

# UNCLASSIFIED

AD NUMBER
AD420622
NEW LIMITATION CHANGE
TO Approved for public release, distribution unlimited
FROM Distribution authorized to U.S. Gov't. agencies and their contractors; Administrative/Operational Use; SEP 1963. Other requests shall be referred to Aeronautical Systems Division, Attn: AF Materials Lab., Wright-Patterson AFB, OH 45433.
AUTHORITY
ASD ltr dtd 20 Jul 1970

THIS PAGE IS UNCLASSIFIED

AD-420622

ASD-TDR-62-729  
PART II, VOL. 1

# **THEORETICAL AND EXPERIMENTAL INVESTIGATION OF ARC PLASMA-GENERATION TECHNOLOGY**

**PAT II: APPLIED RESEARCH ON ELECTRIC ARC PHENOMENA**  
**Vol. 1: A Theoretical and Experimental Study of**  
**Thermionic Arc Cathodes**

TECHNICAL DOCUMENTARY REPORT No. ASD-TDR-62-729  
PART II, VOL. 1

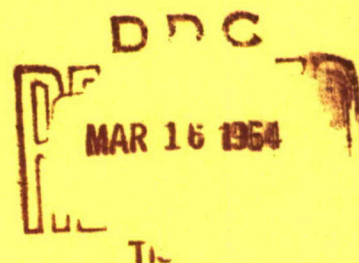
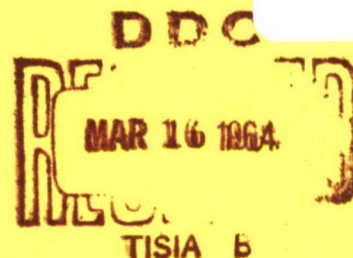
SEPTEMBER 1963

AIR FORCE MATERIALS LABORATORY  
AERONAUTICAL SYSTEMS DIVISION  
AIR FORCE SYSTEMS COMMAND  
WRIGHT-PATTERSON AIR FORCE BASE, OHIO

Project No. 7360, Task No. 736001

(Prepared under Contract No. AF 33(616)-7578 by  
Research and Advanced Development Division, Avco Corporation,  
Wilmington, Massachusetts; W. L. Bade and J. M. Yos, Authors)

20070925181





## NOTICES

When Government drawings, specifications, or other data are used for any purpose other than in connection with a definitely related Government procurement operation, the United States Government thereby incurs no responsibility nor any obligation whatsoever; and the fact that the Government may have formulated, furnished, or in any way supplied the said drawings, specifications, or other data, is not to be regarded by implication or otherwise as in any manner licensing the holder or any other person or corporation, or conveying any rights or permission to manufacture, use, or sell any patented invention that may in any way be related thereto.

DDC release to OTS not authorized.

Qualified requesters may obtain copies of this report from the Defense Documentation Center (DDC), (formerly ASTIA), Arlington Hall Station, Arlington 12, Virginia.

Copies of this report should not be returned to the Aeronautical Systems Division unless return is required by security considerations, contractual obligations, or notice on a specific document.

## FOREWORD

This is Part II, Volume 1 of a final report prepared by the Research and Advanced Development Division of the Avco Corporation on USAF Contract AF33(616)-7578 under Project No. 7360, The Chemistry and Physics of Materials, Task No. 736001, Thermodynamics and Heat Transfer. The work was administered under the direction of the Materials Physics Division of the Air Force Materials Laboratory, Deputy Commander/Research Engineering, Aeronautical Systems Division. The ASD monitor on the program was Mr. Hyman Marcus, Chief of the Thermophysics Section.

The present document reports applied research on thermionic cathodes. Arc column theory, operation in different gases, electrode material investigations and magnetic field arc column interactions are presented in Part II, Volume 2. Part I deals with applied research on electric arc plasma generators.


The present volume was prepared by Drs. William Bade and Jerrold Yos. The program project director was Dr. Richard John. The authors wish to acknowledge many helpful discussions with Mr. Kurt Burkhard and Dr. Peter Neurath. Mr. John Connors expedited the experimental phases of the investigation with his supervisory support. Grateful appreciation is expressed to Mr. C. Simmard for the skill and enthusiasm with which he carried out the experiments. The photographs were taken by Messrs, John Lupo and David Hamilton. Mr. Leonard Comeau aided in the analysis of the data.

This document covers work performed between 1 August 1960 and 30 November 1962.

ABSTRACT

The operating mechanism of thermionic arc cathodes is studied theoretically and experimentally. A theoretical model is formulated including important processes in the plasma of the cathode fall zone, at the plasma cathode interface, and in the cathode interior. In principle, this model permits detailed calculations of cathode performance solely from geometrical considerations and the physical properties of the cathode material and the gas. An approximate analysis indicates that the system has two different types of solution, the occurrence of which depends primarily upon how well the cathode is cooled. Well cooled cathodes tend to operate with a concentrated arc spot, while very poorly cooled cathodes operate without such a spot. Approximate solutions are worked out in numerical detail for spot-mode operation of a semi-infinite cathode and spotless mode operation of a thin rod shaped cathode cooled at one end. The results of a series of experiments on rod shaped thoriated tungsten cathodes are reported. The theory correctly predicts general trends of these data.

This technical documentary report has been reviewed and is approved.



LEO F. SAIZBERG  
Associate Director for  
Materials Physics  
Air Force Materials Laboratory



# TABLE OF CONTENTS

I.	Introduction .....	1
	A. Objectives .....	1
	B. Background .....	2
	C. Present Report .....	4
II.	Summary .....	6
III.	Physical Processes .....	8
	A. Processes in the Cathode Fall Zone .....	8
	B. Processes at the Cathode Surface .....	15
	C. Processes in the Cathode Interior .....	22
IV.	Theory of Thermionic Cathodes .....	25
	A. Phenomenology .....	25
	B. Oversimplified Model .....	25
	C. Theoretical Model for Thermionic Cathodes .....	29
	D. Approximate Methods of Solution .....	40
V.	Quasi-one-dimensional Model .....	53
	A. Preliminary Discussion .....	53
	B. Quasi-one-dimensional Heat Flow in a Thin Rod with Joule Heating and Side Radiation .....	53
	C. Arc Overflow .....	74
	D. Solution of the Quasi-one-dimensional Cathode Model .....	80
	E. Numerical Results .....	85
VI.	Experimental Studies of Rod Shaped Thoriated Tungsten Cathodes .....	123
	A. Apparatus and Procedures .....	123
	B. Results .....	126
	C. Analysis of Data .....	141
	D. Comparison of Theory and Experiment .....	154
VII.	Discussion .....	165
VIII.	Recommendations for Further Work .....	167



TABLE OF CONTENTS (Concl'd)

IX.	References .....	169
X.	Appendixes	
A.	Numerical Procedure for Computation of Surface Heat flux as a Function of Surface Temperature .....	175
B.	Program for Solution of Quasi-one-dimensional Cathode Model .....	177

LIST OF ILLUSTRATIONS

Figure	1	Schematic Cross-sectional Diagram of Fall Zone on a Thermionic Cathode.....	12
	2	Graphical Solution of Oversimplified Model .....	28
	3	Division of Cathode Surface into "Active" and "Inactive" Regions and Interface with Cooling System.....	31
	4	Cathode Heat Flux as a Function of Surface Temperature .....	34
	5	Ion Current Density as a Function of Surface Temperature .....	35
	6	Electron Current Density as a Function of Surface Temperature .....	36
	7	Total Current Density as a Function of Surface Temperature .....	37
	8	Graphical Solution of Equation (63).....	39
	9	Thermal Conductivity of Tungsten .....	56
	10	Electrical Resistivity of Tungsten .....	57
	11	Total Emissivity of Tungsten.....	58

LIST OF ILLUSTRATIONS (Cont'd)

Figure 12	One Dimensional Cathode Function $G(\psi, z)$ .....	63
13	Tip Temperature versus Current and Cathode Length (One Eighth Inch Thoriated Tungsten Cathode in Helium) .....	87
14	Half-Height of Overflow Region versus Current and Cathode Length (One Eighth Inch Thoriated Tungsten Cathode in Helium) .....	88
15	Ratio of Total Current to Current Entering through End versus Current and Cathode Length (One Eighth Inch Thoriated Tungsten Cathode in Helium) .....	89
16	Overflow Parameter $\lambda$ versus Current and Cathode Length (One Eighth Inch Thoriated Tungsten Cathode in Helium) .....	90
17	Current Density through End of Cathode versus Current and Cathode Length (One Eighth Inch Thoriated Tungsten Cathode in Helium) .....	91
18	Heat Transfer from Cathode to Cooling System versus Current and Cathode Length (One Eighth Inch Thoriated Tungsten Cathode in Helium) .....	92
19	Effective Voltage for Heat Transfer to Cooling System versus Current and Cathode Length (One Eighth Inch Thoriated Tungsten Cathode in Helium) .....	93
20	Effective Voltage for Cathode Power Loss versus Current and Cathode Length (One Eighth Inch Thoriated Tungsten Cathode in Helium) .....	94
21	Cathode Fall Voltage versus Current and Cathode Length (One Eighth Inch Thoriated Tungsten Cathode in Helium) .....	95
22	Ion Current Fraction versus Current and Cathode Length (One Eighth Inch Thoriated Tungsten Cathode in Helium) .....	96

LIST OF ILLUSTRATIONS (Cont'd)

Figure 23	Surface Electric Field versus Current and Cathode Length (One Eighth Inch Thoriated Tungsten Cathode in Helium) .....	97
24	Tip Temperature versus Current and Cold End Temperature (One Eighth Inch by One Inch Thoriated Tungsten Cathode in Helium) .....	100
25	Ratio of Total Current to Current Entering through End of Cathode versus Current and Cold-End Temperature (One Eighth Inch by One Inch Thoriated Tungsten Cathode in Helium) .....	101
26	Heat Transfer from Cathode to Cooling System versus Current and Cold End Temperature (One Eighth Inch by One Inch Thoriated Tungsten Cathode in Helium) .....	102
27	Tip Temperature versus Current Density and Cathode Diameter (One Inch Thoriated Tungsten Cathode in Helium) .....	103
28	Ratio of Total Current to Current Entering through End of Cathode versus Current Density and Cathode Diameter (One Inch Thoriated Tungsten Cathode in Helium) .....	104
29	Effective Voltage for Heat Transfer to Cooling System versus Current Density and Cathode Diameter (One Inch Thoriated Tungsten Cathode in Helium) .....	106
30	Effective Voltage for Cathode Power Loss versus Current Density and Cathode Diameter (One Inch Thoriated Tungsten Cathode in Helium) .....	107
31	Ion Current Fraction versus Current Density and Cathode Diameter (One Inch Thoriated Tungsten Cathode in Helium) .....	108
32	Surface Electric Field versus Current Density and Cathode Diameter (One Inch Thoriated Tungsten Cathode in Helium) .....	109



LIST OF ILLUSTRATIONS (Cont'd)

Figure 33	Tip Temperature versus Current and Cathode Material (One Inch by One Eighth Inch Cathodes in Helium) .....	110
34	Ratio of Total Current to Current Entering through End of Cathode versus Current and Cathode Material (One Inch by One Eighth Inch Cathodes in Helium) .....	111
35	Effective Voltage for Heat Transfer to Cooling System versus Current and Cathode Material (One Inch by One Eighth Inch Cathodes in Helium) .....	112
36	Effective Voltage for Cathode Power Loss versus Current and Cathode Material (One Inch by One Eighth Inch Cathodes in Helium) .....	113
37	Cathode Fall Voltage versus Current and Cathode Material (One Inch by One Eighth Inch Cathodes in Helium) .....	114
38	Ion-Current Fraction versus Current and Cathode Material (One Inch by One Eighth Inch Cathodes in Helium) .....	115
39	Surface Electric Field versus Current and Cathode Material (One Inch by One Eighth Inch Cathodes in Helium) .....	116
40	Tip Temperature versus Current and Gas Type (One Inch by One Eighth Inch Thoriated Tungsten Cathode) .....	118
41	Surface Electric Field versus Current and Gas Type (One Inch by One Eighth Inch Thoriated Tungsten Cathode) .....	119
42	Ion Current Fraction versus Current and Gas Type (One Inch by One Eighth Inch Thoriated Tungsten Cathode) .....	120
43	Ratio of Total Current to Current Entering through End of Cathode versus Current and Gas Type (One Inch by One Eighth Inch Thoriated Tungsten Cathode) .....	121

LIST OF ILLUSTRATIONS (Cont'd)

Figure 44	Heat Transfer from Cathode to Cooling System versus Current and Gas Type (One Inch by One Eighth Inch Thoriated Tungsten Cathode) .....	122
45	Arc Assembly for Cathode Studies .....	124
46	Tip Temperature as a Function of Time for a New Thoriated Tungsten Cathode (Five Eighth Inch by One sixteenth Inch, Helium) .....	127
47	Tip Temperature as a Function of Time for a New Thoriated Tungsten Cathode (Two Inch by One Eighth Inch, Helium Argon) .....	129
48	Changes in Appearance of an Arc Operating on a New Thoriated Tungsten Cathode .....	130
49	Appearance of Arc in Helium and Argon as a Function of Current (Two Inch by One Eighth Inch "Used" Thoriated Tungsten Cathode) .....	131
50	Appearance of Arc in Helium and Argon as a Function of Current (One Half Inch by One Eighth Inch "New" Thoriated Tungsten Cathode).....	132
51	Appearance of Arc in Nitrogen (One Inch by One Sixteenth Inch Thoriated Tungsten Cathode) .....	135
52	Current Density versus Temperature for "Used" Thoriated Tungsten Cathodes in Helium .....	145
53	Analysis of Cathode Data for Electrical Resistivity .....	151
54	Results of Error Analysis for Estimates of B from Cathode Data .....	153
55	Heat Transfer to Cathode Cooling System versus Current (Helium).....	155
56	Heat Transfer to Cathode Cooling System versus Current (Argon) .....	156

LIST OF ILLUSTRATIONS (Concl'd)

Figure 57	Heat Transfer to Cathode Cooling System versus Current (Nitrogen) .....	157
58	Cathode Temperature Distribution (Helium, Two Inch by One Eighth Inch Cathode, Twenty five Amperes) .....	158
59	Cathode Temperature Distribution (Helium, Two Inch by One Eighth Inch Cathode, Fifty three Amperes) .....	159
60	Cathode Temperature Distribution (Helium, One Inch by One Sixteenth Inch Cathode, Forty one Amperes) .....	160
61	Cathode Temperature Distribution (Helium, One Inch by One Sixteenth Inch Cathode, Seventy four Amperes) .....	161
62	Cathode Temperature Distribution (Helium, One Inch by One Eighth Inch Cathode, Twenty six Amperes) .....	162
63	Cathode Temperature Distribution (Helium, One Inch by One Eighth Inch Cathode, Ninety six Amperes) .....	163
64	FORTTRAN Listing of Main Program for Solution of Quasi-One-Dimensional Cathode Model .....	178
65	FORTTRAN Listing of Subroutine START .....	180
66	FORTTRAN Listing of Function G .....	181
67	FORTTRAN Listing of Function V .....	182
68	FORTTRAN Listing of Subroutine DISTAN .....	183
69	FORTTRAN Listing of Subroutine OUTPUT .....	184
70	Flow Chart for Main Program between Statements 5 and 200 .....	188



LIST OF TABLES

Table	1	Accommodation Coefficients for Ion Impact upon Tungsten (Billiard Ball Approximation) .....	18
	2	Numerical Results of Approximate Cathode-Spot Theory .....	51
	3	One Dimensional Cathode Function $G(\psi, z)$ .....	60
	4	One Dimensional Cathode Function $V(\psi, z)$ .....	67
	5	One Dimensional Cathode Function $R(\psi, z)$ .....	70
	6	Assumed Cathode Material Properties .....	86
	7	Gas Properties .....	86
	8	Summary of Experimental Data .....	136
	9	Analysis of Cathode Data for Effective Work Function .....	143
	10	Analysis of Cathode Data for Thermal Conductivity.....	148
	11	Analysis of Cathode Data for Electrical Resistivity.....	152



## LIST OF SYMBOLS

The list below defines the principal notations used throughout the report; special symbols used only once and defined in the text are omitted. After each definition, the numbered equation or location where the symbol is first used is given in parentheses.

### Latin Symbols

A	Richardson constant (17)
a	quantity defined by (121)
$\alpha$	accommodation coefficient (Sec. II)
B	parameter in resistivity formula (87)
b	quantity defined by (122)
C	integration constant in (90)
c	specific heat of cathode material (64)
D	cathode diameter (39)
E	electric field intensity (6)
$E_c$	electric field intensity at cathode surface (7)
F	quantity defined by (150)
$F(T_s)$	net heat flux into cathode surface as a function of surface temperature (61)
$G(\psi, z)$	nondimensional distance function for quasi-one-dimensional cathode (93)
H	quantity defined by (158)
I	total current (39)
$I_e$	current through end of cathode (Fig. 34)
j	total-current density (8)

LIST OF SYMBOLS (Cont'd)

$j_0$	uniform current density along cathode (84) current density at cold end of cathode (139j)
$j_e$	electron-current density (2a)
$j_E$	current density through hot end of cathode (130)
$j_i$	ion-current density (2b)
$(j_i)_{\max}$	upper limit to ion-current density based on kinetic theory (16)
$j_s$	current density through side of cathode (110)
$K$	thermal conductivity of cathode (28)
$k$	Boltzmann constant (14)
$L$	cathode length (45)
$M$	ion mass (3a)
$m$	electron mass (3b)
$n$	coordinate along outward-directed normal to cathode surface (28)
$n_e$	electron density (1)
$n_i$	ion density (1)
$p$	pressure (14)
$Q$	total rate of heat transfer to cathode (66)
$Q_0$	heat-transfer rate from cathode to cooling system (Sec. III)
$q$	heat flux (28)
$q'$	$dq/dT$ (70)
$q_0$	heat flux at cold end of cathode (105b)

LIST OF SYMBOLS (Cont'd)

$q_E$	heat flux through hot end of cathode (138)
$R(\psi, z)$	nondimensional function for radiative heat loss from side of cathode (101a)
$r$	radial coordinate (67)
$r_s$	cathode spot radius (66)
$S_1, S_2, S_3$	cathode interface with cooling system, "inactive region" of cathode surface, "active region" of cathode surface, respectively (62)
$s$	temperature exponent in resistivity formula (87)
$T$	cathode temperature (28)
$T_0$	temperature at cathode interface with cooling system (44)
$T_{av}$	average temperature of cathode spot (66)
$T_c$	cutoff temperature for heat-flux function (69)
$T_g$	gas temperature in ion-production zone (14)
$T_m$	temperature at center of cathode spot (Sec. III)
$T_n(x)$	"unperturbed" temperature distribution in cathode with overflow (112)
$T_{ns}$	value of $T_n(x)$ at $x = L$ (113)
$T_{ns}$	temperature gradient at hot tip based on unperturbed solution (116)
$T_s$	cathode surface temperature (17)
$t$	time (64)
$t(x)$	perturbation temperature distribution in cathode with overflow (112)

LIST OF SYMBOLS (Cont'd)

$t_0$	value of $t(x)$ at cathode tip (129)
$U$	electric potential (1)
$\bar{u}_i$	mean thermal speed of ions in any given direction (15)
$V$	quantity defined by (114)
$V(\psi, z)$	nondimensional voltage function for quasi-one-dimensional cathode (98a)
$V_c$	potential fall across space-charge layer (3a)
$V_{eff}$	effective voltage for heat transfer to cooling system (151)
$V_I$	ionization potential (12)
$V_{loss}$	effective voltage for cathode power loss (Sec. IV)
$v_e$	electron velocity (2a)
$v_i$	ion velocity (2b)
$W$	molecular weight of ions (8)
$x$	coordinate in plasma normal to cathode surface (1)
$x$	coordinate along cathode axis (43)
$y$	distance from tip of cathode (115)
$z$	nondimensional Joule-heating parameter (91c)
$z_c$	critical value of $z$ (14)

Greek Symbols

$a$	ion-current fraction, $j_i/j$ (8)
$\gamma$	constant in (72)
$\Delta$	quantity defined by (148)



LIST OF SYMBOLS (Concl'd)

$\Delta T$	temperature difference between center and edge of cathode spot (71a)
$\Delta V$	resistive voltage drop along cathode (98a)
$\delta$	density of cathode material (64)
$\epsilon$	total emissivity (27)
$\epsilon_e$	electronic charge (1)
$\eta$	nondimensional position coordinate (91b)
$\eta_s$	value of $\eta$ at hot end of cathode (139a)
$\theta$	effective work function expressed as a temperature (17)
$\theta_0$	$11609\phi$ (149a)
$\lambda$	nondimensional overflow parameter (127)
$\rho$	electrical resistivity (35)
$\sigma$	Stefan-Boltzmann constant (27)
$r$	nondimensional tip temperature (139n; also (167)
$\phi$	thermionic work function (18)
$\psi$	nondimensional temperature (91a)
$\psi_0$	nondimensional temperature at cold end of cathode (94)
$\psi_s$	nondimensional temperature at hot end of cathode (139a)
$\omega$	quantity defined by (119)

Subscripts

s	cathode surface or tip
av	average over cathode spot.

## I. INTRODUCTION

### A. OBJECTIVES

Electrode phenomena in electric arcs have been studied experimentally and theoretically by a number of investigators. The literature on cathode and anode fall voltages, current densities, and operating mechanisms is voluminous. Nevertheless, the design of electrodes for electric arc plasma generators has been carried out almost entirely on an empirical basis, because there has existed no experimentally verified quantitative theory capable of predicting the performance of an electrode of given properties and geometry operating at a given current in a specified gas.

The development of electrothermal and electromagnetic space propulsion systems and high-energy wind tunnels for simulation of atmospheric re-entry<sup>1</sup> has subjected plasma generator electrode subsystems to requirements of unprecedented severity. The propulsion applications demand operating lifetimes of many hundreds or thousands of hours, while arc driven wind tunnels often call for operation at high currents and pressures with negligible contamination of the gas stream. Rational design procedures based upon proven theoretical models would facilitate meeting these requirements and optimizing electrode configurations, or perhaps, in some instances, establish that the requirements cannot be met with a given type of electrode. The present report describes a series of investigations whose objective has been to develop a quantitative theoretical model for one particular kind of electrode.

Several different types of arc cathode, distinguished by qualitatively different electron emission mechanisms, have been investigated experimentally.<sup>2</sup> Carbon, tungsten, and certain other refractory metals operate as cathodes with high surface temperatures at which the bulk of the observed current density can be accounted for by thermionic emission. Cathodes of copper, mercury, and other low-boiling-point metals carry very high current densities ( $> 10^6$  amp/cm<sup>2</sup>) which cannot be explained on the thermionic hypothesis. The mechanism of the "hollow" or "cavity" cathode<sup>3</sup> is also uncertain.

The present investigation is primarily theoretical in nature, and has been directed toward elucidation of the mechanism of thermionic cathodes. This particular problem area was chosen because of the availability of experimental data for guidance during formulation of the theoretical model and for comparison with predictions of the theory. The data for cold cathodes and hollow cathodes have been too incomplete and inaccurate to permit fruitful theory construction; however, this situation is improving rapidly at the present time.

---

Manuscript released by authors January 1963 for publication as an ASD Technical Documentary Report.



The discovery that electron emission from a tungsten or carbon cathode occurs by the thermionic mechanism does not constitute a complete solution to "the cathode problem" for these materials. On the contrary, it provides only a single relation among the numerous unknown quantities characterizing cathode operation at a given current; namely, a relation among local electron current density, local surface temperature, and local electric field strength at the surface. Standing by itself, the thermionic emission relation throws little light upon such basic questions as why the cathode sometimes operates in the spot mode and sometimes in the spotless mode, and why the occurrence of spot-mode operation depends upon cathode work function, total current, and gas type. Moreover, without additional relations it is impossible to predict quantitatively any of the key parameters of cathode performance, such as the distributions of temperature and current density over the surface and the total cathode power loss. What is required to investigate these questions is a complete mathematical model for thermionic cathodes; i. e., a system of equations which can be solved (given the geometry and physical properties of the cathode, the type of gas in which it is operating, and the total current) to yield the surface temperature and current density, the electric field at the surface, the cathode fall voltage, the ion current fraction, and the net heat flux to the cathode surface. A crude approximation to such a mathematical model is developed in the present report.

## B. BACKGROUND

The current densities observed on carbon and tungsten cathodes operating in the spotless mode are of the order of  $10^3$  amp/cm<sup>2</sup>. These current densities are low enough to be accounted for by assuming thermionic electron emission from the cathode surfaces at the observed temperatures.<sup>4</sup> The higher current densities ( $\sim 10^4$  to  $10^5$  amp/cm<sup>2</sup>) observed during spot-mode operation of hot cathodes can be explained, as suggested by Ecker<sup>5</sup> and Bauer,<sup>6</sup> in terms of electron emission produced by the joint action of a high surface temperature and a high electric field. The field is provided by the net positive space charge in the cathode fall region lying between the surface and the electrically neutral plasma. Lee,<sup>7-8</sup> and Lee and Greenwood,<sup>9</sup> have investigated this approach in considerable detail with the objective of explaining cathode phenomena in metal vapor arcs.

A number of attempts have been made to develop complete theoretical models for particular types of cathodes. Weizel and Thouret,<sup>10</sup> in their "contraction theory," focus attention on processes occurring in the cathode fall zone; i. e., the space charge region in the gas adjacent to the cathode surface. They base their considerations upon the Poisson equation, the equations for electron and ion current densities in terms of mobilities and the electric field intensity, and the heat conduction equation for the gas. By combining these relations, they obtain a formula for cathode fall voltage in terms of the current density, the temperature difference between the cathode and the plasma,



the fraction of the current carried by ions, and certain gas properties. This formula indicates that the fall voltage decreases with increasing current density; thus, contraction of the column into a cathode spot leads to a low cathode fall. For excessively small fall zone thickness, some of the assumed relations break down and the fall voltage begins to increase with further contraction. Weizel and Thouret conclude, from the Steenbeck principle of minimum voltage, that the fall zone on actual cathodes operating in the spot mode must be of the order of a few ion mean free paths. These authors also apply the same set of ideas to cathodes operating in the spotless mode, and conclude that in this case the ion current fraction must be about 0.03; i. e., that the current is carried almost entirely by electron emission.

The Weizel-Thouret theory is not a complete cathode model, since it does not permit prediction of cathode performance solely from cathode geometry and cathode and gas properties. To obtain numerical results from this theory, it is necessary to assume values for some of the unknowns; e. g., current density and ion current fraction. In essence, this shortcoming is a consequence of these authors' disregard for processes occurring on the surface and within the interior of the cathode.

Ecker<sup>5, 11</sup> has constructed a complete cathode model which incorporates some of the physical ideas of the contraction theory. He takes the current density to be given by the sum of the electron emission current, as determined by the surface temperature and the electric field at the surface, and the saturation ion current, which depends upon the rate of production of ions in the contraction region and the rate at which the ions can be drawn to the surface. He considers energy transfer to the surface by ion impact, transfer of neutralization energy, and heat conduction through the gas. He includes heat conduction in the cathode interior and assumes that this heat is given up to the cooler gas outside of the conducting region. The final solution is determined graphically using what Ecker terms the "E diagram," a plot of ion saturation current and ion defect current versus the contraction factor. The theory shows that, in general, two or more solutions exist, corresponding to various degrees of contraction. In other words, the theory predicts operation with and without cathode spots. Ecker states that, for a given case, the operating mode "selected" by the arc is the one with the lowest voltage requirement, in accordance with the Steenbeck principle.

Ecker's theoretical model successfully accounts for many of the qualitative features observed experimentally in cathode operation. In its existing form, however, this theory is not satisfactory as a model for practical cathode design because the cathode geometry assumed for convenience in obtaining a solution is very dissimilar to the cathodes used in actual plasma generators. In addition, some of the physical assumptions employed in the theory appear subject to some improvement.



Bauer<sup>6</sup> has presented a model for the cathode spot on a spherical, radiation cooled cathode. He assumes thermal field electron emission from the surface, and obtains an approximate relation between the electron current fraction and the cathode fall voltage by considering a rough balance between the power injected into the gas by electrons accelerated through the fall zone and the power required for production of ions. The power transferred to the cathode from the fall zone is estimated from the kinetic and neutralization energy of the ions, and is related to the spot temperature on the cathode by means of an approximate heat conduction relation. Finally, a relation between this power and the overall cathode temperature outside of the spot region is obtained by considering radiative cooling of the cathode as a whole. This system of equations is deficient by one relation, so that Bauer is only able to obtain values of the unknown quantities as functions of both current density and total current. Thus, his attempt toward a cathode model is not fully successful; nevertheless, it introduces a number of valuable simple approximations, some of which are employed in the present work.

The most recent cathode model is that of Lee and Greenwood,<sup>9</sup> for the case of metal vapor arcs. Here again, a complete system of equations is not presented. Four relations are given for determining five unknowns, in addition to which the cathode fall voltage is assumed known. However, two inequalities are presented which set limits to the current at which arcs of the type considered can operate. One of these inequalities is considered to be responsible for the phenomenon of "current chop" in an alternating current metal vapor arc.

### C. PRESENT REPORT

Of the cathode theories summarized above, only that of Ecker is "complete" in the sense that, in principle, it permits ab initio calculation of cathode performance solely from geometrical considerations and the physical properties of the cathode and the gas. The present report presents a new cathode model which is complete in this sense. This new theory employs a number of relations used by previous investigators, but focuses attention upon the details of heat flow in the cathode interior as a determinative factor of hitherto unemphasized significance.

Because many of the relations used are crude approximations, this model must be regarded as only a preliminary formulation. However, it appears to offer a conceptual solution to the thermionic arc cathode problem. It can be improved by a straightforward but laborious refinement of its approximations without significant alteration of its overall structure.

Section II of the report reviews the physical processes occurring in the cathode fall zone, at the cathode surface, and in the interior. In section III, a number of rough relations describing these processes are combined to

yield a complete system of equations approximately describing the operation of thermionic cathodes. Various approximate methods for solving this system of equations are considered. Section IV deals with a particular approximate solution, the quasi one dimensional model, which is applicable to long, thin, rod shaped cathodes. Section V then describes a series of experiments carried out with cathodes of this type, and presents a comparison of the experimental results with calculations based upon the theory. Finally, section VI reviews the findings of the present work, and section VII suggests possibly fruitful lines for further investigation.



## II. SUMMARY

This report presents the results of a theoretical and experimental study of the operating mechanism of thermionic arc cathodes. The principal objective is to develop an approximate theoretical model which is "complete," in the sense that it permits detailed calculations of cathode performance solely from geometrical considerations and the physical properties of the cathode material and the gas. If successful, such a theoretical model would have numerous significant applications, including the design of cathodes with low power loss and cathodes capable of operating without significant loss of material at high pressures.

The operation of thermionic cathodes is dependent upon processes occurring in the plasma of the cathode fall zone, at the plasma cathode interface, and in the cathode interior. These processes are represented, in the present formulation, by approximate relations which in some instances are quite crude, but which appear to contain the essential physics of the situation. The entire system of relations can be considered to define a steady state heat conduction problem for the cathode interior, with an unusual boundary condition representing the processes in the plasma and at the surface. An approximate analysis indicates that the system has two different types of solution, the occurrence of which depends primarily upon how well the cathode is cooled.

For a well cooled cathode, the actively emitting region of the surface contracts until the ion current density drawn from the plasma reaches its maximum value as determined by kinetic theory. This type of solution of the theoretical model is provisionally identified with the experimental phenomenon of "spot mode" operation. According to the theory, the current density and surface temperature of a cathode operating in this mode rise with increasing pressure, leading to cathode failure at the pressure level for which the spot temperature reaches the melting point.

The other type of solution predicted by the theoretical model occurs only for poorly cooled (or even heated) cathodes. In these solutions, a large region of the cathode is at a high temperature and carries current. The ion current density is less than the kinetic theory maximum. This type of solution is provisionally identified with "spotless mode" operation as observed experimentally. The present version of the theory indicates that the cathode temperature in spotless mode operation should be pressure independent.

Approximate solutions of these types are worked out in numerical detail for two special cases. Solutions representing spot mode operation are obtained for a semi-infinite cathode with zero temperature at infinity. Spotless mode solutions are calculated for a thin, rod shaped cathode cooled at one end and with the arc striking to the other end. For both cases, the dependence of



cathode operating parameters upon current, gas type, and material properties is explored numerically. In the case of the rod shaped cathode, geometrical factors are also varied.

The results of a series of experiments on rod shaped thoriated tungsten cathodes are reported. The data are analyzed to obtain estimates of the work function, thermal conductivity, and electrical resistivity of the material, and are compared with the results of theoretical calculations based upon the above mentioned approximate theory for rod shaped cathodes. The data follow the general trends predicted by the theory, but fail to provide a quantitative test of the theory owing to occurrence in the experiments of certain phenomena not represented in the theory.

Detailed recommendations are made for further work on the problems of thermionic and cold cathodes.

### III. PHYSICAL PROCESSES

The present section presents a somewhat detailed discussion of the physical processes which are likely to be of substantial importance in the operation of thermionic cathodes. Ecker's recent review article<sup>11</sup> treats many of these topics in greater detail. For convenience of presentation, the various processes are categorized according to their sites of action; i.e., according to whether they take place in the gas, at the surface, or within the cathode interior.

#### A. PROCESSES IN THE CATHODE FALL ZONE

##### 1. Space Charge

The cathode has a negative potential with respect to the arc plasma, and, therefore, attracts positive ions toward its surface. At the same time, plasma electrons are repelled. Thus, a region of positive space charge exists adjacent to the cathode surface. This space charge region is responsible, in large part, for the existence of a cathode fall of potential and of a high electric field at the cathode surface.

These effects are determined essentially by Poisson's equation,

$$d^2U/dx^2 = -4\pi\epsilon_e(n_i - n_e) \quad (1)$$

where

$U$  = electric potential

$x$  = coordinate normal to cathode surface

$\epsilon_e$  = electron charge

$n_i$  = ion density

$n_e$  = electron density.

The particle densities  $n_e$  and  $n_i$  vary through the space charge layer. Back diffusion of electrons from the plasma is neglected in the present discussion, although Ecker<sup>12</sup> has shown that this can be a major effect. The particle densities are then related to the electron and ion current densities,  $j_e$  and  $j_i$ , and the mean velocities of the electrons and ions,  $v_e$  and  $v_i$ , by

$$n_e = j_e / \epsilon_e v_e, \quad (2a)$$

$$n_i = j_i / \epsilon_e v_i \quad . \quad (2b)$$

If the space charge layer is sufficiently thin that collisions within it can be neglected (i. e., if the thickness is of the order of a mean free path or less, as is usually the case<sup>12</sup>), then the current densities  $j_e$  and  $j_i$  are constant, and the electrons and ions execute free trajectories in the electrostatic field resulting from their own space charge. In this case, all of the ions at a given distance from the surface have approximately the same velocity, since the ions start with relatively low thermal velocities at the outer edge of the space charge layer, and all move in essentially the same potential field. A similar statement is valid for the electrons emitted from the cathode surface.

Mackeown,<sup>13</sup> in 1929, obtained a self-consistent solution to Poisson's equation (1) and the equations of motion for the charged particles in this thin, collision free layer. His calculation proceeds as follows. Let  $x$  denote a coordinate normal to the surface, with its origin at the surface. The zero of electric potential is selected to make  $U = 0$  at the surface  $x = 0$ . The thermal energies of the emitted electrons at the cathode surface are always negligible in comparison with the cathode fall voltage. To a somewhat poorer approximation, the thermal velocities of the positive ions at the outer edge of the space charge layer can also be neglected. Then, the energy equations for the two types of charged particle become

$$\frac{1}{2} M v_i^2 = (V_c - U) \epsilon_e \quad , \quad (3a)$$

$$\frac{1}{2} m v_e^2 = U \epsilon_e \quad , \quad (3b)$$

where  $M$  and  $m$  denote the ion and electron masses, respectively, and  $V_c$  is the potential at the outer edge of the space charge layer. Use of (3) to eliminate the velocities  $v_i$  and  $v_e$  from (2) and substitution of the resulting values for  $n_e$  and  $n_i$  into Poisson's equation (1) give a differential equation for the potential:

$$\begin{aligned} \frac{d^2 U}{dx^2} &= -4\pi \left( \frac{j_i}{v_i} - \frac{j_e}{v_e} \right) \\ &= -4\pi \left[ j_i \sqrt{\frac{M}{2\epsilon_e(V_c - U)}} - j_e \sqrt{\frac{m}{2\epsilon_e U}} \right] . \end{aligned} \quad (4)$$

Since  $d^2U/dx^2 = -dE/dx = + E dE/dU$ , where  $E$  denotes the electric field intensity, this differential equation can immediately be integrated to give

$$E^2 = \frac{16\pi}{\sqrt{2\epsilon_e}} \left[ j_i M^{1/2} \sqrt{V_c - U} + j_e m^{1/2} \sqrt{U} \right] + \text{const.} \quad (5)$$

At the outer edge of the space charge layer,  $U = V_c$  and  $E$  has a relatively low value. Approximating  $E = 0$  at this point, one evaluates the constant to obtain

$$E^2 = \frac{16\pi}{\sqrt{2\epsilon_e}} \left[ j_i M^{1/2} \sqrt{V_c - U} + j_e m^{1/2} (\sqrt{U} - \sqrt{V_c}) \right] \quad (6)$$

One further integration, which must be performed numerically, gives  $U$  as a function of  $x$ ; i. e., a relation for the thickness of the space charge zone. This integral has been evaluated by Mackeown<sup>13</sup> and by Lee,<sup>7</sup> with results which are consistent with the original assumption that the space charge layer has a thickness of the order of a mean free path or less. However, the details of these results are not required for the purposes of the present investigation.

Evaluation of (6) at the cathode surface, where  $U = 0$ , gives an expression for the magnitude of the surface field intensity  $E_c$ ,

$$E_c^2 = \frac{16\pi V_c^{1/2}}{\sqrt{2\epsilon_e}} (j_i M^{1/2} - j_e m^{1/2}) \quad (7)$$

Conversion to practical units gives

$$E_c = 873 V_c^{1/4} \left[ (1823 W)^{1/2} j_i - j_e \right]^{1/2} \quad , \quad (8a)$$

or

$$E_c = 873 V_c^{1/4} j^{1/2} \left[ (1823 W)^{1/2} a - (1-a) \right]^{1/2} \quad , \quad (8b)$$



where

$V_c$  = potential drop across space charge layer (volt)

$j$  = total current density,  $j_e + j_i$  (amp/cm<sup>2</sup>)

$W$  = molecular weight of ions (gm/mole)

$\alpha$  = ion current fraction,  $j_i / j$ .

Small discrepancies between the numerical values appearing in (8) and those given by Mackeown, and employed by most subsequent authors, are a consequence of the use in (8) of modern values for the atomic constants.

Unless the ion current fraction  $\alpha$  is very small, the term  $(1823 W)^{1/2} \alpha$  in equation (8) is much larger than  $1 - \alpha$ . In most cases, the latter term can be neglected to a good approximation, and (8) then reduces to the Child-Langmuir formula,

$$E_c = 5700 W^{1/4} V_c^{1/4} j_i^{1/2} \quad , \quad (9)$$

for a space charge layer consisting of particles of a single sign. Physically, the validity of this approximation follows from the fact that the heavy positive ions have much lower velocities than the electrons, and thus require a much longer time to traverse the space charge layer. If the electron and ion current densities are at all comparable, the density of positive ions thus greatly exceeds that of the electrons, so that the Mackeown layer is principally a region of positive space charge.

## 2. Ion Production

Figure 1 schematically illustrates the structure of the active region on a thermionic cathode, as presently understood. The hot, solid surface of the cathode is separated from the still much hotter quasi-equilibrium plasma of the positive column by a relatively thin cathode fall zone. The fall zone, in turn, may be conceptually divided into two regions. The first of these is the Mackeown space charge layer, discussed above, whose thickness is only of the order of a mean free path or less.

In the arc column, the current is carried almost entirely by electrons because their mobility is much higher than that of the heavy positive ions. In the Mackeown zone, however, energy balance considerations indicate that a substantial fraction of the current must be carried by ions, as shown below. Thus, ionization of neutral atoms or molecules must occur in the intervening region. For this reason, the portion of the cathode fall zone

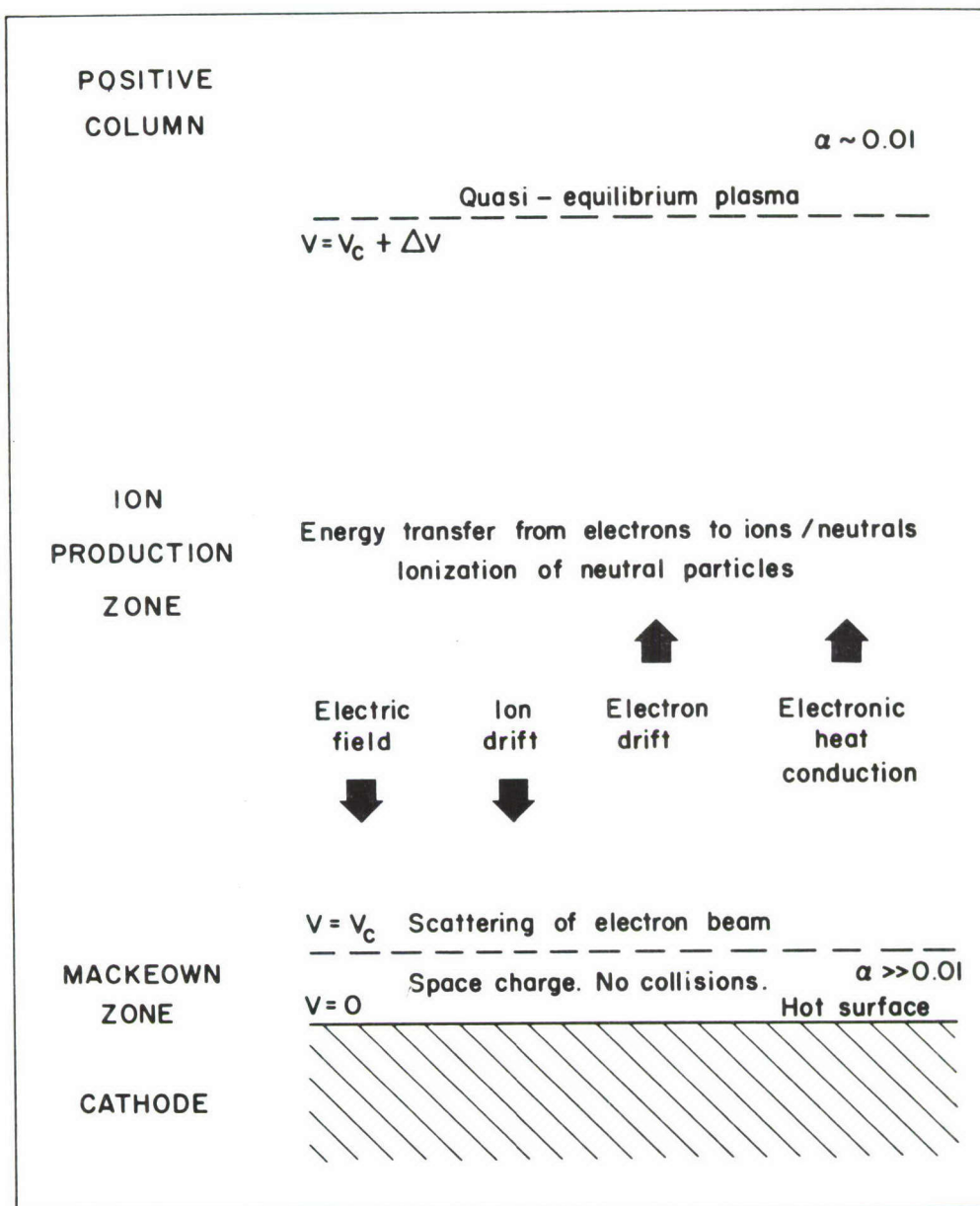


Figure 1 SCHEMATIC CROSS-SECTIONAL DIAGRAM OF FALL ZONE ON A THERMIONIC CATHODE

extending from the outer edge of the Mackeown layer to the boundary of the arc column is designated here as the ion production zone. It occupies the largest fraction of the volume of the fall zone. A large part of the cathode potential drop occurs, however, in the Mackeown zone. Experimentally, the cathode fall is of the order of several volts.

The electrons emitted from the surface are accelerated by the electric field in the Mackeown zone, and thus are injected as a beam into the ion production zone. The kinetic energy  $eV_c$  of these electrons is, in most cases, too low to permit inelastic collisions producing excitation or ionization of atoms or ions. The electrons are thus scattered elastically by the heavy particles but, in general, lose only a little energy per such collision. However, the beam electrons also collide with electrons already present in the gas, and as a result the electron velocity distribution becomes Maxwellian within a few mean free paths from the surface. The directed motion of the beam electrons is thus destroyed, and these electrons join the electron gas in the ion production zone. Their kinetic energy is quickly distributed to a large number of "gas" electrons, and then transferred to heavy particles by elastic collisions. Because of the vast number of collisions occurring in a gas at atmospheric or higher pressure, this transfer is relatively rapid.

The energy transferred from the electrons to the heavy particles is dissipated to some extent by radiation and heat conduction to the cathode, but most of it is presumably consumed in the ionization of neutral particles. This idea provides the basis for a simple and useful approximate relation which has been used previously by Bauer,<sup>6</sup> and which is discussed also by Somerville.<sup>14</sup> Consider the portion of the ion production zone lying above a unit area of the interface between this zone and the Mackeown space charge layer. This region receives an energy influx of amount  $j_e V_c$  as kinetic energy of the electron beam injected from the Mackeown zone. The energy carried out of the region as potential energy of ionization is  $j_i V_I$ . On the assumption that other energy gain and loss terms are negligible or cancel one another, these two quantities can be equated to give  $j_e V_c = j_i V_I$ . With

$$j_i = a j \quad , \quad (10)$$

$$j_e = (1-a) j \quad , \quad (11)$$

this relation becomes

$$V_c = a V_I / (1-a) \quad , \quad (12)$$

or

$$a = V_c / (V_c + V_I) \quad . \quad (13)$$

Equations (12) and (13) have only qualitative validity, because they neglect a large number of energy influx and efflux processes affecting the ion production zone. Some of the energy gain terms omitted are



- a. Joule dissipation in the ion production zone, and
- b. Energy deposition in the zone by Auger electrons ejected from the cathode surface and by neutralized ions rebounding from the surface.

The energy loss terms neglected include

- 1) Thermal energy carried away by electrons diffusing out of the ion production zone into the arc column, \*
- 2) Heat conducted to the cathode surface,
- 3) Radiative losses,
- 4) Energy losses through the side boundaries of the zone, and
- 5) Energy carried out of the zone by convective motions of the gas or by a cathode jet.

Several of these omitted terms are difficult to estimate accurately without a considerable amount of additional work. However, it is clear that equations (12) and (13) give, at best, a very crude approximation to a much more complicated relation which could be obtained, in principle, from a detailed theory of the ion production zone.

In its application to a cathode model, (13) is employed essentially to give the ion current  $j_i$  as a function of  $j_e$ . As  $j_e$  is increased, more electron beam energy is supplied to the ion production zone, and neutral atoms are ionized at a greater rate. It is assumed that all ions thus formed diffuse across the boundary of the Mackeown space charge layer, and then are accelerated by the strong electric field in that region until they strike the cathode surface. It should be noted, however, that there is an upper limit to the ion current density, which would be reached if all of the atoms in the ion production zone were ionized. This limiting ion current density can be estimated<sup>6</sup> in the following way. The ion density in a fully (singly) ionized gas at temperature  $T_g$  and pressure  $p$  is given by

$$(n_i)_{\max} = p/2kT_g \quad (14)$$

since one-half of the particles in such a gas are ions. The mean thermal speed of the ions in any given direction (e. g., normal to the cathode surface) is<sup>15</sup>

$$\bar{u}_i = \sqrt{kT_g/2\pi M} \quad , \quad (15)$$

---

\*Bauer<sup>6</sup> includes a term representing this process in his equation corresponding to (12) or (13).



where  $M$  is the ion mass. Hence, the maximum ion current density is

$$(j_i)_{\max} = e (n_i)_{\max} \bar{u}_i = \frac{P e}{\sqrt{8\pi M k T_g}} \quad (16)$$

In strongly contracted cathode spots, this limit must be rather closely approached over most of the spot area. In such cases equation (13) gives only an upper limit to the value of  $j_i / j$ .

## B. PROCESSES AT THE CATHODE SURFACE

### 1. Electron Emission

In the arc column, almost all of the current is carried by electrons. Thus, a source of electrons must exist at the cathode or in its vicinity. Electrons as well as ions are produced, of course, in the ion production zone, but in arcs of the type under consideration in this report, most of the electrons originate from the cathode itself.

There exist many processes capable of extracting electrons from a metal surface.<sup>11</sup> A number of these depend upon the impact of energetic particles such as ions, excited atoms, and photons. Such processes have been invoked in several theories<sup>16, 17</sup> to explain the operation of cold cathode arcs, but probably do not play an important role in the case of hot, refractory cathodes such as tungsten and carbon, whose surface temperatures are so high that thermionic emission is sufficient to account for most of the observed current.

Electron emission from a metal surface can be produced by a high surface temperature, a high electric field at the surface, or both. The general case is designated as thermal field (T-F) emission.<sup>18</sup> Murphy and Good<sup>19</sup> have presented several analytical approximations, valid in different regions, for the emission current density as a function of temperature, field intensity, and work function. The general case in which both temperature and field are large has not been solved analytically, but Lee<sup>7-9</sup> has presented the results of numerical computations for several values of the work function.

The field intensities for hot cathodes such as tungsten and carbon, calculated from Mackeown's equation (8), turn out to be low enough ( $\lesssim 10^6$  v/cm) that the general T-F emission relation can be approximated with good accuracy by the Richardson-Schottky formula for field enhanced thermionic emission,<sup>19</sup>

$$j_e = A T_s^2 e^{-\theta/T_s} \quad , \quad (17)$$

where

$$\theta = 11609\phi - 4.4\sqrt{E_c} \quad . \quad (18)$$

Here

- A = Richardson constant (amp/cm<sup>2</sup> °K<sup>2</sup>)
- T<sub>s</sub> = surface temperature (°K)
- φ = thermionic work function (volts)
- E<sub>c</sub> = surface electric field intensity (volts/cm).

According to the theoretical derivation of (17), A should be a universal constant having the value 120 amp/cm<sup>2</sup> °K<sup>2</sup> for all materials. However, Nottingham<sup>20</sup> emphasizes that experimental electron emission data are not accurately represented by (17) in any respect. The experimental values for A are usually smaller than the above theoretical values, in some cases by two orders of magnitude or more. The φ value required to fit emission data differs, in general, from the true work function, and is dependent upon temperature, polycrystallinity, and the presence of surface monolayers. Deviations from linear dependence of ln j<sub>e</sub> upon √E<sub>c</sub> occur at low field intensities as well as at high fields, where the approximations upon which (17) is based break down. For these reasons, equation (17) must be regarded, in its application to arc cathodes, as a formula of qualitatively correct form containing two empirical constants whose values can be selected to fit, approximately, the behavior of any given material.

## 2. Heat Transfer

Energy is supplied to the cathode surface by a number of mechanisms.<sup>21</sup> Of these, the most important is ion bombardment. As an ion approaches the metal surface to within a distance of the order of an atomic radius, the potential barrier between the interior of the metal and that of the ion is thinned and weakened until an electron from the conduction band of the cathode can tunnel through and fall into the ground state of the neutralized ion. The neutralization energy  $\epsilon_e (V_I - \phi)$  is delivered to the conduction electrons of the metal, and may cause Auger ejection of an additional electron from the cathode. The yield for this ejection process has been determined by Hagstrum<sup>22</sup> for the inert gas ions incident upon tungsten. It is about one-quarter of an electron per ion for He<sup>+</sup> and Ne<sup>+</sup>, about one-tenth for Ar<sup>+</sup>, and still smaller for Kr<sup>+</sup> and Xe<sup>+</sup>. In all cases, it is roughly independent of ion kinetic energy from 0 to 1000 electron volts. Most of the ejected



electrons have energies in the range from about one-fifth to about three-quarters of the available energy  $V_I - 2\phi$ , the average energy being roughly  $\frac{1}{2}(V_I - 2\phi)$ .

That portion of the available energy  $V_I - 2\phi$  which is not carried away by the emergent electron, as well as the energy given up by ions which fail to produce an Auger ejection, is presumably dispersed among the conduction electrons within the cathode near the surface, and thus appears as heat in the metal. Let  $\gamma_i$  represent the Auger yield. Then, the average amount of neutralization energy transferred to the surface as heat, per incident ion, is given approximately by the expression

$$(1 - \gamma_i)(V_I - \phi) + \gamma_i \cdot \frac{1}{2}(V_I - 2\phi) = V_I \left(1 - \frac{1}{2}\gamma_i\right) - \phi. \quad (19)$$

The first term on the left hand side represents the neutralization energy for that fraction of the ions which do not produce an Auger ejection. The second term is the amount of neutralization energy which is left in the cathode for the ions which do yield an ejection. The right hand side, obtained by simple algebraic reduction, shows that the ion neutralization surface heating is reduced, as a consequence of the Auger effect, by about 20 percent in the case of a tungsten cathode operating in helium. For tungsten in argon, the reduction is about 7 percent. In an accurate theory, one would certainly have to include this effect, at least for gases such as helium and neon, where  $\gamma_i$  is relatively large. However, in view of the uncertainties already present in other relations being used, it appears justifiable to neglect the Auger effect altogether and approximate the heat flux to the cathode surface due to ion neutralization by

$$q_{\text{neut}} = j_i (V_I - \phi) \quad (20)$$

The ions bombarding the surface carry kinetic energy approximately equal to the energy  $eV_c$  which they acquire in falling through the Mackeown space charge layer. An ion or atom striking a solid surface, in general, rebounds instead of transferring all of its kinetic energy to the surface. The fraction of the incident kinetic energy which the particle loses is termed the accommodation coefficient, denoted here by  $a$ . Ecker<sup>21</sup> has reviewed the somewhat contradictory literature on this subject. At energies in the range of a few volts (i.e., of the order of  $V_c$ ), it appears likely that a lower limit to  $a$  can be estimated by considering the "billiard ball" approximation for collision between the ion and an individual atom of the metal surface. This approximation gives, from consideration of energy and momentum conservation for a head on collision,

$$a = 4W_c W_i / (W_c + W_i)^2 \quad (21)$$



where  $W_i$  is the molecular weight of the ion, and  $W_c$  the atomic weight of the cathode material. In the event of a glancing collision, less energy is transferred in the initial collision, but the ion is very likely in this case to collide with a second metal atom before escaping from the vicinity of the surface. It is assumed that the ionic mass is less than the atomic mass for the cathode material; in the opposite case,  $a$  should be essentially equal to unity.

Table 1 lists values of  $a$  calculated from (21) for a number of ions, assumed incident upon a tungsten surface ( $W_c = 183.9$ ). The accommodation coefficient, calculated in this approximation, is very low for helium and other ions of low mass, but approaches unity as the ionic mass approaches the mass of the cathode atoms

TABLE 1  
ACCOMMODATION COEFFICIENTS FOR ION IMPACT  
UPON TUNGSTEN  
(BILLIARD BALL APPROXIMATION)

Ion	$W_i$	$a$
$\text{He}^+$	4.0	0.08
$\text{Ne}^+$	20.2	0.36
$\text{Ar}^+$	39.9	0.59
$\text{Kr}^+$	83.8	0.86
$\text{Xe}^+$	131.3	0.97
$\text{N}^+$	14.0	0.26
$\text{N}_2^+$	28.0	0.46

The portion of the ion kinetic energy which is not transferred directly to the surface is carried by the rebounding atom back into the ion production zone, where it is given up to ions and other atoms by collisions. This energy transfer occurs within a few atomic mean free paths from the surface, and has the effect of raising the temperature of the neutral gas near the surface. As a result, the temperature gradient in the gas in this region is increased, and at least some of the additional heat thus deposited in the ion production zone should flow back to the surface by heat conduction. It is assumed, for the sake of simplicity, that this process brings

all of the rebound energy back to the surface; i. e., that the net heat flux to the surface due directly or indirectly to transfer of ion kinetic energy is given by

$$q_{kin} = j_i V_c . \quad (22)$$

An upper limit to the heat flux reaching the surface by conduction through the gas can be estimated using kinetic theory. The number of ions and neutral particles striking unit area of the surface per second is  $n_h \bar{u}_i$ , where  $n_h$  is the density of heavy particles in the ion-production zone, and  $\bar{u}_i$  is given (15). The thermal energy carried by each such particle is  $3kT_g/2$ , of which a fraction  $a$  is transferred to the surface. Thus,

$$q_k \lesssim \frac{p}{kT_g} \sqrt{\frac{kT_g}{2\pi M}} \cdot \frac{3kT_g}{2} \cdot a = \frac{3ap}{2} \sqrt{\frac{kT_g}{2\pi M}} . \quad (23)$$

With  $T_g \sim 10^4$  °K and  $a \sim 0.6$ , this gives an upper limit of about 5000 w/cm<sup>2</sup> for argon at 1 atmosphere pressure.

Since the ions and neutral particles in the ion production zone are assumed to be in thermal equilibrium with each other, and since the masses are equal, the thermal velocities are the same and the number of particles of each type entering the Mackeown layer from the ion production zone is proportional to the corresponding particle concentration. Most particles of either type which cross the interface between the two zones eventually reach the surface. The accommodation coefficients for transfer of kinetic energy should be about equal. The ions, however, have much more kinetic energy than the neutrals, because the former are accelerated in passing through the Mackeown zone. In addition, the ions transfer most of their neutralization energy  $V_I - \phi$  to the surface. Consequently, each ion hitting the surface delivers an amount of energy which is at least one or two orders of magnitude larger than that transferred by a neutral particle. It follows that ion bombardment heating is always more important than heat conduction, provided that the gas in the ion production zone is substantially ionized (more than about 10 percent). This is certainly the case for the high current densities associated with spot mode operation. It may conceivably not be the case for low current operation without a cathode spot. To determine the answer to this question in general, it would be necessary to construct a detailed theory of the ion production zone. It is assumed in the present report that cathode heating by conduction through the gas is negligible in comparison with ion bombardment heating. Radiative heating and combustion of the surface are also neglected. The total heat flux to the cathode surface is then estimated to be, from (20) and (22),



$$q_{\text{neut}} + q_{\text{kin}} = j_i(V_c + V_I - \phi) . \quad (24)$$

The energy deposited in the cathode surface is disposed of by several mechanisms. The bulk of this energy is consumed by thermionic emission of electrons. Extraction of one electron from the surface by "pure" thermionic emission requires an energy of  $\phi$  electron volts, where  $\phi$  is the thermionic work function. If an electric field producing the Schottky effect is present, this energy requirement is reduced, approximately, to the value of the "effective work function":

$$\phi_{\text{eff}} = \phi - 3.79 \times 10^{-4} \sqrt{E_c} . \quad (25)$$

Calculations by Lee<sup>8</sup> show that the actual cooling energy per electron emitted varies with temperature as well as with electric field intensity, so that (25) is only a rough approximation, even in the region of field strengths where the Richardson-Schottky formula (17) is a good approximation to the exact T-F emission function. Lee's calculations indicate that at a temperature of 3000°K and a field of  $10^7$  v/cm, the cooling effect is about 15 to 20 percent less than it would be in the absence of a field. Since it has been necessary to make several other relatively crude approximations, this correction to the cooling effect of electron emission will be neglected in the present report. The heat flux absorbed by electron emission is then approximated simply by

$$q_{\text{el}} = j_e \phi . \quad (26)$$

The input energy remaining after allowance for the power requirement of electron emission is partly lost by thermal radiation,

$$q_{\text{rad}} = \sigma \epsilon T_s^4 , \quad (27)$$

and partly conducted into the interior of the cathode,

$$q = K (\partial T / \partial n)_s . \quad (28)$$

Here

$\sigma$  = Stefan-Boltzmann constant ( $5.67 \times 10^{-12}$  w/cm<sup>2</sup>°K<sup>4</sup>)

$\epsilon$  = total emissivity of surface



$T_s$  = surface temperature ( $^{\circ}\text{K}$ )

$K$  = thermal conductivity of cathode material

$\partial T/\partial n$  = derivative of cathode temperature along an outward directed normal to the surface ( $^{\circ}\text{K}/\text{cm}$ ).

Under some circumstances, an additional amount of heat is absorbed by vaporization of the cathode material, but this plays little role in the case of tungsten, which is the principal concern of the present study. Certain other processes<sup>21</sup> can become significant in some instances.

Combination of equations (24), (26), (27), and (28) now gives the energy balance relation at the cathode surface,

$$j_i(V_c + V_I - \phi) = j_e \phi + K(\partial T/\partial n)_s + \sigma \epsilon T_s^4 . \quad (29)$$

Substitution of  $j_i = \alpha j$ ,  $j_e = (1 - \alpha)j$  gives

$$j[\alpha(V_c + V_I) - \phi] = K(\partial T/\partial n)_s + \sigma \epsilon T_s^4 . \quad (30)$$

Finally, for cases in which  $j_i < (j_i)_{\max}$ , elimination of  $\alpha$  using (13) yields

$$j(V_c - \phi) = K(\partial T/\partial n)_s + \sigma \epsilon T_s^4 . \quad (31)$$

In (30) or (31), the net electrical heating effect is represented by the expression on the left hand side, while the terms on the right hand side correspond to purely thermal effects.

Equation (30) provides the basis for a rough estimate of the ion current fraction  $\alpha$  for thermionic cathodes. Since the active region of the cathode is at a high temperature, it loses heat by conduction and radiation; thus, the right hand side of (30) is positive. Solution of (30) for  $\alpha$  yields

$$\alpha = \frac{1}{V_c + V_I} \left[ \phi + \frac{K(\partial T/\partial n)_s + \sigma \epsilon T_s^4}{j} \right] . \quad (32)$$

Thus,  $\alpha$  has a lower limit of

$$\alpha_{\min} = \phi/(V_c + V_I) ,$$

which with  $\phi \sim 4$  volts,  $V_c \sim 5$  volts,  $V_I \sim 20$  volts gives  $\alpha_{\min} \sim 0.16$ . The presence of the second term in the bracketed expression of (32) makes the

actual  $\alpha$  value somewhat larger than this. This argument shows that a much larger fraction of the current is carried by ions at the surface of the cathode than in the arc column.<sup>23</sup>

Thus far, attention has been paid only to processes occurring on the electrically active portion of the cathode surface. Over the remainder of the surface, there is no electrical heating. Heating by radiation from the arc or from other hot surfaces in the system may occur, but, if so, will depend to a major extent upon the details of the plasma generator configuration. The same may be said of convective heating by arc heated gas flowing over the cathode surface. These effects will not be considered further.

Energy losses occur from the entire exposed surface of the cathode, and play a role of considerable significance. The radiative loss is, of course, a flux  $\sigma\epsilon T^4$  where  $\epsilon$  is the total emissivity, and  $T$  the local surface temperature. The convective loss is less readily calculable, since it depends upon the distribution of gas temperature and velocity in the flow field near the cathode. These quantities are strongly dependent upon the plasma generator configuration and are difficult to calculate or to determine experimentally. In general, the convective loss should be larger, under otherwise identical conditions, when the cathode is operated in a gas of high thermal conductivity such as helium or hydrogen.

## C. PROCESSES IN THE CATHODE INTERIOR

### 1. Heat Conduction

For a thermionic cathode to operate, a portion of its surface must be maintained at high temperature. Heat then flows from this hot region toward the cooler regions of the cathode. The steady flow of heat in a solid with no interior sources or sinks is governed by the partial differential equation,

$$\nabla \cdot (K \nabla T) = 0 , \quad (33)$$

where  $K$  denotes the thermal conductivity. If  $K$  is independent of position, (33) reduces to Laplace's equation

$$\nabla^2 T = 0 . \quad (34)$$

Equation (33) or (34), of course, has an infinite variety of solutions. Determination of the solution  $T(x, y, z)$  describing a particular physical situation, such as the temperature field in a certain cathode, requires the specification of an adequate set of boundary conditions. The steady heat flow problem for a thermionic cathode has ordinary fixed temperature

and radiative cooling conditions over certain portions of the surface, and the boundary condition (29) or (31) over the region where flow of current is possible.

## 2. Joule Heating

Not only heat but also electric current flows in the interior of a cathode. The flow of current produces a distributed source of resistive heating throughout the interior with the magnitude  $\rho j^2$  per unit volume, where  $\rho$  is the resistivity of the metal (a function of temperature), and  $j$  the current density. Equation (33) is, thus, replaced by<sup>24</sup>

$$\nabla \cdot (K \nabla T) + \rho j^2 = 0 . \quad (35)$$

The current density is a function of position and is not "given," but is part of the solution of the problem. It is a vector determined locally by Ohm's law

$$\mathbf{j} = \mathbf{E} / \rho , \quad (36)$$

where  $\mathbf{E}$  denotes the electric field vector, which in turn is equal to the negative gradient of the electric potential function,

$$\mathbf{E} = - \nabla U . \quad (37)$$

Since no sources of current exist in the cathode interior,  $\mathbf{j}$  is solenoidal,

$$\nabla \cdot \mathbf{j} = - \nabla \cdot \left[ \frac{1}{\rho(T)} \nabla U \right] = 0 . \quad (38)$$

One is thus confronted with a system of two coupled partial differential equations (35), (38).

Rich<sup>25</sup> has obtained an approximate solution to the problem of Joule heating in the vicinity of a cathode spot, by assuming  $\rho = \text{constant}$  and a uniform current density over a circular portion of the surface of a semi-infinite body. His results show that for hot tungsten ( $\rho \sim 100 \times 10^{-6}$  ohm-cm) with a current density of  $10^5$  amp/cm<sup>2</sup>, the Joule power in the spot region is about  $10^6 a^3$  watts, where  $a = \text{spot radius (cm)}$ . The current is  $10^5 \pi a^2$ . Thus, the voltage associated with Joule heating under these conditions is about  $3a$  volts. A current of 1000 amperes with the assumed current density would require a spot size of only about 0.06 centimeter, so that this effective voltage is small ( $\sim 0.2$  volt) even for the rather severe case assumed. It may be concluded that Joule heating in the spot region is negligible for



thermionic cathodes. This outcome is a consequence of the fact that radial spreading of the current causes the power density  $\rho j^2$  to decrease extremely steeply with distance from the spot, so that the volume in which significant heating occurs is very small.

If the cathode is not effectively semi-infinite, but is a rather long thin body with axial current flow, Joule heating can become very significant at high total currents, because a moderate power density is produced throughout the entire volume of the cathode. The theory of Joule heating of long, cylindrical tungsten cathodes is developed in section IV below.

## IV. THEORY OF THERMIONIC CATHODES

### A. PHENOMENOLOGY

The variety of behavior exhibited by cathodes is impressive. Even a single cathode, simply observed visually, presents a bewildering sequence of qualitatively different appearances as its environment and operating current are varied. In a given gas, for example, at low currents, a tungsten cathode may operate in the spot mode with a high current density. An increase of current beyond a certain level causes transition to the spotless mode, with a lower current density. An increase in pressure brings back the spot. Operating in a different gas at the same pressure and over the same range of currents, the cathode may run either always in the spot mode or always without a spot. This richness of phenomenology presents a severe and interesting challenge to any theoretical model which may be proposed.

Apart from qualitative features such as those just mentioned, a successful theoretical cathode model must predict quantitatively the observables of cathode operation. For a given total current, these include the cathode fall voltage, the power losses from the cathode by radiation and heat conduction to the cooling system (if any), the temperature distribution in the cathode, and the distribution of current density over the surface. In the absence of significant radiative or convective heat transfer from the arc column to the cathode, this prediction must be based solely upon the cathode geometry and the physical properties of the cathode and gas.

### B. OVERSIMPLIFIED MODEL

The cathode model presented below (section III C) is, in spite of the crudity of many of its approximations, a fairly complex mathematical construction. To clarify some of the basic ideas before undertaking a discussion of the complete problem, the present section considers an oversimplified model for which the analysis is elementary. This model is defined by the following assumptions:

1. The cathode is a cylindrical rod of diameter  $D$  and length  $L$ , one end of which is held at a low temperature  $T_0$ . The other end is operating as a cathode spot with a uniform current density.
2. The electron emission is purely thermionic (no Schottky effect).
3. Joule heating and radiative energy loss from the surface are neglected. The current emission does not "overflow" down onto the curved side surface of the cathode.
4. The thermal conductivity is a constant.

It is virtually certain that no cathode satisfying these assumptions even roughly can be constructed. This model is presented solely to illustrate a few of the fundamental features of the more realistic cathode theory formulated in the next section.

One parameter characterizing the operation of a cathode can always be chosen arbitrarily, at least within certain limits. For the oversimplified model, the total current  $I$  can be specified. Then, the current density is

$$j = 4I/\pi D^2 . \quad (39)$$

The current density, in turn, is related to the surface temperature  $T_s$  of the active end of the cathode by Richardson's equation,

$$j_e = (1 - a) j = AT_s^2 e^{-11609\phi/T_s} , \quad (40)$$

where  $a$  denotes the fraction of the current carried by ions. This quantity is given approximately by (13),

$$a = \frac{V_c}{V_c + V_I} , \quad (41)$$

in which the ionization potential  $V_I$  is known. However,  $V_c$  is not yet known and does not appear in (40). At this stage, there are three unknowns,  $a$ ,  $T_s$ , and  $V_c$ , and only two equations, (40) and (41). It is now necessary to invoke the surface energy balance relation (31),

$$j(V_c - \phi) = K(\partial T/\partial n)_s . \quad (42)$$

The temperature gradient on the right hand side must be determined from the solution of Laplace's equation (34). Under the assumptions of this oversimplified model, the heat flow is one dimensional, and hence (34) becomes

$$d^2T/dx^2 = 0 , \quad (43)$$

with the boundary conditions

$$T(0) = T_0 \quad (44)$$

$$T(L) = T_s . \quad (45)$$

The solution of (43) satisfying (44) and (45) is obviously

$$T = T_0 + (T_s - T_0)(x/L) . \quad (46)$$



Hence,

$$(\partial T / \partial n)_s = (T_s - T_0) / L \quad (47)$$

Substitution of (47) into (46) gives

$$j(V_c - \phi) = K(T_s - T_0) / L \quad (48)$$

Equations (40), (41), and (48) now provide a system of three equations for the three unknowns  $\alpha$ ,  $T_s$ , and  $V_c$ .

From (41)

$$1 - \alpha = \frac{V_I}{V_c + V_I}.$$

Hence, (40) becomes

$$V_c = \frac{j V_I}{A T_s^2 e^{-11609 \phi / T_s}} - V_I \quad (49)$$

Equation (48) can be rewritten

$$V_c = \phi + \frac{K(T_s - T_0)}{jL} \quad (50)$$

The pair of equations (49), (50) can be solved for  $V_c$  and  $T_s$  by a graphical procedure, as illustrated in figure 2 for the case  $j = 1000 \text{ amp/cm}^2$ ,  $V_I = 15 \text{ volts}$ ,  $A = 120 \text{ amp/cm}^2 \text{ } ^\circ\text{K}^2$ ,  $\phi = 4 \text{ volts}$ ,  $K = 1 \text{ w/cm } ^\circ\text{K}$ ,  $T_0 = 300^\circ\text{K}$ , and  $L = 3 \text{ centimeters}$ . The solution for this particular case is  $V_c = 4.97 \text{ volts}$ ,  $\alpha = 0.249$ ,  $T_s = 3240^\circ\text{K}$ . The corresponding net heat flux to the surface is  $980 \text{ w/cm}^2$ .

It is worth noting that to determine the solution, even for this extremely simple model, it is necessary to use relations describing processes in the gas, in the cathode interior, and at the interface. Thus, the operation of a thermionic cathode depends upon phenomena in both the solid and the gas and upon the coupling between the two regions across the interface.

The system of equations (49), (50) is sufficiently simple that one easily sees qualitatively how the solution depends upon various parameters. For example, a change in  $L$  affects the slope of the straight line representing equation (50) in figure 2 without modifying the curve for (49). The latter is so steep that a substantial change in  $L$  produces only a slight alteration of the temperature  $T_s$  for the solution, although the cathode fall voltage  $V_c$  changes considerably. For

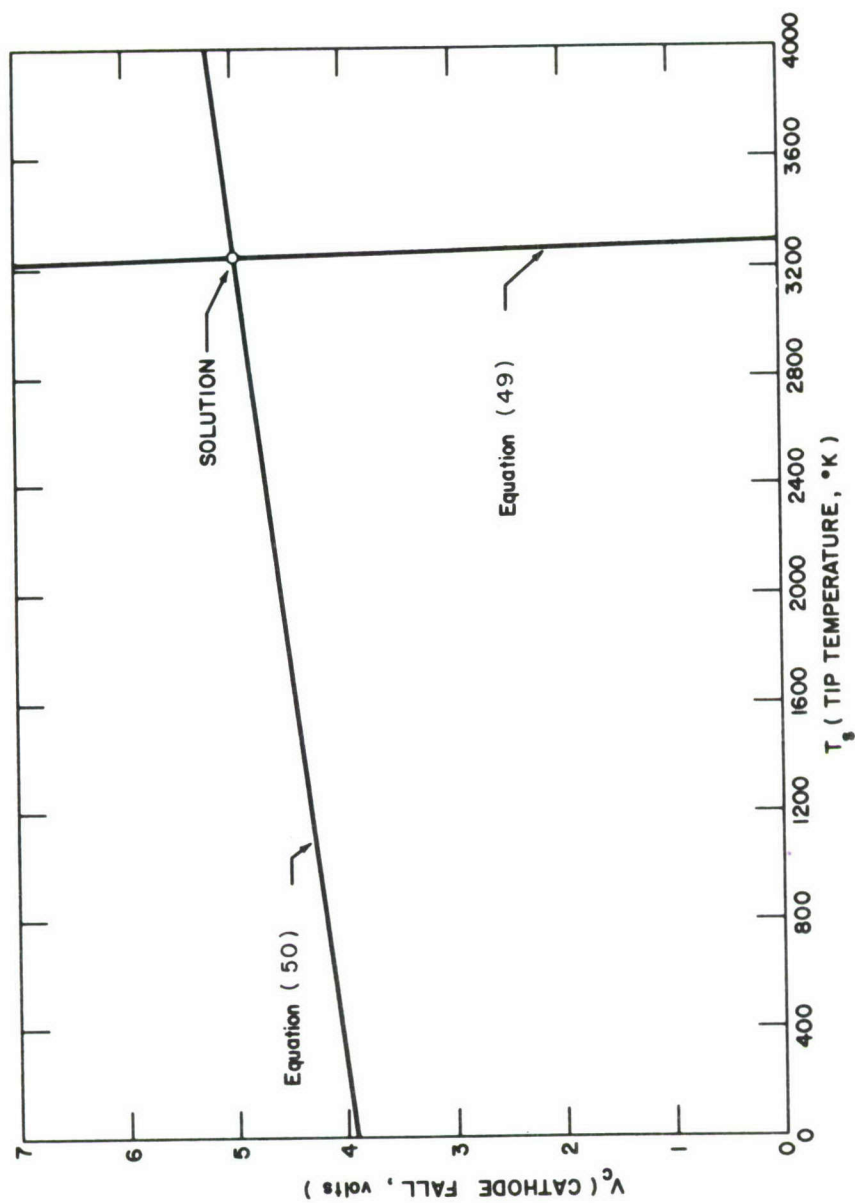


Figure 2 GRAPHICAL SOLUTION OF OVERSIMPLIFIED MODEL

this model, at least, stronger cooling of the cathode (achieved by reducing the length), thus accomplishes very little by way of reducing the temperature which the material must endure without melting. Of course, this is a consequence of the fact that most of the cathode current is carried by electrons emitted thermionically. The stronger cooling achieves its slight reduction of tip temperature at constant current by increasing the ion current fraction  $\alpha$ , so that the requirement for electron emission is reduced a little. The additional ion current thus drawn from the gas naturally increases the heat flux to the cathode. The extra heat flux can be handled by internal heat conduction, because the shortening of the cathode with little change in tip temperature has increased the axial temperature gradient.

### C. THEORETICAL MODEL FOR THERMIONIC CATHODES

The relations set down in section II to describe the processes occurring in the gas region, in the cathode interior, and at the interface between these two regions provide the basis for an approximate but complete mathematical model for thermionic cathodes. The central feature of this model is the heat conduction problem for the cathode interior. The present section formulates and discusses this cathode model for the case in which Joule heating in the cathode interior is neglected. It has been shown in paragraph 2 of section II C, on the basis of Rich's<sup>25</sup> results, that Joule heating contributes little to the heating of a thermionic cathode operating in the spot mode, and omission of this effect simplifies the formulation of the problem considerably. When Joule heating is neglected, the differential equation for the temperature distribution within the cathode is (33)

$$\nabla \cdot (K \nabla T) = 0 \quad (51)$$

To discuss the boundary conditions for this equation, it is necessary to introduce some notation for providing a generalized description of the cathode geometry.

The bounding surface of the cathode can be divided conceptually into three portions,  $S_1, S_2, S_3$ :

- $S_1$ : Interface between cathode and external cooling system.
- $S_2$ : "Inactive region"; i. e., surface through which no current can flow because of geometrical separation from anode.
- $S_3$ : "Active region"; i. e., portion of surface through which current can enter the cathode from the arc column. The entire region  $S_3$  need not be covered by current flow however. The actual cathode spot may be much smaller than  $S_3$ .



Possible ways of dividing the cathode surface into these three regions are illustrated for several cases in figure 3. The dividing curve between  $S_2$  and  $S_3$  is rather arbitrary in most cases. For the geometries (c) and (d) of figure 3  $S_2$  can be omitted.

The boundary conditions on the temperature field within the cathode can now be formulated with reference to this division of the cathode surface into regions. This formulation of the boundary conditions is not necessarily applicable to all geometrical configurations, but is reasonably general and can be modified readily to treat special cases.

It is assumed that the material in contact with the cathode over the region  $S_1$  of the surface is an excellent thermal conductor, such as copper. Then,  $S_1$  is a surface of constant temperature to a good approximation, and the boundary condition over this region is

$$T = T_0 \quad \text{on } S_1 \quad . \quad (52)$$

Over the region  $S_2$ , by assumption, there is no current flow. Hence, there is also no surface heating by ion bombardment. It is assumed for the present formulation that radiative heating of the surface and convective heat exchange between the surface and the gas can be neglected, although this is not always the case. Then,

$$K \left( \frac{\partial T}{\partial n} \right)_s = - \sigma \epsilon T^4 \quad \text{on } S_2 \quad , \quad (53)$$

where  $\partial/\partial n$  denotes the outward directed normal derivative.

In the "active region"  $S_3$ , the boundary condition is considerably more complicated because it involves relations pertaining to the cathode fall zone and the electrical heating of the surface. The condition in this region is essentially equation (29),

$$K \left( \frac{\partial T}{\partial n} \right)_s = j_i (V_c + V_I - \phi) - j_e \phi - \sigma \epsilon T_s^4 \quad \text{on } S_3 \quad . \quad (54)$$

However, (54) contains the ion and electron current densities, which are not "given" but are part of the solution of the problem. The electron current density is related to the local surface temperature  $T_s$  and field intensity  $E_c$  by the Richardson-Schottky equation (17),

$$j_e = A T_s^2 e^{-\theta/T_s} \quad . \quad (55a)$$

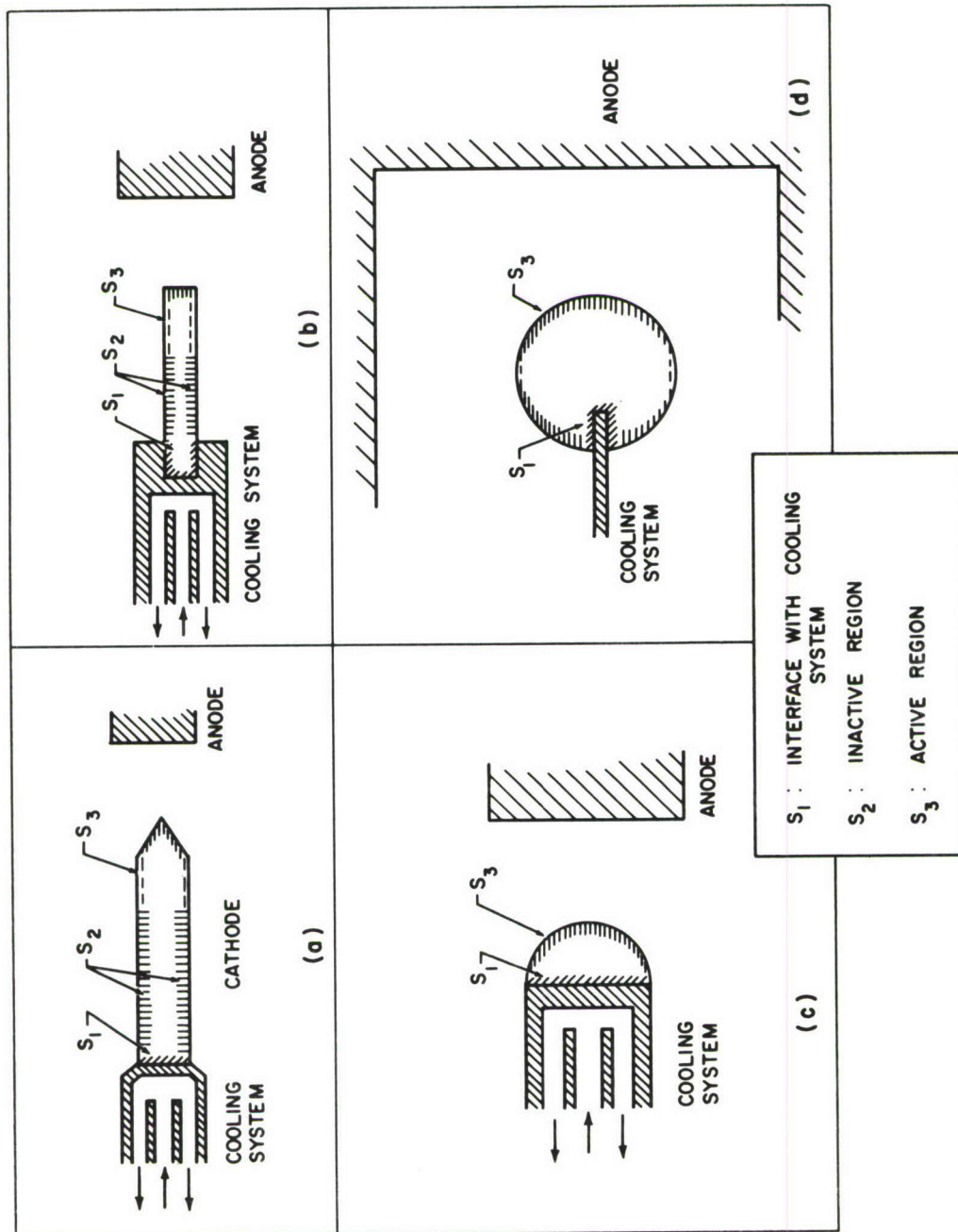


Figure 3 DIVISION OF CATHODE SURFACE INTO "ACTIVE" AND "INACTIVE" REGIONS AND INTERFACE WITH COOLING SYSTEM

Here,

$$\theta = 11609 \phi - 4.40 \sqrt{E_c} \quad , \quad (55b)$$

and  $E_c$  is given by Mackeown's formula (8a)

$$E_c = 873 V_c^{1/4} [(1823W)^{1/2} j_i - j_e]^{1/2} \quad . \quad (56)$$

The ion current density  $j_i$  is represented by

$$j_i = \min [aj_e/(1-a), (j_i)_{\max}] \quad , \quad (57)$$

where  $\min(x, y) = x$  or  $y$ , whichever is smaller;  $a$  is given by the rough energy balance relation (13) for the ion production zone,

$$a = V_c / (V_c + V_I) \quad ; \quad (58)$$

and  $(j_i)_{\max}$  is the upper limit to the ion current density based on kinetic theory, equation (16),

$$(j_i)_{\max} = \frac{P\epsilon_e}{\sqrt{8\pi M k T_g}} \quad . \quad (59)$$

The gas temperature  $T_g$  in the ion production zone is roughly equal to  $0.15 V_I/k$  if the gas in that zone is just fully ionized. The idea expressed by equation (57) is that the power  $j_e V_c$  brought into the ion production zone by the electron beam emerging from the space charge layer is all consumed in producing the ions which flow to the cathode, unless the ion current has reached its limiting value  $(j_i)_{\max}$ , in which case the excess power  $j_e V_c - j_i V_I$  is simply lost by unspecified mechanisms. Actually, some of this excess power is likely to produce extra ions in neighboring parts of the ion production zone where the electron current density is not so high, and one could with equal justification use other approximations in place of (57).

In this formulation, the quantities  $(\partial T / \partial n)_s$ ,  $T_s$ ,  $j_i$ ,  $j_e$ ,  $\theta$ ,  $E_c$  are functions of position over the surface region  $S_3$ . The cathode fall voltage is taken to be independent of position over the emitting region, since it is the potential difference between two good electrical conductors, the cathode and the plasma. According to equation (58),  $a$  is, then, also constant. The ratio  $j_i/j_e$  is constant, from (57), except in the region (if any) where  $j_i = (j_i)_{\max}$ . The total current is given by the surface integral of the total current density,



$$I = \int_{S_3} (j_e + j_i) dS \quad . \quad (60)$$

One of the position independent parameters of the problem, such as the total current, can be selected arbitrarily. For the following discussion, it is convenient to let this arbitrary parameter be  $V_c$  instead of  $I$ . If  $V_c$  is given, then  $\alpha$  is known from (58). At each point of the surface  $S_3$ , there are then six unknowns  $T_s$ ,  $(\partial T/\partial n)_s$ ,  $j_e$ ,  $j_i$ ,  $E_c$ ,  $\theta$ , which are related to one another by the five algebraic relations (54) to (57). These relations can be solved for  $(\partial T/\partial n)_s$  as a function of  $T_s$ ,

$$q_s = K (\partial T/\partial n)_s = F(T_s) \quad . \quad (61)$$

A rapidly convergent numerical procedure for computing values of this function is described in appendix A. Figure 4 illustrates the form of the function for a cathode with the thermionic constants  $\phi = 3.5$  volts,  $A = 120$  amp/cm<sup>2</sup> °K<sup>2</sup> operating in argon at 1 atmosphere. (The ordinate in figure 4 is the net electrical heat flux,  $K (\partial T/\partial n)_s + \sigma \epsilon T_s^4$ , rather than  $F(T_s)$  itself.) Figures 5, 6, and 7 show the ion, electron, and total current densities based upon the same calculations. Comparison of figures 4 and 5 shows that the maximum electrical heat flux occurs at the temperature for which the ion current density reaches its maximum value. Below this temperature, the ion current is proportional to the electron current, and thus increases with increasing temperature. The increase of ion current is responsible for the increase of heat flux which occurs in this region. Above the temperature at which  $j_i$  reaches  $(j_i)_{\max}$ , the ion current is constant while the electron current continues to increase with temperature. The resulting increase of the cooling effect of electron emission without any compensating increase of ion bombardment heating produces the decrease of heat flux shown in figure 4.

The reduction of equations (55) through (59) to the single relation (61) makes it possible to summarize the cathode problem concisely as follows: Find solutions of the partial differential equation,

$$\nabla \cdot (K \nabla T) = 0 \quad , \quad (62a)$$

satisfying the boundary conditions

$$T = T_0 \quad \text{on } S_1 \quad (62b)$$

$$\frac{\partial T}{\partial n} = - \frac{\sigma \epsilon T^4}{K} \quad \text{on } S_2 \quad (62c)$$

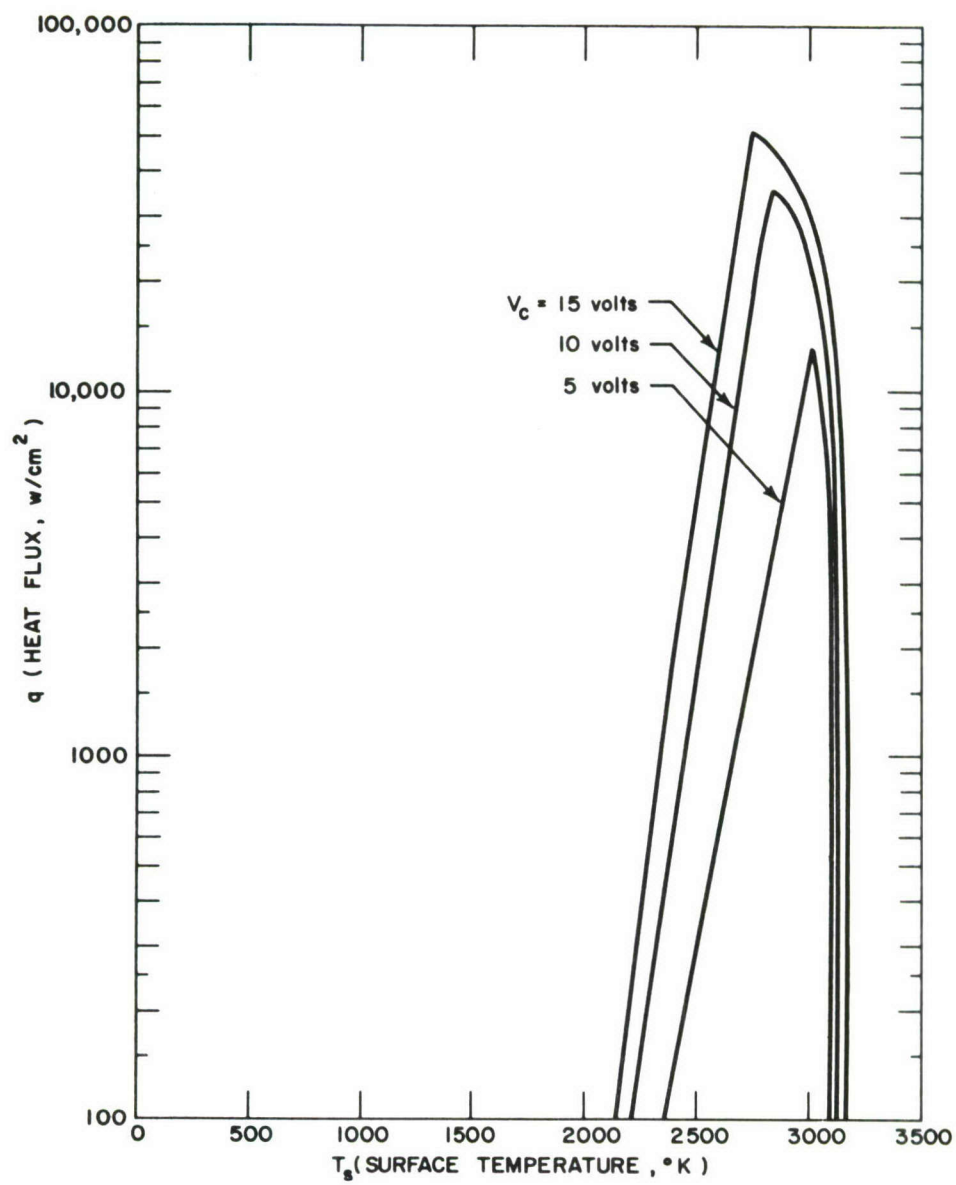


Figure 4 CATHODE HEAT FLUX AS A FUNCTION OF SURFACE TEMPERATURE

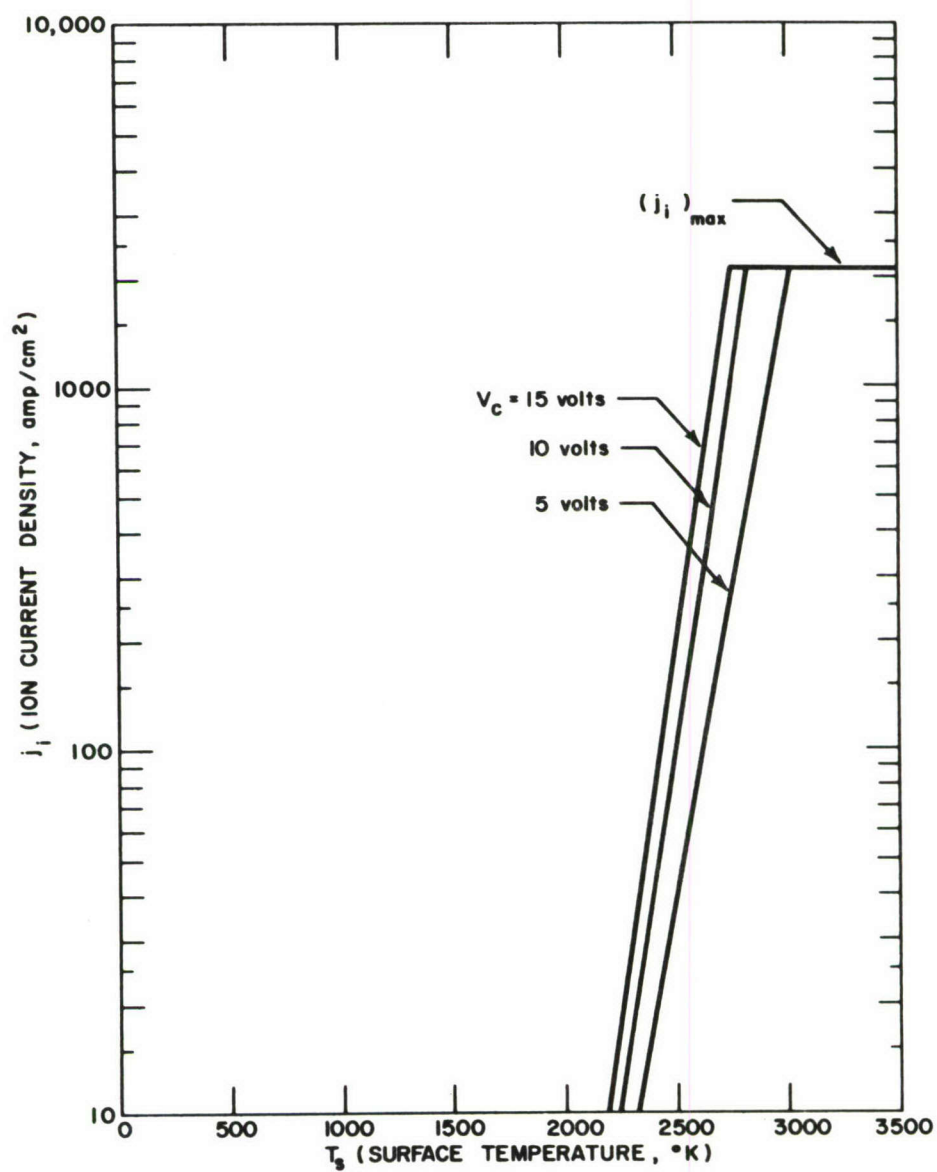


Figure 5 ION CURRENT DENSITY AS A FUNCTION OF SURFACE TEMPERATURE



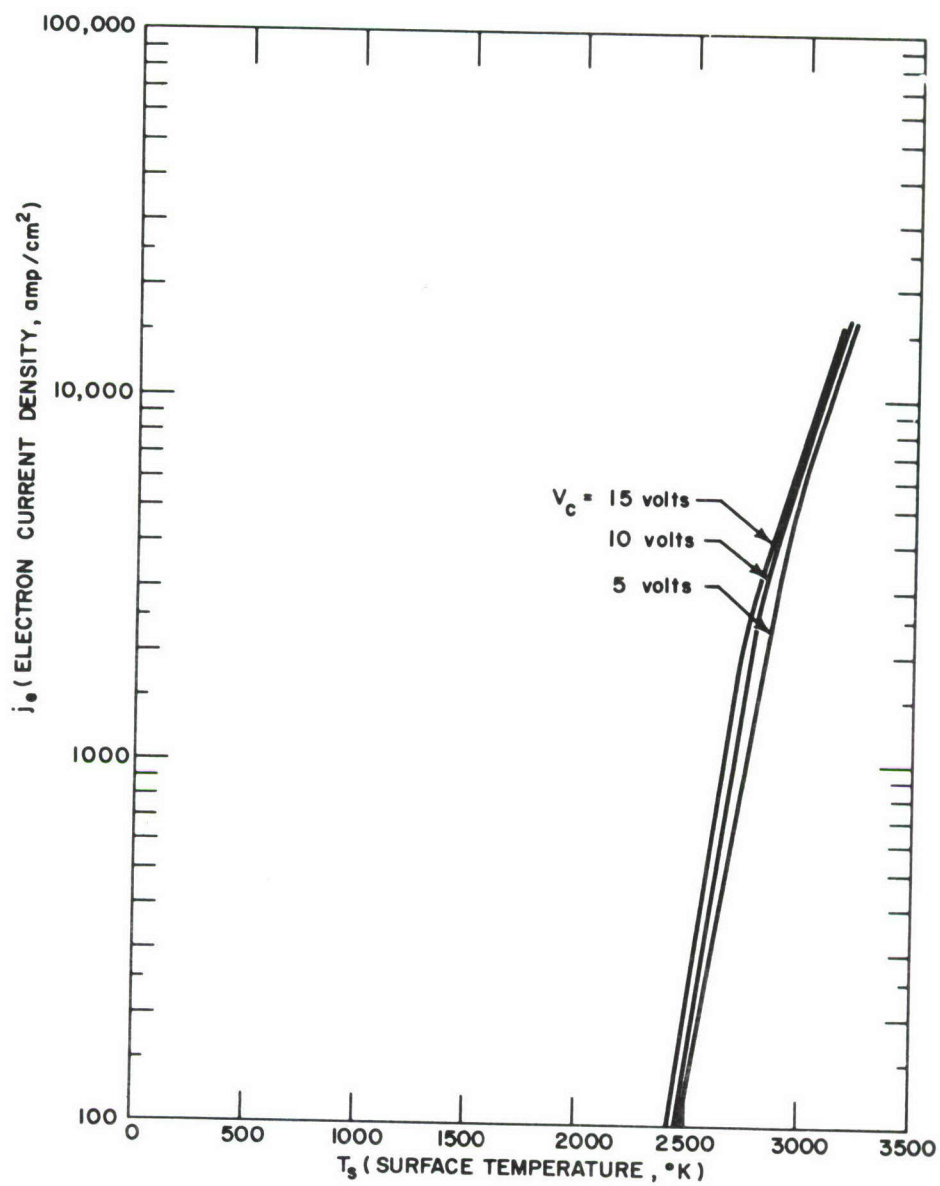


Figure 6 ELECTRON CURRENT DENSITY AS A FUNCTION OF SURFACE TEMPERATURE

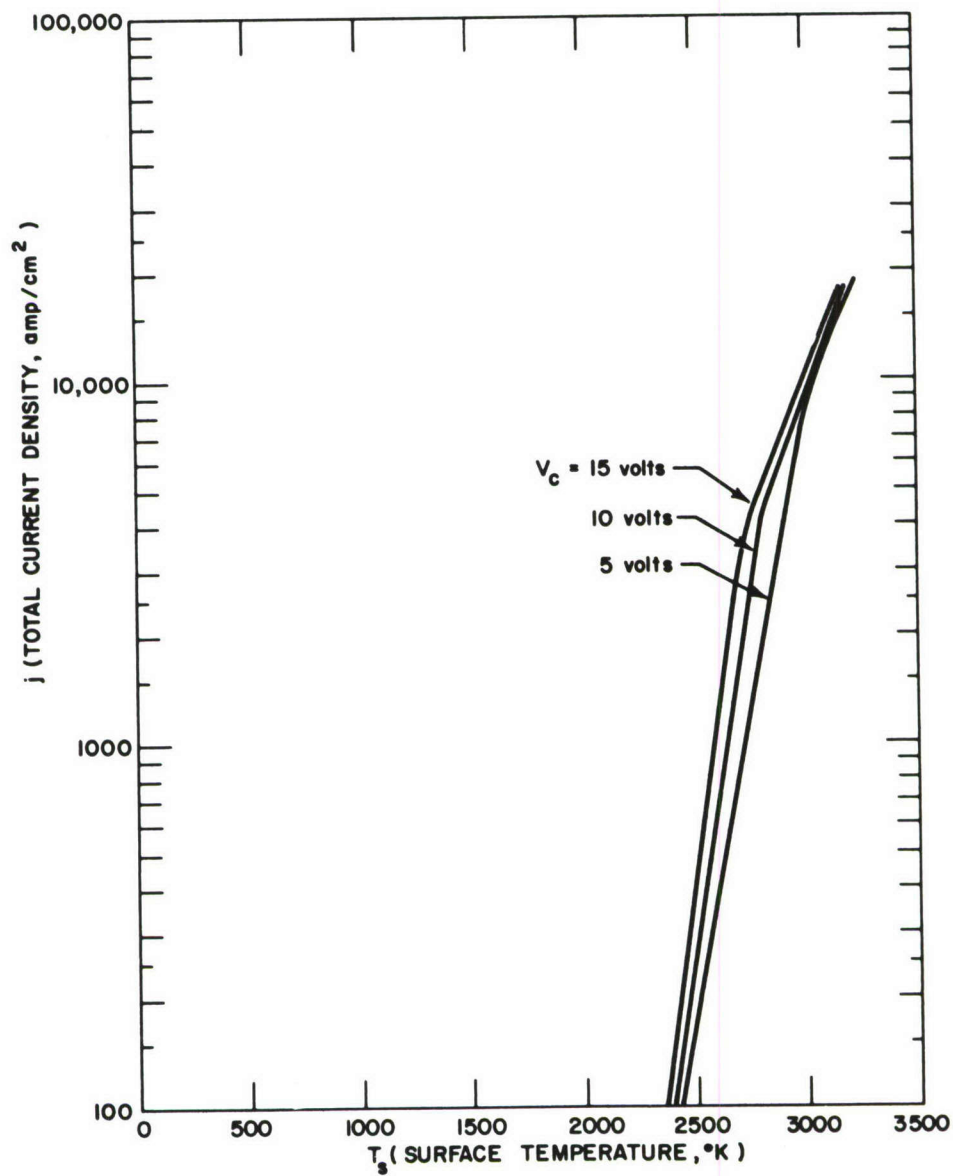


Figure 7 TOTAL CURRENT DENSITY AS A FUNCTION OF SURFACE TEMPERATURE

$$\frac{\partial T}{\partial n} = \frac{F(T; V_c)}{K} \quad \text{on } S_3, \quad (62d)$$

where  $\partial/\partial n$  denotes the outward directed normal derivative, and  $F(T; V_c)$  is a positive, nonlinear function of local surface temperature of the general form illustrated in figure 4.  $F(T; V_c)$  depends parametrically upon the cathode fall  $V_c$ . The cathode fall is regarded as an input parameter. Assuming that (62) has been solved for series of  $V_c$  values, the total current  $I$  can be computed from (60) for each case, giving  $I = I(V_c)$ . Inversion of this relation gives  $V_c = V_c(I)$ , so that one can obtain the temperature distribution, current density distribution, and other quantities of interest as parametric functions of total current.

The system of equations (62) represents an unusual type of heat conduction problem which does not appear to have been considered previously in the literature. In general, two or more solutions may exist for any given set of input conditions, corresponding to different modes of cathode operation. The possible nonuniqueness of solutions can be illustrated by considering a physically unreal but mathematically acceptable case of (62), in which the cathode is a circular cylinder of length  $L$ ,  $S_1$  is the circular area of one end and  $S_3$  that of the other, and  $S_2$  is the curved side surface. The emissivity  $\epsilon$  and end temperature  $T_0$  are assumed to be zero. Depending upon the value of  $L$ , the problem thus defined may have one, two, three, or more solutions. Some of these are one dimensional solutions of the form  $T = T_s x/L$ , where  $T_s$  is obtained by solving the equation

$$\frac{KT_s}{L} = F(T_s) \quad (63)$$

This is the form to which (62d) reduces in the case of one dimensional heat flow in a rod with zero temperature at one end. Figure 8 illustrates the graphical solution of (63) for a particular value of  $V_c$ . The  $F(T_s)$  curve in this figure is identical with the curve for  $V_c = 10$  volts in figure 4. Figure 8 shows that (63) always has at least one solution  $T_s = 0$ , corresponding to  $T = 0$  throughout the cathode. In this case, the cathode is not operating. If  $L$  is not too small, the straight line  $q_s = KT_s/L$  intersects the curve  $q_s = F(T_s)$  in two points (see figure 8). The point lying at a lower value of  $T_s$  corresponds to a cathode mode in which the ion current is less than  $(j_i)_{\max}$ . The higher point represents a mode with much higher current density for which the ion current has essentially reached its limiting value. If  $L$  is too small, the line  $q_s = KT_s/L$  passes above the peak of the curve for  $F(T_s)$ , and there is no nonzero one dimensional solution for the given cathode fall voltage. Solutions can still be obtained, however, for higher  $V_c$ . In addition to these various one dimensional solutions, the problem may possess non one dimensional solutions in which the current flow is contracted into a spot on the end of the cathode.



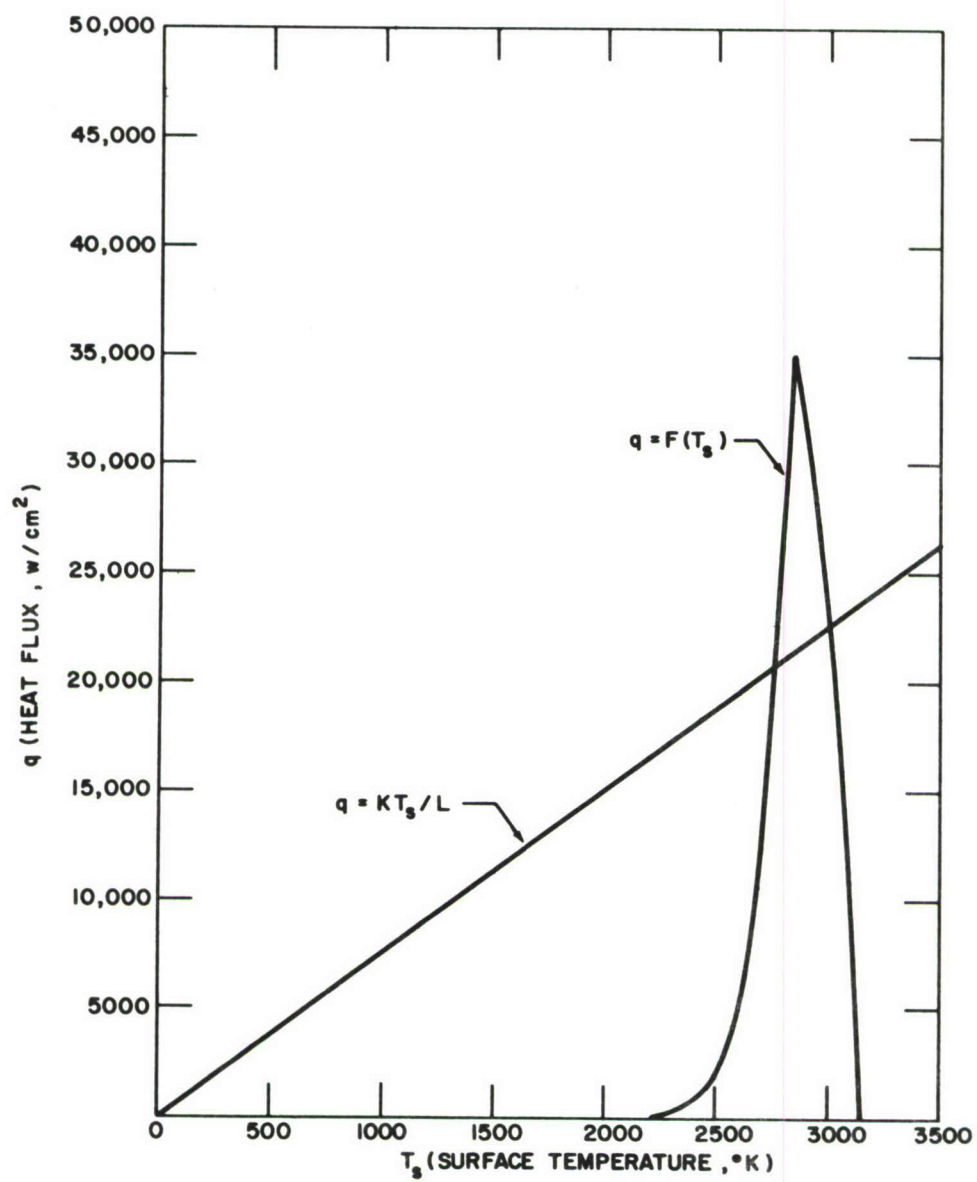


Figure 8 GRAPHICAL SOLUTION OF EQUATION (63)

The mathematical techniques for treating problems of the type of (62) are not well developed at the present time. The most important lack is that of a practical numerical procedure, adaptable to machine computation, for obtaining axisymmetric and three dimensional solutions. However, a number of approximate methods for solving the cathode heat conduction problem are considered in subsequent sections.

#### D. APPROXIMATE METHODS OF SOLUTION

##### 1. Numerical Methods for Two and Three dimensional Problems

A numerical method for high speed digital computation of solutions to the cathode model (62) is needed for investigating the mathematical consequences of the theory and testing its predictions against experimental data. If the theory, or some modification of it, proves to be approximately valid, such a computation technique will also be required for applications to cathode design studies.

The standard methods for numerical solution of elliptical partial differential equations do not appear to be directly applicable to (62), because of the peculiar nature of the boundary condition (62). The function  $F(T)$  is so strongly varying (see figure 4) that it tends to amplify greatly the effects of any errors in the surface temperature distribution. This tendency probably will lead to instability and convergence failure in any iterative numerical process which does not contain a special stabilizing feature.

It appears that the most suitable method for stabilizing a numerical solution of (62) may be to take the total current  $I$  as the input parameter in place of the cathode fall voltage  $V_c$ . This, of course, entails some inconvenience in the computation because the algebraic structure of equations (54) through (59) practically requires that  $V_c$  be retained as an intermediate parameter. However, holding  $I$  constant during a series of successive approximations at least ensures that the calculation will not skid off toward some extreme cathode operating condition with zero or infinite current.

Use of  $I$  as the independent input parameter also practically rules out some techniques of solution such as the relaxation method, in which the temperature distribution throughout the body is adjusted piecemeal. The total current is given by an integral (60) over the active region of the surface, and, thus, refers to a single complete temperature distribution. What thus appears to be suggested is a method of successive approximations to the entire temperature distribution, starting with a rather arbitrary trial function. Assuming that the procedure converges, one might, then, hope to find solutions corresponding to various cathode "modes" by choosing different trial functions. Two approaches of this type are suggested here. Neither has actually been tried. Testing and developing either of these methods will require a major programming and computing effort.



The first suggested method presumes the existence of a program for solving equation (62a) with mixed Dirichlet-Neumann conditions. It proceeds by iterating the following sequence of steps:

- a. Choose a trial function\*  $T(r, z)$ .
- b. Using the temperature given by this function at the surface in region  $S_3$ , solve for the  $V_c$  value required to give total current  $I$ .
- c. Using this  $V_c$ , calculate the surface heat flux distribution over  $S_3$  using (62d). Also, calculate the heat flux over  $S_2$  using (62c).
- d. Solve  $\nabla \cdot (KV_T) = 0$  with the boundary conditions that  $T$  is prescribed on  $S_1$  and  $\partial T / \partial n$  is prescribed (from c above) over  $S_2$  and  $S_3$ .
- e. Go to (b) above.

A second plausible looking procedure for solving (62) is to obtain solutions to this steady state problem by following the evolution of a corresponding solution of the transient heat equation

$$\nabla \cdot (KV_T) = \delta c \partial T / \partial t \quad (64)$$

to late times. The boundary conditions in (64) are again (62a, b, c, d). The total current is taken as an input parameter and held constant in time. This requires that the cathode fall voltage  $V_c$  be adjusted at each time step of integration of (64).

Both of these procedures will require relatively large amounts of machine time per case. The approach through the transient problem is likely to be exceptionally costly in this respect, so that alternatives such as the first method suggested above should be explored thoroughly before a solution by this technique is tried.

## 2. Approximate Relationships for the Cathode Heat-Conduction Problem

Although the cathode heat conduction problem (62) is quite difficult to solve accurately, the general nature of the solutions can be seen rather clearly from simple qualitative considerations. A general discussion of this type of heat conduction problem is given in the present section, and approximate conditions are derived relating the nature of the solutions to the form of the assumed heat input function  $q(T)$ . In the following section, the results of this analysis are applied to the actual heat input function  $q(T)$  defined by equations (54) through (59) to obtain an approximate solution for the properties of the cathode burning spot for a particular cathode geometry.

\*The notation in this discussion assumes the case of an axisymmetric problem.



The discussion can be carried out most simply by choosing a semi-infinite cathode geometry with the boundary condition that the temperature goes to a fixed value  $T_0$  at infinity. The parameter  $T_0$  then represents the strength of the cooling applied to the cathode. The effects of a finite geometry can be simulated qualitatively by choosing  $T_0$  in such a way as to reproduce the actual boundary conditions on the cathode as well as possible. For example, if the actual cathode has typical dimension  $R$  and the surface is held at temperature  $T_1$ , then  $T_0$  would be chosen so as to give a temperature  $T_1$  at the distance  $R$  from the center of the spot. Thus, a long, rod shaped cathode of the type to be discussed in section IV below would be simulated by a large positive value of  $T_0$ , while a small, strongly cooled cathode would correspond to a negative  $T_0$ .

For the semi-infinite cathode with  $T = T_0$  at infinity, the boundary conditions (62b,c,d) on the cathode temperature distribution become

$$\begin{aligned} T &= T_0 && \text{at infinity} \\ K \partial T / \partial n &= q(T) && \text{on the cathode surface,} \end{aligned} \quad (65)$$

where  $q(T)$  is a specified function of surface temperature which depends parametrically upon the cathode fall voltage  $V_c$ . The latter quantity may be regarded as the independent variable for the problem, in place of total current, as discussed above. The general nature of the solutions can be studied by conceptually dividing the surface into a cathode spot region of radius  $r_s$  in which the heat input  $q$  is appreciable, and an external region  $r > r_s$  in which the heat input is negligible. The total heat input to the cathode per unit time is, then, approximately

$$Q \approx \pi r_s^2 q(T_{av}) \quad , \quad (66)$$

where  $T_{av}$  is the average spot temperature. A second relation between these parameters is furnished by the heat flow relation outside the spot region. On the assumption of radial heat flow in the external region, the differential equation (62a) for the temperature distribution becomes simply

$$2\pi r^2 K \partial T / \partial r = -Q \quad . \quad (67)$$

Integration of equation (67) gives, with the aid of the boundary condition at  $r = \infty$ ,

$$Q \approx 2\pi K r_s (T_{av} - T_0) \quad . \quad (68)$$

Relations analogous to (68) have been derived previously by a number of authors<sup>6, 11, 26</sup> for various cathode geometries, using arguments similar

to those given here. Elimination of  $Q$  from equations (66) and (68) gives a relation between the spot radius  $r_s$  and spot temperature  $T_{av}$ , which must be satisfied approximately by any solution of the cathode heat conduction problem (62).

Equations (66) and (68) do not, however, exhaust the conditions which must be satisfied by the temperature distribution in the cathode. The initial assumption that the heat flux is appreciable for  $r < r_s$  and inappreciable for  $r > r_s$  remains to be formulated. This assumption requires that the temperature gradient across the spot, in combination with the known dependence of the heat flux  $q$  on temperature, must be just sufficient to cut the heat flux essentially to zero at the edge of the spot,  $r = r_s$ . This condition can be represented symbolically by

$$T(r_s) \approx T_c, \quad (69)$$

where  $T(r_s)$  is the actual temperature at the edge of the spot, and  $T_c$  is the cutoff temperature, defined as the temperature for which the heat flux  $q(T_c)$  becomes negligible in comparison with the average heat flux  $q(T_{av})$  over the spot.  $T_c$  is, of course, in general a function of  $T_{av}$ . There is evidently some arbitrariness in the choice of the cutoff temperature  $T_c$ , just as there is in the spot radius  $r_s$ ; however, if  $q(T)$  is a sufficiently strong function of  $T$ , this arbitrariness leads to only a small uncertainty in the numerical value of  $T_c$ .

If the function  $q(T)$  can be approximated by a straight line over the range of temperatures occurring in the spot, it is possible to give a more explicit formulation of (69). This type of approximation is applicable, for example, to the rising part of the heat flux curve defined by equations (54) to (57) and illustrated for a special case in figure 4. The linear approximation to  $q(T)$  is given by the first two terms of its Taylor expansion,  $q(T) = q(T_{av}) + q'(T_{av})(T - T_{av})$ . A logical choice of the cutoff temperature, based upon this approximation, is the temperature for which this expression gives  $q = 0$ . Then equation (69) becomes

$$\frac{q'(T_{av})}{q(T_{av})} \Delta T \approx 1, \quad (70)$$

where  $\Delta T$  is the temperature difference across the cathode spot. A rough estimate of  $\Delta T$  may be obtained by taking  $\Delta T = r_s (dT/dr)_{r_s}$ , where  $(dT/dr)_{r_s}$  is the surface temperature gradient at the edge of the spot, as given by equation (67). Eliminating  $Q$  using (68), one finds in this way that

$$\Delta T \approx Q/2\pi K r_s \approx T_{av} - T_0; \quad (71a)$$



i. e., the temperature difference across the spot is of the same order of magnitude as the temperature difference between the spot and the cooling system. Since the surface temperature gradient  $dT/dr$  is actually not constant across the spot, but increases from zero at the center to a maximum absolute value at the edge of the spot, the estimate (71a) is probably somewhat too large and should be replaced by a relation of the form

$$\Delta T \simeq \gamma (T_{av} - T_0) , \quad (72)$$

where  $\gamma$  is some constant of value less than unity. A uniform variation of  $dT/dr$  across the spot, for example, would give  $\gamma = 1/2$ .

Another estimate of  $\Delta T$  can be obtained by assuming a uniform heat flux over the spot area and no heat input outside the spot. An analytic solution for the temperature distribution in this case<sup>27</sup> gives the relation

$$\Delta T = \left(1 - \frac{2}{\pi}\right) [T(0) - T_0] \simeq \frac{1}{3} (T_{av} - T_0) , \quad (71b)$$

where  $T(0)$  is the temperature at  $r = 0$ . Since for the linear approximation to  $q(T)$  considered here the heat flux actually increases toward the center of the spot, equation (71b) probably represents a lower limit for  $\Delta T$ . It may, thus, be concluded from (71a,b) that the constant  $\gamma$  in equation (72) lies within the range

$$\frac{1}{3} \leq \gamma \leq 1 , \quad (73)$$

the most likely value being about  $1/2$ . Substitution (72) into (70) gives the approximate condition

$$\frac{q'(T_{av})}{q(T_{av})} (T_{av} - T_0) \simeq \frac{1}{\gamma} \simeq 2 , \quad (74)$$

which must be satisfied by the spot temperature  $T_{av}$  for cases in which the heat flux function  $q(T)$  can be approximated reasonably well by the first two terms of its Taylor expansion.

Equation (74) is a condition on the possible operating temperatures  $T_{av}$  of the cathode spot. The quantity  $q'(T_{av}) (T_{av} - T_0) / q(T_{av})$  appearing in the left hand side of the equation is termed the "steepness" of the heat flux function. In general, of course, the steepness is a function of spot temperature. Solutions of the cathode heat conduction problem can exist only for spot temperatures such that the steepness is exactly right (i. e., equal to  $1/\gamma$ ).



The possibility of a relationship between the formation of cathode burning spots and the steepness of the dependence of heat flux  $q$  upon surface temperature was apparently first suggested by Bauer.<sup>6</sup> He pointed out that, because of the very strong dependence of thermionic emission on the surface temperature, any nonuniformity in temperature over the cathode surface would lead to a concentration of the arc current, and hence also the heat flux, at the hot spots. The increased heat input at these points would then tend to raise their temperature even more, and this, in turn, would produce a further concentration of current and heat flux. Thus, the arc would tend to contract into a spot, with a spot temperature considerably higher than that of the surrounding cathode.

Bauer did not indicate how steep a temperature dependence would be required to cause spot formation, or what would determine the ultimate operating temperature reached by the contracted spot. These questions can be answered approximately, however, for a fairly smoothly varying heat flux function  $q(T)$ , by reference to equation (74) which gives the critical steepness required for stable operation of the spot. If the steepness of  $q(T)$  at the initial cathode temperature exceeds this critical value, then the arc contracts and the spot temperature rises until a temperature is reached for which the steepness of  $q(T)$  has fallen to the critical value  $1/\gamma$  given by (74). Once this critical steepness has been reached, the concentration of heat flux produced by the temperature gradients across the spot is no longer sufficient to cause a further rise in temperature, and stable operation thus ensues.

In the case of an irregularly shaped function  $q(T)$ , for which the Taylor series expansion is not a good approximation, equation (74) is naturally not applicable. However, the more general relation (69), which states that the temperature gradient across the spot must be just sufficient to cut the heat flux off at the spot radius, remains valid. It is, thus, expected that, in general, stable operation of the spot is possible only for certain specific temperatures for which the dependence of the heat flux on temperature is just "steep" enough, in some sense, to produce the required cutoff.

The general nature of solutions to the cathode heat conduction problem (62) can be seen from the approximate relations (66), (68), and (74) or (69) deduced above. For a given cathode fall voltage  $V_c$  and boundary temperature  $T_0$ ,  $q(T)$  is a known function of  $T$ , and the possible operating temperatures  $T_{av}$  of the cathode spot are determined completely by the solutions of equation (74) or its more general form (69).

Depending on the form of  $q(T)$ , there may be zero, one, two or more solutions for  $T_{av}$ . For each of these possible values of  $T_{av}$ , the spot radius  $r_s$  is uniquely determined by equations (66) and (68). Thus, the heat conduction problem in the cathode has stable solutions only for certain specific values of the spot radius  $r_s$  and temperature  $T_{av}$ , and the arc is,

therefore, forced to contract in front of the cathode so as to take on one of these permitted values for the spot radius. Each solution of the heat conduction problem corresponds to a possible mode of operation of the cathode.

Once  $T_{av}$  and  $r_s$  have been determined, approximate values for the other significant cathode operating parameters can be calculated from the equations given in section IIIC. In particular, the average electron and ion current densities over the spot,  $(j_e)_{av}$  and  $(j_i)_{av}$ , can be determined approximately by evaluating the implicit equations (55) through (59) at the average spot temperature  $T_{av}$ , and the total current can, then, be found from (60) in the integrated form

$$I = \pi r_s^2 [(j_e)_{av} + (j_i)_{av}] \quad (75)$$

### 3. Approximate Theory of Cathode Spots

An approximate theory for the burning spot on a semi-infinite cathode with temperature  $T_0 = 0$  at infinity is developed in this section. The heat input function  $q(T)$  for this problem is given by equations (54) through (59) and has the form illustrated in figure 4.

It is convenient to consider separately the case in which the ion current density  $j_i$  is everywhere less than its limiting value  $(j_i)_{max}$ , and the case in which  $j_i = (j_i)_{max}$  over part of the cathode surface. In the former case, the function  $q(T)$  can be approximated fairly well by a straight line over the entire range of temperatures occurring in the cathode spot (see figure 8), so that equation (74) may be applied to determine the approximate spot temperature  $T_{av}$ . An implicit differentiation of the equations (54) through (59) defining  $q(T)$  gives for the steepness function (neglecting the radiative heat loss from the spot)

$$\frac{q'(T_{av})}{q(T_{av})} T_{av} = \frac{2 + (11609\phi - 4.4\sqrt{E_c})/T_{av}}{1 - 1.1\sqrt{E_c}/T_{av}} \quad (76)$$

For reasonable values of the parameters, this quantity is always  $\gtrsim 10$ , so that equation (74) can be satisfied only if  $T_0$  has a fairly large positive value. Thus, the burning spot on a thermionic cathode cannot operate with an ion current density less than the limiting value  $(j_i)_{max}$  unless the cathode is rather poorly cooled. It may be concluded, in particular, that this mode of operation is not possible for the semi-infinite cathode with  $T_0 = 0$ , which is under consideration in the present section.



If the ion current density  $j_i$  is equal to the limiting value  $(j_i)_{\max}$  over part of the spot, then it is no longer possible to approximate  $q(T)$  even roughly by a straight line, and equation (74) for the spot temperature is not applicable. However, qualitative arguments similar to those used in the preceding section can be employed to show that a stable spot should be possible in this temperature regime. It was pointed out in the discussion of equation (74) that, if the heat flux  $q$  is too steep a function of temperature, the spot must contract and its temperature must rise until a stable situation is reached. As seen above, for  $j_i < (j_i)_{\max}$ , the heat flux function  $q(T)$  is always much too steep to permit the existence of stable solutions, so that the spot must continue to contract and its temperature to rise at least until  $j_i = (j_i)_{\max}$  at the center. On the other hand, the peak temperature in the spot cannot rise above the temperature at which  $q(T)$  becomes negative owing to the cooling effect of excessive electron emission, since the heat flow in the cathode interior must always be away from the region of peak temperature, and this heat flow must be supplied by the flux into the surface. It therefore appears that a stable situation must be reached with a spot temperature somewhere between that at which  $j_i = (j_i)_{\max}$  and that at which  $q(T)$  becomes negative. For the particular case illustrated in figure 4, this argument indicates a spot temperature between about 2850° and 3150°K for a cathode fall of 10 volts, and between about 3000° and 3100°K for a fall of 5 volts.

Although the qualitative considerations of the preceding paragraph serve to determine the average spot temperature to within rather narrow limits, it appears possible to obtain a somewhat more accurate solution by considering the average electron and ion current densities in the spot. It is assumed, for this calculation, that all of the power brought into the ion production zone by the electron current  $\pi r_s^2 (j_e)_{\text{av}}$  is consumed in producing the ion current  $\pi r_s^2 (j_i)_{\text{av}}$  which flows to the cathode surface. This assumption leads to the simple energy balance relation (13) for the average current densities  $(j_e)_{\text{av}}$  and  $(j_i)_{\text{av}}$ , although not for the current densities at each individual point. Then,

$$(j_i)_{\text{av}} = \frac{\alpha}{1 - \alpha} (j_e)_{\text{av}} , \quad (77)$$

where  $\alpha$  is given by (58). A somewhat different assumption was made in deriving equation (57) above; however, the present assumption appears equally well justified by the facts of the physical situation, and is more convenient for the present analysis.

Since according to (76) the heat flux function  $q(T)$  for  $j_i < (j_i)_{\max}$  is very much steeper than would be required to satisfy (74), it appears likely that, in a stable spot, a large part of the spot area must operate with  $j_i = (j_i)_{\max}$ . It, therefore, seems reasonable to take



$$(j_i)_{av} \simeq (j_i)_{max} \quad (78)$$

in equation (77). Since  $j_e$  is a rather smoothly varying function of  $T$  over the spot (see figure 6),  $(j_e)_{av} \simeq j_e(T_{av})$ , and equation (77) becomes

$$j_e(T_{av}) = \frac{1-a}{a} (j_i)_{max} \quad (79)$$

In combination with the defining equations (55) and (56) for  $i_e$ , equation (79) gives a relation for determining the average spot temperature  $T_{av}$ . This relation takes the place of (74). Once the spot temperature  $T_{av}$  has been determined as a function of  $V_c$  from equation (79), an approximate solution for the remaining spot properties can be obtained by the methods outlined in paragraph 2 of section III D above, using equations (54), (66), (68), and (75).

For the present case, a somewhat more accurate version of equation (68) can be obtained from consideration of the temperature distribution in the cathode spot. It is apparent from figure 4 that the heat flux  $q(T)$  to the cathode surface is significant only for a rather narrow range of surface temperatures whose width is of the order of 500°K or less. Thus, the temperature difference across the spot is not very large, and the heat flow should be about the same as it would be if the spot were at a constant temperature. This latter problem, however, has been solved,<sup>27</sup> and the total heat flow  $Q$  is

$$Q = 4Kr_s (T_{av} - T_0) \quad (80)$$

where  $T_{av}$  is the spot temperature, and  $T_0$  the temperature at infinity. This equation differs from the approximate relation (68) only in that the factor  $2\pi$  in (68) is replaced by the factor 4 in (80).

An estimate of the actual temperature difference across the spot can also be obtained from a comparison with the solution for a constant temperature spot. The heat flux per unit area at the center of the constant temperature spot is<sup>27</sup>

$$q = \frac{2K(T_{av} - T_0)}{\pi r_s} \quad (81)$$

On the assumption that this same heat flux exists at the center of the actual spot, the temperature  $T_m$  at the center of the spot can be calculated from the relation between  $q$  and  $T$  given by equations (54) through (59).

The calculated maximum spot temperature  $T_m$  can, then, be compared with the average spot temperature  $T_{av}$  to check how well the assumption of a constant spot temperature is satisfied.

Calculations of the cathode spot parameters have been carried out as a function of arc current  $I$  for a thoriated tungsten cathode operating in argon and helium at 1 atmosphere pressure, using the approximate spot theory developed above. For convenience, the equations used in the calculation are summarized below:

$$q = (V_c + V_i - \phi) j_i - \phi j_e - \sigma \epsilon T_{av}^4 \quad (54)$$

$$j_e = A T_{av}^2 e^{-\theta/T_{av}} \quad (55a)$$

$$\theta = 11609 \phi - 4.40 \sqrt{E_c} \quad (55b)$$

$$E_c = 873 V_c^{1/4} \left[ (1823 W)^{1/2} j_i - j_e \right]^{1/2} \quad (56)$$

$$\alpha = V_c / (V_c + V_i) \quad (58)$$

$$(j_i)_{\max} = p \epsilon_e / \sqrt{8\pi M k T_g} \quad (59)$$

$$Q = \pi r_s^2 q \quad (66)$$

$$I = \pi r_s^2 (j_e + j_i) \quad (75)$$

$$j_i = (j_i)_{\max} \quad (78)$$

$$j_e = (1 - \alpha) j_i / \alpha \quad (79)$$

$$Q = 4 K r_s T_{av} \quad (80)$$

These equations are solved iteratively by the following procedure. For a given value of the independent parameter  $I$ , a guess is made as to the value of the cathode fall voltage  $V_c$ . Values of  $\alpha$ ,  $j_i$ , and  $j_e$  are then calculated from equations (58), (59), (78), and (79). These values are substituted into equations (55) and (56) to obtain a first approximation to the average spot temperature  $T_{av}$ . An improved approximation to  $V_c$  is then obtained by substituting the known total current

I and the first approximation to  $T_{av}$  into the relation

$$V_c = \phi + 4 K T_{av} \sqrt{\frac{a}{\pi j_i I}} - \frac{\sigma \epsilon T_{av}^4 a}{j_i}, \quad (82)$$

which is obtained by combining equations (54), (58), (66), (75), (79), and (80). The entire sequence of steps is then iterated until satisfactory convergence is obtained.

The results of the numerical calculations are presented in Table 2. These results are based upon the material property values,

$$\phi = 2.6 \text{ volts}$$

$$A = 1 \text{ amp/cm}^2 \text{ } ^\circ\text{K}^2$$

$$K = 0.94 \text{ w/cm } ^\circ\text{K}$$

$$\epsilon = 0.4, \quad (83)$$

obtained by analysis of experimental data on rod shaped thoriated tungsten cathodes (section V below).

Although the approximate nature of the theory and the uncertainties in the material property values probably preclude any meaningful quantitative comparison of the calculations with experimental data, the magnitudes of the various spot properties given in Table 2, and their general trend with current and gas type, are in very satisfactory qualitative agreement with experiment. Thus, for an increase in total arc current by a factor of 100, the calculated current density increases by only a factor of 3 or 4, in agreement with the general observation that an increased arc current is carried mainly by an increase in spot size, but also to some extent by a slight increase in the current density over the spot. The calculated results also show a drop in cathode fall voltage<sup>28</sup> and a slight rise in spot temperature with increasing current, in agreement with experimental observations. The generally lower values of spot temperature found experimentally\* by Neurath<sup>29</sup> might be explained by a slight difference of the work function  $\phi$  or the Richardson constant A from the values assumed in these calculations.

Comparison of the results for the two gases shows that the spot temperatures and current densities are distinctly higher in helium than in argon, as was also found experimentally by Neurath.<sup>29\*</sup> The primary reason for this difference, according to the theory given here, is the lower molecular weight of helium, which permits a higher limiting value  $(j_i)_{\max}$  for the ion current density. Since, in this theory, the limit on the ion current density

---

\* Vol. 2, part I of this report.



TABLE 2

## NUMERICAL RESULTS OF APPROXIMATE CATHODE-SPOT THEORY

Gas	I amperes	T <sub>av</sub> °K	r <sub>s</sub> cm	$j \equiv j_e + j_i$ amp/cm <sup>2</sup>	V <sub>c</sub> volts	$\alpha$	Q watts	E <sub>c</sub> 10 <sup>6</sup> v/cm	T <sub>m</sub> °K	j <sub>m</sub> amp/cm <sup>2</sup>	(T <sub>m</sub> -T <sub>av</sub> )/T <sub>av</sub> percent
Argon	10	2730	0.032	3010	36.0	0.695	334	1.61	3750	22,100	37
	30	2900	0.051	3640	21.2	0.574	558	1.41	3660	16,500	26
	100	3100	0.081	4830	12.0	0.433	946	1.22	3600	13,400	16
	300	3280	0.122	6450	7.56	0.324	1500	1.09	3590	12,400	10
	1000	3440	0.192	8600	5.06	0.243	2490	0.98	3620	12,500	5
Helium	10	3310	0.017	10,700	24.0	0.494	214	1.29	4270	54,400	29
	30	3540	0.026	14,600	13.9	0.362	340	1.12	4215	46,200	19
	100	3810	0.039	21,300	8.13	0.248	554	0.97	4220	43,600	11
	300	4000	0.057	29,100	5.45	0.182	862	0.87	4260	44,700	6
	1000	4170	0.092	37,600	4.03	0.141	1440	0.80	4310	47,500	4

plays an essential role in stopping the contraction of the cathode spot, a higher limiting value  $(j_i)_{\max}$  permits the spot to contract further, and thus to reach a higher operating temperature.

Another interesting feature of the present theory is the prediction of the shape of the temperature distribution across the cathode spot, as shown in the last column of Table 2. The results indicate that, as the total arc current increases, the maximum temperature  $T_m$  in the spot remains about the same while the average spot temperature increases somewhat. This leads to a rather "flat topped" temperature distribution across the spot at the higher currents, in agreement with qualitative observations by Neurath.<sup>29</sup> The slight increase in the maximum temperature  $T_m$  at low currents which is indicated in Table 2 is believed to be spurious, and to be due to the breakdown of the assumption of a constant temperature spot used in deriving equation (81).

Calculations of the cathode spot properties have been carried out for several different values of the cathode work function  $\phi$  to investigate the dependence of the solutions on this parameter. In general, it is found that a change in the cathode work function produces a nearly proportional change in the spot temperature  $T_{av}$ , while the other spot properties are changed very little. Again, this conclusion is in qualitative agreement with Neurath's<sup>29</sup> experimental results on cathodes of different materials.\*

Although no calculations have been carried out for pressures other than atmospheric, it is readily seen that a higher pressure increases the limiting value (59) of the ion current density, so that according to the theory the spot should contract and the spot temperature and current density should rise with increasing pressure. This behavior is again in good agreement with the general trend of experimental observations.<sup>6</sup> The increase of cathode spot temperature with pressure, predicted by this theory and observed empirically, evidently places a very severe requirement on the design of thermionic cathodes for operation at high pressures, unless its effects can be counteracted in some way. One possible method for extending the pressure capabilities of thermionic cathodes is use of low work function, high melting point materials. Another is development of cathodes with sufficiently poor cooling (or even heating) to prevent the ion current density from reaching its limiting value  $(j_i)_{\max}$ . As discussed after equation (76), such cathodes would operate in the spotless mode with a substantially lower maximum surface temperature than that occurring in spot mode operation. On the basis of the approximations underlying the present theory, the surface temperature of a thermionic cathode running in the spotless mode is pressure independent.

---

\* Vol. 2, part I of this report.



## V. QUASI ONE DIMENSIONAL MODEL

### A. PRELIMINARY DISCUSSION

The solution of the cathode model (62) can be approximated rather simply for a rod shaped cathode with the arc striking to one end, because in this case the heat flow problem becomes approximately one dimensional. True one dimensional heat flow can never actually be realized in a cathode, because of occurrence of one or more of the following effects:

1. Radiative heat loss from the sides of the cathode.
2. "Overflow" of the arc current onto the side of the cathode near the tip.
3. Spot mode operation.

However, radiative losses can be allowed for by inserting a fictitious sink term into the one dimensional steady heat flow equation. Arc overflow can also be represented approximately by modifying one dimensional solutions, as shown below in section V C. A rod shaped cathode with heat loss by side radiation, arc overflow, and Joule heating can thus be described approximately by means of a quasi one dimensional theory. Spot mode operation is more difficult to treat in such a theory because it produces more extreme departures from one dimensional heat flow in the tip region.

The quasi one dimensional theory of a thin, rod shaped thermionic cathode operating in the spotless mode provides a case in which the consequences of the cathode model (62) can be worked out in considerable detail. This theory is of interest also because it is possible, under certain circumstances, to operate rod shaped cathodes in the spotless mode, and, thus, to obtain a comparison between theoretical predictions and experimental data.

Section B below presents the solution of the quasi one dimensional heat flow problem for a rod with Joule heating and radiative loss of heat from the sides. Section C develops an analytical approximation to the temperature distribution in the tip region in the presence of arc overflow. The results of these two sections are combined, in section D, with the relations describing processes in the cathode fall zone and at the surface. A numerical procedure is developed for solving the resulting cathode model. Numerical results are given in section E.

### B. QUASI ONE DIMENSIONAL HEAT FLOW IN A THIN ROD WITH JOULE HEATING AND SIDE RADIATION

The quasi one dimensional flow of heat and electric current in a rod can be analyzed without considering the mechanism by which the end of the rod is



heated. Such a procedure is advantageous because the results can then be used in conjunction with various approximations to the theory of cathode fall zone and surface processes. However, the temperature dependence of electrical and thermal conductivities makes it convenient to specialize the theory with respect to the type of cathode material. In the present section, the quasi one dimensional theory is developed for the case of tungsten cathodes, possibly containing small quantities of low work function additives. The theory could also be worked out for carbon cathodes, but this has not been done because operating lifetime and contamination considerations make carbon less interesting than tungsten for most plasma generation applications.

The following analysis pertains to a cylindrical rod of length  $L$  and diameter  $D \ll L$ . The diameter is assumed to be sufficiently small that radial temperature differences can be neglected in comparison with axial ones. Then the temperature field in the rod's interior is approximately one dimensional,  $T = T(x)$ , where  $x$  is a coordinate along the axis of the rod with its origin at the cold end and with its positive direction toward the heated end.

It is assumed that the rod carries an electric current in the axial direction with a uniform current density  $j_0$ . This current is assumed, for the present, to enter and leave the rod only through the ends. Conservation of charge then requires that  $j_0(x) = \text{constant}$ . Joule dissipation produces a distributed heat source with a power density  $\rho j_0^2$ , where  $\rho$  denotes the resistivity of the material. Heat is lost from the sides of the rod at a rate  $\sigma \epsilon T^4$ , where  $\sigma$  is the Stefan-Boltzmann constant ( $5.67 \times 10^{-12} \text{ w/cm}^2\text{°K}^4$ ),  $\epsilon$  the total emissivity of the material, and  $T$  the local temperature.

The steady state energy balance for the volume bounded by the side surface of the rod and the two planes  $x$  and  $x + dx$  is

$$\left( q + \frac{dq}{dx} dx \right) \cdot \frac{\pi D^2}{4} - q \cdot \frac{\pi D^2}{4} = \rho j_0^2 \cdot \frac{\pi D^2}{4} dx - \sigma \epsilon T^4 \cdot \pi D dx$$

or

$$\frac{dq}{dx} = \rho j_0^2 - \frac{4\sigma \epsilon T^4}{D}, \quad (84)$$

in which  $q$  represents the local axial heat flux in the rod,

$$q = -K \frac{dT}{dx} \quad (85)$$

The differential equation describing steady heat flow in the rod is, then,

$$\frac{d}{dx} \left( K \frac{dT}{dx} \right) + \rho j_0^2 = \frac{4\sigma \epsilon T^4}{D} \quad (86)$$

Integration of this equation requires specification of the temperature dependence of the material properties  $K$ ,  $\rho$ ,  $\epsilon$ . Literature data on the values of these quantities for pure tungsten are shown in figures 9, 10, and 11. Figure 9 indicates that the thermal conductivity<sup>30,31</sup> of tungsten does not change in any systematic fashion with temperature. For fully dense pure tungsten, a mean value of about 1.1 or 1.2 w/cm<sup>2</sup>°K represents the literature values with reasonable accuracy over the temperature range from 300° to 3000°K. In contrast, the electrical resistivity<sup>32</sup> varies widely over the same temperature range, as shown in figure 10. The values can be fitted by an empirical formula,

$$\rho = B T^s, \quad (87)$$

where, for pure tungsten,\*

$$B = 5.0 \times 10^{-9} \text{ ohm-cm/}^\circ\text{K}^s \quad (88)$$

$$s = 1.234.$$

Figure 11 shows that the total emissivity<sup>33</sup> of pure tungsten increases with rising temperature, but does not vary greatly in the high temperature region, where the radiative heat flux from a cathode surface is large. In view of other approximations being used, it appears that  $\epsilon = \text{constant}$  should be an acceptable approximation.

When  $K$  and  $\epsilon$  are assumed to be constant and  $\rho$  is represented by (87), the differential equation (86) becomes

$$\frac{d^2T}{dx^2} = \frac{4\sigma\epsilon}{KD} T^4 - \frac{B j_0^2}{K} T^s, \quad (89)$$

which, with the substitution  $u = dT/dx$ ,  $d^2T/dx^2 = u du/dT$ , readily yields the first integral

$$\frac{dT}{dx} = \sqrt{\frac{8\sigma\epsilon}{5KD} T^5 - \frac{2B j_0^2}{(s+1)K} T^{s+1}} + C. \quad (90)$$

---

\* Equation (87) could also be written in the form  $\rho = B' (T/T_u)^s$  with  $T_u = 1^\circ\text{K}$  and  $B' = 5.0 \times 10^{-9} \text{ ohm-cm}$ . The form actually given in (87) is obtained by setting  $B = B'/T_u^s$ , which gives (88) with its somewhat strange-looking unit, ohm-cm/°K<sup>s</sup>. Writing (87) in terms of  $B$  rather than  $B'$  simplifies the appearance of the many subsequent formulas based in part upon (87).

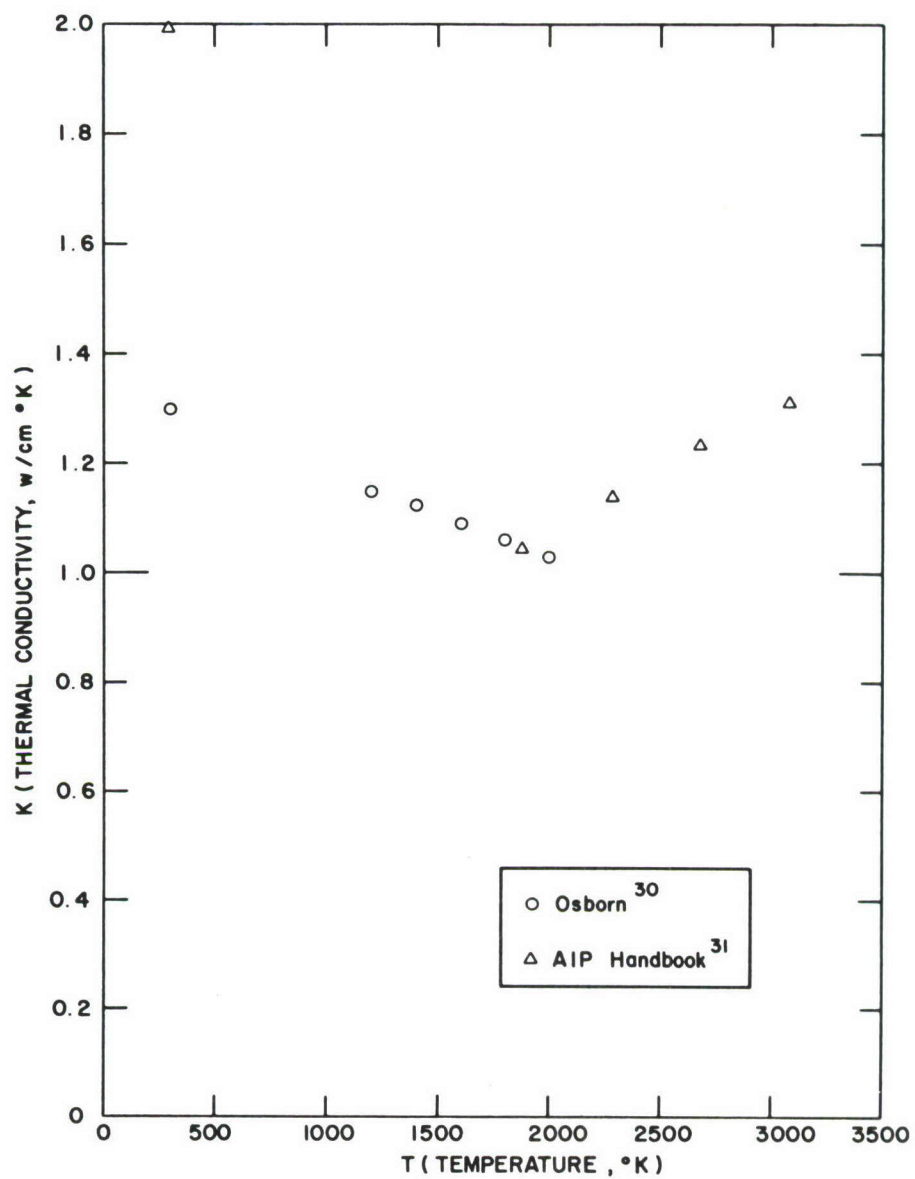


Figure 9 THERMAL CONDUCTIVITY OF TUNGSTEN



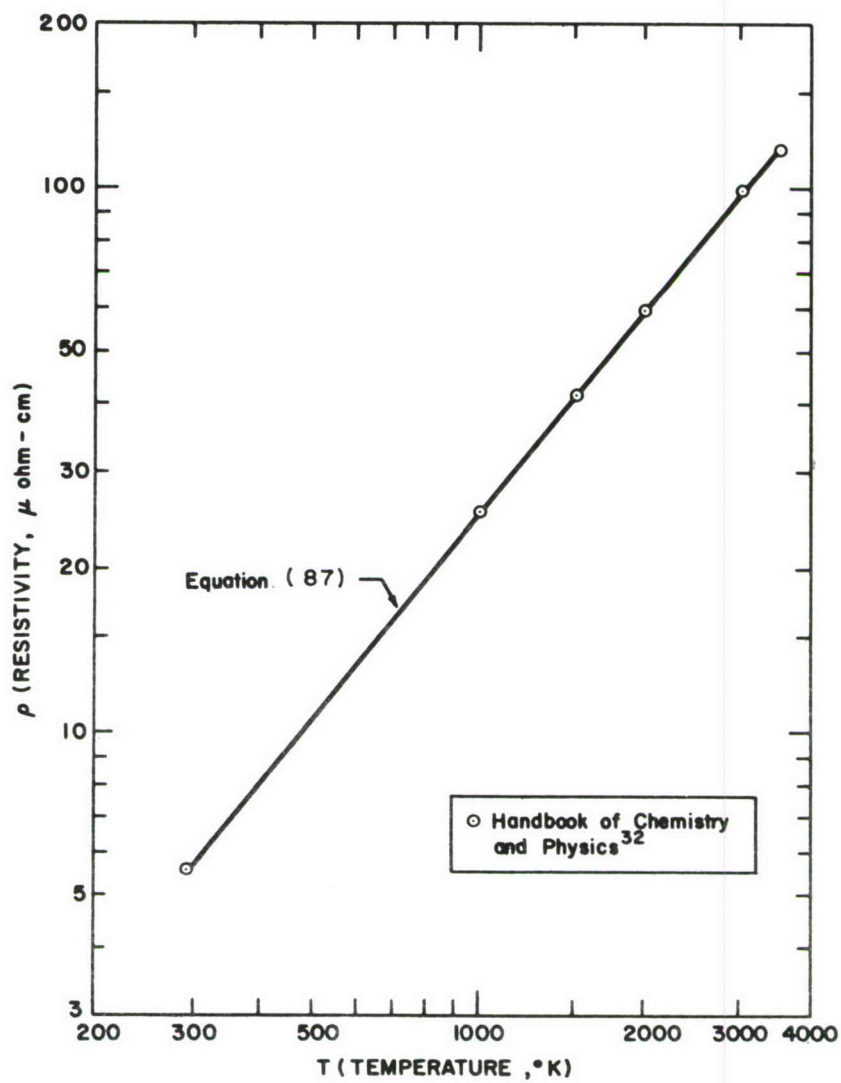


Figure 10 ELECTRICAL RESISTIVITY OF TUNGSTEN

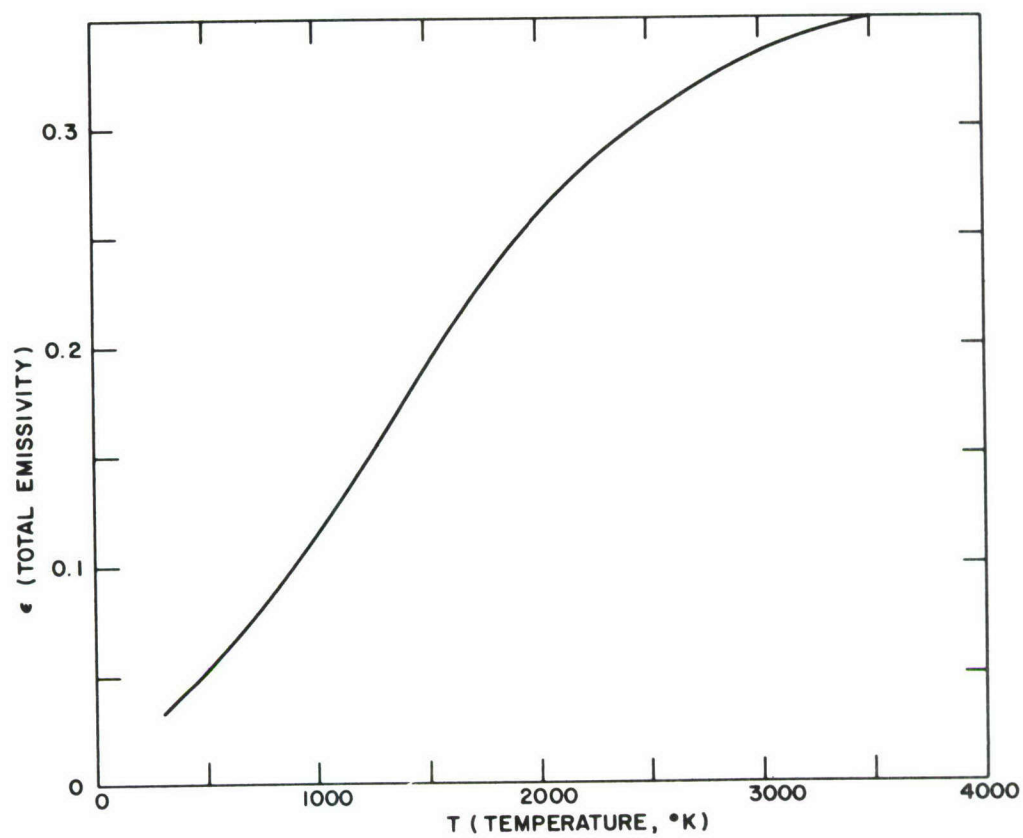


Figure 11 TOTAL EMISSIVITY OF TUNGSTEN

The remaining integration necessary to obtain  $T$  as a function of  $x$  must be performed numerically. To minimize the number of cases, it is advantageous to introduce nondimensional variables, as follows: Let

$$\psi = \left( \frac{8\sigma\epsilon}{5KDC} \right)^{1/5} T \quad (91a)$$

$$\eta = \sqrt{C} \left( \frac{8\sigma\epsilon}{5KDC} \right)^{1/5} x, \quad (91b)$$

and define the parameter

$$z = \frac{2B j_0^2}{(s+1)KC} \left( \frac{8\sigma\epsilon}{5KDC} \right)^{-(s+1)/5}. \quad (91c)$$

Then, the differential equation (90) reduces to

$$\frac{d\psi}{d\eta} = \sqrt{1 + \psi^5 - z\psi^{s+1}}. \quad (92)$$

Define the function

$$G(\psi', z) \equiv \int_0^{\psi'} \frac{d\psi}{\sqrt{1 + \psi^5 - z\psi^{s+1}}}. \quad (93)$$

Then, the general solution of (92) can be expressed as

$$\eta = G(\psi, z) - G(\psi_0, z), \quad (94)$$

where  $\psi_0$  is the value of  $\psi$  corresponding to  $\eta = 0$ .

The function  $G(\psi, z)$  has been evaluated numerically for  $s = 1.234$  using a program for Simpson rule integration. The results are given in Table 3 and illustrated in figure 12 for a few values of  $z$ . The shapes of the curves become intelligible on physical grounds when it is noted that  $\psi$  is proportional to temperature and  $G$  to distance from the cold end of the cathode (apart from the relatively small shift represented by  $G(\psi_0, z)$  in equation (94). For  $z = 0$ , there is no Joule heating since  $j_0^2 = 0$  from (91c). For small  $\psi$  (low temperature), the curve representing  $G(\psi, z)$  for  $z = 0$  is nearly linear, since radiative losses are negligible in this region. As  $\psi$  increases, radiative losses



TABLE 3

ONE DIMENSIONAL CATHODE FUNCTION  $G(\psi, z)$ 

$\begin{array}{c} z \\ \psi \end{array}$	0.0	0.1	0.2	0.3	0.4	0.5	0.6	0.7	0.8	0.9	1.0
0.0	0.0000	0.0000	0.0000	0.0000	0.0000	0.0000	0.0000	0.0000	0.0000	0.0000	0.0000
0.1	0.1000	0.1000	0.1000	0.1000	0.1000	0.1000	0.1000	0.1001	0.1001	0.1001	0.1001
0.2	0.2000	0.2001	0.2002	0.2002	0.2003	0.2004	0.2005	0.2006	0.2007	0.2008	0.2008
0.3	0.2999	0.3002	0.3006	0.3009	0.3012	0.3015	0.3019	0.3022	0.3025	0.3029	0.3032
0.4	0.3997	0.4005	0.4013	0.4021	0.4029	0.4038	0.4046	0.4054	0.4063	0.4072	0.4081
0.5	0.4987	0.5003	0.5020	0.5037	0.5054	0.5072	0.5090	0.5108	0.5127	0.5146	0.5166
0.6	0.5962	0.5991	0.6021	0.6051	0.6082	0.6114	0.6148	0.6182	0.6218	0.6254	0.6292
0.7	0.6908	0.6953	0.7000	0.7049	0.7100	0.7153	0.7209	0.7267	0.7328	0.7391	0.7459
0.8	0.7806	0.7871	0.7939	0.8011	0.8086	0.8165	0.8249	0.8338	0.8432	0.8534	0.8642
0.9	0.8638	0.8724	0.8814	0.8910	0.9011	0.9119	0.9234	0.9358	0.9492	0.9637	0.9796
1.0	0.9389	0.9494	0.9605	0.9724	0.9850	0.9986	1.0132	1.0290	1.0462	1.0650	1.0859
1.1	1.0051	1.0173	1.0303	1.0442	1.0590	1.0749	1.0921	1.1107	1.1312	1.1536	1.1786
1.2	1.0628	1.0764	1.0908	1.1062	1.1227	1.1404	1.1597	1.1805	1.2034	1.2286	1.2566
1.3	1.1125	1.1271	1.1427	1.1592	1.1770	1.1962	1.2168	1.2393	1.2639	1.2911	1.3212
1.4	1.1553	1.1706	1.1870	1.2045	1.2232	1.2433	1.2651	1.2887	1.3145	1.3430	1.3745
1.5	1.1920	1.2080	1.2250	1.2431	1.2625	1.2833	1.3058	1.3303	1.3570	1.3863	1.4188
1.6	1.2238	1.2402	1.2576	1.2762	1.2961	1.3174	1.3405	1.3655	1.3928	1.4227	1.4559
1.7	1.2513	1.2680	1.2858	1.3047	1.3250	1.3467	1.3702	1.3956	1.4233	1.4537	1.4874
1.8	1.2753	1.2923	1.3103	1.3295	1.3500	1.3720	1.3957	1.4214	1.4495	1.4802	1.5142
1.9	1.2963	1.3135	1.3317	1.3511	1.3718	1.3940	1.4180	1.4439	1.4721	1.5031	1.5373
2.0	1.3148	1.3321	1.3505	1.3700	1.3909	1.4133	1.4374	1.4635	1.4919	1.5230	1.5575
3.0	1.4215	1.4393	1.4581	1.4782	1.4996	1.5225	1.5471	1.5737	1.6027	1.6344	1.6694
4.0	1.4664	1.4842	1.5032	1.5233	1.5448	1.5678	1.5925	1.6192	1.6482	1.6800	1.7151
5.0	1.4901	1.5080	1.5269	1.5471	1.5686	1.5916	1.6163	1.6430	1.6721	1.7039	1.7390

TABLE 3  $G(\psi, z)$  (Cont'd)

$\begin{array}{c} z \\ \psi \end{array}$	1.0	1.1	1.2	1.3	1.4	1.5	1.6	1.7	1.8	1.9
0.0	0.0000	0.0000	0.0000	0.0000	0.0000	0.0000	0.0000	0.0000	0.0000	0.0000
0.1	0.1001	0.1001	0.1001	0.1001	0.1001	0.1001	0.1001	0.1002	0.1002	0.1002
0.2	0.2008	0.2009	0.2010	0.2011	0.2012	0.2013	0.2014	0.2015	0.2016	0.2016
0.3	0.3032	0.3035	0.3039	0.3042	0.3045	0.3049	0.3052	0.3056	0.3059	0.3063
0.4	0.4081	0.4090	0.4099	0.4108	0.4118	0.4127	0.4137	0.4147	0.4157	0.4167
0.5	0.5166	0.5186	0.5206	0.5227	0.5249	0.5270	0.5293	0.5316	0.5340	0.5365
0.6	0.6292	0.6332	0.6373	0.6416	0.6460	0.6507	0.6555	0.6606	0.6660	0.6717
0.7	0.7459	0.7530	0.7606	0.7686	0.7772	0.7864	0.7964	0.8073	0.8192	0.8325
0.8	0.8642	0.8760	0.8888	0.9028	0.9182	0.9356	0.9553	0.9781	1.0052	1.0390
0.9	0.9796	0.9971	1.0165	1.0385	1.0636	1.0929	1.1283	1.1727	1.2326	1.3258
1.0	1.0859	1.1091	1.1354	1.1656	1.2010	1.2436	1.2970	1.3679	1.4728	1.6703
1.1	1.1786	1.2067	1.2386	1.2755	1.3192	1.3722	1.4394	1.5299	1.6656	1.9239
1.2	1.2566	1.2882	1.3241	1.3656	1.4147	1.4744	1.5498	1.6509	1.8011	2.0810
1.3	1.3212	1.3551	1.3936	1.4381	1.4906	1.5541	1.6341	1.7406	1.8975	2.1859
1.4	1.3745	1.4100	1.4502	1.4965	1.5511	1.6169	1.6994	1.8089	1.9692	2.2616
1.5	1.4188	1.4553	1.4966	1.5442	1.6000	1.6672	1.7513	1.8625	2.0246	2.3190
1.6	1.4559	1.4931	1.5352	1.5835	1.6402	1.7083	1.7933	1.9055	2.0688	2.3644
1.7	1.4874	1.5250	1.5676	1.6164	1.6737	1.7424	1.8280	1.9409	2.1048	2.4012
1.8	1.5142	1.5522	1.5951	1.6443	1.7020	1.7711	1.8572	1.9705	2.1349	2.4317
1.9	1.5373	1.5756	1.6187	1.6683	1.7261	1.7956	1.8819	1.9956	2.1603	2.4575
2.0	1.5575	1.5959	1.6392	1.6890	1.7470	1.8167	1.9033	2.0171	2.1820	2.4795
3.0	1.6694	1.7084	1.7523	1.8026	1.8613	1.9316	2.0188	2.1333	2.2989	2.5970
4.0	1.7151	1.7541	1.7982	1.8486	1.9073	1.9777	2.0650	2.1795	2.3452	2.6434
5.0	1.7390	1.7780	1.8221	1.8725	1.9313	2.0017	2.0890	2.2036	2.3693	2.6675



TABLE 3  $G(\psi, z)$  (Concl'd)

$\psi \backslash z$	1.90	1.92	1.94	1.95	1.96	1.97	1.98	1.983	1.986	1.9875
0.0	0.0000	0.0000	0.0000	0.0000	0.0000	0.0000	0.000	0.000	0.000	0.000
0.1	0.1002	0.1002	0.1002	0.1002	0.1002	0.1002	0.100	0.100	0.100	0.100
0.2	0.2016	0.2017	0.2017	0.2017	0.2017	0.2017	0.202	0.202	0.202	0.202
0.3	0.3063	0.3064	0.3064	0.3065	0.3065	0.3065	0.307	0.307	0.307	0.307
0.4	0.4167	0.4169	0.4171	0.4172	0.4173	0.4174	0.417	0.418	0.418	0.418
0.5	0.5365	0.5370	0.5375	0.5377	0.5380	0.5382	0.538	0.539	0.539	0.539
0.6	0.6717	0.6728	0.6740	0.6746	0.6752	0.6758	0.676	0.677	0.677	0.677
0.7	0.8325	0.8353	0.8382	0.8397	0.8412	0.8427	0.844	0.845	0.845	0.845
0.8	1.0390	1.0469	1.0552	1.0596	1.0641	1.0688	1.074	1.075	1.077	1.077
0.9	1.3258	1.3528	1.3853	1.4044	1.4261	1.4515	1.482	1.493	1.504	1.510
1.0	1.6703	1.7409	1.8394	1.9076	1.9991	2.1363	2.399	2.552	2.835	3.154
1.1	1.9239	2.0158	2.1427	2.2291	2.3432	2.5093	2.812	2.981	3.282	3.612
1.2	2.0810	2.1787	2.3121	2.4020	2.5199	2.6902	2.997	3.168	3.470	3.800
1.3	2.1859	2.2856	2.4211	2.5122	2.6312	2.8027	3.111	3.282	3.585	3.915
1.4	2.2616	2.3621	2.4985	2.5900	2.7095	2.8815	3.190	3.361	3.664	3.995
1.5	2.3190	2.4201	2.5569	2.6486	2.7684	2.9406	3.249	3.420	3.724	4.054
1.6	2.3644	2.4657	2.6027	2.6946	2.8145	2.9868	3.296	3.467	3.770	4.101
1.7	2.4012	2.5026	2.6399	2.7318	2.8518	3.0242	3.333	3.504	3.808	4.138
1.8	2.4317	2.5333	2.6706	2.7626	2.8826	3.0551	3.364	3.535	3.839	4.169
1.9	2.4575	2.5591	2.6964	2.7885	2.9086	3.0810	3.390	3.561	3.865	4.195
2.0	2.4795	2.5811	2.7185	2.8106	2.9307	3.1032	3.412	3.584	3.887	4.218
3.0	2.5970	2.6987	2.8363	2.9285	3.0486	3.2212	3.530	3.702	4.005	4.336
4.0	2.6434	2.7452	2.8828	2.9749	3.0951	3.2677	3.577	3.748	4.051	4.382
5.0	2.6675	2.7693	2.9069	2.9990	3.1192	3.2918	3.601	3.772	4.076	4.406



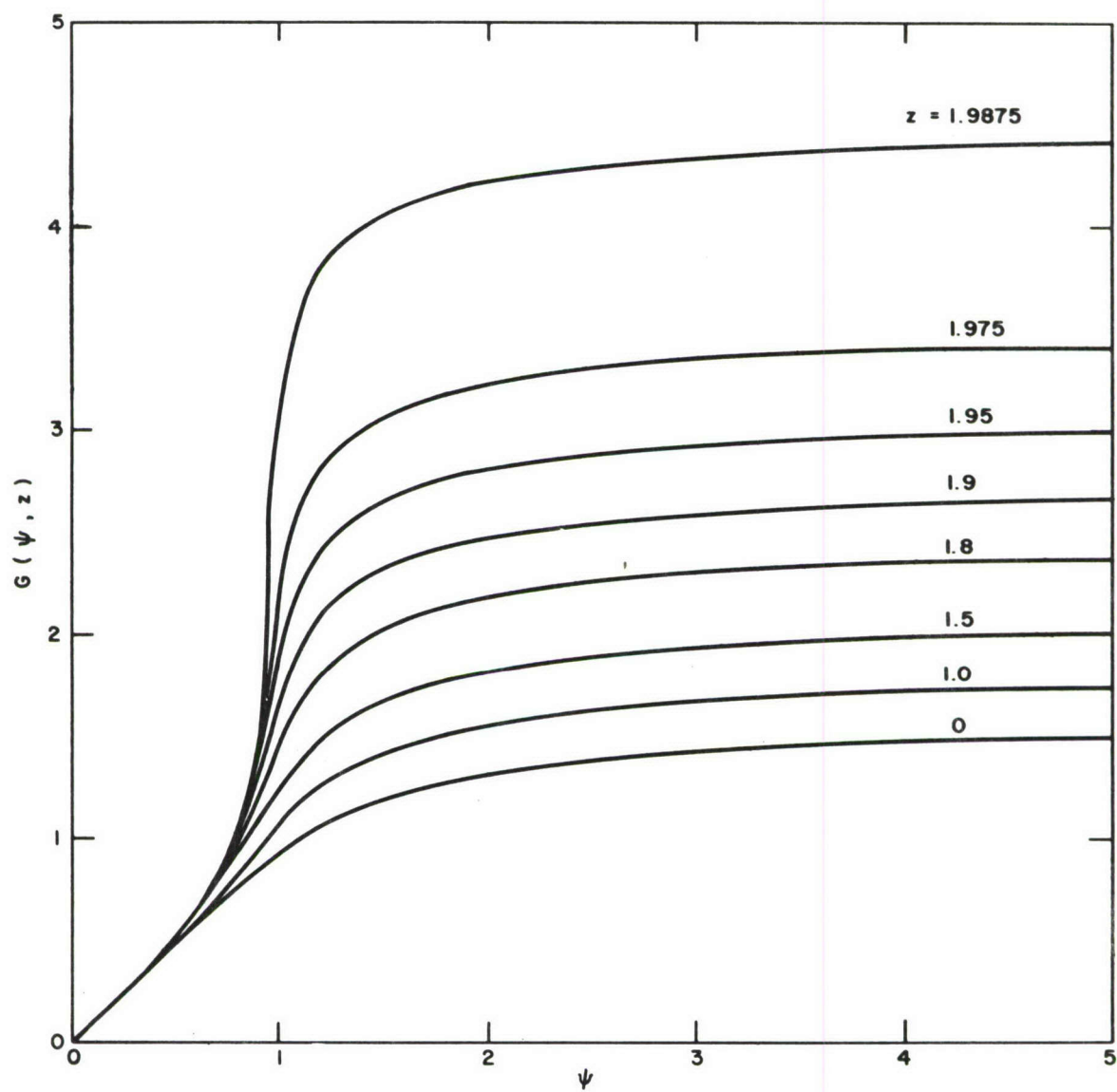


Figure 12 ONE DIMENSIONAL CATHODE FUNCTION  $G(\psi, z)$

rise as  $\psi^4$  and the temperature gradient  $d\psi/dG$  steepens, because the rod in this region has to carry not only the heat flux reaching the cold end but also the heat escaping through the sides above the end. For  $z > 0$ , Joule heating contributes to the energy balance for the rod. This heat addition tends to decrease the temperature gradient  $d\psi/dG$  at points distant from the cold end of the rod, since some of the heat flux reaching the cold end is now supplied by Joule dissipation, and, thus, need not be carried by conduction at the point in question. The curves for  $z > 0$ , thus, bend upward initially before reaching the high temperature region where radiation dominates and  $d\psi/dG$  becomes large.

For  $z$  values a little less than 2, the curves become quite sensitive to  $z$  for  $\psi \gtrsim 0.9$ . The reason for this behavior is that the radicand  $1 + \psi^5 - z\psi^{s+1}$  in (93) becomes small for  $\psi \sim 1$  in these cases. For  $z = z_c$ , where

$$z_c = 5 [(s+1)^{s+1} (4-s)^{4-s}]^{-0.2} , \quad (95)$$

the radicand has a minimum of zero at  $\psi = \psi_m \equiv [(s+1)/(4-s)]^{0.2}$ , and  $G(\psi, z)$  goes to infinity at  $\psi = \psi_m$ . For  $s = 1.234$ ,  $z_c$  is approximately 1.9887. Since  $\psi$  and  $G$  are essentially proportional to temperature and distance, respectively, the solution for  $z = z_c$  predicts a region of almost constant temperature extending downward from the heated end of the cathode. In this region, Joule heating is virtually in local equilibrium with side radiation.

In addition to  $G(\psi, z)$ , certain other one dimensional cathode functions are useful. The resistive voltage drop between the points  $x_1$  and  $x_2$  along the cathode is given by

$$\Delta V = \int_{x_1}^{x_2} \rho j_0 dx = j_0 B \int_{x_1}^{x_2} T^s dx , \quad (96)$$

using (87). Substitution of (91) gives

$$\Delta V = \frac{j_0 B}{\sqrt{C}} \left( \frac{8\sigma\epsilon}{5KDC} \right)^{-(s+1)/5} \int_{\eta_1}^{\eta_2} \psi^s d\eta . \quad (97)$$

Since  $d\eta = (d\eta/d\psi) d\psi$ , the integral can be transformed, using (92), to

$$\Delta V = \frac{j_0 B}{\sqrt{C}} \left( \frac{8\sigma\epsilon}{5KDC} \right)^{-(s+1)/5} [V(\psi_2, z) - V(\psi_1, z)] , \quad (98a)$$

where

$$V(\psi', z) \equiv \int_0^{\psi'} \frac{\psi^s d\psi}{\sqrt{1+\psi^5 - z\psi^{s+1}}} , \quad (98b)$$

and  $\psi_1, \psi_2$  are the values of  $\psi$  at the points  $x_1, x_2$ . The electrical resistance of the cathode between  $x_1$  and  $x_2$  is equal to  $\Delta V/I$ , where  $I$  denotes the total current. The Joule heating power evolved in the cathode between  $x_1$  and  $x_2$  is  $I \cdot \Delta V$ .

Similarly, the total power lost by side radiation between the points  $x_1$  and  $x_2$  along the cathode is

$$\Delta P_R = \int_{x_1}^{x_2} \sigma\epsilon T^4 \cdot \pi D dx = \sigma\epsilon\pi D \int_{x_1}^{x_2} T^4 dx . \quad (99)$$

Substitution of (91) gives

$$\Delta P_R = \frac{\sigma\epsilon\pi D}{\sqrt{C}} \cdot \frac{5KDC}{8\sigma\epsilon} \int_{\eta_1}^{\eta_2} \psi^4 d\eta . \quad (100)$$

Transformation to an integral over  $\psi$  gives

$$\Delta P_R = \frac{5\pi D^2 K \sqrt{C}}{8} [R(\psi_2, z) - R(\psi_1, z)] , \quad (101a)$$



where

$$R(\psi', z) \equiv \int_0^{\psi'} \frac{\psi^4 d\psi}{\sqrt{1+\psi^5 - z\psi^{s+1}}} . \quad (101b)$$

The functions V and R satisfy a simple algebraic relation.

Consider

$$\int_0^{\psi'} \frac{d(1+\psi^5 - z\psi^{s+1})}{\sqrt{1+\psi^5 - z\psi^{s+1}}} = 2 \sqrt{1+(\psi')^5 - z(\psi')^{s+1}} - 1 . \quad (102)$$

On the other hand,

$$\int_0^{\psi'} \frac{d(1+\psi^5 - z\psi^{s+1})}{\sqrt{1+\psi^5 - z\psi^{s+1}}} = 5 \int_0^{\psi'} \frac{\psi^4 d\psi}{\sqrt{1+\psi^5 - z\psi^{s+1}}} - (s+1)z \int_0^{\psi'} \frac{\psi^s d\psi}{\sqrt{1+\psi^5 - z\psi^{s+1}}} . \quad (103)$$

Hence,

$$5 R(\psi, z) - (s+1) z V(\psi, z) = \sqrt{1+\psi^5 - z\psi^{s+1}} - 1 . \quad (104)$$

This relation corresponds physically to the complete energy balance for the cathode. The functions V( $\psi, z$ ) and R( $\psi, z$ ) are presented in Tables 4 and 5 respectively, for  $s = 1.234$ .

Application of the nondimensional cathode functions requires that the constant of integration C appearing in (90) and (91) be specified. This constant is determined by the boundary conditions, which can be of several types. Two cases are discussed here as follows:

TABLE 4

ONE DIMENSIONAL CATHODE FUNCTION  $V(\psi; z)$ 

$\begin{array}{c} z \\ \psi \end{array}$	0.0	0.1	0.2	0.3	0.4	0.5	0.6	0.7	0.8	0.9	1.0
0.0	0.0000	0.0000	0.0000	0.0000	0.0000	0.0000	0.0000	0.0000	0.0000	0.0000	0.0000
0.1	0.0026	0.0026	0.0026	0.0026	0.0026	0.0026	0.0026	0.0026	0.0026	0.0026	0.0026
0.2	0.0123	0.0123	0.0123	0.0123	0.0123	0.0123	0.0123	0.0123	0.0124	0.0124	0.0124
0.3	0.0304	0.0304	0.0305	0.0305	0.0306	0.0306	0.0307	0.0308	0.0308	0.0309	0.0309
0.4	0.0577	0.0579	0.0581	0.0583	0.0585	0.0587	0.0589	0.0591	0.0593	0.0595	0.0597
0.5	0.0947	0.0952	0.0957	0.0962	0.0968	0.0973	0.0979	0.0984	0.0990	0.0996	0.1002
0.6	0.1413	0.1424	0.1436	0.1447	0.1460	0.1472	0.1485	0.1498	0.1512	0.1527	0.1542
0.7	0.1969	0.1990	0.2011	0.2034	0.2058	0.2082	0.2109	0.2136	0.2165	0.2195	0.2228
0.8	0.2598	0.2633	0.2669	0.2708	0.2749	0.2792	0.2838	0.2887	0.2940	0.2996	0.3058
0.9	0.3273	0.3330	0.3384	0.3443	0.3505	0.3572	0.3644	0.3721	0.3806	0.3899	0.4001
1.0	0.3982	0.4052	0.4126	0.4206	0.4292	0.4385	0.4485	0.4595	0.4715	0.4849	0.4998
1.1	0.4685	0.4773	0.4867	0.4967	0.5076	0.5194	0.5322	0.5462	0.5617	0.5789	0.5982
1.2	0.5369	0.5473	0.5584	0.5704	0.5832	0.5972	0.6124	0.6290	0.6474	0.6678	0.6907
1.3	0.6024	0.6141	0.6267	0.6402	0.6547	0.6705	0.6876	0.7064	0.7270	0.7500	0.7756
1.4	0.6642	0.6771	0.6908	0.7056	0.7215	0.7387	0.7574	0.7778	0.8002	0.8250	0.8528
1.5	0.7223	0.7361	0.7508	0.7666	0.7836	0.8019	0.8218	0.8434	0.8672	0.8935	0.9227
1.6	0.7768	0.7913	0.8068	0.8234	0.8412	0.8604	0.8812	0.9039	0.9286	0.9560	0.9864
1.7	0.8278	0.8429	0.8591	0.8763	0.8948	0.9147	0.9362	0.9596	0.9852	1.0133	1.0446
1.8	0.8756	0.8912	0.9079	0.9256	0.9446	0.9651	0.9872	1.0112	1.0374	1.0662	1.0981
1.9	0.9205	0.9365	0.9536	0.9717	0.9912	1.0121	1.0346	1.0591	1.0858	1.1151	1.1475
2.0	0.9627	0.9790	0.9964	1.0149	1.0347	1.0560	1.0789	1.1037	1.1308	1.1605	1.1933
3.0	1.2802	1.2979	1.3167	1.3367	1.3580	1.3807	1.4051	1.4315	1.4601	1.4914	1.5259
4.0	1.4867	1.5048	1.5240	1.5443	1.5659	1.5890	1.6138	1.6405	1.6695	1.7011	1.7359
5.0	1.6365	1.6547	1.6740	1.6944	1.7162	1.7394	1.7643	1.7911	1.8202	1.8520	1.8869



TABLE 4  $V(\psi, z)$  (Cont'd)

$\psi \backslash z$	1.0	1.1	1.2	1.3	1.4	1.5	1.6	1.7	1.8	1.9
0.0	0.0000	0.0000	0.0000	0.0000	0.0000	0.0000	0.0000	0.0000	0.0000	0.0000
0.1	0.0026	0.0026	0.0026	0.0026	0.0026	0.0026	0.0026	0.0026	0.0026	0.0026
0.2	0.0124	0.0124	0.0124	0.0124	0.0124	0.0124	0.0124	0.0124	0.0124	0.0124
0.3	0.0309	0.0310	0.0310	0.0311	0.0311	0.0312	0.0313	0.0313	0.0314	0.0314
0.4	0.0597	0.0599	0.0601	0.0603	0.0606	0.0608	0.0610	0.0613	0.0615	0.0617
0.5	0.1002	0.1009	0.1015	0.1022	0.1029	0.1036	0.1043	0.1050	0.1058	0.1066
0.6	0.1542	0.1558	0.1574	0.1591	0.1609	0.1628	0.1648	0.1669	0.1691	0.1714
0.7	0.2228	0.2262	0.2299	0.2339	0.2381	0.2427	0.2478	0.2533	0.2594	0.2663
0.8	0.3058	0.3125	0.3199	0.3280	0.3371	0.3474	0.3593	0.3733	0.3902	0.4117
0.9	0.4001	0.4115	0.4244	0.4390	0.4560	0.4763	0.5010	0.5328	0.5767	0.6474
1.0	0.4998	0.5166	0.5359	0.5583	0.5849	0.6176	0.6592	0.7159	0.8020	0.9706
1.1	0.5982	0.6201	0.6453	0.6748	0.7102	0.7539	0.8101	0.8874	1.0061	1.2387
1.2	0.6907	0.7167	0.7467	0.7817	0.8235	0.8750	0.9410	1.0308	1.1666	1.4247
1.3	0.7756	0.8047	0.8381	0.8770	0.9232	0.9798	1.0518	1.1487	1.2933	1.5625
1.4	0.8528	0.8841	0.9199	0.9614	1.0107	1.0706	1.1463	1.2475	1.3969	1.6717
1.5	0.9227	0.9557	0.9932	1.0367	1.0880	1.1501	1.2282	1.3320	1.4844	1.7625
1.6	0.9864	1.0205	1.0594	1.1042	1.1569	1.2205	1.3003	1.4059	1.5601	1.8403
1.7	1.0446	1.0797	1.1194	1.1652	1.2190	1.2837	1.3646	1.4715	1.6270	1.9085
1.8	1.0981	1.1338	1.1743	1.2208	1.2754	1.3409	1.4227	1.5304	1.6868	1.9693
1.9	1.1475	1.1838	1.2248	1.2719	1.3270	1.3932	1.4755	1.5839	1.7410	2.0242
2.0	1.1933	1.2300	1.2715	1.3190	1.3746	1.4412	1.5241	1.6330	1.7906	2.0743
3.0	1.5259	1.5642	1.6073	1.6566	1.7138	1.7822	1.8669	1.9776	2.1370	2.4227
4.0	1.7359	1.7746	1.8181	1.8677	1.9254	1.9941	2.0791	2.1902	2.3500	2.6360
5.0	1.8869	1.9258	1.9694	2.0191	2.0769	2.1458	2.2309	2.3421	2.5020	2.7882



TABLE 4  $V(\psi, z)$  (Concl'd)

$z \backslash \psi$	1.90	1.92	1.94	1.95	1.96	1.97	1.98	1.983	1.986	1.9875
0.0	0.0000	0.0000	0.0000	0.0000	0.0000	0.0000	0.000	0.000	0.000	0.000
0.1	0.0026	0.0026	0.0026	0.0026	0.0026	0.0026	0.003	0.003	0.003	0.003
0.2	0.0124	0.0124	0.0124	0.0125	0.0125	0.0125	0.012	0.012	0.012	0.012
0.3	0.0314	0.0314	0.0315	0.0315	0.0315	0.0315	0.032	0.032	0.032	0.032
0.4	0.0617	0.0618	0.0618	0.0619	0.0619	0.0619	0.062	0.062	0.062	0.062
0.5	0.1066	0.1068	0.1069	0.1070	0.1071	0.1072	0.107	0.107	0.107	0.107
0.6	0.1714	0.1719	0.1724	0.1727	0.1729	0.1732	0.173	0.174	0.174	0.174
0.7	0.2663	0.2678	0.2693	0.2701	0.2709	0.2717	0.272	0.273	0.273	0.273
0.8	0.4117	0.4168	0.4222	0.4250	0.4280	0.4310	0.434	0.435	0.436	0.437
0.9	0.6474	0.6684	0.6939	0.7090	0.7264	0.7468	0.772	0.780	0.790	0.795
1.0	0.9706	1.0326	1.1202	1.1815	1.2645	1.3903	1.634	1.778	2.044	2.345
1.1	1.2387	1.3230	1.4403	1.5206	1.6272	1.7831	2.068	2.228	2.513	2.826
1.2	1.4247	1.5158	1.6407	1.7252	1.8362	1.9970	2.287	2.449	2.736	3.049
1.3	1.5625	1.6562	1.7838	1.8698	1.9823	2.1446	2.436	2.599	2.886	3.199
1.4	1.6717	1.7667	1.8956	1.9823	2.0955	2.2585	2.551	2.713	3.001	3.314
1.5	1.7625	1.8582	1.9878	2.0748	2.1884	2.3518	2.645	2.807	3.095	3.408
1.6	1.8403	1.9364	2.0665	2.1537	2.2675	2.4311	2.724	2.887	3.174	3.488
1.7	1.9085	2.0049	2.1353	2.2227	2.3366	2.5003	2.794	2.956	3.244	3.558
1.8	1.9693	2.0659	2.1965	2.2840	2.3980	2.5619	2.855	3.018	3.306	3.619
1.9	2.0242	2.1210	2.2517	2.3393	2.4534	2.6173	2.911	3.073	3.361	3.675
2.0	2.0743	2.1712	2.3020	2.3896	2.5038	2.6677	2.961	3.124	3.412	3.726
3.0	2.4227	2.5199	2.6511	2.7389	2.8533	3.0174	3.311	3.474	3.762	4.076
4.0	2.6360	2.7333	2.8646	2.9525	3.0669	3.2311	3.525	3.688	3.976	4.289
5.0	2.7882	2.8855	3.0168	3.1047	3.2191	3.3833	3.650	3.840	4.128	4.442

TABLE 5

ONE DIMENSIONAL CATHODE FUNCTION  $R(\psi, z)$ 

$\begin{array}{c} z \\ \psi \end{array}$	0.0	0.1	0.2	0.3	0.4	0.5	0.6	0.7	0.8	0.9	1.0
0.0	0.000	0.000	0.000	0.000	0.000	0.000	0.000	0.000	0.000	0.000	0.000
0.1	0.000	0.000	0.000	0.000	0.000	0.000	0.000	0.000	0.000	0.000	0.000
0.2	0.000	0.000	0.000	0.000	0.000	0.000	0.000	0.000	0.000	0.000	0.000
0.3	0.000	0.000	0.000	0.000	0.000	0.000	0.000	0.000	0.000	0.000	0.000
0.4	0.002	0.002	0.002	0.002	0.002	0.002	0.002	0.002	0.002	0.002	0.002
0.5	0.006	0.006	0.006	0.006	0.006	0.006	0.006	0.007	0.007	0.007	0.007
0.6	0.015	0.015	0.016	0.016	0.016	0.016	0.016	0.017	0.017	0.017	0.017
0.7	0.032	0.033	0.033	0.034	0.034	0.035	0.035	0.036	0.037	0.038	0.038
0.8	0.061	0.062	0.063	0.064	0.066	0.067	0.069	0.070	0.072	0.074	0.076
0.9	0.104	0.107	0.109	0.111	0.114	0.117	0.120	0.124	0.128	0.132	0.137
1.0	0.166	0.169	0.174	0.178	0.183	0.188	0.194	0.199	0.207	0.214	0.223
1.1	0.246	0.252	0.258	0.265	0.273	0.281	0.289	0.299	0.310	0.322	0.336
1.2	0.347	0.355	0.364	0.374	0.384	0.395	0.407	0.421	0.436	0.453	0.472
1.3	0.468	0.479	0.491	0.503	0.516	0.531	0.547	0.564	0.584	0.605	0.630
1.4	0.610	0.624	0.638	0.653	0.670	0.687	0.707	0.728	0.752	0.777	0.806
1.5	0.773	0.788	0.805	0.824	0.843	0.864	0.887	0.912	0.939	0.969	1.002
1.6	0.956	0.974	0.994	1.014	1.037	1.061	1.087	1.115	1.145	1.179	1.216
1.7	1.159	1.180	1.202	1.226	1.251	1.277	1.306	1.337	1.371	1.408	1.448
1.8	1.384	1.407	1.432	1.458	1.485	1.514	1.546	1.580	1.616	1.656	1.700
1.9	1.630	1.656	1.682	1.710	1.740	1.772	1.806	1.842	1.881	1.924	1.970
2.0	1.898	1.925	1.954	1.984	2.016	2.050	2.087	2.125	2.167	2.212	2.261
3.0	5.848	5.891	5.936	5.983	6.031	6.082	6.135	6.191	6.250	6.312	6.379
4.0	12.406	12.460	12.515	12.572	12.631	12.692	12.756	12.822	12.892	12.965	13.043
5.0	21.964	22.025	22.088	22.152	22.219	22.288	22.359	22.433	22.510	22.591	22.677



TABLE 5  $R(\psi, z)$  (Cont'd)

$z \backslash \psi$	1.0	1.1	1.2	1.3	1.4	1.5	1.6	1.7	1.8	1.9
0.0	0.000	0.000	0.000	0.000	0.000	0.000	0.000	0.000	0.000	0.000
0.1	0.000	0.000	0.000	0.000	0.000	0.000	0.000	0.000	0.000	0.000
0.2	0.000	0.000	0.000	0.000	0.000	0.000	0.000	0.000	0.000	0.000
0.3	0.000	0.000	0.000	0.000	0.000	0.000	0.000	0.001	0.001	0.001
0.4	0.002	0.002	0.002	0.002	0.002	0.002	0.002	0.002	0.002	0.002
0.5	0.007	0.007	0.007	0.007	0.007	0.007	0.007	0.007	0.007	0.007
0.6	0.017	0.017	0.018	0.018	0.018	0.019	0.019	0.019	0.020	0.020
0.7	0.038	0.039	0.040	0.041	0.042	0.043	0.044	0.046	0.048	0.049
0.8	0.076	0.078	0.081	0.084	0.087	0.091	0.095	0.101	0.107	0.116
0.9	0.137	0.142	0.148	0.155	0.164	0.174	0.187	0.203	0.228	0.269
1.0	0.223	0.233	0.245	0.259	0.276	0.297	0.324	0.363	0.424	0.550
1.1	0.336	0.352	0.370	0.392	0.419	0.453	0.497	0.559	0.657	0.855
1.2	0.472	0.494	0.520	0.550	0.586	0.631	0.689	0.769	0.892	1.128
1.3	0.630	0.657	0.689	0.726	0.770	0.825	0.894	0.988	1.126	1.382
1.4	0.806	0.839	0.876	0.920	0.971	1.033	1.111	1.214	1.364	1.632
1.5	1.002	1.039	1.081	1.130	1.187	1.255	1.339	1.450	1.608	1.886
1.6	1.216	1.257	1.303	1.356	1.418	1.491	1.581	1.698	1.862	2.147
1.7	1.448	1.493	1.543	1.600	1.666	1.744	1.838	1.959	2.129	2.419
1.8	1.700	1.748	1.801	1.862	1.931	2.012	2.111	2.236	2.410	2.705
1.9	1.970	2.021	2.078	2.141	2.214	2.299	2.401	2.530	2.707	3.006
2.0	2.261	2.314	2.374	2.440	2.516	2.603	2.708	2.840	3.021	3.323
3.0	6.379	6.451	6.529	6.614	6.708	6.815	6.940	7.092	7.293	7.615
4.0	13.043	13.125	13.214	13.310	13.416	13.534	13.669	13.833	14.045	14.379
5.0	22.677	22.767	22.863	22.967	23.080	23.206	23.350	23.521	23.741	24.082



TABLE 5  $R(\psi, z)$  (Concl'd)

$z \backslash \psi$	1.90	1.92	1.94	1.95	1.96	1.97	1.98	1.983	1.986	1.9875
0.0	0.000	0.000	0.000	0.000	0.000	0.000	0.00	0.00	0.00	0.00
0.1	0.000	0.000	0.000	0.000	0.000	0.000	0.00	0.00	0.00	0.00
0.2	0.000	0.000	0.000	0.000	0.000	0.000	0.00	0.00	0.00	0.00
0.3	0.001	0.001	0.001	0.001	0.001	0.001	0.00	0.00	0.00	0.00
0.4	0.002	0.002	0.002	0.002	0.002	0.002	0.00	0.00	0.00	0.00
0.5	0.007	0.007	0.007	0.007	0.007	0.007	0.01	0.01	0.01	0.01
0.6	0.020	0.020	0.020	0.020	0.020	0.020	0.02	0.02	0.02	0.02
0.7	0.049	0.050	0.050	0.050	0.051	0.051	0.05	0.05	0.05	0.05
0.8	0.116	0.118	0.120	0.122	0.123	0.124	0.13	0.13	0.13	0.13
0.9	0.269	0.282	0.297	0.307	0.318	0.331	0.35	0.35	0.36	0.36
1.0	0.550	0.599	0.669	0.719	0.787	0.893	1.10	1.23	1.46	1.73
1.1	0.855	0.929	1.032	1.103	1.197	1.336	1.59	1.73	1.99	2.26
1.2	1.128	1.211	1.325	1.402	1.503	1.648	1.91	2.05	2.31	2.59
1.3	1.382	1.470	1.589	1.669	1.773	1.921	2.19	2.33	2.59	2.87
1.4	1.632	1.723	1.845	1.926	2.031	2.181	2.45	2.59	2.85	3.13
1.5	1.886	1.978	2.102	2.184	2.291	2.442	2.71	2.86	3.11	3.39
1.6	2.147	2.241	2.366	2.449	2.556	2.708	2.98	3.12	3.38	3.66
1.7	2.419	2.514	2.641	2.724	2.832	2.984	3.25	3.40	3.66	3.94
1.8	2.705	2.801	2.928	3.012	3.120	3.273	3.54	3.69	3.95	4.23
1.9	3.006	3.103	3.231	3.315	3.424	3.577	3.85	3.99	4.25	4.53
2.0	3.323	3.421	3.550	3.634	3.743	3.897	4.17	4.31	4.57	4.85
3.0	7.615	7.717	7.850	7.937	8.048	8.203	8.48	8.62	8.88	9.16
4.0	14.379	14.483	14.618	14.706	14.818	14.975	15.25	15.40	15.66	15.94
5.0	24.082	24.188	24.325	24.414	24.526	24.684	24.96	25.11	25.37	25.65

## 1. Case 1

A cathode experiment, such as the one discussed below in section V, may provide data on the temperature and heat flux at the cold end of the cathode. In this event, the boundary conditions on the problem are

$$T(0) = T_0 \quad (105a)$$

$$(K dT/dx)_{x=0} = q_0 \quad (105b)$$

Then, from equation (90),

$$C = \left(\frac{q_0}{K}\right)^2 - \frac{8\sigma\epsilon}{5KD} T_0^5 + \frac{2B j_0^2}{(s+1)K} T_0^{s+1} \quad (106)$$

## 2. Case 2

The boundary conditions for the theoretical cathode model are a given temperature at the cold end of the rod and a relation such as (62d) between temperature and heat flux at the hot end. The heat flow problem does not stand by itself in this case, but may conveniently be represented as a problem in which the heat flux at the hot end is given. The boundary conditions may, then, be taken to be

$$T(0) = T_0 \quad (107a)$$

$$(K dT/dx)_{x=L} = q_s \quad (107b)$$

and from (90),

$$C = \left(\frac{q_s}{K}\right)^2 - \frac{8\sigma\epsilon}{5KD} T_s^5 + \frac{2B j_0^2}{(s+1)K} T_s^{s+1} \quad (108)$$

where  $T_s$  denotes the temperature at  $x=L$ .

The solutions of the quasi one dimensional heat flow problem are given by equations (91) and (94), with  $C$  represented by (106) or (108) according as the boundary conditions are (105) or (107).

### C. ARC OVERFLOW

When a thin, rod shaped thermionic cathode operates in the spotless mode, the entire tip region is at an approximately uniform high temperature. Electron emission, therefore, occurs from the entire end surface. In addition, the side of the cathode just below the end is almost as hot as the end surface itself, so that some emission occurs from this surface also; i. e. , arc "overflow" onto the side of the cathode takes place. This phenomenon affects cathode operation in a rather significant way, since it reduces the surface current density required to yield a given total current, and, thus, reduces the tip operating temperature.

It is assumed that the current density is low enough that the ion current is less than  $(j_i)_{\max}$  (16) over the entire surface. Then, equation (29) for the net heat flux to the cathode surface reduces, with  $j_i = \alpha j$ ,  $j_e = (1 - \alpha) j$ , and equation (13), to the simpler form

$$K (\partial T / \partial n)_s = j (V_c - \phi) - \sigma \epsilon T^4 \quad . \quad (109)$$

The current flow through the side of the cathode gives rise to an additional fictitious heat source term in the quasi one dimensional heat flow equation (89), and also affects the Joule heating term by making the current density along the rod a function of position. Equation (89) is replaced by

$$\frac{d^2 T}{dx^2} = \frac{4\sigma\epsilon}{KD} T^4 - \frac{4(V_c - \phi)}{KD} j_s - \frac{Bj^2 T^s}{K} \quad . \quad (110)$$

Here,  $j_s$  denotes the current density through the side of the cathode, a function of temperature; and  $j$  is a function of  $x$ .

These overflow effects can be incorporated into the quasi one dimensional heat flow theory most conveniently by means of a perturbation approach, which assumes that the extent of the overflow region is small in comparison with the cathode length. This assumption is usually satisfied, because the current density,

$$j_s = \frac{j_e}{1 - \alpha} = \frac{A(V_c + V_I)}{V_I} T^2 e^{-\theta/T} \quad , \quad (111)$$

is a strong function of temperature, and because in most cases the temperature gradient in the tip region is large on account of radiative heat losses from the side. However, if Joule heating is comparable with radiative losses in the tip region, the temperature gradient may be so low that the overflow region becomes large. The perturbation theory of arc overflow effects is thus inapplicable to cathodes operating at such high currents that Joule heating and radiation nearly balance one another in the tip region.



On the assumption that the extent of the overflow region is small in comparison with the cathode length, the actual temperature distribution  $T(x)$  is indistinguishable from a solution  $T_n(x)$  of the heat flow equation (89) without overflow, except in a small region near the tip. The actual temperature is then represented by

$$T(x) = T_n(x) + t(x), \quad (112)$$

where the perturbation term  $t(x)$  is small in comparison with  $T_n(x)$  and approaches zero rapidly with increasing distance from the tip. Since the overflow region is assumed to be small,  $T_n$  does not vary greatly in the region where  $t(x)$  differs significantly from zero. Reasonably simple results can then be obtained from (110) by systematically neglecting all but the very strongest temperature dependence in the terms appearing on the right hand side. In addition, Joule heating is neglected in the tip region because the perturbation approach is invalid in cases where it cannot be neglected in this region. \*

These approximations bring (110) into the form

$$\frac{d^2 T_n}{dx^2} + \frac{d^2 t}{dx^2} = \frac{4\sigma\epsilon}{KD} T_{ns}^4 - \frac{4(V_c - \phi) A (V_c + V_I)}{KD V_I} T_{ns}^2 e^{-\theta/(T_n + t)},$$

where  $T_{ns} = T_n(L)$  is the temperature given by the unperturbed solution at the tip of the cathode, and the weak variation of  $\theta$  with current density given by (18) is neglected.  $T_n(x)$  satisfies (89), which becomes, with the same approximations,

$$\frac{d^2 T_n}{dx^2} = \frac{4\sigma\epsilon}{KD} T_{ns}^4.$$

The differential equation satisfied by  $t(x)$  is, thus,

$$\frac{d^2 t}{dx^2} = - \frac{4 A V T_{ns}^2}{KD} e^{-\theta/(T_n + t)}, \quad (113)$$

---

\*This restriction does not rule out cases in which Joule heating is important along a large fraction of the cathode's length; so long as the cathode tip is significantly hotter than the midsection, the radiative loss decreases rapidly (as  $T^4$ ) with distance from the tip, whereas the resistivity falls off more slowly (only as  $T^{1.234}$ ).

in which

$$V \equiv (V_c - \phi) \left( 1 + \frac{V_c}{V_I} \right) . \quad (114)$$

Let  $y$  represent the distance of a given point from the hot end of the cathode,

$$y = L - x . \quad (115)$$

Then, in the overflow region,

$$T_n \approx T_{ns} - T_{ns}' y , \quad (116)$$

where

$$T_{ns}' = (dT_n/dx)_{x=L} , \quad (117)$$

and in the region under consideration,  $y$  is small enough that  $T_{ns}' y \ll T_{ns}$ .  
Also

$$\frac{1}{T_n + t} = \frac{1}{T_n} \left( 1 - \frac{t}{T_n} \right) = \frac{1}{T_{ns}} \left( 1 - \frac{t - T_{ns}' y}{T_{ns}} \right) . \quad (118)$$

Let

$$\omega \equiv t - T_{ns}' y . \quad (119)$$

Substitution of (118) and (119) into (113) gives a differential equation for  $\omega$ ,

$$d^2 \omega / dy^2 = - a e^{b \omega} , \quad (120)$$

with

$$a = \frac{4 A T_{ns}^2 V e^{-\theta/T_{ns}}}{KD} \quad (121)$$

$$b = \theta / T_{ns}^2 . \quad (122)$$

The first integral of (120) is

$$\left(\frac{d\omega}{dy}\right)^2 = -\frac{2a}{b} e^{b\omega} + \text{const.} \quad (123)$$

For large  $y$ ,  $t$  approaches zero and, from (119),  $d\omega/dy$  approaches  $-T_{ns}'$ . Hence, the integration constant is equal to  $T_{ns}'^2$ ,

$$\frac{d\omega}{dy} = \sqrt{T_{ns}'^2 - \frac{2a}{b} e^{b\omega}}. \quad (124)$$

A final integration gives

$$by + \text{const.} = \frac{2}{T_{ns}'} \tanh^{-1} \sqrt{1 - \frac{2a}{b T_{ns}'^2} e^{b\omega}}. \quad (125)$$

Since, for large  $y$ ,  $\omega \sim -T_{ns}' y$ , the integration constant in this equation is equal to  $[\ln(2b T_{ns}'^2/a)]/T_{ns}'$ . Hence,

$$e^{b\omega} = \frac{b T_{ns}'^2}{2a} \text{sech}^2 \left[ \frac{b T_{ns}' y}{2} + \frac{1}{2} \ln \left( \frac{2b T_{ns}'^2}{a} \right) \right]. \quad (126)$$

Elimination of  $\omega$ ,  $a$ , and  $b$  using (119), (121), and (122), then gives the perturbation function  $t(y)$ ,

$$t = T_{ns}' y + \frac{T_{ns}'^2}{\theta} \ln \left[ \frac{1}{4\lambda} \text{sech}^2 \left( \frac{\theta T_{ns}' y}{2 T_{ns}'^2} - \frac{1}{2} \ln \lambda \right) \right], \quad (127)$$

where

$$\lambda \equiv \frac{2 \Lambda V T_{ns}'^4 e^{-\theta/T_{ns}'}}{\theta K D T_{ns}'^2} \quad (128)$$



is a nondimensional parameter characterizing the amount of arc overflow. The value of  $\tau$  at the cathode tip ( $y = 0$ ) is

$$\tau_0 = - \frac{2T_{ns}^2}{\theta} \ln(1 + \lambda) \quad , \quad (129)$$

so that for  $\lambda = 0$  there is no change of the tip temperature.

The current  $\pi D^2 j/4$  carried by the cathode at any given point along its length is equal to the current  $\pi D^2 j_E/4$  entering through the hot end, plus the integral of the "overflow" current density into the side between the hot end and the point in question. Hence,

$$j = j_E + \frac{4}{D} \int_0^y j_s dy \quad . \quad (130)$$

Now from (111),

$$j_E = \frac{A(V_c + V_I)}{V_I} T_{ns}^2 e^{-\theta/(T_{ns} + \tau_0)} \quad . \quad (131)$$

Substitution of (118), (119), (121), (122), and (126) gives

$$j_E = \frac{A(V_c + V_I)}{(1 + \lambda)^2 V_I} T_{ns}^2 e^{-\theta/T_{ns}} \quad . \quad (132)$$

The second term of (130) can be evaluated using the same relations. The integral is

$$\int_0^y j_s dy = \frac{A(V_c + V_I)}{V_I} T_{ns}^2 e^{-\theta/T_{ns}} \int_0^y e^{b\omega} dy \quad . \quad (133)$$

The integrand on the right hand side is given by (126). Thus,

$$j = j_E + \frac{K T_{ns}'}{V_c - \phi} \left\{ \tanh \left[ \frac{\theta T_{ns}' y}{2 T_{ns}^2} - \frac{1}{2} \ln \lambda \right] - \frac{1-\lambda}{1+\lambda} \right\} . \quad (134)$$

According to (134), one-half of the total overflow current (represented by the second term on the right hand side) has entered the cathode at a distance  $y_{0.5}$  from the tip, where

$$y_{0.5} = \frac{T_{ns}^2}{\theta T_{ns}'} \ln(2+\lambda) . \quad (135)$$

For large  $y$ ,  $j$  approaches the current density  $j_0$  for the unperturbed solution. Setting  $y = \infty$  in (134) and substituting (132) for  $j_E$ , one obtains

$$j_0 = \frac{A(V_c + V_I) T_{ns}^2 e^{-\theta/T_{ns}}}{(1+\lambda)^2 V_I} \left[ 1 + (1+\lambda) \frac{4 T_{ns}^2}{D \theta T_{ns}'} \right] . \quad (136)$$

This is the expression for the current density  $j_0$  at the cold end of the cathode in terms of the actual values of  $\theta$  and  $V_c$  for the "perturbed" case with overflow and the quantities  $T_{ns}$  and  $T_{ns}'$  for the fictitious "unperturbed" (no overflow) case.

The heat flux  $q_E$  into the end of the cathode is given by (112) and (119) in the form

$$q_E = K \left( \frac{dT}{dx} \right)_E = K \left[ T_{ns}' - \left( \frac{dt}{dy} \right)_0 \right] = - K \left( \frac{d\omega}{dy} \right)_0 . \quad (137)$$

Equation (124), together with the integrated expression for  $\omega$ , gives

$$q_E = K T_{ns}' \frac{1-\lambda}{1+\lambda} . \quad (138)$$

This equation shows that, for  $\lambda > 1$ , the heat flux into the end of the cathode is negative; i.e., the temperature near the cathode tip decreases with increasing  $x$ . This situation cannot arise in actual cathodes, except perhaps in cases in which the cathode is heated almost entirely by Joule dissipation. As indicated previously, the perturbation theory of arc overflow effects is inapplicable to such cases. Thus, for situations in which the theory is valid,  $\lambda$  always lies in the range between zero and one.

#### D. SOLUTION OF THE QUASI ONE DIMENSIONAL CATHODE MODEL

The results of the preceding sections B and C provide the means of solving the heat conduction part of the quasi one dimensional cathode problem. The present section combines these results with the relations describing processes in the cathode fall zone and at the surface, to obtain a complete system of equations which can be solved to yield predictions of performance for rod shaped cathodes.

It is assumed that the dimensions L, D and physical properties  $A, \phi, K, \epsilon, B$  of the cathode are known, and that the electrical resistivity is given by equation (87) with  $s = 1.234$ . This is the value of  $s$  for pure tungsten, and it should be approximately the same for tungsten with additives, even though the value of  $B$  might be a little different for such materials. The gas properties  $W, V_I$  and the temperature  $T_0$  of the cold end are also assumed to be known.

The "unperturbed" solution, which correctly describes the temperature field in the cathode everywhere except in the overflow region near the tip, is governed by equations (91) and (94). At the tip, these equations give the following relations involving the quantities  $T_{ns}$  and  $T_{ns}'$  which appear in the perturbation theory of arc overflow:

$$\eta_s = G(\psi_s, z) - G(\psi_0, z) \quad (139a)$$

$$\eta_s = \sqrt{C} \left( \frac{8\sigma\epsilon}{5KDC} \right)^{1/5} L \quad (139b)$$

$$\psi_s = \left( \frac{8\sigma\epsilon}{5KDC} \right)^{1/5} T_{ns} \quad (139c)$$

$$\psi_0 = \left( \frac{8\sigma\epsilon}{5KDC} \right)^{1/5} T_0 \quad (139d)$$

$$z = \frac{2Bj_0^2}{(s+1)KC} \left( \frac{8\sigma\epsilon}{5KDC} \right)^{-(s+1)/5} \quad (139e)$$



The constant C is given by (108),

$$C = T_{ns}'^2 - \frac{8\sigma\epsilon}{5KD} T_{ns}^5 + \frac{2Bj_0^2}{(s+1)K} T_{ns}^{s+1} . \quad (139f)$$

Here,  $T_{ns}$  and  $T_{ns}'$  are fictitious values for the temperature and temperature gradient at the hot tip of the cathode, based upon an extrapolation of the unperturbed solution to the tip, neglecting overflow. The actual heat flux into the end of the cathode is (138)

$$q_E = K T_{ns}' (1-\lambda)/(1+\lambda) , \quad (139g)$$

with (128),

$$\lambda = \frac{2A(V_c - \phi)(V_c + V_I) T_{ns}^4 e^{-\theta/T_{ns}}}{\theta KD V_I T_{ns}'^2} . \quad (139h)$$

Here,  $V_c$  and  $\theta$  are the values for these quantities in the actual case with overflow. The current density at the hot end is (132)

$$j_E = \frac{A(V_c + V_I) T_{ns}^2 e^{-\theta/T_{ns}}}{(1+\lambda)^2 V_I} , \quad (139i)$$

while the current density at the cold end is (136).

$$j_0 = j_E \left[ 1 + (1+\lambda) \frac{4 T_{ns}^2}{D \theta T_{ns}'} \right] , \quad (139j)$$

$\theta$  is given by (55b)

$$\theta = 11609 \phi - 4.4 \sqrt{E_c} , \quad (139k)$$

with  $E_c$  given by (8) and (58)

$$E_c = 873 V_c^{1/4} j_E^{1/2} \left[ (1823 W)^{1/2} \frac{V_c}{V_c + V_I} - \frac{V_I}{V_c + V_I} \right]^{1/2} . \quad (139l)$$

The energy balance (109) becomes

$$q_E = j_E (V_c - \phi) - \sigma \epsilon T_{ns}^4 , \quad (139m)$$

in which the radiative energy loss is approximated in terms of the unperturbed temperature  $T_{ns}$  at the end of the cathode. Let

$$r = T_{ns}/\theta . \quad (139n)$$

Then equations (139a to n) constitute a system of 14 equations for the 15 quantities  $\eta_s, \psi_s, \psi_0, z, C, T_{ns}, T_{ns}', j_0, \lambda, j_E, q_E, \theta, E_c, V_c$ , and  $r$ . The value of one of these quantities can be selected arbitrarily (within, perhaps, certain limits), since the cathode can operate over a range of total current values. After this selection has been made, the 14 equations (139) can be solved numerically for the 14 remaining unknown quantities. From the solution, various other quantities such as the actual tip temperature,

$$T_s = T_{ns} \left[ 1 - \frac{2 T_{ns}}{\theta} \ln(1 + \lambda) \right] , \quad (140)$$

and the total current,

$$I = \pi D^2 j_0 / 4 , \quad (141)$$

can be calculated. Equation (140) is based upon (112) and (129).

The solution of equations (139) can be accomplished by selecting  $r$  as the independent variable and noting that when values of  $\theta$  and  $T_{ns}'$  are given, all of the other unknowns can be calculated analytically in the following way. With  $r$  specified, assumption of a value for  $\theta$  gives  $T_{ns}$  by (139n). Elimination of  $q_E$  and  $j_E$  from (139g, i, m) gives

$$\frac{A V T_{ns}^2 e^{-1/r}}{(1 + \lambda)^2} - \sigma \epsilon T_{ns}^4 = K T_{ns}' \frac{1 - \lambda}{1 + \lambda} . \quad (142)$$

Then, elimination of  $V$  using (139h) and (114) gives a quadratic equation for  $\lambda$  in terms of  $T_{ns}'$

$$\lambda = \frac{2T_{ns}'^2}{\theta K D T_{ns}'} \left[ (1+\lambda)^2 \sigma \epsilon T_{ns}'^4 + (1-\lambda^2) K T_{ns}' \right] , \quad (143)$$

the solution of which is

$$\lambda = \frac{1}{2(K T_{ns}' - \sigma \epsilon T_{ns}'^4)} \left\{ 2\sigma \epsilon T_{ns}'^4 - \frac{\theta K D T_{ns}'^2}{2 T_{ns}'^2} + \sqrt{\left( \frac{\theta K D T_{ns}'^2}{2 T_{ns}'^2} - 2\sigma \epsilon T_{ns}'^4 \right)^2 + 4 (K^2 T_{ns}'^2 - \sigma^2 \epsilon^2 T_{ns}'^8)} \right\} . \quad (144)$$

Thus, with values assumed for  $\theta$  and  $T_{ns}'$ ,  $\lambda$  can be calculated. The quantity  $V$  can then be obtained from (139h) and (114),

$$V = \frac{\lambda \theta K D T_{ns}'^2}{2 A T_{ns}'^4 e^{-1/\tau}} . \quad (145)$$

Equation (114) can then be solved to give  $V_c$ ,

$$V_c = -\frac{1}{2} (V_I - \phi) + \frac{1}{2} \sqrt{(V_I + \phi)^2 + 4 V_I V} . \quad (146)$$

The current density  $j_0$  for the unperturbed solution is, then, from (139i and j),

$$j_0 = \frac{A (V_c + V_I) T_{ns}'^2 e^{-1/\tau}}{(1+\lambda)^2 V_I} \left[ 1 + (1+\lambda) \frac{4 T_{ns}'^2}{D \theta T_{ns}'} \right] . \quad (147)$$

Now  $C$  can be calculated from (139f), and  $\eta_s, \psi_s, \psi_0$ , and  $z$  from (139b, c, d, e). Substitution of these values into (139a) gives a measure  $\Delta$  of the error in the original choice of  $T_{ns}'$ :

$$\Delta = \eta_s - [G(\psi_s, z) - G(\psi_0, z)] . \quad (148)$$



By trial and error and interpolation, the value of  $T_{ns}'$  (if any) which makes  $\Delta = 0$  can be found.\* This is the "correct" value of  $T_{ns}'$  based upon the originally assumed value of  $\theta$ . An improved value of  $\theta$  can now be obtained by solving (139k and l), using the values of  $V_c$  and  $\lambda$  based upon the initial "correct" value of  $T_{ns}'$ . Elimination of  $E_c$  and  $j_E$  from (139i, k, l) gives

$$\left(\frac{\theta_0 - \theta}{4.4}\right)^2 = \frac{873 V_c^{1/4} A^{1/2} \theta r e^{-1/2r}}{1 + \lambda} \left[ (1823 W)^{1/2} \frac{V_c}{V_I} - 1 \right]^{1/2}, \quad (149a)$$

where

$$\theta_0 \equiv 11609 \phi.$$

The solution of (149a) for  $\theta$  is

$$\theta = \frac{1}{2} (2\theta_0 + F) - \frac{1}{2} \sqrt{F^2 + 4F\theta_0}, \quad (149b)$$

where

$$F = \frac{16900 A^{1/2} V_c^{1/4} r e^{-1/2r}}{1 + \lambda} \sqrt{(1823 W)^{1/2} \frac{V_c}{V_I} - 1}. \quad (150)$$

Since  $F$  depends rather weakly upon  $V_c$  and  $\lambda$ , and since  $F \ll \theta_0$ , the errors in  $V_c$  and  $\lambda$  have little effect upon the value of  $\theta$  calculated from (149).

The procedure for solving the system of equations (139) may now be summarized briefly. The independent parameter is  $r$ . For a given value of  $r$ , the following iterative numerical calculation yields the values for all of the unknowns.

1. Approximate  $\theta$  initially by  $\theta_0 = 11609 \phi$ .
2. Calculate  $T_{ns} = \theta r$ .
3. Solve the equation  $\Delta = 0$ , where  $\Delta$  is given by (148), for  $T_{ns}'$ . This can be accomplished by trial and error and interpolation using equations (144), (145), (146), (147), (139f), and (139b, c, d, e). This procedure gives values for  $T_{ns}'$ ,  $\lambda$ , and  $V_c$  based upon the current approximation to  $\theta$ .

---

\*If two such solutions exist, as happens in some cases, the larger of these is chosen. The other solution, which has small  $T_{ns}'$  and, consequently, large overflow, corresponds to a condition of cathode operation for which the perturbation theory of overflow effects is invalid.

4. Calculate an improved value for  $\theta$  using (149) and (150).
5. Go to step (2) with this new value of  $\theta$  and iterate until  $\theta$  has been determined with sufficient accuracy. Normally, the second or third pass through steps (2), (3), and (4) will give an excellent approximation to the value of  $\theta$ .

As pointed out previously, the perturbation calculation of overflow effects is physically meaningful only for  $\lambda < 1$ . As  $r$  increases,  $\lambda$  eventually begins to increase rapidly. When  $r$  is further increased beyond this region, the procedure described above gives either no solution or a physically unrealistic solution with  $\lambda \gg 1$ . The range of  $r$  values giving physically significant solutions must be determined by trial. A satisfactory starting value for  $r$  can be estimated from  $r \sim (10 + \ln A)^{-1}$ .

A program for solving the quasi one dimensional cathode model (139) has been developed. A FORTRAN listing and flow chart for this program are given and discussed in appendix B.

## E. NUMERICAL RESULTS

The mathematical model for quasi one dimensional cathodes operating in the spotless mode involves the following material and gas properties, geometrical factors, and physical parameters: total current ( $I$ ), ion molecular weight ( $W$ ), ionization potential ( $V_I$ ), diameter ( $D$ ), length ( $L$ ), cold end temperature ( $T_0$ ), Richardson constant ( $A$ ), thermionic work function ( $\phi$ ), thermal conductivity ( $K$ ), electrical resistivity parameter ( $B$ ), and total emissivity ( $\epsilon$ ). Because these quantities are so numerous, it is neither feasible nor desirable to undertake a comprehensive parameter variation study involving all combinations. Instead, several series of solutions have been obtained in which most of the parameters are held constant, and the dependence of the operating conditions upon a single variable is explored as a function of current. These results are discussed in physical terms to illustrate the principal properties of the model.

### 1. Material and Gas Properties

To limit the number of cases which must be considered, it is desirable to select a "standard" set of cathode and gas properties, which can be held fixed while geometrical and other factors are varied. The effects of varying the material properties themselves probably can be studied most usefully by varying the "material" rather than its individual properties. Table 6 lists the values assumed for the three cathode materials considered in this section. The "thoriated tungsten" values are based upon an analysis of experimental data presented in section V.



This "thoriated tungsten" is chosen as the standard material for most of the calculations. The properties given for "pure tungsten" are from the literature.<sup>30-33</sup> In the case of "barium oxide impregnated tungsten," the thermionic properties are obtained from Nottingham's<sup>34</sup> tabulation, while the other properties are assumed to be the same as for the "thoriated tungsten." Similarly, Table 7 gives the gas property values used in the calculations. Helium is taken as the standard gas. In the case of nitrogen, the ions are assumed to be  $N^+$  (rather than  $N_2^+$ ). The standard value for  $T_0$  is chosen to be 300°K.

## 2. Dependence upon Cathode Length

The theoretical behavior of 1/8 inch diameter thoriated tungsten cathodes of various lengths operating in the spotless mode in helium is shown in figures (13 to 23). The primary effect of an increase in cathode length is to decrease the cooling of the tip region. Most of the effects illustrated in these figures can be explained qualitatively as consequences of this dependence of tip cooling upon cathode length.

TABLE 6  
ASSUMED CATHODE MATERIAL PROPERTIES

Material	A amp/cm <sup>2</sup> °K <sup>2</sup>	$\phi$ volts	K w/cm°K	B ohm-cm/°K <sup>3</sup>	s	$\epsilon$
Pure Tungsten	60	4.51	1.1	$5.0 \times 10^{-9}$	1.234	0.32
Tungsten + ThO <sub>2</sub>	1	2.6	0.94	$5.3 \times 10^{-9}$	1.234	0.40
Tungsten + BaO	15	2.0	0.94	$5.3 \times 10^{-9}$	1.234	0.40

TABLE 7  
GAS PROPERTIES

Gas	w gm/mole	V <sub>I</sub> volts
Helium	4	24.5
Argon	40	15.7
Nitrogen	14	14.5



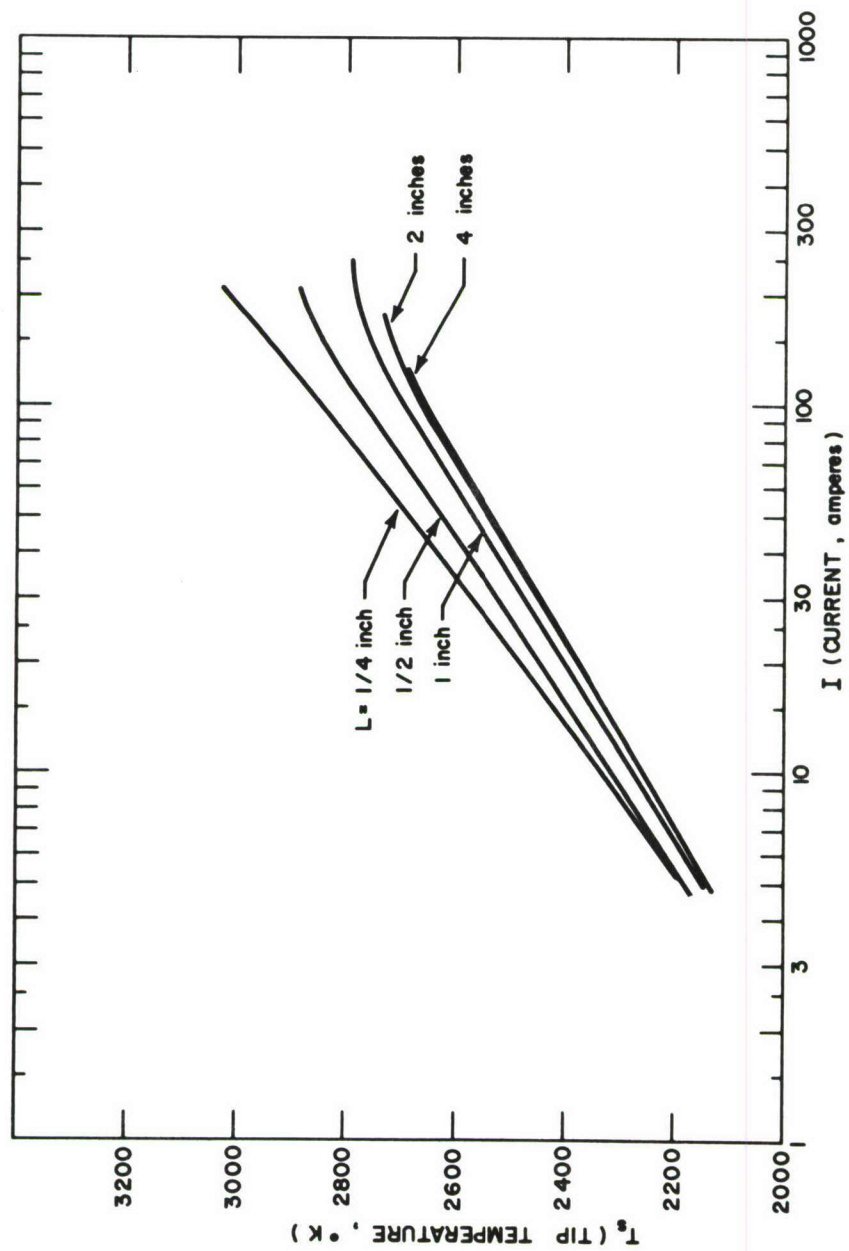


Figure 13 TIP TEMPERATURE VERSUS CURRENT AND CATHODE LENGTH  
(ONE EIGHTH INCH THORIATED TUNGSTEN  
CATHODE IN HELIUM)

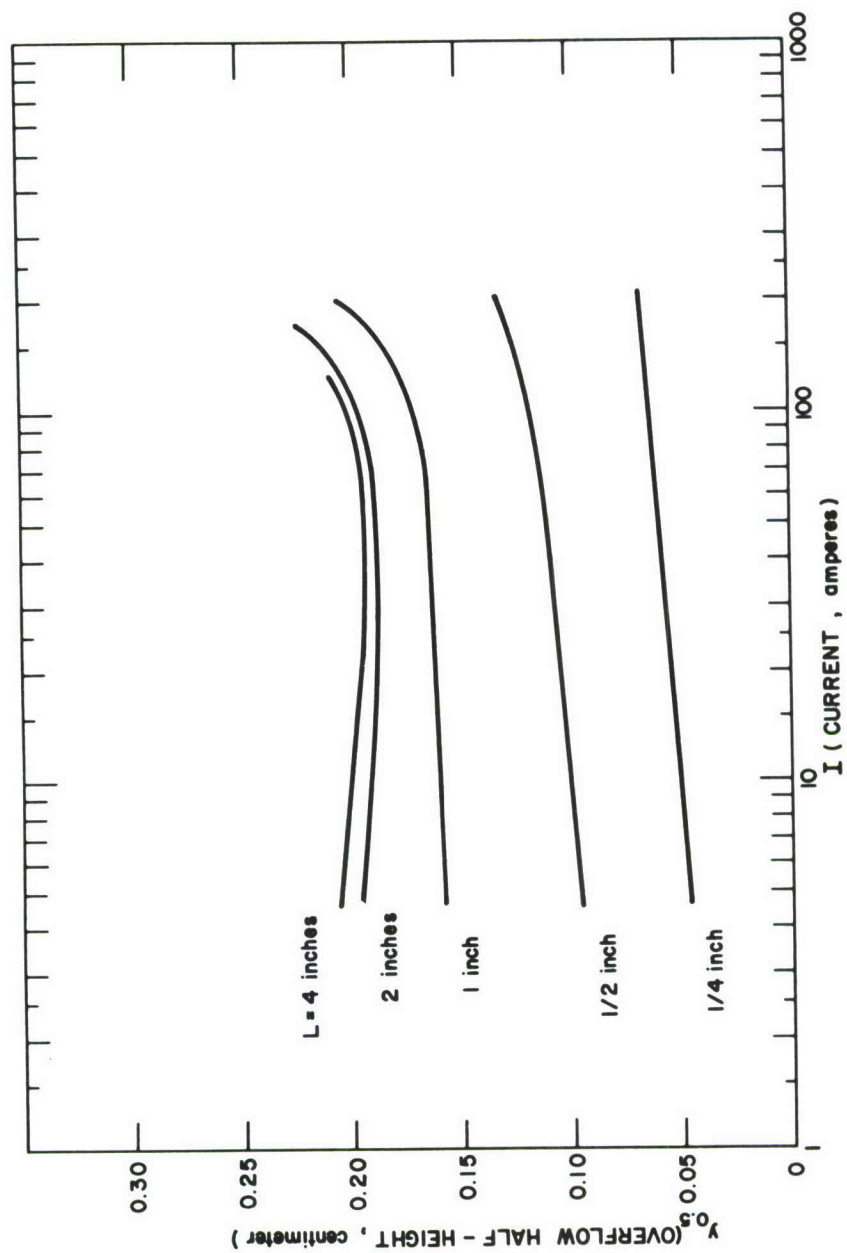


Figure 14 HALF-HEIGHT OF OVERFLOW REGION VERSUS CURRENT AND  
CATHODE LENGTH (ONE EIGHTH INCH THORIATED TUNGSTEN  
CATHODE IN HELIUM)

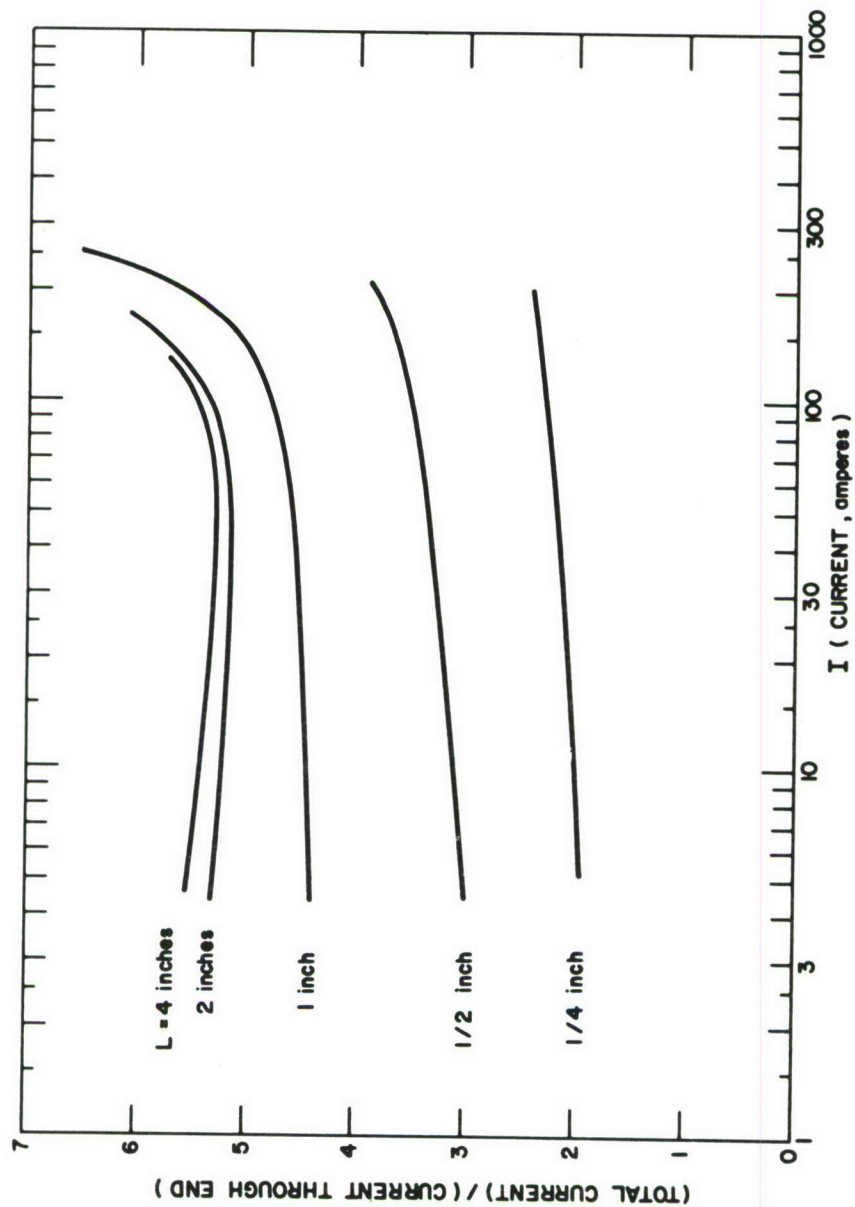


Figure 15 RATIO OF TOTAL CURRENT TO CURRENT ENTERING THROUGH  
END VERSUS CURRENT AND CATHODE LENGTH (ONE EIGHTH  
INCH THORIATED TUNGSTEN CATHODE IN HELIUM)



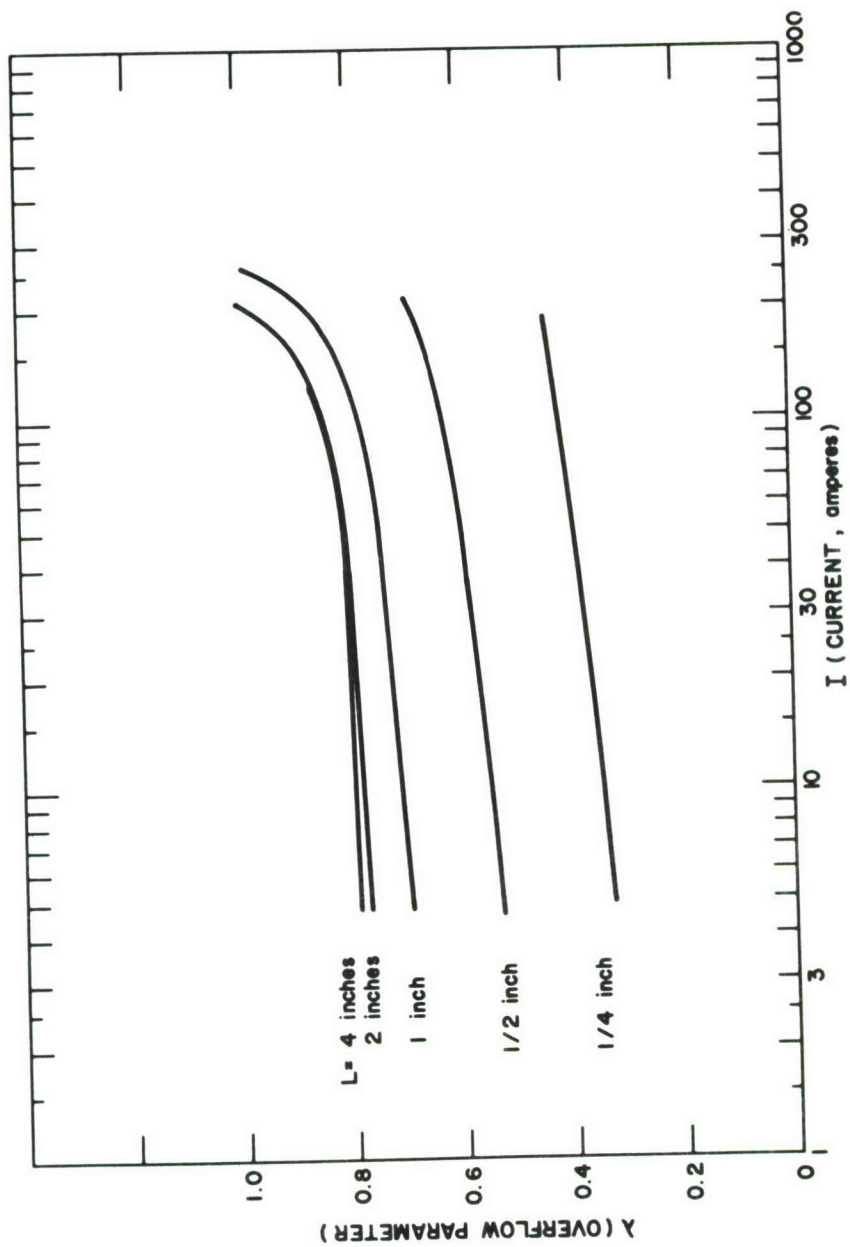


Figure 16. OVERFLOW PARAMETER  $\lambda$  VERSUS CURRENT AND CATHODE LENGTH (ONE EIGHTH INCH THORIATED TUNGSTEN CATHODE IN HELIUM)

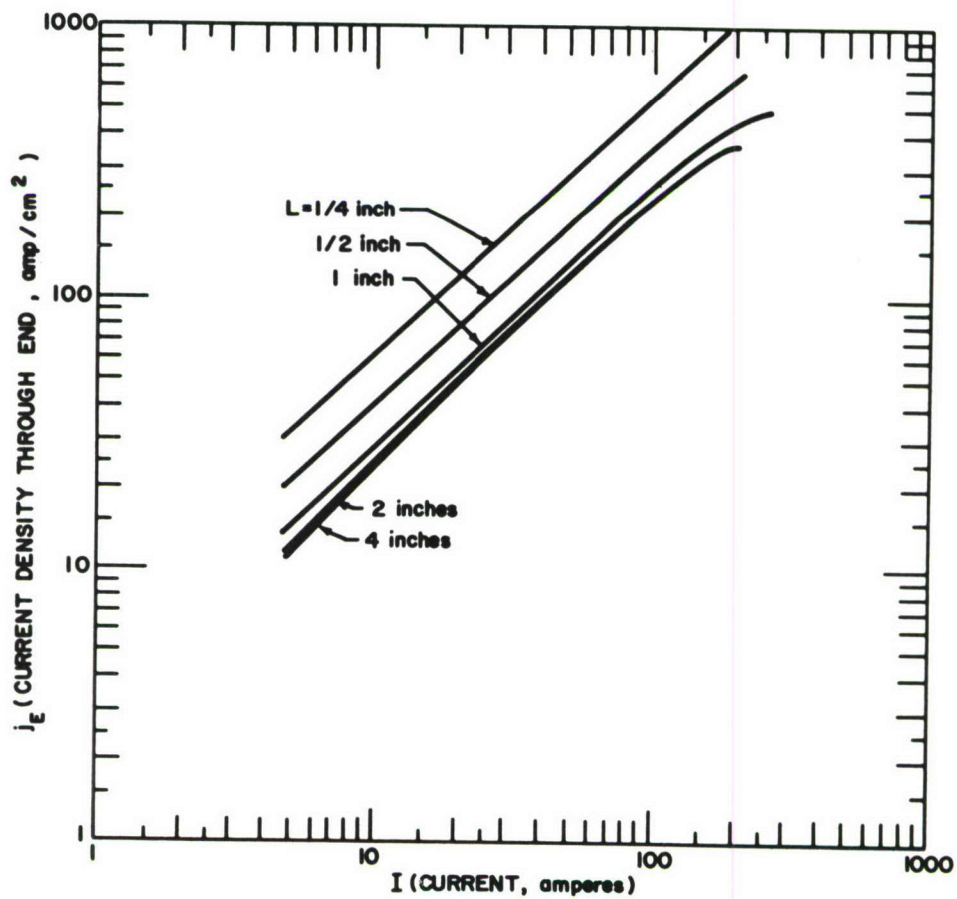


Figure 17 CURRENT DENSITY THROUGH END OF CATHODE VERSUS CURRENT AND CATHODE LENGTH (ONE EIGHTH INCH THORIATED TUNGSTEN CATHODE IN HELIUM)

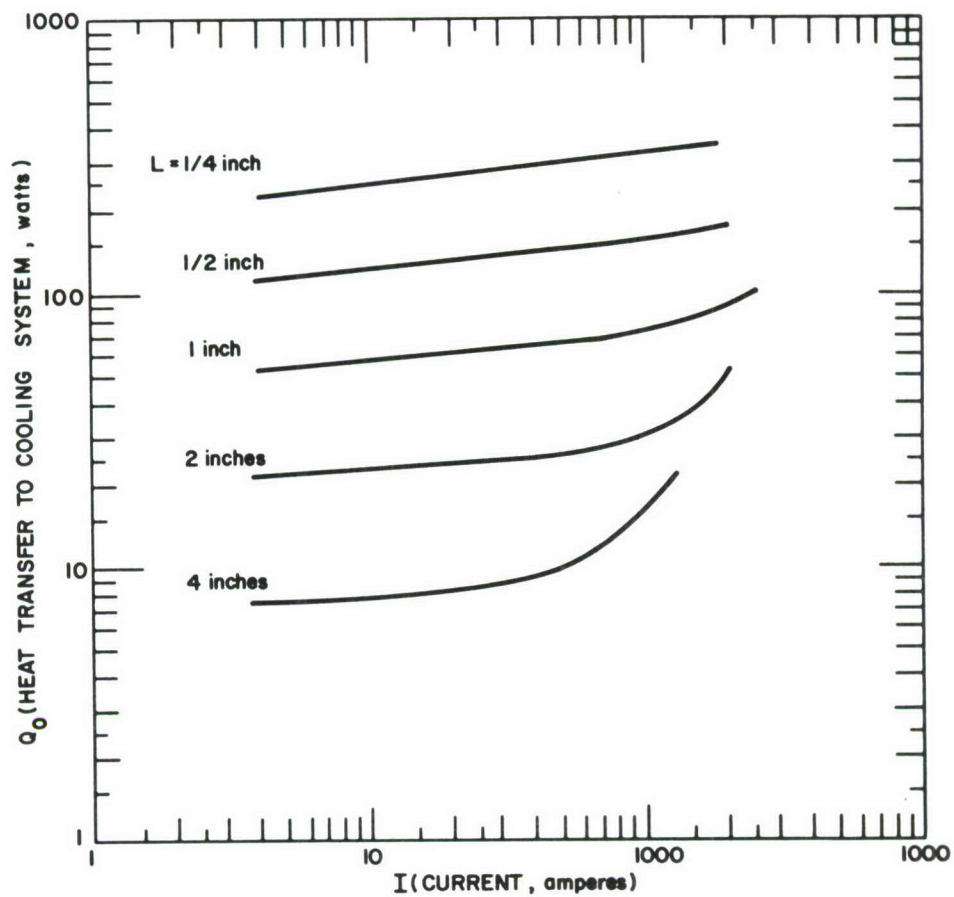


Figure 18 HEAT TRANSFER FROM CATHODE TO COOLING SYSTEM  
VERSUS CURRENT AND CATHODE LENGTH (ONE EIGHTH INCH  
THORIATED TUNGSTEN CATHODE IN HELIUM)



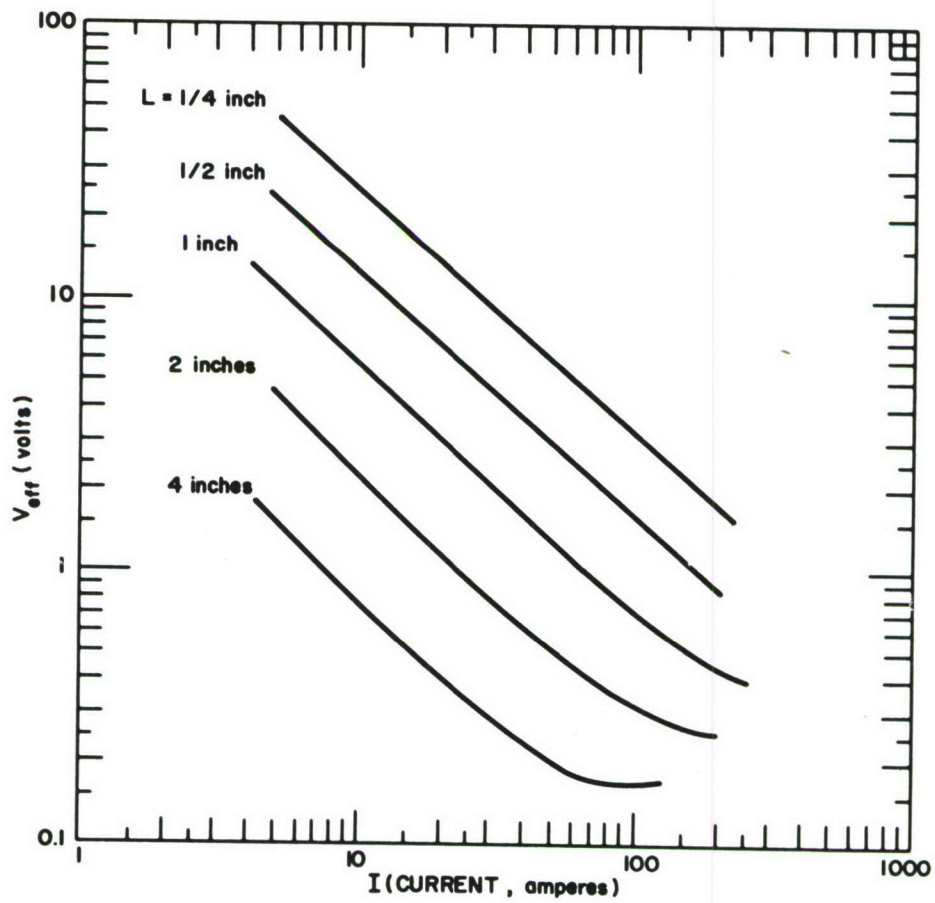


Figure 19 EFFECTIVE VOLTAGE FOR HEAT TRANSFER TO COOLING SYSTEM VERSUS CURRENT AND CATHODE LENGTH (ONE EIGHTH INCH THORIATED TUNGSTEN CATHODE IN HELIUM)

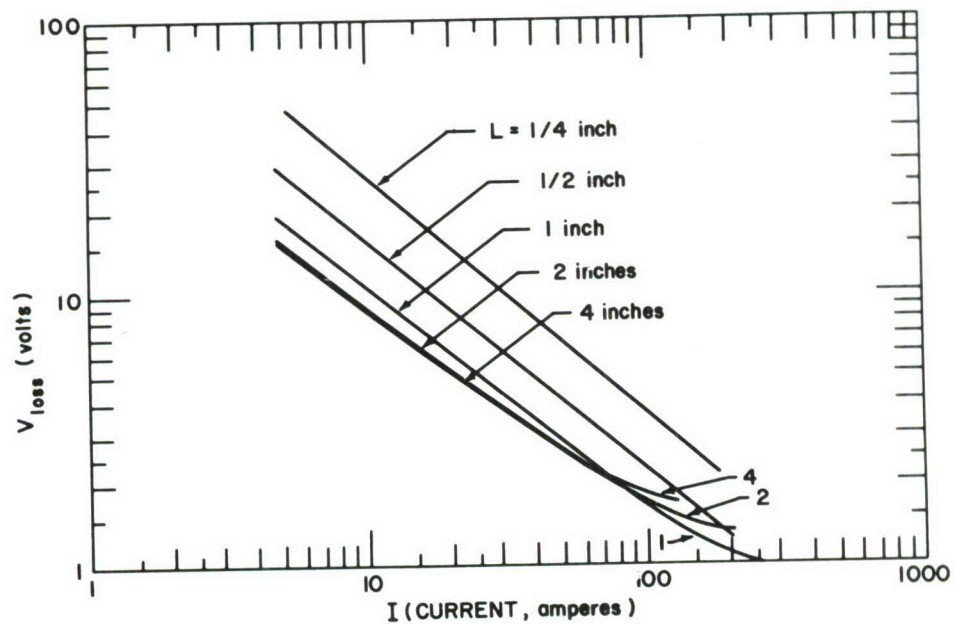


Figure 20 EFFECTIVE VOLTAGE FOR CATHODE POWER LOSS VERSUS CURRENT AND CATHODE LENGTH (ONE EIGHTH INCH THORIATED TUNGSTEN CATHODE IN HELIUM)

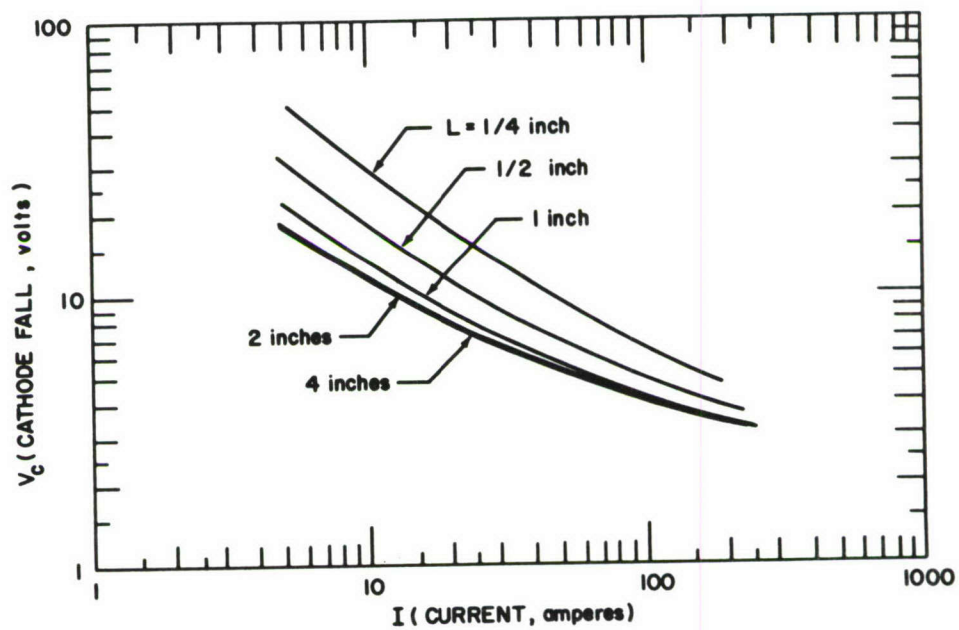


Figure 21 CATHODE FALL VOLTAGE VERSUS CURRENT AND CATHODE LENGTH (ONE EIGHTH INCH THORIATED TUNGSTEN CATHODE IN HELIUM)



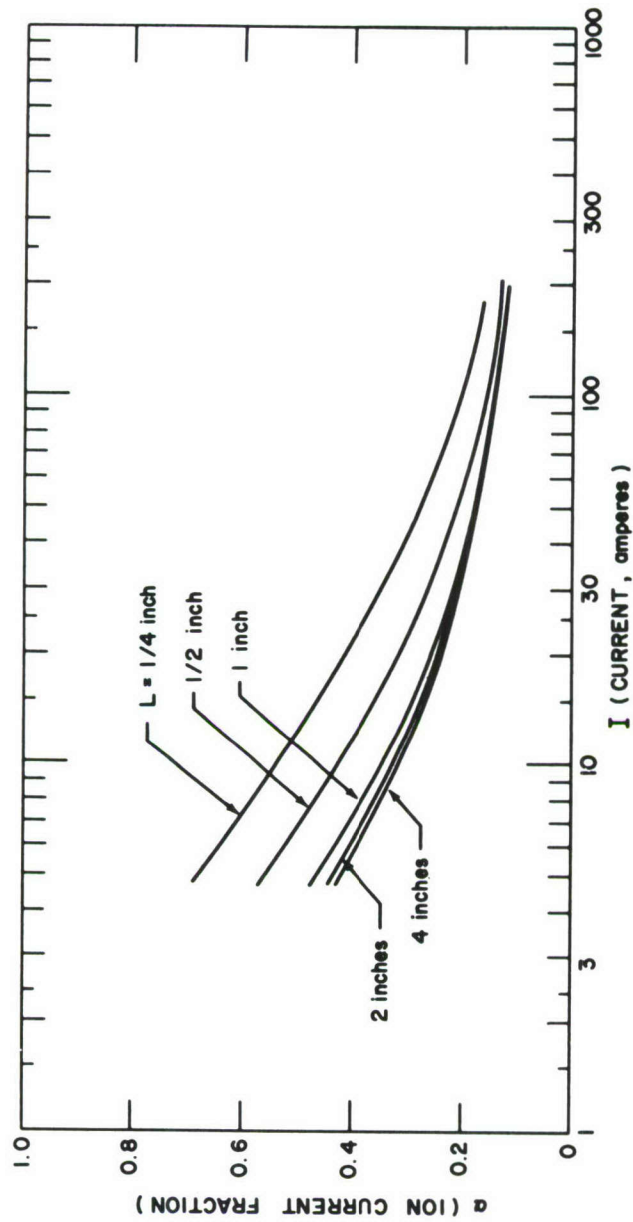


Figure 22 ION CURRENT FRACTION VERSUS CURRENT AND CATHODE LENGTH (ONE EIGHTH INCH THORIATED TUNGSTEN CATHODE IN HELIUM)

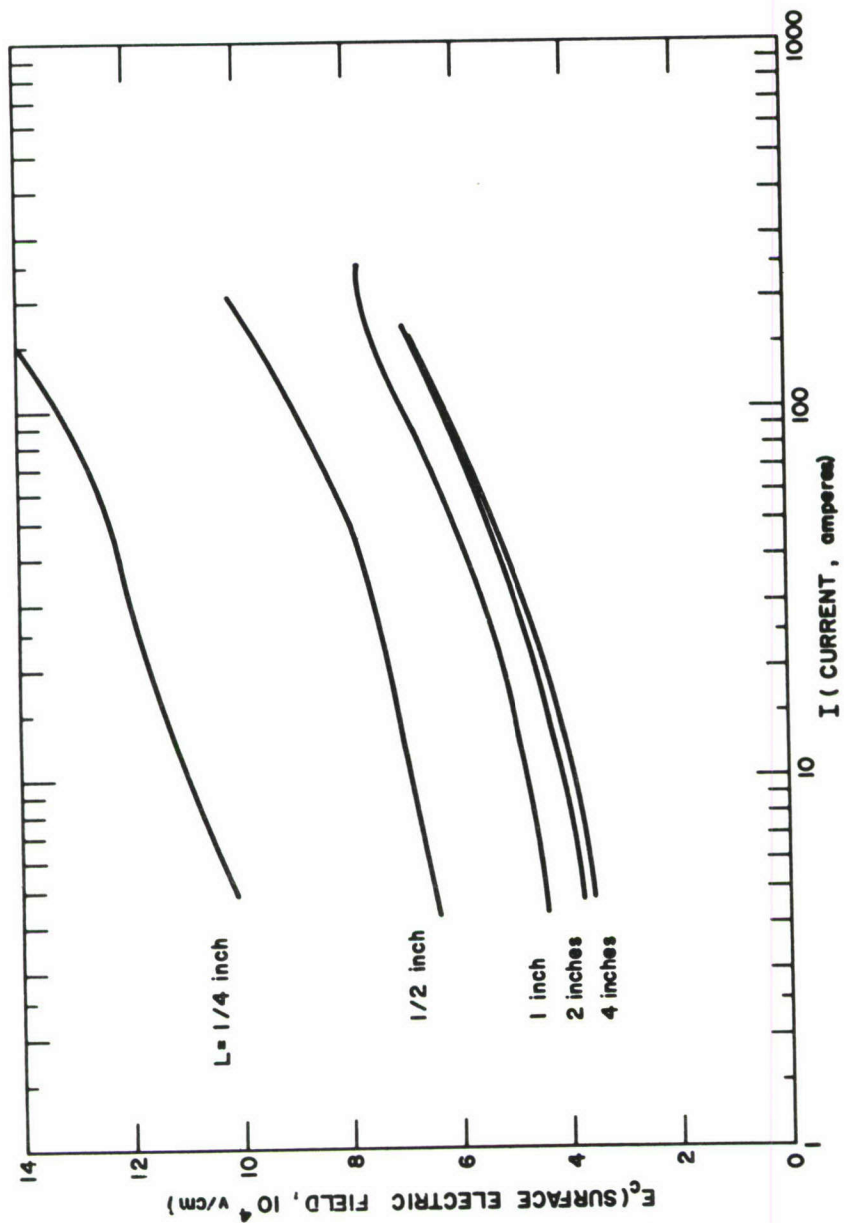


Figure 23 SURFACE ELECTRIC FIELD VERSUS CURRENT AND CATHODE LENGTH (ONE EIGHTH INCH THORIATED TUNGSTEN CATHODE IN HELIUM)

For example, the tip temperature (see figure 13) increases with decreasing cathode length; i. e., at a given total current the tip becomes hotter, the more strongly it is cooled. This result, paradoxical at first sight, is an effect of the dependence of arc overflow upon tip cooling. As the cathode length is decreased, the temperature gradient along the cathode increases. This steepening of the temperature gradient causes the overflow current density through the side of the cathode to cut off more rapidly with increasing distance from the tip, so that a larger fraction of the fixed total current flows through the end of the cathode rather than its sides. Since the current flow is predominantly thermionic, an increased current density through the end implies an increase of tip temperature, as shown in figure (13). For very long cathodes, the cooling is mainly radiative rather than conductive, so that increase of length beyond a certain point has no significant effect upon tip temperature. This limit has been reached, for the cases shown in figure 13, at a length of about 2 inches.

Further details of the mechanism just described are illustrated in figures 14 through 17. Figure 14 shows the "half height" (135) of the overflow region (defined as the distance from the tip at which one-half of the overflow current has entered the cathode) as a function of cathode length and total current. The decrease in overflow half height with decreasing length causes a larger fraction of the total current to enter the cathode through the end, as shown in figure 15. The turning upward of the curves in figure 14 at high currents is a consequence of Joule heating, which tends to decrease the temperature gradient in the tip region, and, thus, tends to increase the amount of overflow. The same effect can be seen in figures 13 and 15, as well as in figure 16, which shows the variation of the overflow parameter  $\lambda$ . Figure 17 gives the current density through the end surface of the cathode. The effects of Joule heating and overflow variation are apparent in these curves also.

The thermal power  $Q_0$  transferred from the cathode to its cooling system is shown in figure 18. This quantity is seen to be rather insensitive to current, except at high currents where Joule heating steepens the temperature gradient near the cold end of the cathode. However,  $Q_0$  is rather strongly dependent upon cathode length, because changes in length have no major effect upon tip temperature (see figure 13), while the heat flux at the cooled end is roughly proportional to  $(T_s - T_0)/L$ . The quantity  $Q_0/I$  is a voltage denoted by  $V_{eff}$ . This quantity is shown in figure 19. The total power dissipated by the cathode is the sum of  $Q_0$  and the radiative losses. The ratio of this total power loss to the total current is a voltage  $V_{loss}$ , the dependence of which upon length and current is shown in figure 20. This quantity is a measure of inefficiency; it is the voltage "wasted" by the cathode at a given current. Figure 20 shows that for long cathodes,  $V_{loss}$  becomes insensitive to length. The reason for this behavior is that long cathodes are cooled predominantly by radiation from the region near the



tip.  $V_{\text{loss}}$  decreases with increasing current, for a given cathode length up to the point at which Joule heating becomes important; beyond this point,  $V_{\text{loss}}$  increases with current. The onset of major Joule heating effects occurs at different currents for cathodes of different lengths, so that the curves cross one another in this region. At a given current, the optimum cathode length for minimizing power loss is the length corresponding to the lowest lying curve at that current.

The cathode fall voltage (see figure 21) decreases with increasing current and with increasing cathode length. The dependence upon length is a consequence of the assumption that the electrical heat flux to the cathode surface is proportional to  $V_c - \phi$ , equation (139m). As the cathode length decreases at a given current, the heat flux required to maintain the surface temperature rises, and  $V_c$  rises to meet this demand. This increasing demand for heat input is also met partially by an increase in the ion current fraction, as shown in figure 22. The corresponding increase of ion density in the space charge layer produces an increase of surface electric field with decreasing cathode length, as illustrated in figure 23.

### 3. Dependence upon Cold End Temperature

Just as figure 13 above shows that cooling the cathode more strongly causes its tip temperature to rise, figure 24 indicates that "heating" the cathode by raising the temperature of its "cold end" causes the tip temperature to fall a little. The explanation of this phenomenon is, of course, that an increase of  $T_0$  implies a decrease of the temperature gradient along the cathode, and, thus, leads to an increase in the amount of arc overflow, as shown in figure 25. The heat transfer  $Q_0$  from the cathode to the cooling system (see figure 26) decreases, as would be expected, when the cold end temperature rises.

### 4. Dependence upon Cathode Diameter

When the cathode diameter is varied at constant tip temperature, the total current varies almost in proportion to the area of the tip (i. e., as  $D^2$ ). For this reason, it appears that the operating behavior of cathodes of various diameters can best be compared using the current density  $j_0$  at the cold end as the independent variable in place of total current. If the cathode were operating in a truly one dimensional fashion (with no side radiation or overflow), the tip temperature and effective power loss voltage would depend upon current density only, not upon diameter.

Figure 27 shows the effect of non one dimensional effects upon the tip temperature for 1 inch long thoriated tungsten cathodes of various diameters operating in helium. The calculated tip temperature falls with decreasing cathode diameter because, as shown in figure 28, the fraction of the current carried by overflow through the sides of the cathode increases

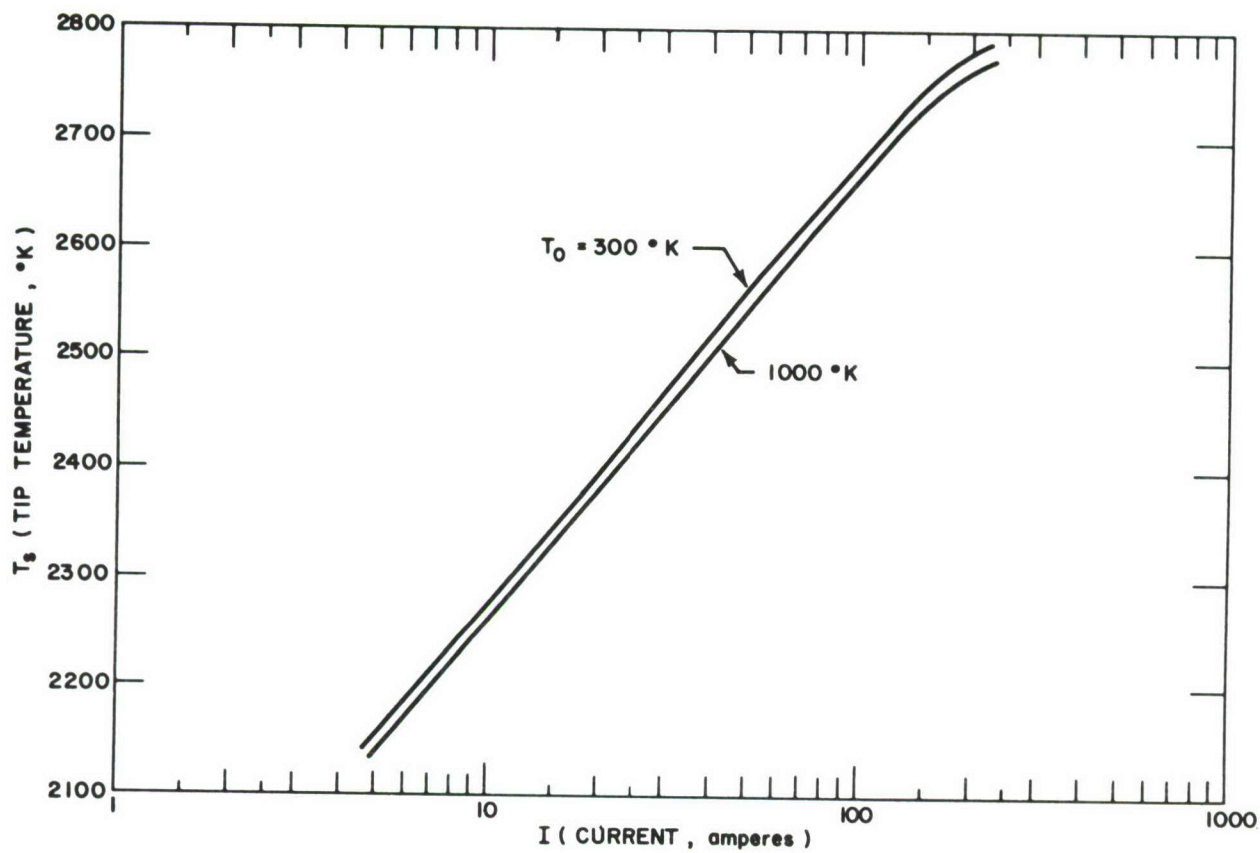


Figure 24 TIP TEMPERATURE VERSUS CURRENT AND COLD END TEMPERATURE (ONE EIGHTH INCH BY ONE INCH THORIATED TUNGSTEN CATHODE IN HELIUM)

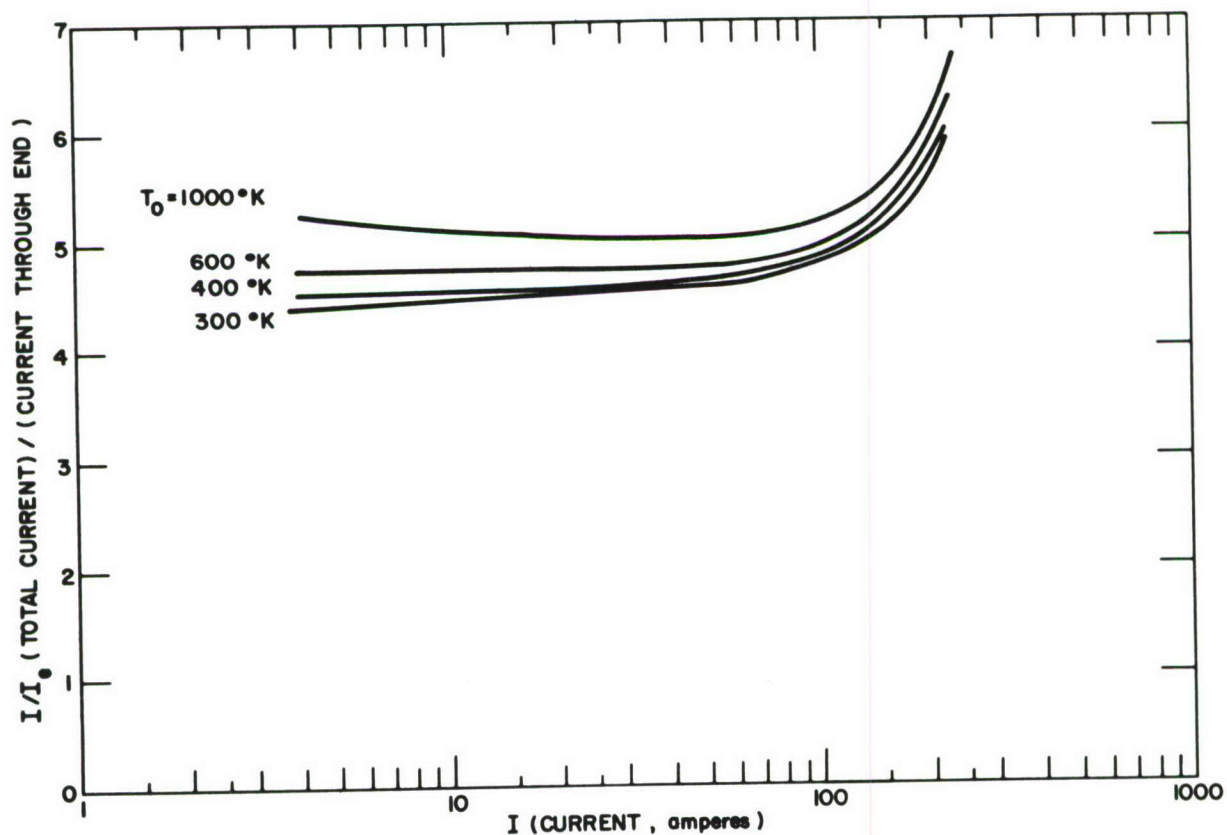


Figure 25 RATIO OF TOTAL CURRENT TO CURRENT ENTERING THROUGH  
END OF CATHODE VERSUS CURRENT AND COLD END TEMPERATURE  
(ONE EIGHTH INCH BY ONE INCH THORIATED TUNGSTEN  
CATHODE IN HELIUM)



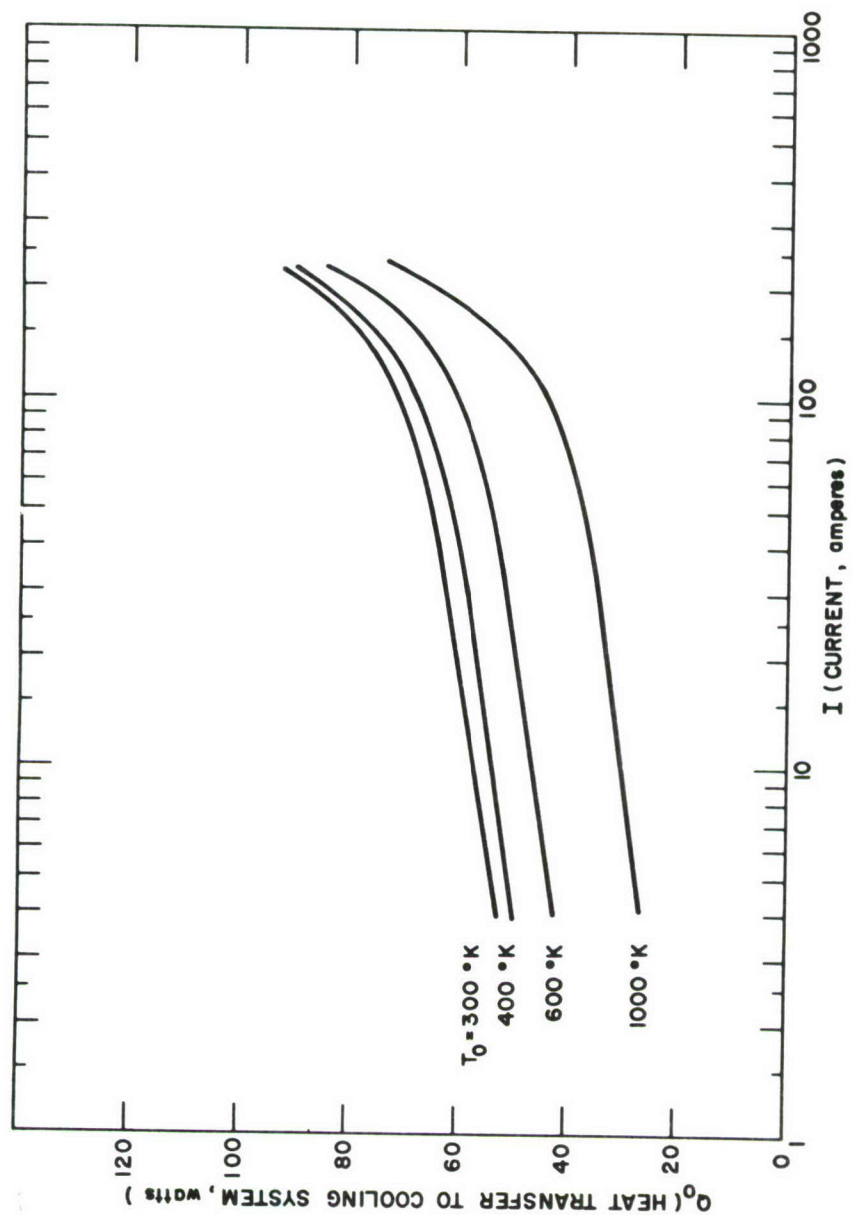


Figure 26 HEAT TRANSFER FROM CATHODE TO COOLING SYSTEM VERSUS  
CURRENT AND COLD END TEMPERATURE (ONE EIGHTH INCH BY  
ONE INCH THORIATED TUNGSTEN CATHODE IN HELIUM)

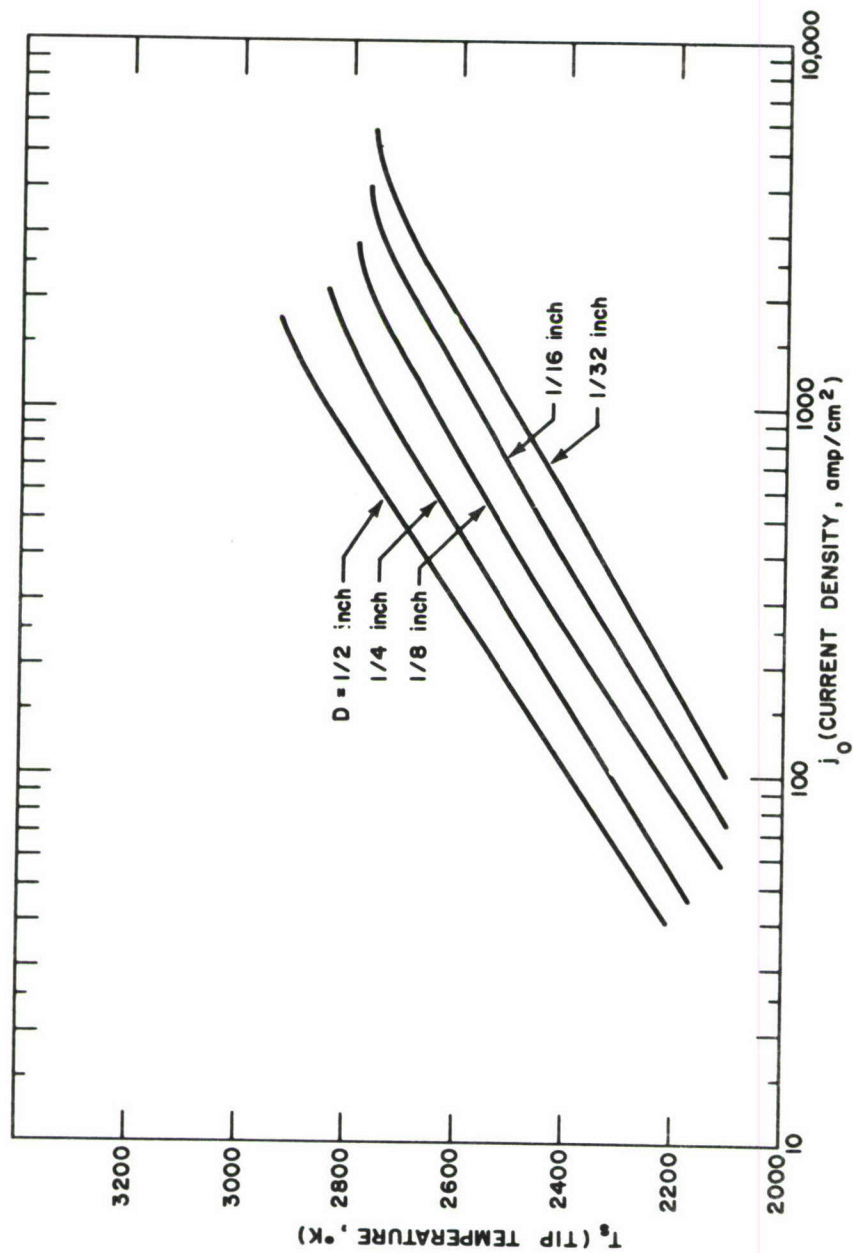


Figure 27 TIP TEMPERATURE VERSUS CURRENT DENSITY AND CATHODE DIAMETER (ONE INCH THORIATED TUNGSTEN CATHODE IN HELIUM)

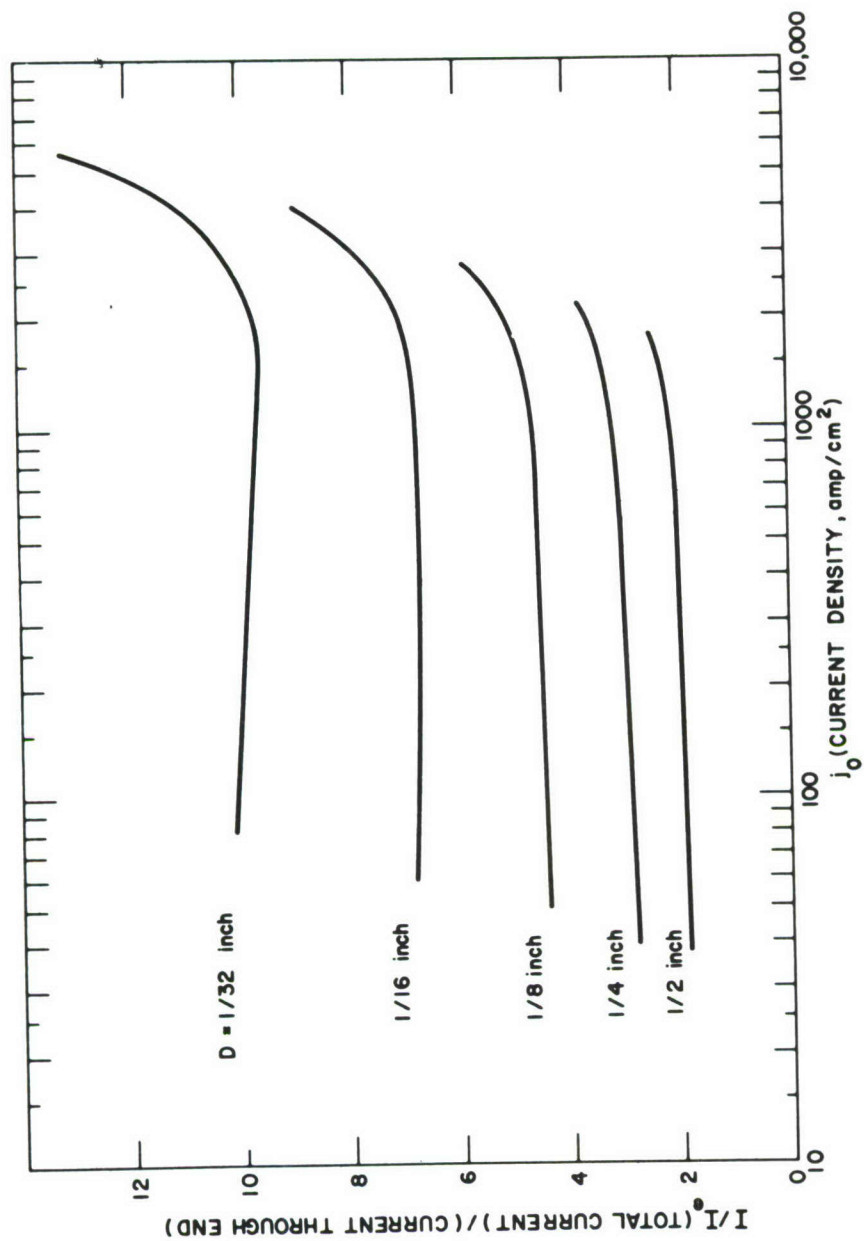


Figure 28 RATIO OF TOTAL CURRENT TO CURRENT ENTERING THROUGH  
END OF CATHODE VERSUS CURRENT DENSITY AND CATHODE  
DIAMETER (ONE INCH THORIATED TUNGSTEN  
CATHODE IN HELIUM)



as the diameter is decreased. This occurs because the height of the overflow region is roughly independent of diameter for a given current density, so that the overflow current varies about as  $D$  while the current through the end goes as  $D^2$ .

The effective voltage for heat transfer to the cooling system (see figure 29) also decreases with the cathode diameter. In this case, the departure from one dimensional behavior is caused by side radiation. The radiative heat loss is roughly proportional to  $D$ , while the heat conduction toward the cold end varies as  $D^2$ , so that a decrease in diameter favors the former process at the expense of the latter. The same effect shows up also in the curves of effective voltage for cathode power loss, figure 30. Here, the fact that the smaller cathodes are more strongly cooled (by radiation) than the larger ones implies that the smaller cathodes must lose more power to operate at a given current density. In accord with this argument, the ion current fraction (see figure 31) also rises with decreasing cathode diameter. The surface electric field (see figure 32) decreases with cathode diameter because the decrease of surface current density, shown in figure 28, more than offsets the rise of  $\alpha$  (see figure 31) in Mackeown's equation (8a).

#### 5. Dependence upon Cathode Material

The theoretical effects of low work function additives upon tungsten cathode performance are illustrated in figures 33 through 39, for 1 inch by 1/8 inch cathodes operating in helium. The primary effect of such additives is a reduction of tip operating temperature, as shown in figure 33. Pure tungsten, even if it could be made to operate in the spotless mode (which is doubtful), would approach its melting point ( $3653^\circ\text{K}$ ) at a current of a few hundred amperes. In contrast, tungsten impregnated with barium oxide operates, according to these calculations, below  $2000^\circ\text{K}$  over the entire current range considered. This large difference in operating temperatures is primarily a consequence of the difference in work functions assumed (Table 6), but is also exaggerated by the presence of a greater tendency toward arc overflow in the impregnated cathodes as shown in figure 34.

The reduction in surface temperature resulting from use of low work function additives significantly reduces the cathode losses. The effective voltage  $V_{\text{eff}}$  for heat transfer to the cooling system (see figure 35) is lower by about a factor of 2 in barium oxide impregnated tungsten as compared with pure tungsten. The differences in total power loss as represented by  $V_{\text{loss}}$  are even larger (see figure 36), because the radiative loss increases in a nonlinear fashion with increasing temperature. The reduction in power requirements for the impregnated cathodes results in a lowering of the cathode fall voltage (see figure 32) and the ion current fraction (see figure 38), in accordance with qualitative arguments given previously.

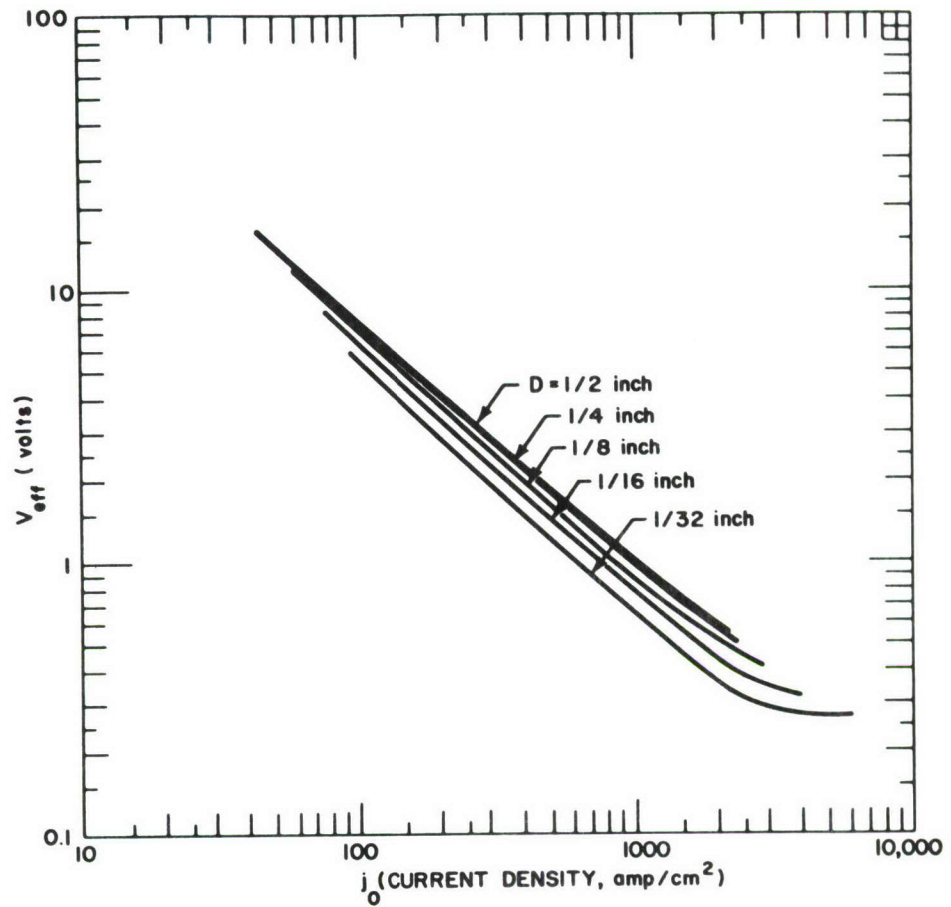


Figure 29 EFFECTIVE VOLTAGE FOR HEAT TRANSFER TO COOLING SYSTEM VERSUS CURRENT DENSITY AND CATHODE DIAMETER (ONE INCH THORIATED TUNGSTEN CATHODE IN HELIUM)

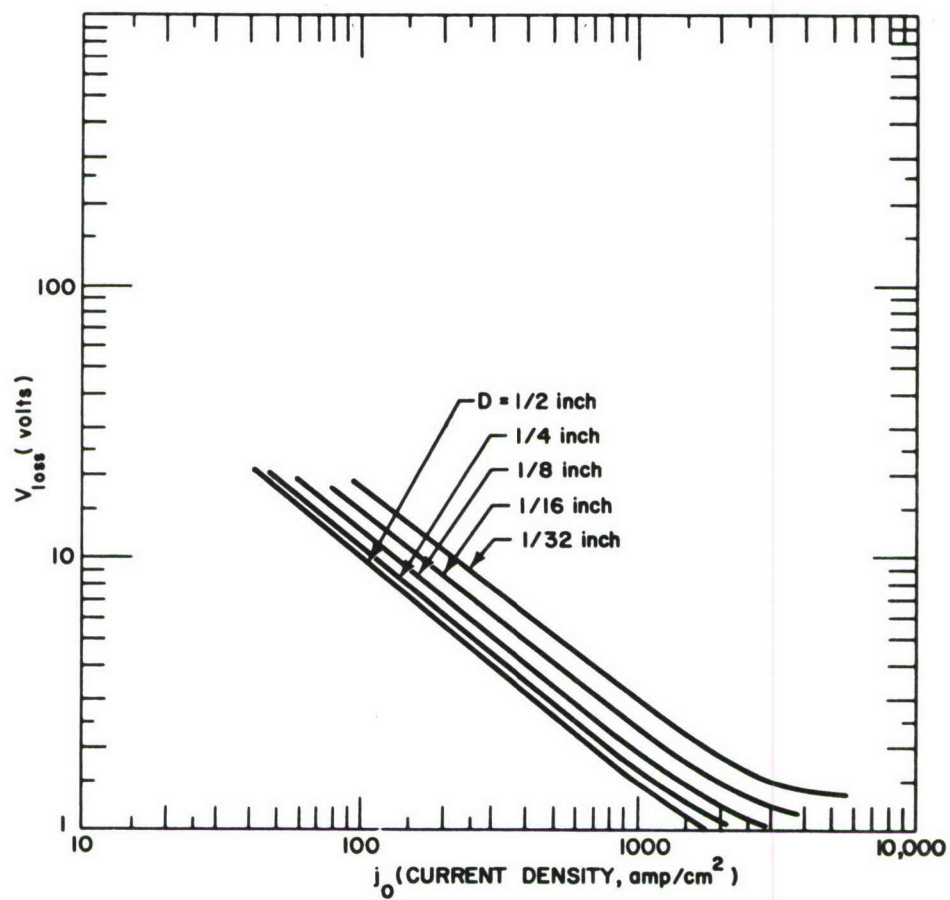


Figure 30 EFFECTIVE VOLTAGE FOR CATHODE POWER LOSS VERSUS CURRENT DENSITY AND CATHODE DIAMETER (ONE INCH THORIATED TUNGSTEN CATHODE IN HELIUM)



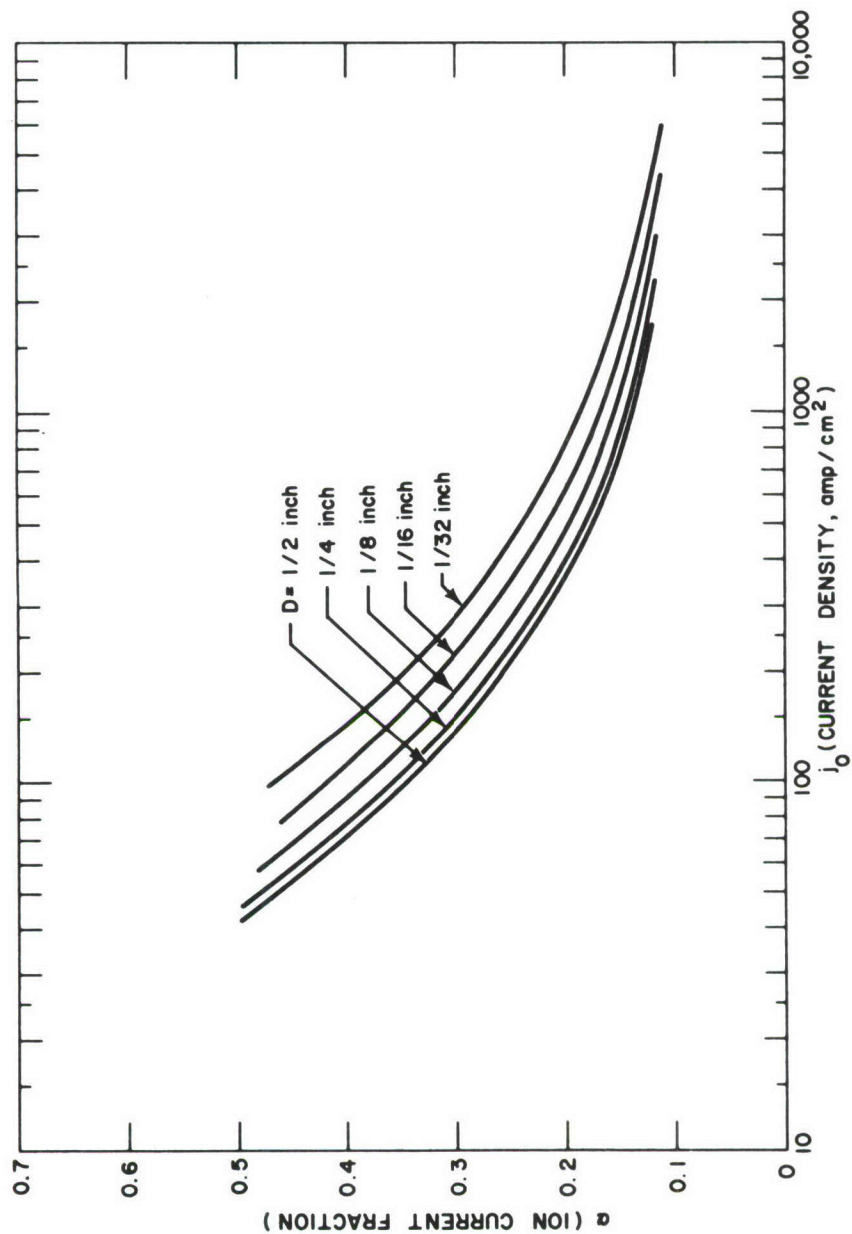


Figure 31 ION CURRENT FRACTION VERSUS CURRENT DENSITY AND  
CATHODE DIAMETER (ONE INCH THORIATED TUNGSTEN  
CATHODE IN HELIUM)

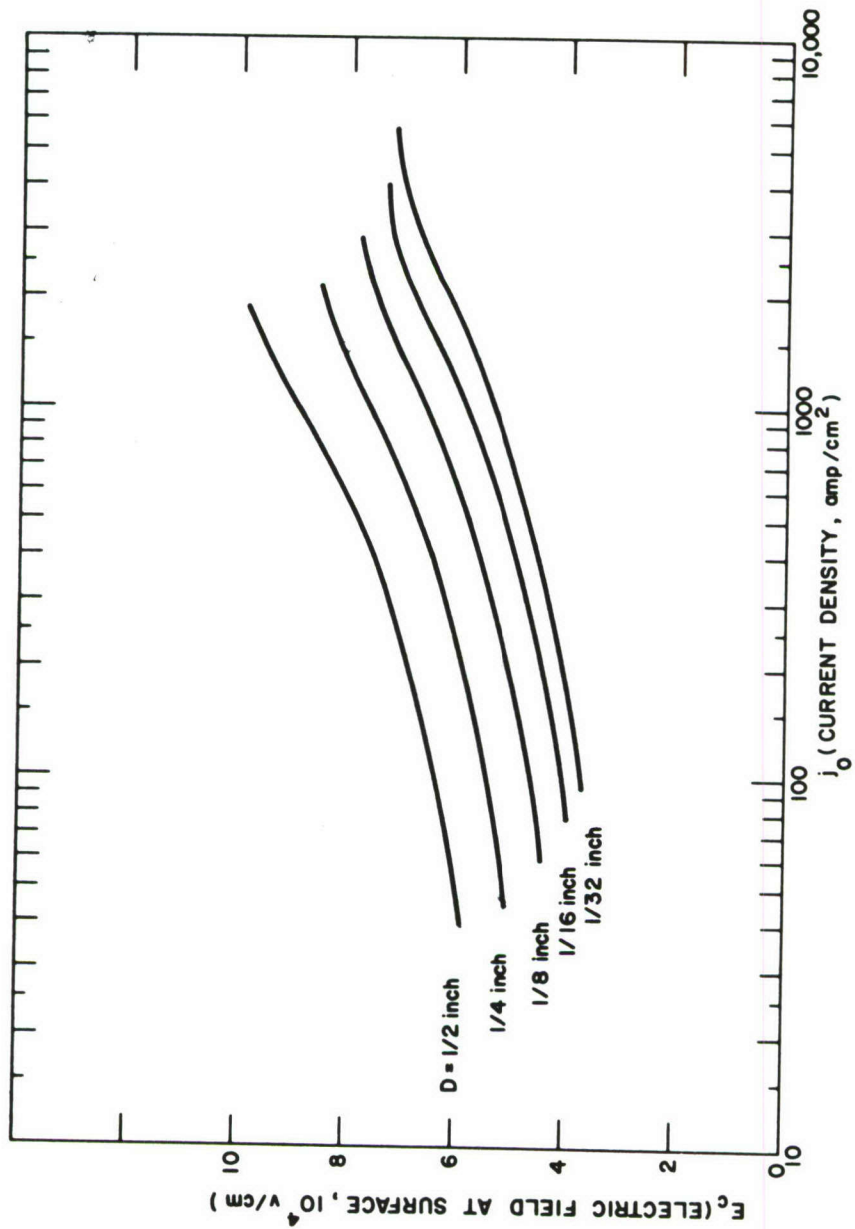


Figure 32 SURFACE ELECTRIC FIELD VERSUS CURRENT DENSITY AND CATHODE DIAMETER (ONE INCH THORIATED TUNGSTEN CATHODE IN HELIUM)

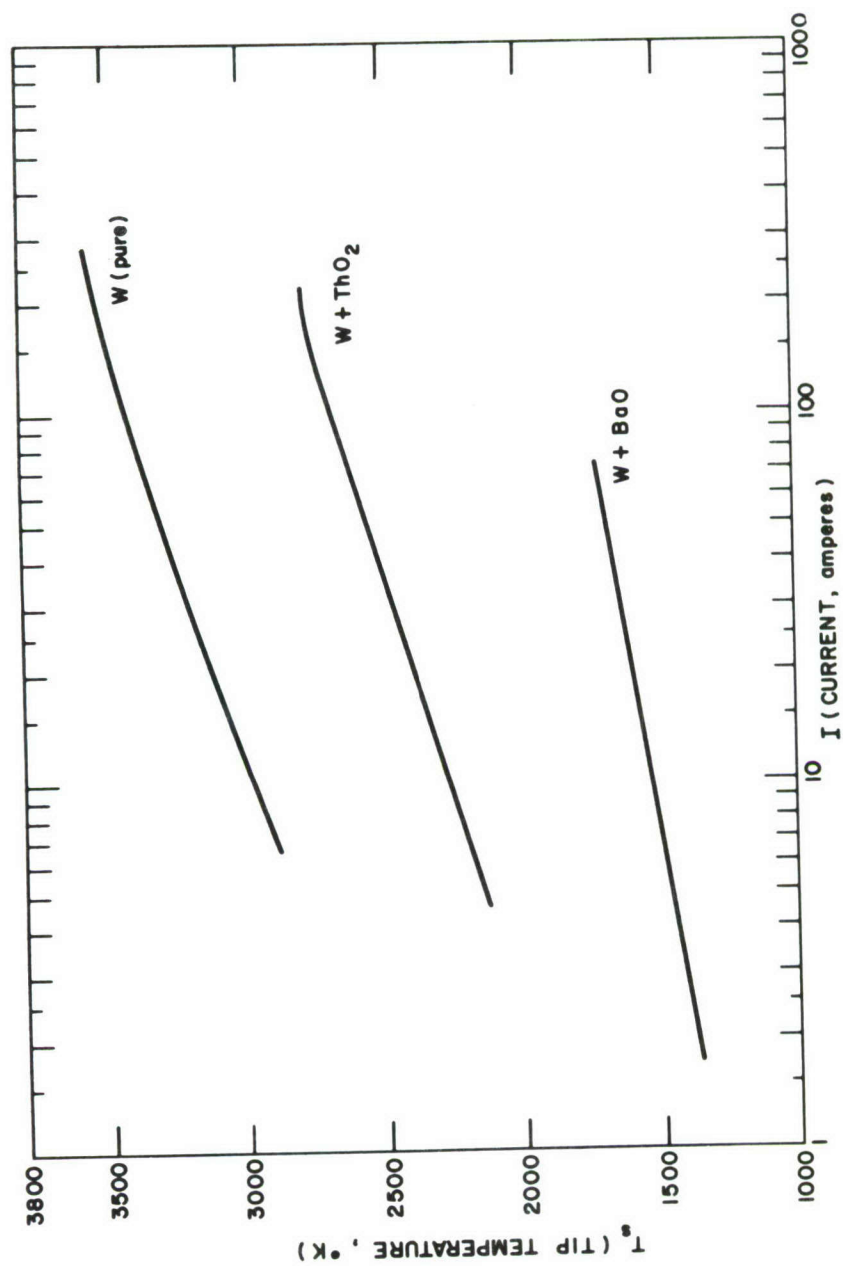


Figure 33 TIP TEMPERATURE VERSUS CURRENT AND CATHODE MATERIAL  
(ONE INCH BY ONE EIGHTH INCH CATHODES IN HELIUM)



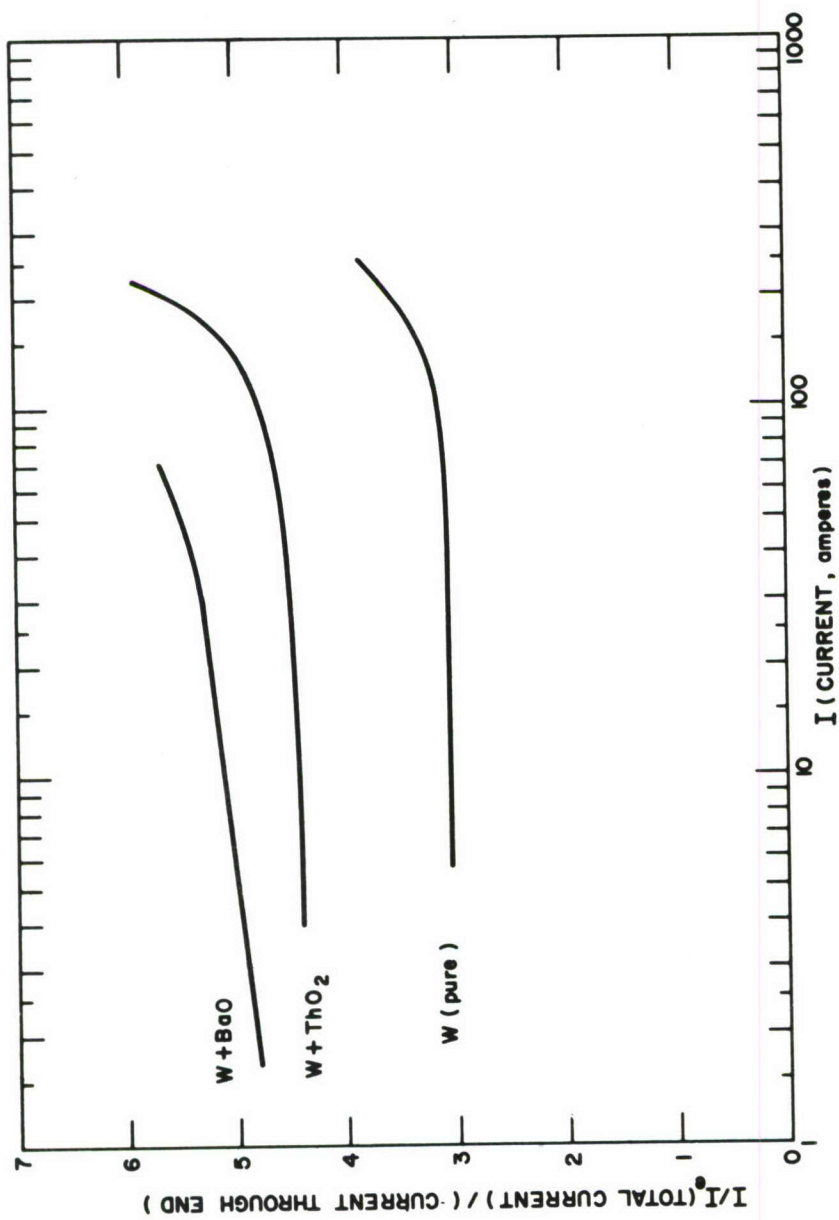


Figure 34 RATIO OF TOTAL CURRENT TO CURRENT ENTERING THROUGH  
END OF CATHODE VERSUS CURRENT AND CATHODE MATERIAL  
(ONE INCH BY ONE EIGHTH INCH CATHODES IN HELIUM)

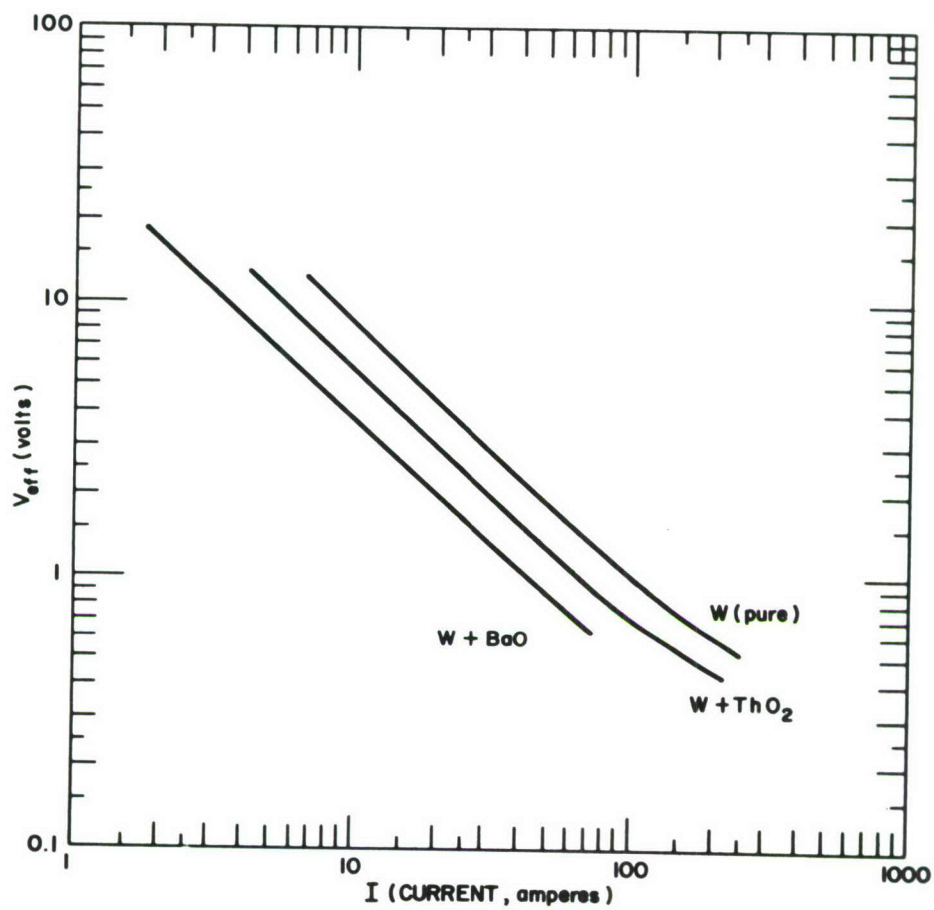


Figure 35 EFFECTIVE VOLTAGE FOR HEAT TRANSFER TO COOLING SYSTEM VERSUS CURRENT AND CATHODE MATERIAL (ONE INCH BY ONE EIGHTH INCH CATHODES IN HELIUM)

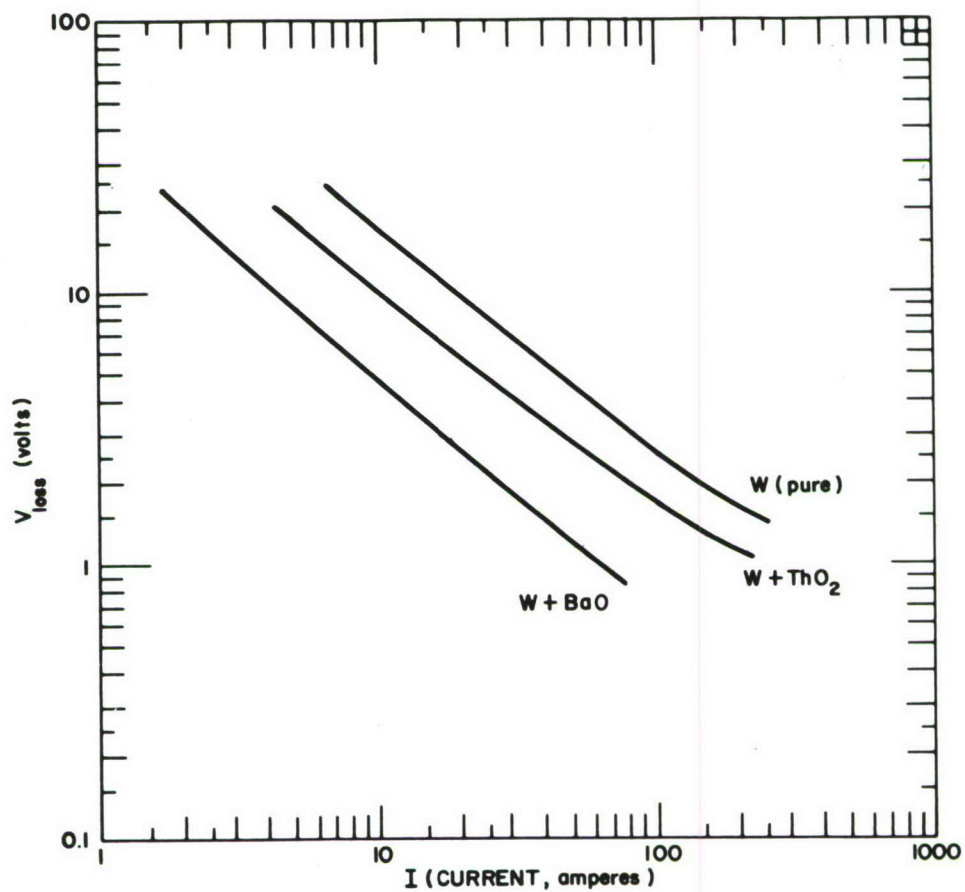


Figure 36 EFFECTIVE VOLTAGE FOR CATHODE POWER LOSS VERSUS CURRENT AND CATHODE MATERIAL  
(ONE INCH BY ONE EIGHTH INCH CATHODES IN HELIUM)



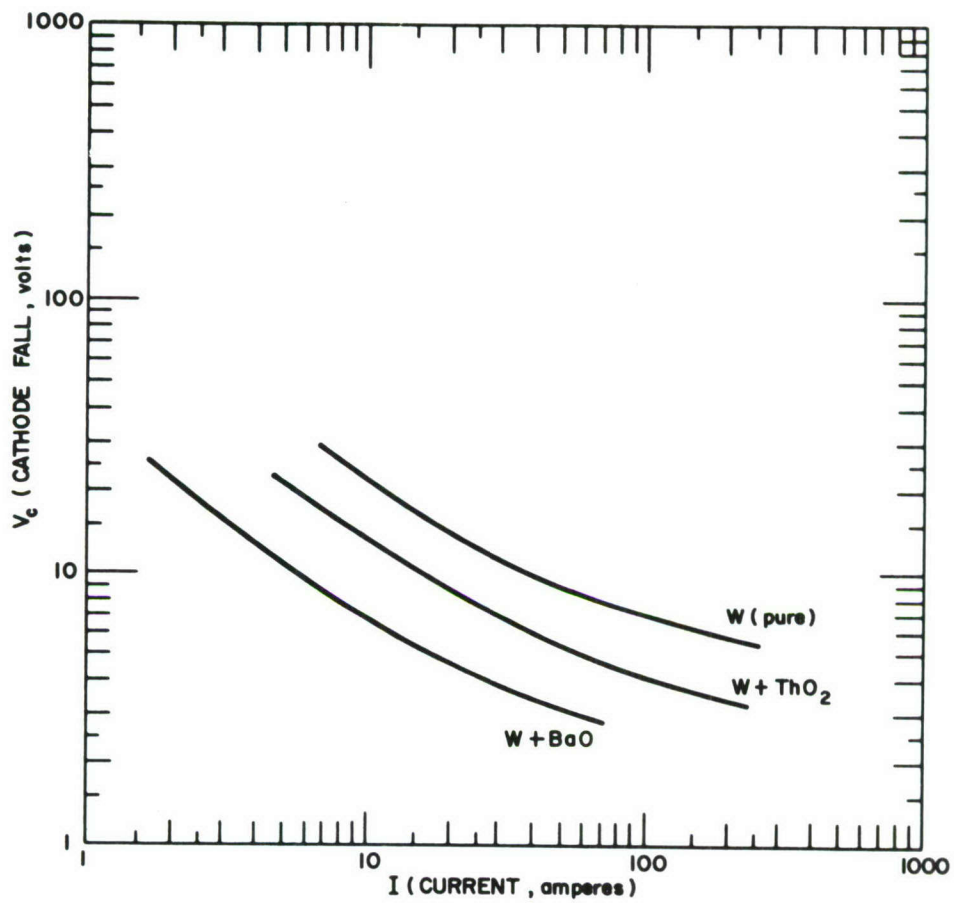


Figure 37 CATHODE FALL VOLTAGE VERSUS CURRENT AND CATHODE MATERIAL (ONE INCH BY ONE EIGHTH INCH CATHODES IN HELIUM)

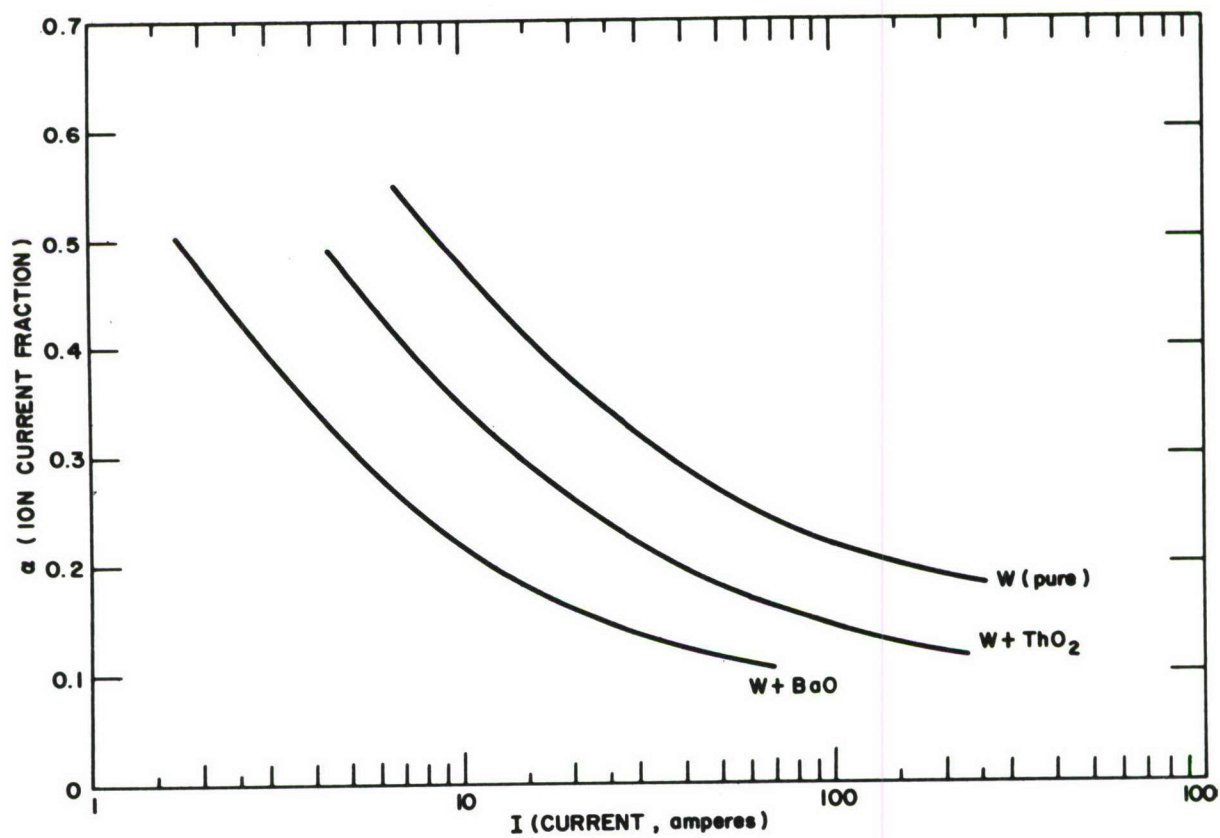


Figure 38 ION CURRENT FRACTION VERSUS CURRENT AND CATHODE MATERIAL (ONE INCH BY ONE EIGHTH INCH CATHODES IN HELIUM)

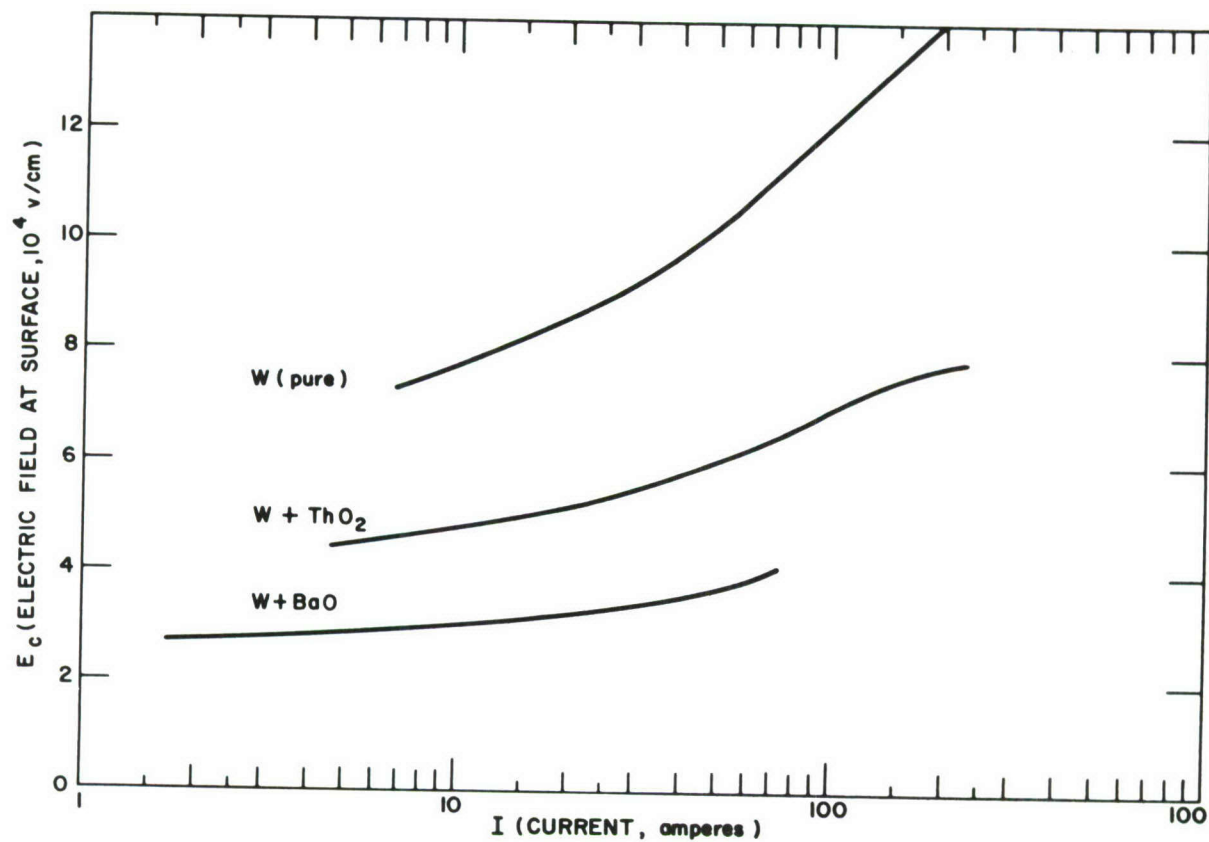


Figure 39 SURFACE ELECTRIC FIELD VERSUS CURRENT AND CATHODE MATERIAL (ONE INCH BY ONE EIGHTH INCH CATHODES IN HELIUM)



The decrease in ion current fraction, in turn, entails a reduction in the surface electric field, as shown in figure 39.

The predictions of cathode performance represented by figures 33 through 39 are based upon the hypothesis that the cathodes under consideration are operating in the spotless mode in helium. It is very doubtful that a pure tungsten cathode would obey this hypothesis. At the lower currents (below about 20 amperes), even thoriated tungsten tends to operate in the spot mode, as discussed in section V below.

## 6. Dependence upon Gas Properties

Figures 40 through 44 show the differences in theoretical characteristics for a 1 inch by 1/8 inch thoriated tungsten cathode operating in the spotless mode in three different gases, helium, argon, and nitrogen. The tip temperature (see figure 40), is highest in helium and lowest in argon; however, the differences are not large, covering a range of about 60°C. These differences in tip temperature result mainly from the variation of surface electric field, shown in figure 41, which in turn is a consequence of the differences in ionic mass. The ion current fraction is noticeably lower in helium than in argon and nitrogen, primarily because the high ionization potential of helium makes it possible for a smaller ion current to deliver sufficient heat to maintain the cathode surface temperature. Figures 43 and 44 show that the differences in overflow and heat transfer to the cooling system are negligible under the assumptions upon which the theoretical model is based.

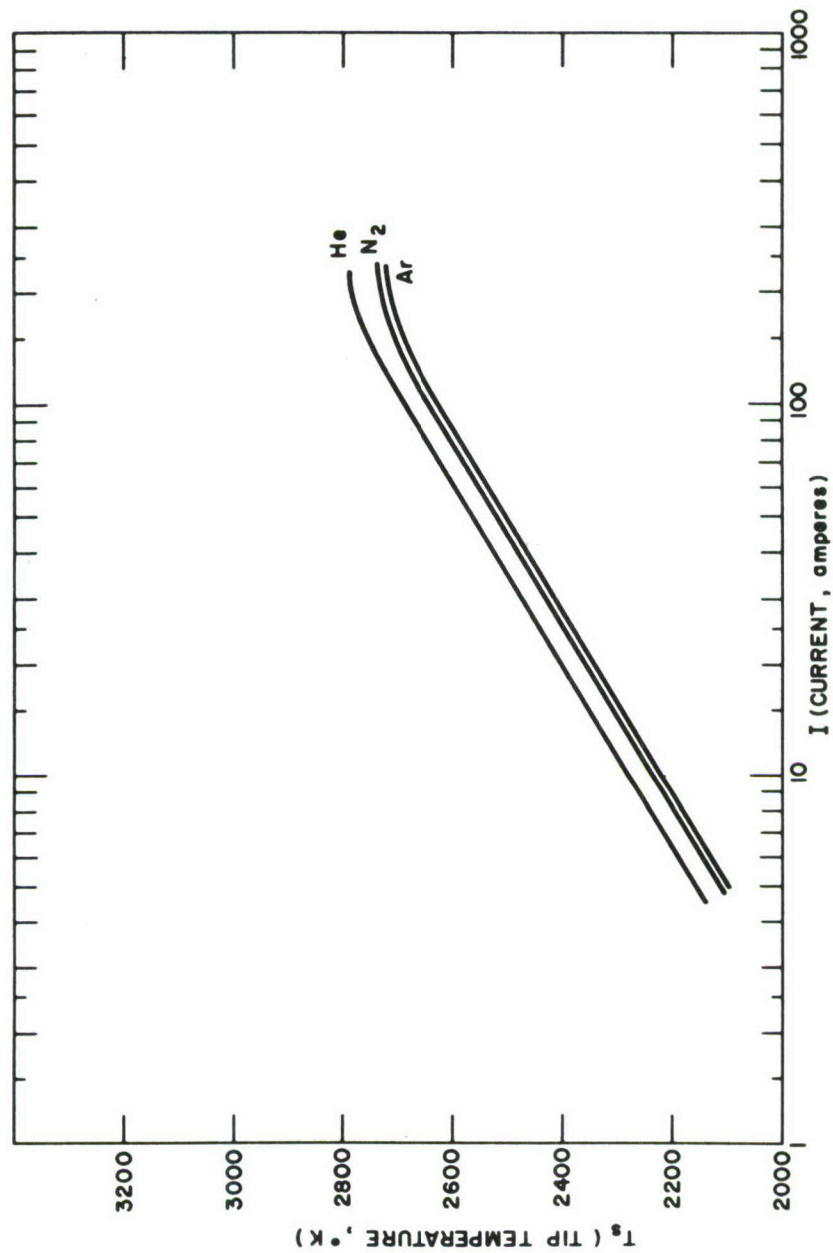


Figure 40 TIP TEMPERATURE VERSUS CURRENT AND GAS TYPE (ONE INCH BY ONE EIGHTH INCH THORIATED TUNGSTEN CATHODE)

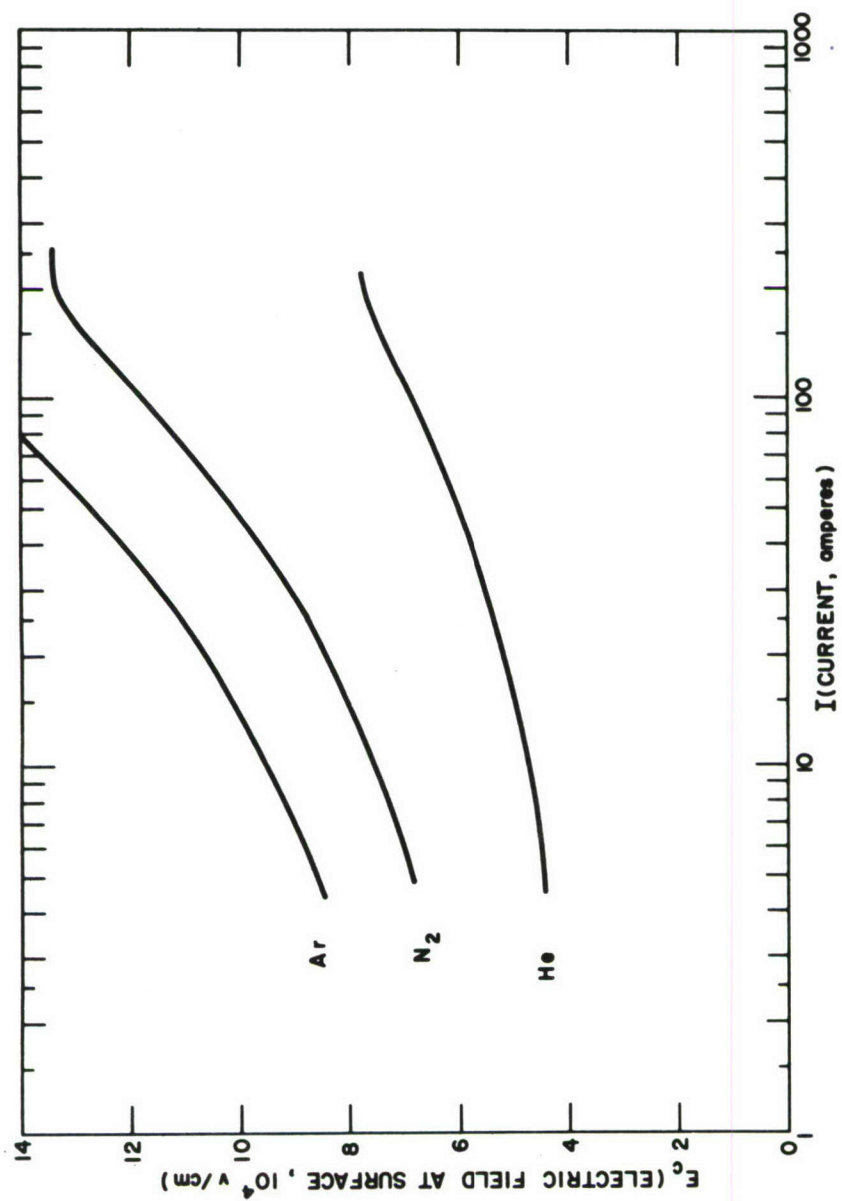


Figure 41 SURFACE ELECTRIC FIELD VERSUS CURRENT AND GAS TYPE (ONE INCH BY ONE EIGHTH INCH THORIATED TUNGSTEN CATHODE)



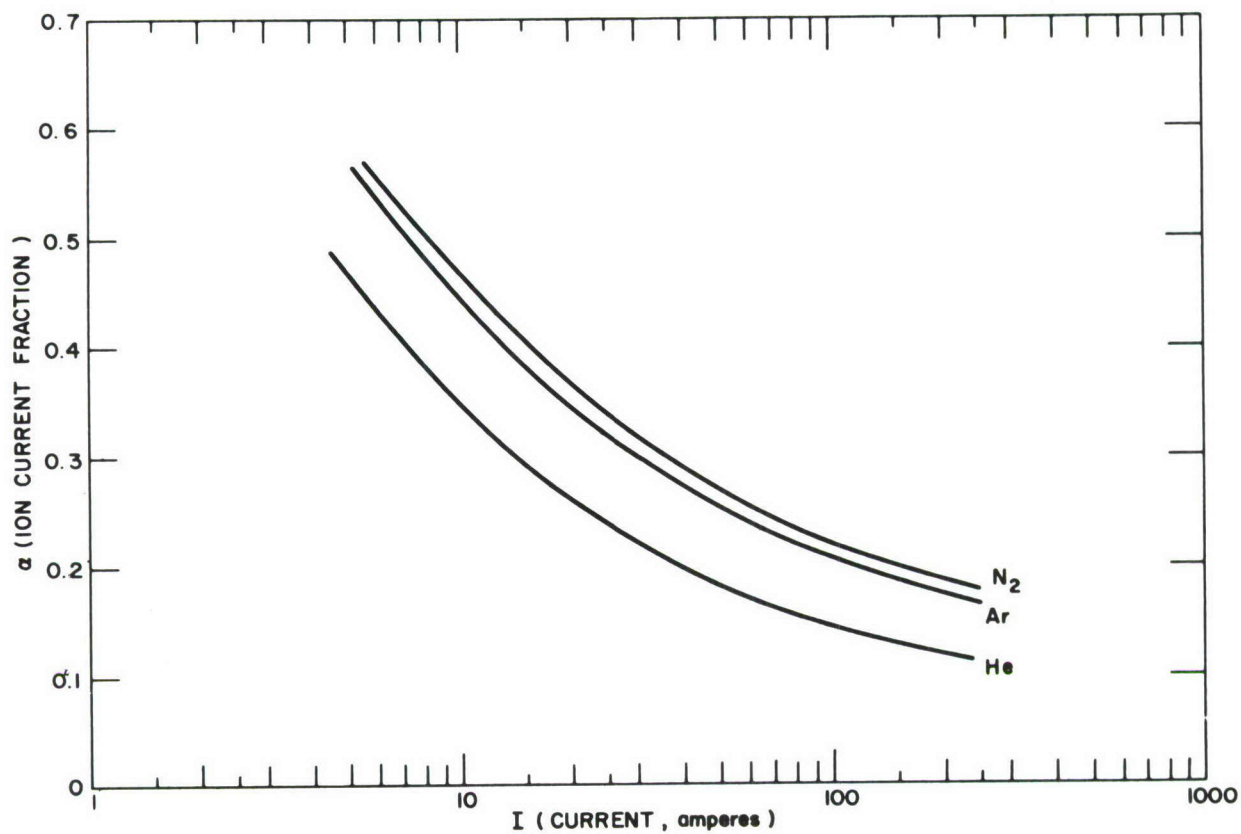


Figure 42 ION CURRENT FRACTION VERSUS CURRENT AND GAS TYPE  
(ONE INCH BY ONE EIGHTH INCH THORIATED TUNGSTEN CATHODE)

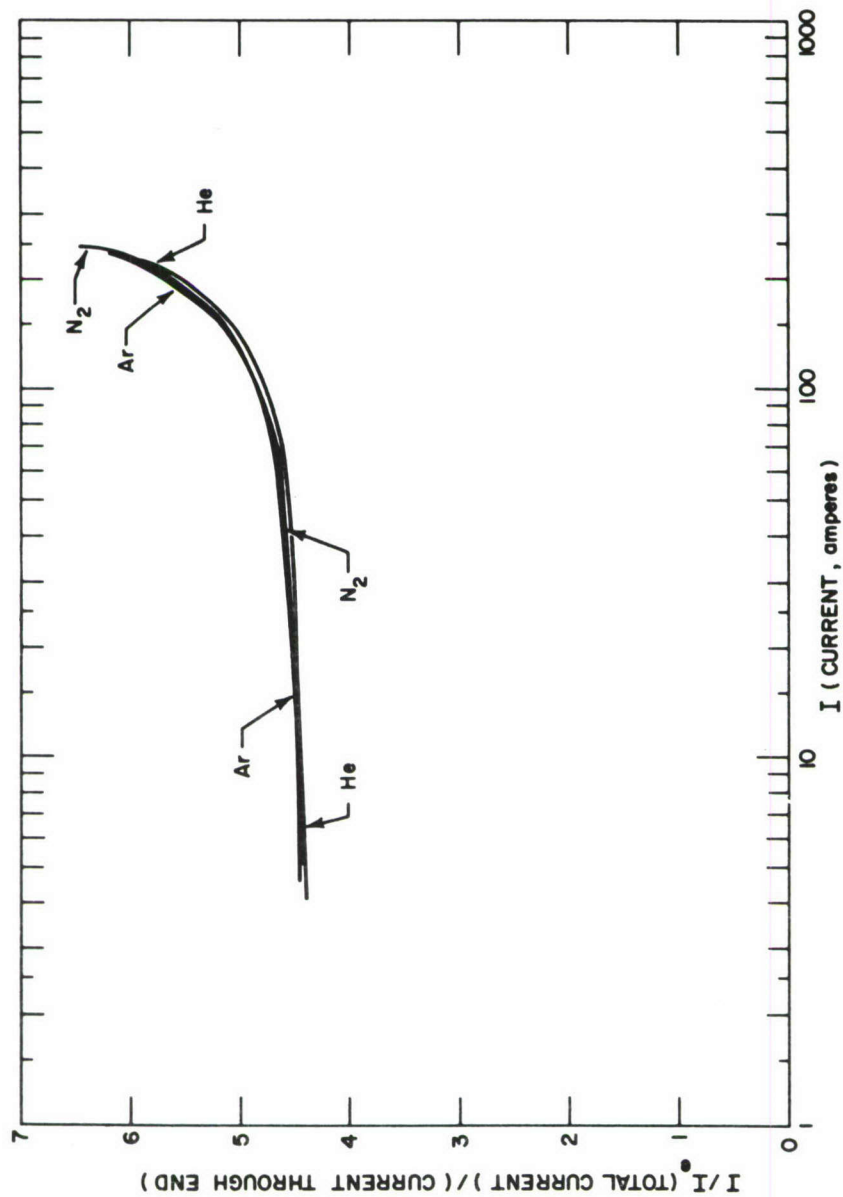


Figure 43 RATIO OF TOTAL CURRENT TO CURRENT ENTERING THROUGH END OF CATHODE VERSUS CURRENT AND GAS TYPE (ONE INCH BY ONE EIGHTH INCH THORIATED TUNGSTEN CATHODE)

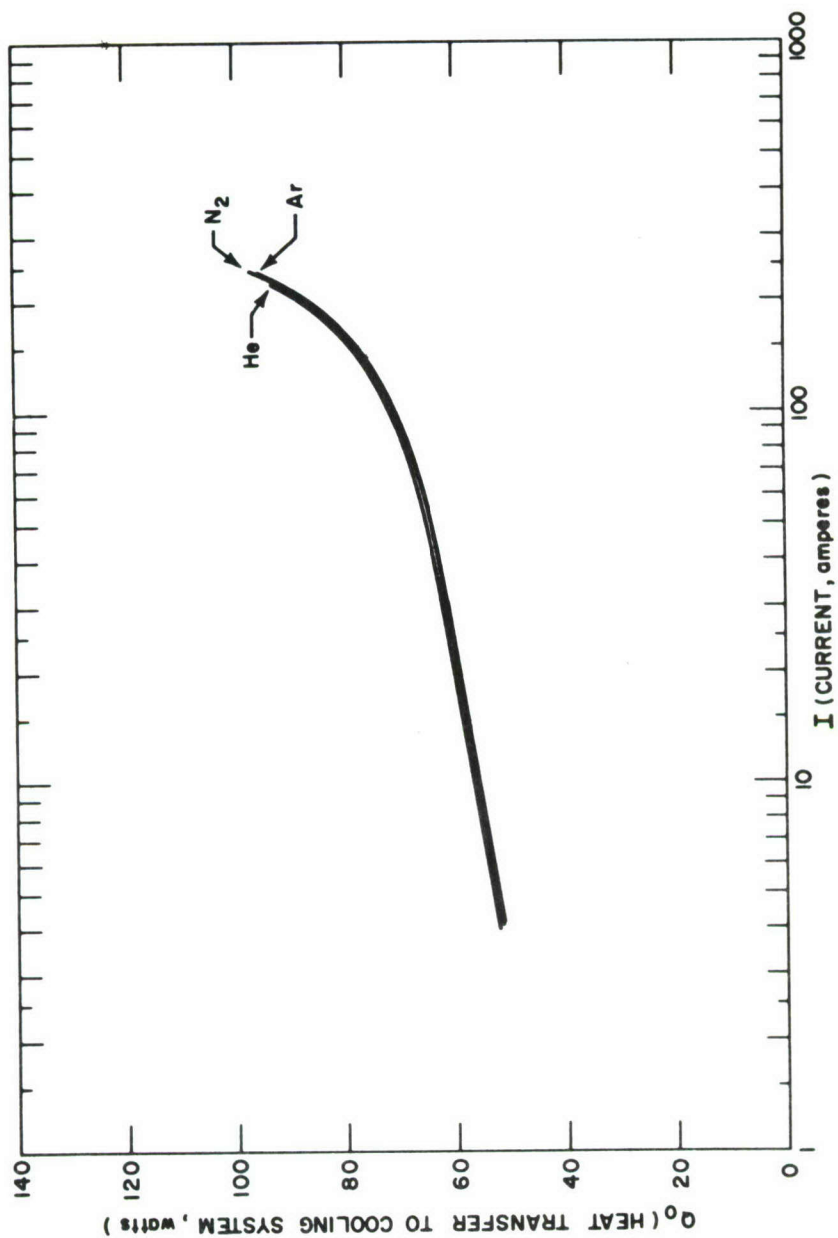


Figure 44 HEAT TRANSFER FROM CATHODE TO COOLING SYSTEM VERSUS  
CURRENT AND GAS TYPE (ONE INCH BY ONE EIGHTH INCH  
THORIATED TUNGSTEN CATHODE)



## VI. EXPERIMENTAL STUDIES OF ROD SHAPED THORIATED TUNGSTEN CATHODES

A series of experiments have been carried out to provide laboratory data for comparison with the quasi one dimensional theory presented in the preceding section. The objectives of this work were as follows:

1. To determine whether rod shaped, thoriated tungsten cathodes can actually be operated in the spotless mode, and, if so, under what conditions spot mode and spotless mode operation occur;
2. To determine effective material property values for thoriated tungsten operated as a cathode; and
3. To test the validity of the theory.

Since a major experimental program using sophisticated techniques would have absorbed an excessively large fraction of the effort, these experiments were intended to supply only those data which could be obtained using simple and crude methods of measurement.

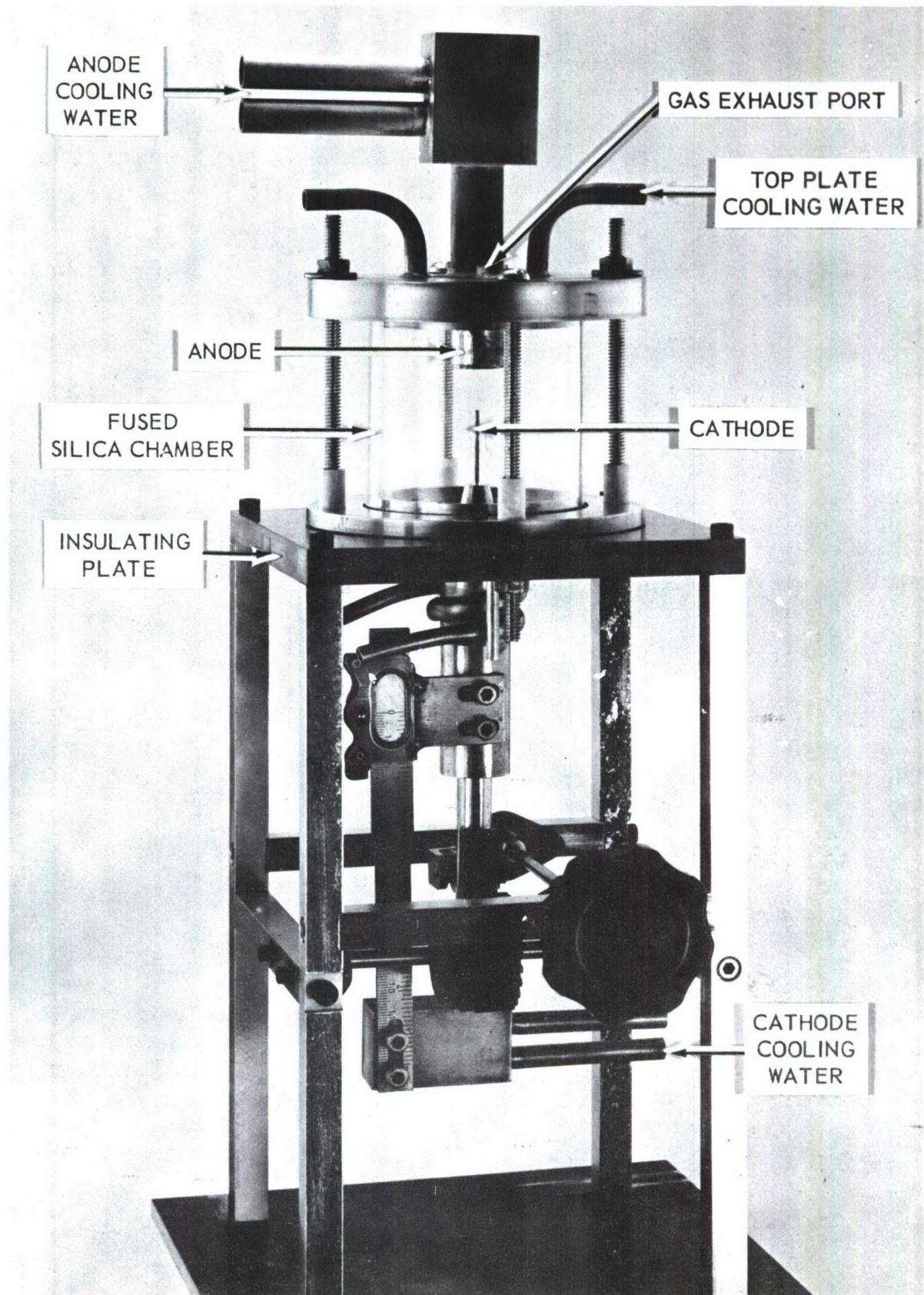
### A. APPARATUS AND PROCEDURES

Figure 45 shows the special arc unit used in the experimental program. The cathode is a cylindrical rod of 2 percent thoriated tungsten, embedded in a copper base. A threaded stud on the bottom of the base mates with a socket in the top of a water cooled holder. A number of cathodes having various dimensions with exposed lengths up to 2 inches and diameters up to 1/8 inch have been used. The cathode holder slides within a tubular support attached to the bottom plate of the arc chamber, the bearing surfaces being two rubber O rings. The holder is raised and lowered by means of a rack and pinion to adjust the arc gap independently of cathode length. The anode is a 3/4 inch diameter tungsten plate, brazed to a water cooled copper support. The top and bottom of the arc chamber are water cooled metal; the side wall is a cylinder of clear fused silica so that the arc and the electrodes can be observed visually and pyrometrically during operation. Gas injection ports are provided in the bottom of the chamber and exhaust ports in the top.

Power was supplied to the arc by a pair of Miller rectifiers, and regulated by means of a large rheostat. The arc was initiated using a high frequency oscillator.

In the experiments being reported, the following types of measurement were made:

1. The steady state heat flow from the cathode to the cooling water was determined by measuring the flow rate and temperature rise of the water.



Arc Assembly for Cathode Studies



Water flow was regulated using a pump and measured with the aid of a flowmeter. The calibration of the flowmeter was checked by measuring the total effluent volume over a certain period of time, and was found to be accurate. Inlet and outlet temperatures for the cathode cooling water were determined using 0° to 50°C chemical thermometers. Steady values of these temperatures, obtained after 3 to 5 minutes of arc operation at fixed current, were measured.

2. Arc current was measured using a millivoltmeter connected across a shunt. An 80 or a 200 ampere shunt was used, depending upon the level of current being measured.

3. Cathode temperatures at various distances from the tip of the cathode were measured using an optical pyrometer. The resulting brightness temperature values were converted into "true" temperature assuming the cathode to have the same spectral emissivity as pure tungsten.<sup>33</sup> Since the surface was somewhat rough and not clean, the temperatures calculated by this procedure might be a little too high. No allowance was made for reflective losses at the two silica glass/air interfaces traversed by the light before reaching the pyrometer. The coefficient of reflection was estimated<sup>35</sup> to be about 0.035 at each interface, corresponding to a total loss of about 7 percent. This error would tend to make the calculated temperatures too low, and thus might be partially compensated by an error in the emissivity assumption.

4. For points other than the cathode tip, the distance of the spot viewed through the pyrometer from the cathode tip was determined before or after the arc run using a scale placed behind the arc chamber. Observation of the scale during the run was precluded by the brightness of the cathode. The error due to thermal expansion of the cathode during the run was estimated and found to be negligible. However, it was found that the position of the cathode tip as seen through the pyrometer changed by 1/32 inch when the pyrometer's red filter was moved into position. This effect was attributed to optical imperfection of the filter and was allowed for in reduction of the data.

5. Gas flow rate was monitored using a flowmeter and a gauge to measure injection pressure.

6. Arc voltage was measured using a voltmeter.

7. The cathode-anode gap was determined either using the vernier scale attached to the cathode holder or by viewing a scale placed behind the arc chamber through the pyrometer.

8. The amount of arc overflow onto the side of the cathode was estimated visually in terms of the cathode diameter.



## B. RESULTS

### 1. Changes of Cathode Properties with Operating Time

The cathodes used in these experiments were 2 percent thoriated tungsten. A number of qualitative observations made during the early part of the program suggested that the properties of the cathode material might be changing gradually as the material was operated for prolonged periods at high temperatures. To determine whether such changes were actually taking place, two special runs were made in which the tip temperatures of new cathodes were measured pyrometrically as functions of time beginning immediately after arc initiation.

Figure 46 shows the results of the first of these runs, which was carried out at 16 amperes in helium using a cathode 1/16 inch in diameter and 5/8 inch in length. In this case, the tip temperature rises by nearly 400°K during the one-half hour long run. Most of the rise occurs during the first 15 minutes of operation.

Figure 47 similarly shows tip temperature as a function of running time for a 2 inch by 1/8 inch cathode operating at 52 amperes in a helium-argon mixture. The temperature again rises substantially during the run. The rise appears to be a little slower than for the 5/8 inch by 1/16 inch cathode, probably because of the larger mass and greater thickness of the 2 inch cathode. Figure 48 presents a series of photographs of this cathode during the same run. The first picture, taken at 30 seconds after arc initiation, shows the arc striking rather uniformly over the end of the cathode. As the run progresses, the cathode attachment of the arc becomes more and more asymmetrical until, at 12.5 minutes, the cathode definitely appears to be operating in the spot mode.

The visual appearance of the cathode itself changes during prolonged operation, especially at high currents. A new cathode has a bright, machine finished surface. Cathodes which have been run at high temperature for several hours, or even for shorter periods at very high current, have a roughened surface in the region near the tip, apparently because of recrystallization. Other qualitative observations tending to confirm the change of cathode properties with "hot time" are reported in the next section.

The rise of tip temperature with time presumably reflects an increase of the effective work function of the cathode. Such a property change might result from gradual loss of the low work function additive during high temperature operation. It is clear that other properties of the material might change to a certain extent at the same time, although the data presented thus far throw no light on this question.

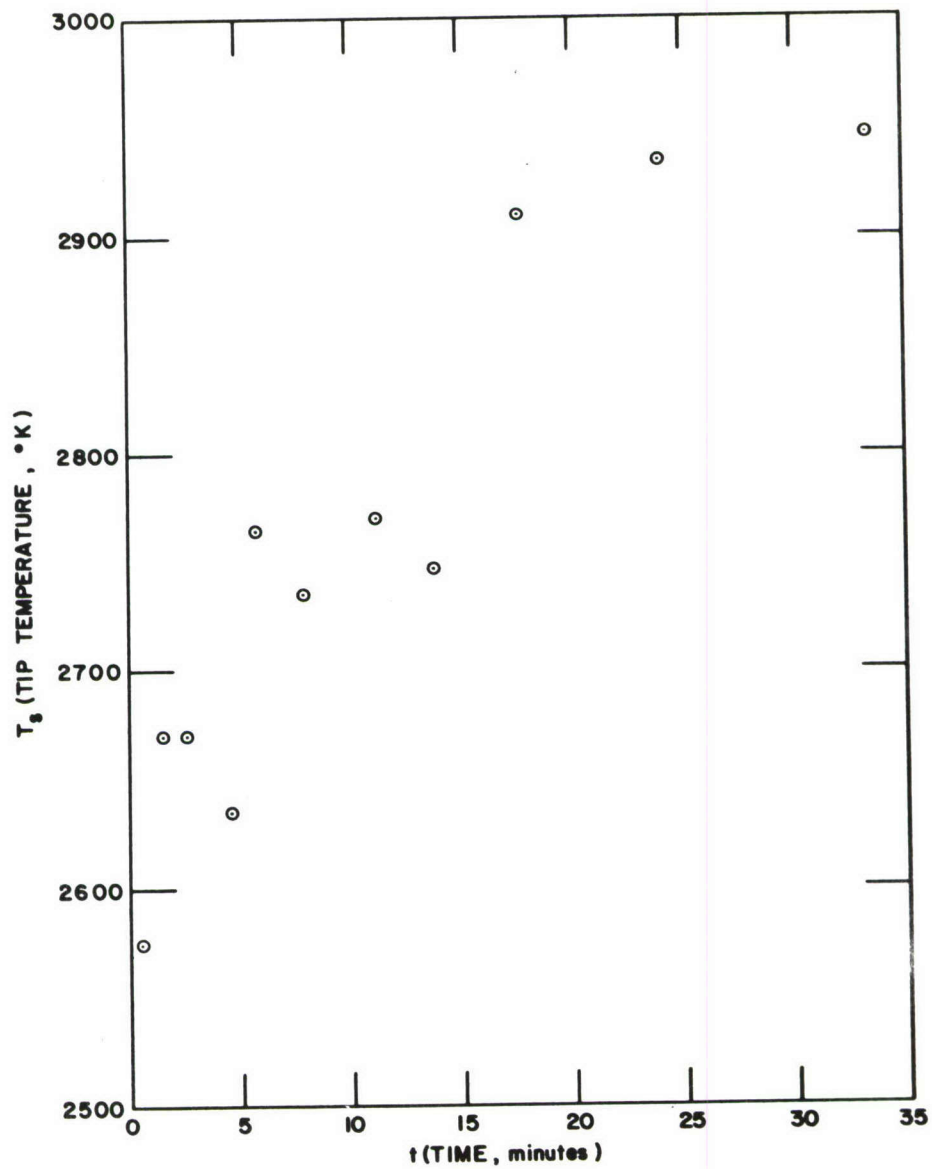


Figure 46 TIP TEMPERATURE AS A FUNCTION OF TIME FOR A NEW THORIATED TUNGSTEN CATHODE (FIVE EIGHTH INCH BY ONE SIXTEENTH INCH, HELIUM)



The time dependence of cathode work function poses a problem in quantitative studies such as those reported below. During the 3 to 5 minutes required for a heat flux measurement by the method used in this work, the change in tip temperature for a new cathode is substantial, as shown by figures 47 and 48. To avoid this difficulty, the quantitative experiments in the present investigation have been made using cathodes which have already been "run in" at moderate currents for periods of one-half hour or more. Figures 47 and 48 suggest that the change in tip temperature becomes very slow after the first one-half hour, so that the use of cathodes conditioned in this way should provide reasonable stability of material properties. This supposition is confirmed by the fact that reruns of certain cases on the same cathode after extensive periods of operation have shown good reproducibility.

## 2. Qualitative Observations

The rod shaped cathodes have been operated in three gases, helium, argon, and nitrogen. The visual appearance of the arc in the cathode region is different in each of these gases, and is also different for new and used cathodes. Figure 49 shows a 2 inch long, 1/8 inch diameter cathode operating at four current levels in helium and argon. The exposure is the same (0.5 second at f/32 through a 2.0 neutral density filter on Polaroid Type 55 P/N film, ASA 100) for all of the pictures in figures 48, 49, and 50.

The cathode shown in figure 49 had been operated for several hours prior to the time at which the photographs were taken, so that the pictures shown in this figure are representative of the behavior of "used" thoriated tungsten. As illustrated by the figure, the cathode operates in the spot mode in both helium and argon at the lowest current. In argon, the spot mode persists over the entire current range, but in helium a transition to spotless operation occurs with increasing current.

The behavior of a "new" thoriated tungsten cathode is shown in figure 50. In this case, the cathode appears to operate without a spot even at 10 amperes in helium, but again runs in the spot mode at all currents in argon, even though the argon runs were made first in this case.

Comparison of the photographs for argon and helium at a given current shows that the tip is usually less bright in argon, except in the spot region. This illustrates the fact that spot mode operation leads to a generally lower tip temperature. Such observations can be explained by noting that the electron emission current is a very strong function of temperature, so that contraction of the cathode attachment of the arc into a spot permits a given current to flow from a much smaller area without a very large increase in the temperature of the emitting region. Quasi-radial heat flow within the cathode, then, permits most of the cathode tip to be at a substantially lower temperature than in the spotless case.



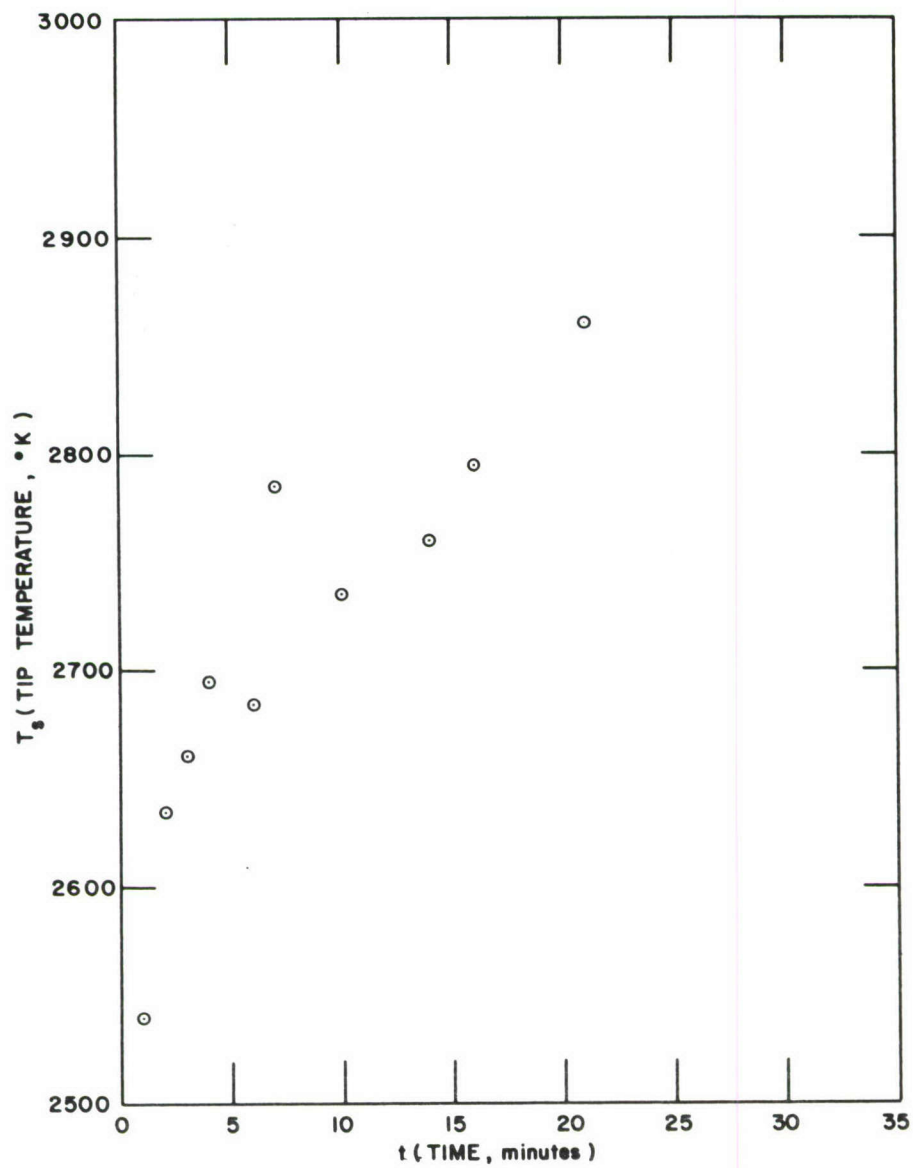
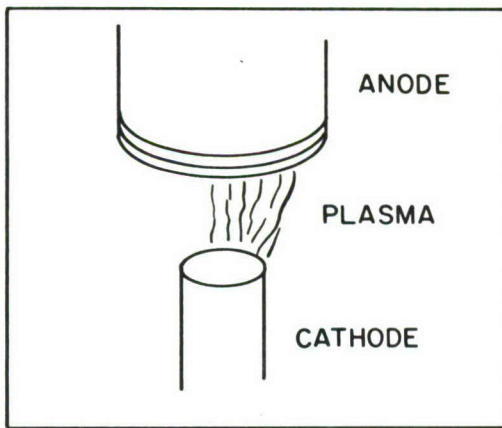
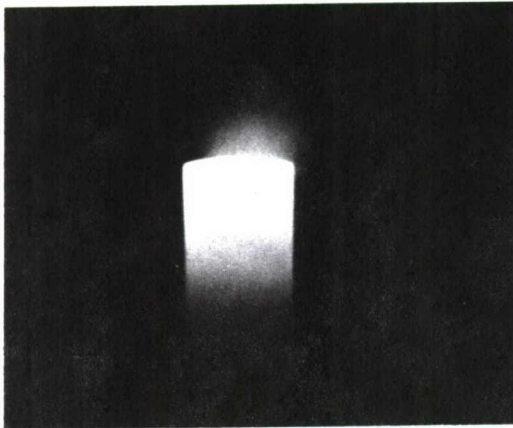


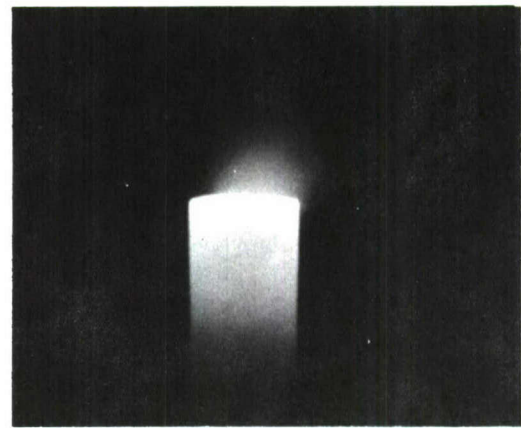
Figure 47 TIP TEMPERATURE AS A FUNCTION OF TIME FOR A NEW THORIATED TUNGSTEN CATHODE (TWO INCH BY ONE EIGHTH INCH, HELIUM ARGON)



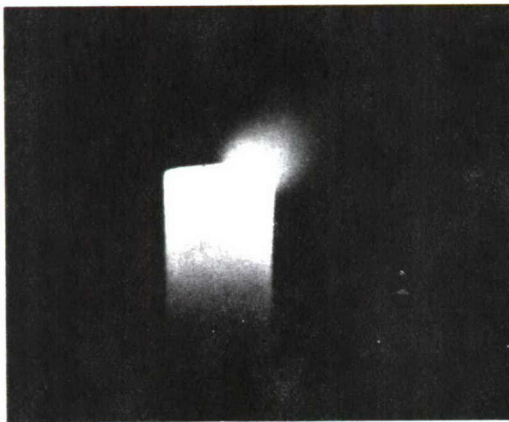
MATERIAL: 2 percent thoriated tungsten  
 CATHODE DIMENSIONS: 2 x 1/8 inch  
 CURRENT: 52 amperes  
 GAS: helium - argon mixture



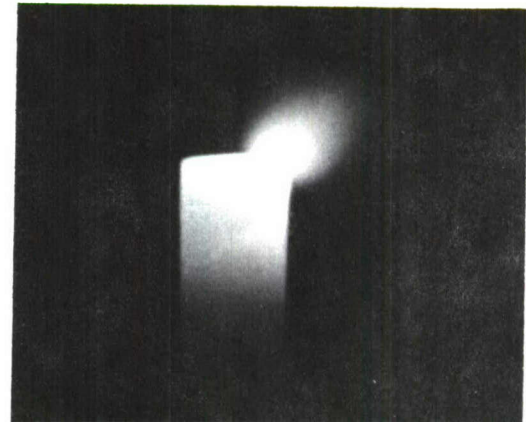
(a) 0.5 minute



(b) 3.5 minutes



(c) 7.5 minutes



(d) 12.5 minutes

Figure 48 CHANGES IN APPEARANCE OF AN ARC OPERATING ON A NEW THORIATED-TUNGSTEN CATHODE

62-5020

MATERIAL : 2 percent thoriated tungsten ("used")

CATHODE DIMENSIONS : 2 x 1/8 inch

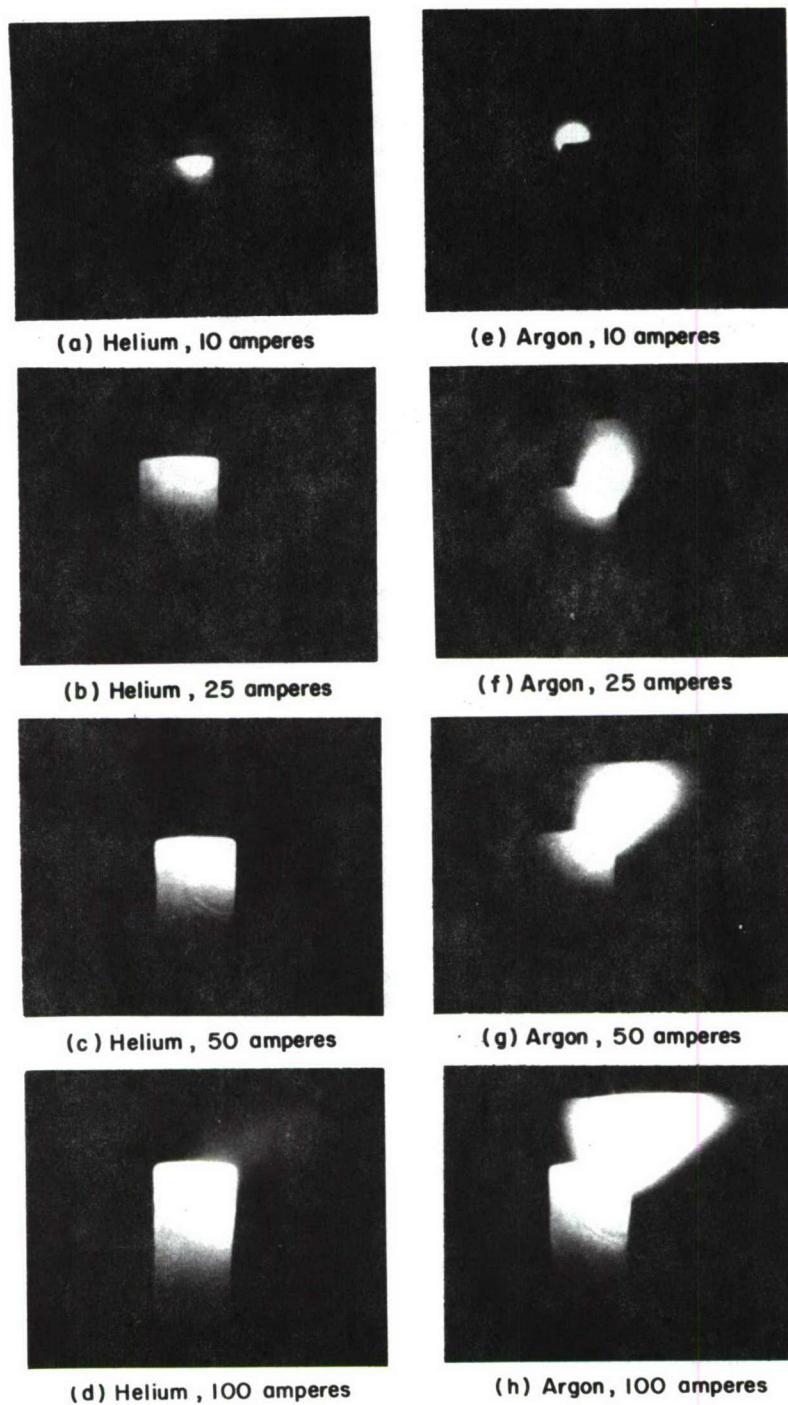


Figure 49 APPEARANCE OF ARC IN HELIUM AND ARGON AS A FUNCTION OF CURRENT (TWO INCH BY ONE EIGHTH INCH "USED" THORIATED TUNGSTEN CATHODE)

62-5021

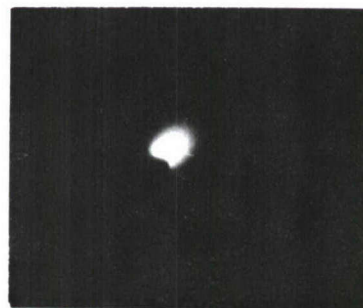


MATERIAL : 2 percent thoriated tungsten ("new")

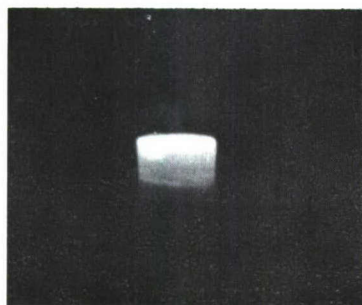
CATHODE DIMENSIONS :  $1/2 \times 1/8$  inch



(a) Helium , 10 amperes



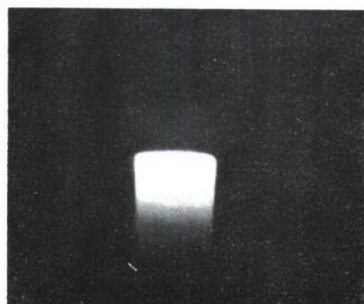
(e) Argon , 10 amperes



(b) Helium , 25 amperes



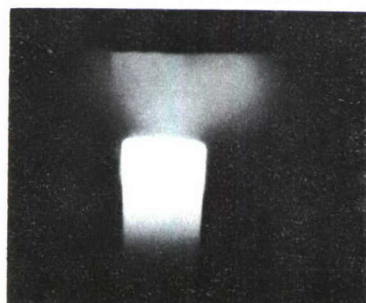
(f) Argon , 25 amperes



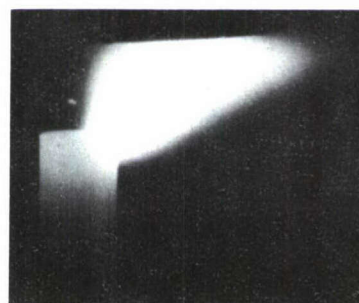
(c) Helium , 50 amperes



(g) Argon , 50 amperes



(d) Helium , 100 amperes



(h) Argon , 100 amperes

Figure 50 APPEARANCE OF ARC IN HELIUM AND ARGON AS A FUNCTION  
OF CURRENT (ONE-HALF INCH BY ONE EIGHTH INCH "NEW"  
THORIATED TUNGSTEN CATHODE)  
62-5022

The observations on cathode operation in helium, argon, and nitrogen may be summarized as follows.

a. Helium

1) "New" cathodes

The arc operates invariably in the spotless mode (at least at the current levels used in these experiments). The arc appears symmetrical with respect to the cathode axis, and a considerable amount of arc "overflow" onto the side of the cathode is noted at some current levels. No contraction at the anode is apparent.

2) "Used" cathodes

The arc operates in the spot mode at low currents, but reverts to spotless operation at high currents. However, on cathodes which have accumulated a large amount of "hot time," the cathode attachment of the arc is often asymmetrical, covering the end surface of the cathode and overflowing to one side. In such cases, a cathode jet sometimes appears.

b. Argon

1) "New" Cathodes

In a few instances, brand new 1 inch by 1/16 inch cathodes have been observed to operate symmetrically, and apparently in the spotless mode, in argon. After a few minutes, however, a spot develops on the rim of the cathode end. In all cases, a sheath of brilliant plasma covers the emitting region of the cathode. During symmetrical operation on new cathodes, little or no overflow is visible. Slight contraction at the anode is generally noted in argon.

2) "Used" cathodes

The arc operates invariably in the spot mode. The general tip temperature away from the spot is lower than in helium operating without a cathode spot at the same current. At the higher currents, a cathode jet appears to issue from the spot region.

c. Nitrogen

No "new" cathodes have been operated in nitrogen during these experiments. "Used" cathodes appear to operate in the spot mode. A distinct, thin arc column is usually visible, and flits back and forth over

the surfaces of the electrodes. The cathode surface shows signs of local melting after operation in nitrogen, but no loss of material has been detected. The general tip temperature of the cathode in nitrogen is as high as, or higher than, that in helium. Figure 51 shows a 1 inch by 1/16 inch cathode operating in nitrogen at 20 amperes. The anode attachment is strongly contracted and terminates in an incandescent spot on the tungsten surface. At higher currents, material is lost from the anode at a noticeable rate.

### 3. Heat Flux and Temperature Data

The principal series of experiments to study cathode performance was carried out using three cathode geometries (1 inch by 1/16 inch, 2 inch by 1/8 inch, and 1 inch by 1/8 inch) and three gases (helium, argon, and nitrogen). The cathodes employed were all "used"; i.e., previously run for extended periods of time. The data obtained are summarized in Table 8. In this table  $I$  denotes total current, and  $Q_0$  total heat flow from the cathode to its cooling water.  $j_0$  and  $q_0$  are the corresponding fluxes, based upon the cathode cross sectional area  $\pi D^2/4$ . The effective voltage  $V_{\text{eff}}$  for heat transfer to the cooling system is defined as

$$V_{\text{eff}} = Q_0/I \quad . \quad (151)$$

$x$  represents the distance from the cold end of the cathode, and  $T$  the absolute temperature of the cathode side surface. In Table 8, the runs are categorized according to gas type and cathode geometry, and within each set are arranged in order of increasing total current. For each run, the measured surface temperatures are arranged in order of increasing distance from the tip, the first value being the tip temperature in each case.

The electrode gap and gas flow are not given in Table 8, but have the following values:

$$\begin{aligned} \text{Electrode gap} &= \begin{cases} 0.25 \text{ inch for He and Ar} \\ 0.125 \text{ inch for N}_2 \end{cases} \\ \text{Gas mass flow} &= \begin{cases} 0.23 \text{ gm/sec for He} \\ 0.71 \text{ gm/sec for Ar} \\ 0.59 \text{ gm/sec for N}_2 \end{cases} \quad . \end{aligned}$$

Based upon estimated errors in the measurement of water flow, water temperature rise, and the potential drop across the shunt, the minimum



MATERIAL : 2 percent thoriated tungsten ("used")

CATHODE DIMENSIONS : 1 x 1/16 inch

CURRENT : 20 amperes

GAS : nitrogen

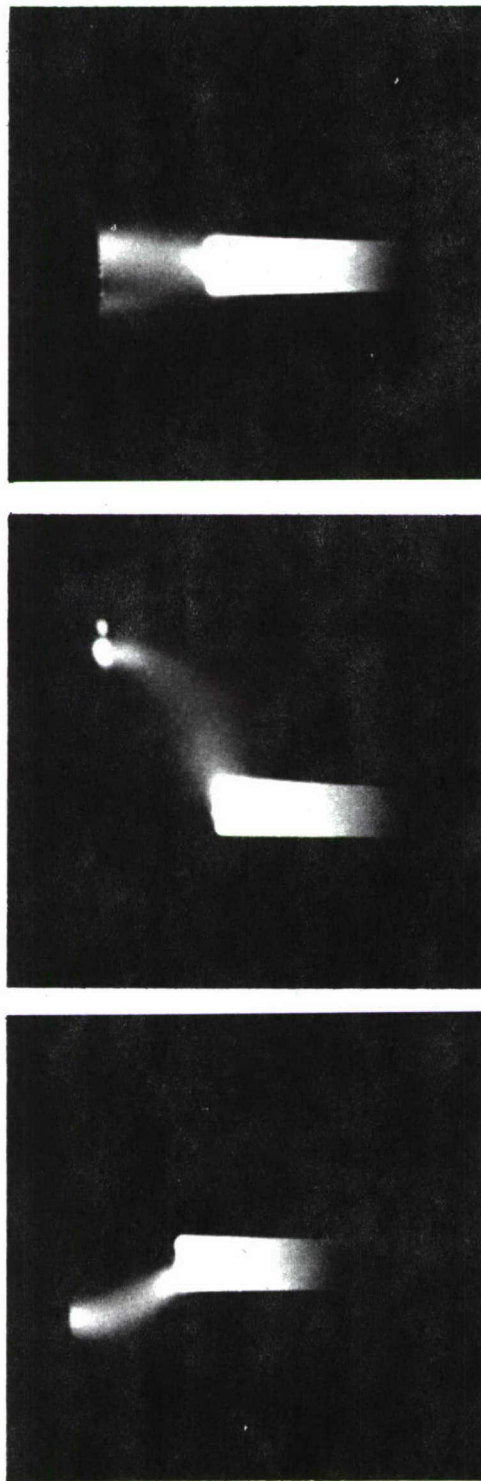


Figure 51 APPEARANCE OF ARC IN NITROGEN (ONE INCH BY  
ONE SIXTEENTH INCH THORIATED  
TUNGSTEN CATHODE)  
62-5023

TABLE 8

## SUMMARY OF EXPERIMENTAL DATA


Gas	Run Number	Diameter inch	Length inch	I amperes	Q <sub>0</sub> watts	i <sub>0</sub> amp/cm <sup>2</sup>	q <sub>0</sub> w/cm <sup>2</sup>	V <sub>eff</sub> volts	x cm	T °K	Remarks
Helium	1	1/16	1	6.8	13.5	344	684	1.98	2.54 2.06	2710 2220	Spot on side 1D below tip
Helium	2	1/16	1	12.6	17.1	634	865	1.36	2.54 2.14 1.90	3030 2590 2070	Asymmetric
Helium	3	1/16	1	20.2	19.2	1021	973	0.95	2.54 2.14 1.90	3010 2510 1900	Asymmetric
Helium	4	1/16	1	40.8	18.5	2062	936	0.45	2.54 2.14 1.90	3060 2390 1900	Approx. symmetric
Helium	5	1/16	1	50.0	24.2	2527	1225	0.48	2.54	3180	Overflow 1.5D
Helium	6	1/16	1	73.6	32.1	3719	1621	0.44	2.54 2.14 1.75	3330 2610 2080	Symmetric
Helium	7	1/16	1	80.8	26.4	4080	1333	0.33	2.54	3300	No visible overflow
Helium	8	1/16	1	124.0	40.6	6270	2050	0.33	2.54	3410	
Helium	9	1/16	1	162	58.4	8190	2950	0.36	2.54	3275	
Helium	10	1/16	1	192	82.0	9700	4140	0.43	2.54 1.11	3420 2930	

TABLE 8 (Cont'd)

Gas	Run Number	Diameter inch	Length inch	I amperes	Q <sub>0</sub> watts	j <sub>0</sub> amp/cm <sup>2</sup>	q <sub>0</sub> w/cm <sup>2</sup>	V <sub>eff</sub> volts	x cm	T °K	Remarks
Helium	11	1/8	2	23.9	12.8	302	162	0.54	5.08 4.68 4.21	2800 2010 1710	Asymmetric toward pyrometer
Helium	12	1/8	2	24.2	11.4	306	144	0.47	5.08 4.37	2750 1690	Symmetric
Helium	13	1/8	2	24.8	12.8	313	162	0.52	5.08 4.68 4.21	2740 1980 1690	Asymmetric
Helium	14	1/8	2	35.6	15.0	450	189	0.42	5.08 4.68 4.05	2920 2300 1660	Asymmetric
Helium	15	1/8	2	52.6	20.0	664	252	0.38	5.08 4.52 3.81	3110 2130 1740	Asymmetric
Helium	16	1/8	2	98.4	26.4	1243	333	0.27	5.08 4.52	3120 2150	Asymmetric
Helium	17	1/8	1	11.6	37.1	147	468	3.20	2.54 2.14 1.87	2220 1720 1560	Cathode spot on rim
Helium	18	1/8	1	25.8	44.2	325	558	1.71	2.54 2.14 1.71	2820 2010 1610	Asymmetric toward pyrometer
Helium	19	1/8	1	50.6	50.6	639	639	1.00	2.54 2.14 1.75	2930 2200 1760	Asymmetric toward pyrometer



TABLE 8 (Cont'd)


Gas	Run Number	Diameter inch	Length inch	I amperes	Q <sub>0</sub> watts	i <sub>0</sub> amp/cm <sup>2</sup>	q <sub>0</sub> w/cm <sup>2</sup>	V <sub>eff</sub> volts	x cm	T °K	Remarks
Helium	20	1/8	1	96.0	66.3	1213	837	0.69	2.54 2.14 1.75	3130 2300 1880	Asymmetric toward pyrometer
Argon	21	1/16	1	5.3	12.1	267	612	2.30	2.54 2.18 2.14	2370 1940 1800	Spot on side 1 mm below tip
Argon	22	1/16	1	8.1	12.1	408	612	1.50	2.54 2.14 1.78	2520 1800 1580	Spot on side 1 mm below tip
Argon	23	1/16	1	15.4	13.5	780	684	0.88	2.54 2.14 1.90	2550 1860 1725	Spot on rim of cathode tip
Argon	24	1/16	1	24.0	14.3	1213	720	0.59	2.54 1.67	2635 1590	
Argon	25	1/16	1	24.9	15.3	1258	775	0.62	2.54 2.14 1.87	2610 2070 1780	
Argon	26	1/16	1	45.6	18.5	2304	936	0.41	2.54 2.14 1.79	2760 2250 1820	
Argon	27	1/16	1	78.4	27.8	3962	1405	0.35	2.54 2.14	2950 2520	
Argon	28	1/8	2	23.8	20.7	301	261	0.87	5.08 4.68 4.05	2250 1800 1540	

TABLE 8 (Cont'd)



Gas	Run Number	Diameter inch	Length inch	I amperes	Q <sub>0</sub> watts	i <sub>0</sub> amp/cm <sup>2</sup>	q <sub>0</sub> w/cm <sup>2</sup>	V <sub>eff</sub> volts	x cm	T °K	Remarks
Argon	29	1/8	2	24.0	19.2	303	243	0.80	5.08	2160	Spot on rim
Argon	30	1/8	2	48.4	22.1	611	279	0.46	5.08	2340	
Argon	31	1/8	2	95.6	27.8	1208	351	0.29	5.08 3.73	2540 1700	
Argon	32	1/8	1	12.4	43.5	157	549	3.51	2.54 1.83	1980 1500	
Argon	33	1/8	1	23.8	49.2	301	621	2.07	2.54	2250	
Argon	34	1/8	1	47.2	53.5	597	675	1.13	2.54	2250	Symmetrical, very steady Spot on rim
Argon	35	1/8	1	96.0	64.2	1213	810	0.67	2.54 2.14	2490 2080	
Nitrogen	36	1/16	1	5.0	15.7	251	792	3.14	2.54	2840	
Nitrogen	37	1/16	1	9.0	15.7	453	792	1.74	2.54	2980	
Nitrogen	38	1/16	1	14.9	16.4	752	828	1.10	2.54	3140	
Nitrogen	39	1/16	1	23.6	18.5	1192	936	0.78	2.54	3100	
Nitrogen	40	1/16	1	46.7	22.8	2361	1153	0.49	2.54	3300	
Nitrogen	41	1/16	1	76.8	31.4	3880	1585	0.41	2.54	3540	
Nitrogen	42	1/8	2	24.4	17.8	308	225	0.73	5.08	2350	Spot on end
Nitrogen	43	1/8	2	50.4	22.1	637	279	0.44	5.08	2470	

TABLE 8 (Concl'd)

Gas	Run Number	Diameter inch	Length inch	I amperes	Q <sub>0</sub> watts	i <sub>0</sub> amp/cm <sup>2</sup>	q <sub>0</sub> w/cm <sup>2</sup>	V <sub>eff</sub> volt	x cm	T °K	Remarks
Nitrogen	44	1/8	2	93.0	27.8	1175	351	0.30	5.08 3.89	2560 1720	
Nitrogen	45	1/8	1	15.0	40.6	189	513	2.71	2.54 1.90	1850 1430	
Nitrogen	46	1/8	1	22.8	46.3	288	585	2.03	2.54	1920	
Nitrogen	47	1/8	1	49.6	57.0	627	720	1.15	2.54	2300	
Nitrogen	48	1/8	1	98.0	69.1	1238	873	0.71	2.54 1.83	--- 1790	



uncertainties in  $Q_0$  and  $I$  are about 2 watts and 0.2 ampere, respectively. Actual errors are probably larger than these values in some instances because of fluctuations in water flow and arc current. The pyrometer readings are probably accurate to within  $\pm 50^\circ\text{C}$  in brightness temperature, but the "true" temperatures listed in Table 8 are more uncertain than this because of a possible difference between the spectral emissivity of the cathode and that of pure tungsten, and because of the presence of strong temperature gradients in the surface region viewed through the pyrometer.

### C. ANALYSIS OF DATA

The thermal and electrical conductivities and total emissivity for pure tungsten have been reviewed in section IV. In summary, the literature values are

$$\text{pure tungsten} \left\{ \begin{array}{l} \epsilon \approx 0.32 \\ K \approx 1.1 \text{ w/cm}^\circ\text{K} \\ \rho = \text{BT}^s \end{array} \right.$$

with

$$\text{pure tungsten} \left\{ \begin{array}{l} B = 5.0 \times 10^{-9} \text{ ohm-cm/}^\circ\text{K}^s \\ s = 1.234 \end{array} \right.$$

The thermionic constants for pure tungsten are<sup>34</sup>

$$\text{pure tungsten} \left\{ \begin{array}{l} A = 60 \text{ amp/cm}^2 \text{ }^\circ\text{K}^2 \\ \phi = 4.51 \text{ volts} \end{array} \right.$$

It is clear, however, that these thermionic properties cannot be applied to thoriated tungsten. The  $A$  and  $\phi$  values must be determined for the particular material being used, especially because there is good reason to believe that the "used" cathodes, upon which the data of Table 8 are based, have different thermionic properties from the original material.

The other properties listed above may also differ to some extent from their values for pure tungsten.

#### 1. Total Emissivity

It is probable that the effective total emissivity for the "used" cathode material is somewhat higher than that for pure tungsten, since the cathode surface is "dirty" and also rather rough in the region which reaches high temperatures during operation. With allowance for the effects of these conditions, it is estimated that

$$\epsilon \approx 0.4 \quad .$$

(152)

## 2. Thermionic Constants

The values of the thermionic constants  $A$  and  $\phi$  can be estimated from the measurements of tip temperature and current density presented in Table 8. The argon and nitrogen data are not useful for this purpose, of course, since the cathode always operates in the spot mode in these gases, and the spot area has not been measured. The helium data must also be rejected for those runs in which spot-mode operation or a large amount of overflow occurred. The high current runs 7 to 10 also omitted, because a considerable amount of overflow probably occurred in these runs but was not visible owing to the extreme brightness of the Joule heated cathode. The remaining data, which ought to be suitable for estimating thermionic constants, are run numbers 3, 4, 6, 11, 13, 14, 15, 16, 18, 19 and 20.

The accuracy of the data is not good enough to permit determination of both  $A$  and  $\phi$ . For this reason, the data are analyzed by assuming a value for  $A$  and calculating a corresponding "effective" value for  $\phi$ . Experimental values of  $A$  for tungsten with low work function additives are usually very low,<sup>34</sup> of the order of unity. The present analysis assumes

$$A = 1 \text{ amp/cm}^2 \text{ } ^\circ\text{K}^2 \quad . \quad (153)$$

The current density is given theoretically by equation (111),

$$j = A \left( 1 + \frac{V_c}{V_I} \right) T^2 e^{-\theta/T} \quad , \quad (154a)$$

where

$$\theta = 11609 \phi - 4.4 \sqrt{E_c} \quad , \quad (154b)$$

and the surface field strength is given by Mackeown's formula (1391) which can be approximated by

$$E_c \simeq 873 V_c^{1/4} j_E^{1/2} (1823 W)^{1/4} \left( \frac{V_c}{V_c + V_I} \right)^{1/2} \quad . \quad (154c)$$

Elimination of  $E_c$  and  $\theta$  from these equations gives

$$\ln j = \ln A + \ln \left( 1 + \frac{V_c}{V_I} \right) + 2 \ln T - \frac{1}{T} \left[ 11609 \phi - 130 V_c^{1/8} \left( \frac{V_c}{V_c + V_I} \right)^{1/4} (1823 W)^{1/8} j^{1/4} \right] . \quad (155)$$

This is now regarded as an equation for  $\phi$  in terms of experimental values of  $j$  and  $T$  and an assumed value (153) of the Richardson constant  $A$ . The value of  $\phi$  obtained is rather insensitive to the unknown value of  $V_c$ ; a typical value  $V_c \sim 5$  volts is assumed for all cases. Then, with  $V_I = 24.5$  and  $W = 4$ ,

$$\phi = 8.61 \times 10^{-5} \left[ T \left( \ln \frac{T^2}{j} + 0.2 \right) + 311 j^{1/4} \right] . \quad (156)$$

TABLE 9

ANALYSIS OF CATHODE DATA FOR EFFECTIVE WORK FUNCTION

Run Number	Diameter inch	Length inches	$j_0$ amp/cm <sup>2</sup>	$T_s$ °K	$\phi$ volts
3	1/16	1	1021	3010	2.56
4	1/16	1	2062	3060	2.45
6	1/16	1	3719	3330	2.56
11	1/8	2	302	2800	2.61
13	1/8	2	313	2740	2.53
14	1/8	2	450	2920	2.64
15	1/8	2	664	3110	2.75
16	1/8	2	1243	3120	2.62
18	1/8	1	325	2820	2.58
19	1/8	1	639	2930	2.54
20	1/8	1	1213	3130	2.64



Table 9 shows the results of applying this formula to the data on tip temperature and current for the runs listed above. In this table, the surface current density at the tip is approximated by  $j_0$ , since there was little visual indication of overflow in any of these runs and the computed value of  $\phi$  is not very sensitive to  $j$ . The mean of the values shown in the last column, together with its root mean square deviation, is  $2.59 \pm 0.07$  volts. In the subsequent analysis, it is assumed that, for the "used" thoriated tungsten cathodes,

$$\phi = 2.6 \text{ volts} , \quad (157)$$

based upon  $A = 1 \text{ amp/cm}^2 \text{ }^\circ\text{K}^2$ . The current density-temperature relation calculated from (156) using these values is compared with the data of Table 8 in figure 52. It is interesting, but probably not significant, that (157) agrees fairly well with the value ( $\phi = 2.63$ ,  $A = 3$ ) listed by Nottingham<sup>34</sup> for W + Th.

### 3. Thermal Conductivity

The data of Table 8 also permit analysis for thermal conductivity. This property can best be determined using temperatures measured at points below the tip, where the effects of strong temperature gradients in the tip region have largely died out and the heat flow is nearly one dimensional. Data from all three gases can be used. However, it is best to restrict consideration at this stage to data taken at low current densities where Joule heating does not affect the heat flow to a major extent. This analysis for thermal conductivity does not involve any of the "arc" relations pertaining to the cathode fall zone or the surface, but only the heat conduction problem with radiative loss from the sides.

If the temperature distribution in the cathode were linear, the thermal conductivity could be calculated using the simple relation  $K = q_0 x / (T - T_0)$ . In fact, this formula gives fairly good values when applied to the lowest temperature data of Table 8. However, radiative loss of heat from the side of the cathode is always significant in regions of the cathode surface which are bright enough to yield a good pyrometer reading. For this reason, it is desirable to use the quasi one dimensional heat flow theory of section V B in carrying out the analysis. It is convenient to define

$$H = K^2 C = q_0^2 - \frac{8\sigma\epsilon K}{5D} T_0^5 + \frac{2BKj_0^2}{s+1} T_0^{s+1} , \quad (158)$$

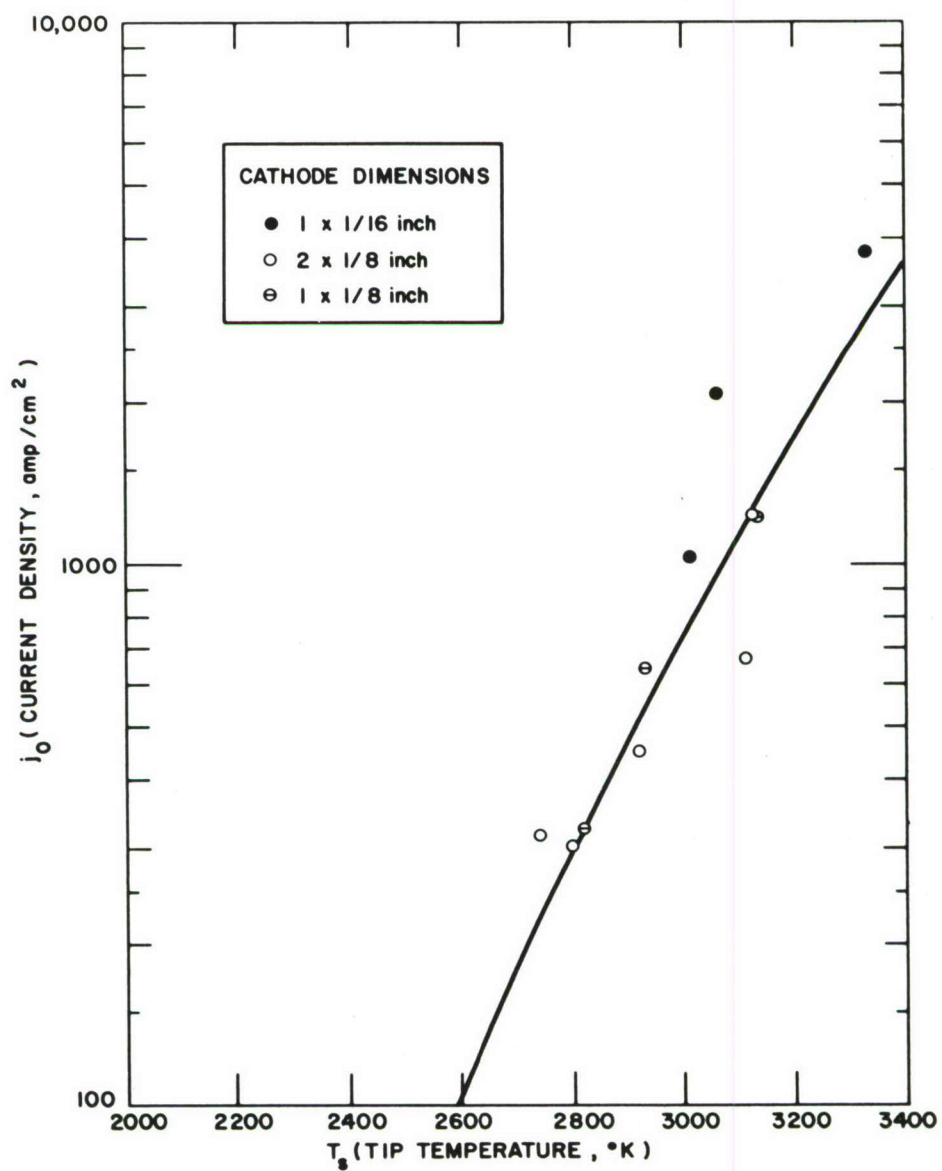


Figure 52 CURRENT DENSITY VERSUS TEMPERATURE FOR "USED" THORIATED TUNGSTEN CATHODES IN HELIUM

where C is the integration constant (106), determined from the temperature and heat flux at the cold end of the cathode. Then, equations (91) become

$$\psi = \left( \frac{8\sigma\epsilon K}{5DH} \right)^{1/5} T \quad (159a)$$

$$K\eta = \sqrt{H} \left( \frac{8\sigma\epsilon K}{5DH} \right)^{1/5} x \quad (159b)$$

$$z = \frac{2BKj_0^2}{(s+1)H} \left( \frac{8\sigma\epsilon K}{5DH} \right)^{-(s+1)/5} \quad (159c)$$

The term  $q_0^2$  on the right-hand side of (158) is much larger than the other two terms, so that the experimental value of  $q_0$  gives a good determination of H without knowledge of the exact value of K. Because of the exponent 1/5, the quantity  $(8\sigma\epsilon K/5DH)^{1/5}$  appearing in (159a and b) is insensitive to errors in an assumed K value. Equation (159c) is somewhat more sensitive to variations in K, but this has little effect upon the calculations since z is small in the runs selected for thermal conductivity determination. Thus, knowing only that K should be of the order of 1 w/cm°K, one can determine  $\psi$  and the quantity  $K\eta$  with reasonable accuracy from experimental values of  $q_0$ , T, and x. The quantity

$$\psi_0 = \left( \frac{8\sigma\epsilon K}{5DH} \right)^{1/5} T_0 \quad (160)$$

is not known accurately, since the temperature  $T_0$  at the cold end of the cathode was not measured in these experiments. However, the cathode is embedded in a 1/2 inch diameter copper base which is screwed tightly into a water cooled holder, so that  $T_0$  should not be much above room temperature. It is assumed that

$$T_0 = 300^\circ\text{K} \quad (161)$$

This assumption is most likely to be in error in runs with the 1 inch by 1/8 inch cathode. The unusually high heat flows obtained with this geometry might force  $T_0$  to rise appreciably above the value (161).

With  $\psi$  given by (159a),  $\psi_0$  by (160), and z by (159c), one can calculate  $\eta$  from equation (94), using Table 3 to evaluate  $G(\psi, z)$  and  $G(\psi_0, z)$ .



Then, since  $K\eta$  is known from (91b),  $K$  can be obtained. The results of applying this procedure to data from Table 8 are shown in Table 10. The runs used have been selected to avoid excessively large values of  $z$ , and tip temperature data have not been employed (with one exception). The value  $B = 5.3 \times 10^{-9}$  has been assumed in the calculations, on the basis of a discussion presented below.

The thermal conductivity values shown in the last column of Table 10 are of the correct order of magnitude, but vary considerably. It is noted that

- a. The thermal conductivity values obtained from the argon and nitrogen data are all essentially in agreement, independently of cathode geometry.
- b. In the case of helium, the calculated  $K$  depends markedly upon the cathode geometry. For the 1 inch by 1/16 inch cathode, the  $K$  values are in the vicinity of 0.9, which happens to be roughly the value obtained from the argon and nitrogen data. For the 2 inch by 1/8 inch cathode in helium,  $K$  is calculated to be about 0.65. For the 1 inch by 1/8 inch cathode, the value is intermediate, near 0.75.

These differences can be accounted for, at least qualitatively, by considering the effects of convective cooling of the cathode, convective heating of the cathode base and holder, and variation of  $T_0$  with the total heat flow from the cathode to the cooling water.

The gas flow field in the arc chamber is not known in detail, but presumably contains large scale circulatory motions fed by the jets emerging from the two injection ports in the bottom plate. Gas heated by the arc column must mix, to some extent, with the surrounding cooler gas, and the gas flowing over the surfaces of the cathode and its copper holder is likely to be at some temperature above 300°K but far below the temperature of the arc.

The construction of the arc unit is such that the top of the copper holder for a 2 inch cathode is about flush with the surface of the bottom plate. Thus, a 2 inch by 1/8 inch cathode is immersed in the gas flow field in the chamber, but its holder is not. Such a cathode operating in helium can lose a considerable amount of heat from its side by convective heat transfer to the gas. The same type of cathode operating in argon or nitrogen will lose much less heat by convection, because the thermal conductivities of these gases are only one eighth that of helium.

A 1 inch long cathode operating in this arc unit has 1 inch of its base and holder, with an area of about 4 cm<sup>2</sup>, immersed in the heated gas. It is reasonable to assume that some heat transfer takes place from the gas to this cold copper surface. This could account for the fact that the 1 inch by 1/16 inch cathode gives higher calculated thermal conductivity values than

TABLE 10

## ANALYSIS OF CATHODE DATA FOR THERMAL CONDUCTIVITY

Gas	Run Number	Diameter inch	Length inch	z	$\psi_0$	x cm	T °K	$\psi$	$\eta$	K w/cm °K
Argon	21	1/16	1	0.015	0.168	2.14	1800	1.010	0.779	0.94
Argon	22	1/16	1	0.035	0.168	2.18	1940	1.085	0.829	0.90
Argon	24	1/16	1	0.255	0.157	2.14	1800	1.010	0.782	0.94
						1.79	1580	0.883	0.685	0.89
						2.14	1770	0.926	0.751	1.08
						1.67	1590	0.832	0.669	0.94
Argon	28	1/8	2	0.066	0.205	4.68	1800	1.235	0.895	0.94
						4.05	1540	1.057	0.786	0.92
Argon	32	1/8	1	0.008	0.153	1.83	1500	0.763	0.595	0.86
Nitrogen	45	1/8	1	0.012	0.157	1.91	1430	0.748	0.578	0.89
Helium	1	1/16	1	0.021	0.161	2.06	2220	1.192	0.905	0.84
Helium	2	1/16	1	0.058	0.146	2.14	2590	1.261	0.956	0.94
						1.91	2070	1.008	0.805	1.00
Helium	11	1/8	2	0.113	0.248	4.68	2010	1.664	1.012	0.62
						4.21	1710	1.415	0.930	0.61
Helium	12	1/8	2	0.135	0.260	5.08	2750	2.383	1.133	0.56
Helium	13	1/8	2	0.121	0.248	4.37	1690	1.465	0.939	0.58
Helium	14	1/8	2	0.225	0.233	4.68	1980	1.640	1.006	0.63
						4.21	1690	1.400	0.924	0.61
Helium	15	1/8	2	0.119	0.208	4.68	2300	1.788	1.079	0.64
						4.05	1660	1.290	0.909	0.66
						4.52	2130	1.473	0.994	0.80
						3.81	1740	1.204	0.869	0.77
Helium	17	1/8	1	0.023	0.163	2.14	1720	0.935	0.734	0.74
						1.87	1560	0.848	0.664	0.71
Helium	18	1/8	1	0.012	0.152	2.14	2010	1.016	0.804	0.75
						1.71	1610	0.814	0.644	0.75



the 2 inch by 1/8 inch cathode in helium. The same effect must occur also with the 1 inch by 1/8 inch cathode, but, in this latter case, an additional phenomenon may affect the results.

The temperature difference between the bottom end of the cathode and the cooling water stream is proportional to the total heat flow from the cathode. The proportionality constant involves the thermal resistances of the copper base, the holder, and the interface between these two pieces. A lower limit to the temperature difference for the case of a 1 inch by 1/8 inch cathode discharging 40 watts of heat into its base can be estimated by considering the base and holder as a single 1/2 inch diameter cylinder of copper 1.25 inches long, carrying a uniform heat flux. This gives  $\Delta T = QL/KA \sim 25^\circ\text{C}$ . Allowance for thermal resistance of the interface between the base and holder, radial spreading of the heat as it goes from the tungsten into the copper, and the reduction in cross section by the empty part of the socket in the holder could increase this estimate substantially. The average of the K values from argon data, excluding the run made with the 1 inch by 1/8 inch cathode, is  $0.94 \text{ w/cm}^\circ\text{K}$ . The change  $\Delta T$  in  $T_0$  required to bring the values from this excluded run into agreement with the mean of the other values would be about  $100^\circ\text{C}$ . It is certainly believable that  $\Delta T$  could be this large.

On the basis of the preceding discussion, it is suggested that the thermal conductivity values obtained by analysis of the data from 1 inch by 1/16 inch and 2 inch by 1/8 inch cathodes operating in argon are approximately correct. The mean of these values is  $0.94 \pm 0.05 \text{ w/cm}^\circ\text{K}$ . In the subsequent analysis, the value,

$$K = 0.94 \text{ w/cm}^\circ\text{K} \quad , \quad (162)$$

will be assumed.

If experiments of this type are again undertaken in the future, it should be possible to eliminate these sources of uncertainty by installing a suitable anti-convection shield surrounding the cathode and a temperature sensor at the bottom end of the cathode for measurement of  $T_0$ .

#### 4. Electrical Resistivity

The runs at high current provide data from which the electrical resistivity temperature function for the cathode material can be estimated. As in the preceding section, the analysis does not involve "arc" relations but only heat conduction with Joule heating and radiative losses. The data are too few and of too poor a quality to permit determination of more than one parameter in the resistivity formula (87). In the present study, it is assumed that  $s$  in



that formula has the value for pure tungsten (about 1.234), but that B might differ somewhat from the value  $5.0 \times 10^{-9}$  ohm-cm/°K<sup>8</sup> obtained from figure 10.

Since the quantity H defined by equation (158) is nearly equal to  $q_0^2$ , equations (159a, b) and (160) can be written approximately

$$\psi = (1.6 \sigma \epsilon K)^{0.2} \frac{T}{D^{0.2} q_0^{0.4}} \quad (163a)$$

$$\psi_0 = (1.6 \sigma \epsilon K)^{0.2} \frac{T_0}{D^{0.2} q_0^{0.4}} \quad (163b)$$

$$\eta = (1.6 \sigma \epsilon K)^{0.2} \frac{x q_0^{0.6}}{K D^{0.2}} \quad (163c)$$

Since  $\psi_0$  is small enough that  $G(\psi_0, z) \approx \psi_0$ , equation (162) becomes

$$\eta + \psi_0 \approx G(\psi, z) \quad (164)$$

Since  $\psi, \psi_0$ , and  $\eta$  can be calculated from the experimental data, (164) can be solved for  $z$ . Then, equation (159c) gives an estimate for B,

$$B = \frac{(s+1)z q_0^2}{2K j_0^2} \left( \frac{8 \sigma \epsilon K}{5 D q_0^2} \right)^{(s+1)/5} \quad (165)$$

Table 11 and figure 53 illustrate the application of this procedure to high current data selected from Table 8. No helium data are used because the measured  $q_0$  values for runs in this gas are probably affected significantly by convective heat transfer, as discussed in the preceding section. Tip temperature data are also excluded because of spot mode operation in argon and nitrogen, and data from the 1 inch by 1/8 inch cathode are omitted because of unreliability of the  $T_0$  estimate (161). Table 11 shows that, in spite of this screening of the data, the scatter in the computed B values is large. The reason for this scatter can be seen from figure 53, in which the  $\psi, G$  values computed from the data are plotted on top of the family of curves representing the function  $G(\psi, z)$ . The horizontal and vertical bars on the points represent the estimated uncertainties in G and  $\psi$ , respectively, arising from estimated uncertainties of

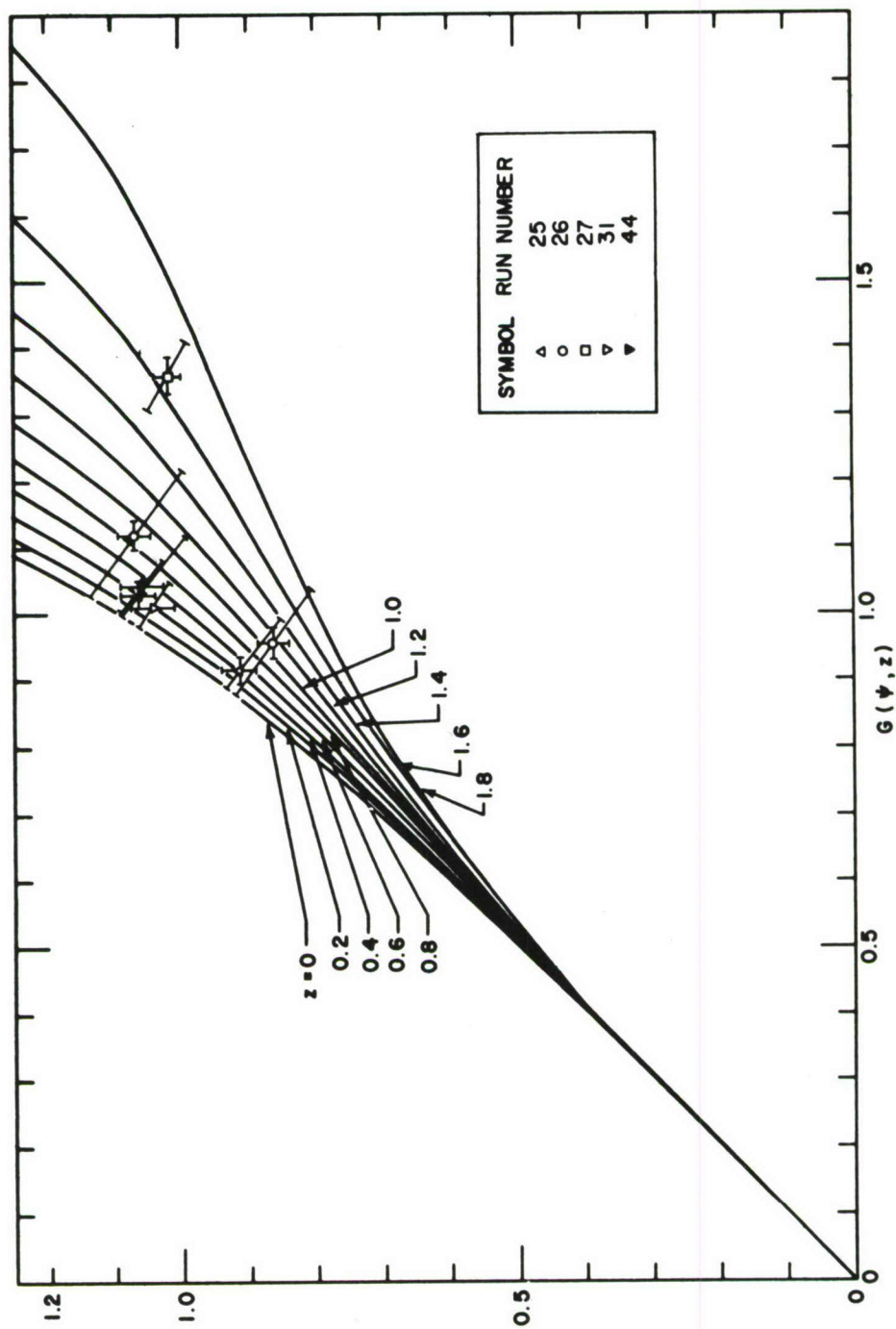


Figure 53 ANALYSIS OF CATHODE DATA FOR ELECTRICAL RESISTIVITY

$\pm 0.05$  centimeter in  $x$  and  $\pm 50^\circ\text{K}$  in  $T$ . The diagonal bars passing through the points indicate the uncertainties resulting from a possible error of 2 watts in the measurement of the total heat flow  $Q_0$  from the cathode to its cooling water. An error in  $Q_0$  gives rise to one in the heat flux  $q_0$ , and thus affects the position of the experimental point in figure 53 in accordance with equations (163). It is seen that the uncertainties arising from possible errors in the heat flow measurements are generally a good deal larger than those originating in uncertainties in  $x$  and  $T$ , so that the latter can be neglected. The two ends of each diagonal bar in figure 53 thus define upper and lower limiting values of  $z$  which would be consistent with the experimental data in view of their limited accuracy. Substitution of these limiting values into equation (165) gives corresponding upper and lower limits to  $B$ , provided that the  $q_0$  in (165) is also assigned its corresponding upper and lower limits. The results of applying this error analysis procedure to the data of Table 11 are shown in figure 54. The  $B$  values of Table 11 are represented by circles, and the vertical bars connect the upper and lower limits of accuracy. It is apparent that most of the runs provide only an order of magnitude for  $B$ . However, the data from run 27 set the reasonably narrow limits  $B = (6.4 \pm 1.1) \times 10^{-9} \text{ ohm-cm/}^\circ\text{K}^s$ .

TABLE 11

ANALYSIS OF CATHODE DATA FOR ELECTRICAL RESISTIVITY

Gas	Run Number	Diameter inch	Length inch	$x$ cm	$T$ $^\circ\text{K}$	$z$	$B$ $10^{-9} \text{ ohm-cm/}^\circ\text{K}^s$
Argon	25	1/16	1	2.14	2070	0.40	7.9
				1.87	1780	0.44	8.7
Argon	26	1/16	1	2.14	2250	0.88	6.3
				1.79	1820	1.12	8.2
Argon	27	1/16	1	2.14	2520	1.65	6.4
Argon	31	1/8	2	3.73	1700	0.39	2.6
Nitrogen	44	1/8	2	3.89	1720	0.53	3.7

The literature value of  $B$  for pure tungsten,  $5.0 \times 10^{-9}$ , is below these limits. However, the electrical resistivity of two specimens of the thoriated tungsten cathode material has been measured by Peterson<sup>36</sup> at  $23^\circ\text{C}$ . The resulting values ( $6.04 \times 10^{-6}$  and  $5.74 \times 10^{-6} \text{ ohm-cm}$ ) give an average  $B$  of  $5.3 \times 10^{-9}$ , which is just at the bottom of the range of values consistent with the data from run 27. This agreement between electrical resistivity as determined from high temperature and room temperature data provides at least a rough confirmation of the correctness of the value  $s = 1.234$  for the temperature exponent in (87). Peterson's room temperature value is selected as the "standard" value of  $B$  for subsequent calculations:



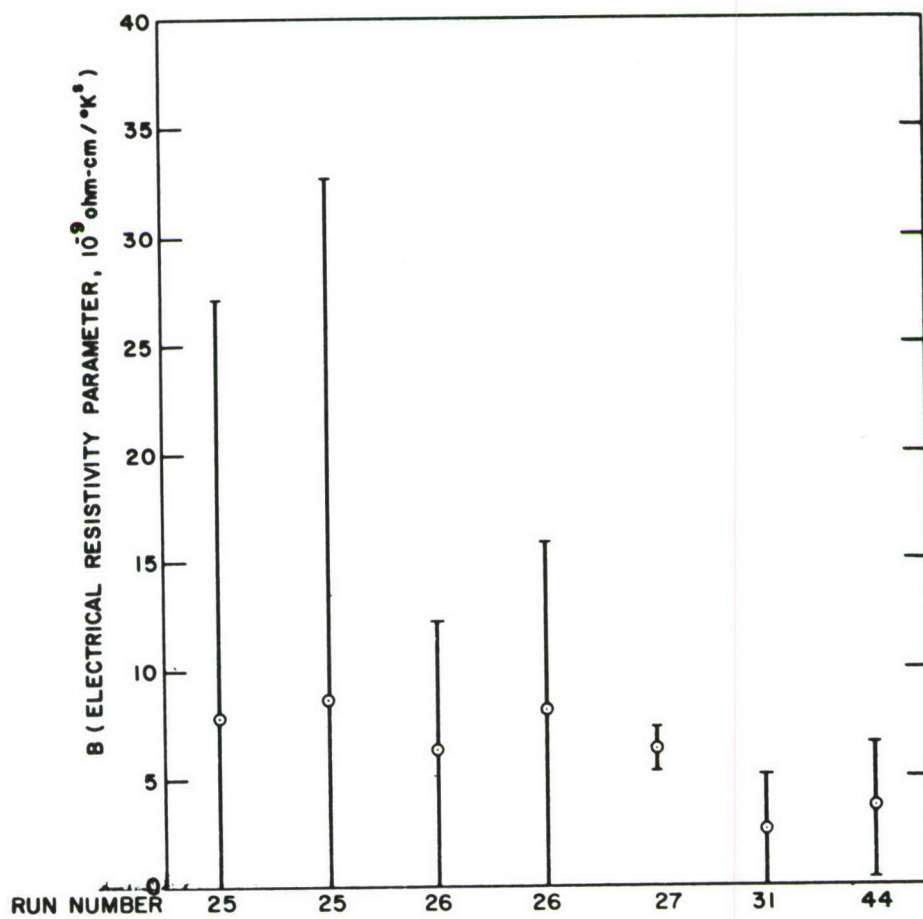


Figure 54 RESULTS OF ERROR ANALYSIS FOR ESTIMATES OF B FROM CATHODE DATA

$$B = 5.3 \times 10^{-9} \text{ ohm-cm/}^\circ\text{K}^3 .$$

(166)

#### D. COMPARISON OF THEORY AND EXPERIMENT

The experiments under discussion are significantly affected, as shown in the preceding section, by two phenomena which are not represented in the theoretical model. The rod shaped thoriated tungsten cathodes operate in the spot mode in argon and nitrogen, and even in helium at low currents, while the model assumes spotless mode operation. Furthermore, the performance of the cathode in helium is influenced very considerably by convective heat losses. The fact that the cold end temperature  $T_0$  was not measured introduces a further uncertainty which becomes fairly large in the case of the 1 inch by 1/8 inch cathode, as shown by figure 26. As a result of these factors, the experiments have produced no data which provide an unambiguous quantitative test of the theory. Nevertheless, a comparison of the experimental results with theoretical predictions is worthwhile, because it shows just what the discrepancies are and tests the usefulness of the model as a basis for rough estimates of cathode performance.

Figures 55, 56 and 57 are plots of the heat transfer to the cathode cooling system versus total current. The curves in these figures are based upon theoretical values calculated from the quasi-one-dimensional model, while the points represent the experimental data for the three cathode geometries. Figure 55 shows the results for helium. The fact that the curve for the 2 inch by 1/8 inch cathode lies above the corresponding experimental points is attributed mainly to the neglect of convective heat losses in the theoretical model. The similar discrepancy for the 1 inch by 1/8 inch cathode is believed to result from the same deficiency in the model, and from the assumption of a value (300 °K) for the cold end temperature which is unrealistically low in the case of this cathode geometry. The approximate agreement between theory and experiment for the 1 inch by 1/16 inch cathode is considered fortuitous; it probably occurs because the convective heat loss from the side of the cathode is roughly balanced by convective heating of the cathode base and holder, which are partially immersed in the heated gas of the arc chamber in this case. The theoretical curve for this geometry is not extended beyond 95 amperes, because, at this current,  $\lambda$  is already slightly larger than unity. For higher currents, the perturbation calculation of overflow effects used in the model becomes completely unrealistic.

In the cases of argon and nitrogen, the applicability of the model is questionable because of the occurrence of spot mode operation in these gases. Nevertheless, figures 56 and 57 show that, as in helium, the model reproduces the general trend of the experimental heat transfer data reasonably well.

Figures 58 through 63 present a comparison of experimental and theoretical axial temperature distributions for cathodes of the three geometries operating in helium. In each figure, the curve is based upon calculations using the

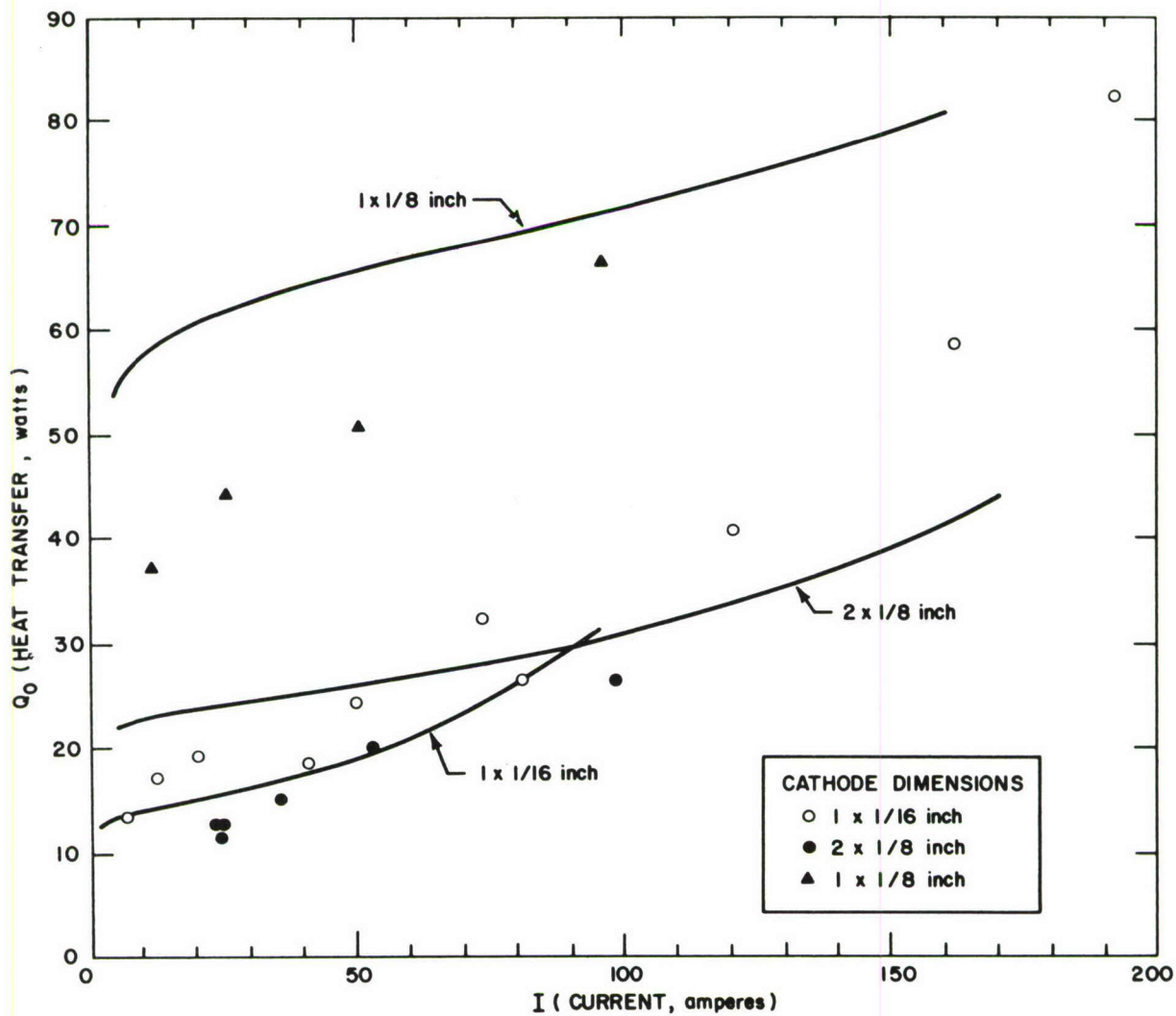


Figure 55 HEAT TRANSFER TO CATHODE COOLING SYSTEM VERSUS CURRENT (HELIUM)



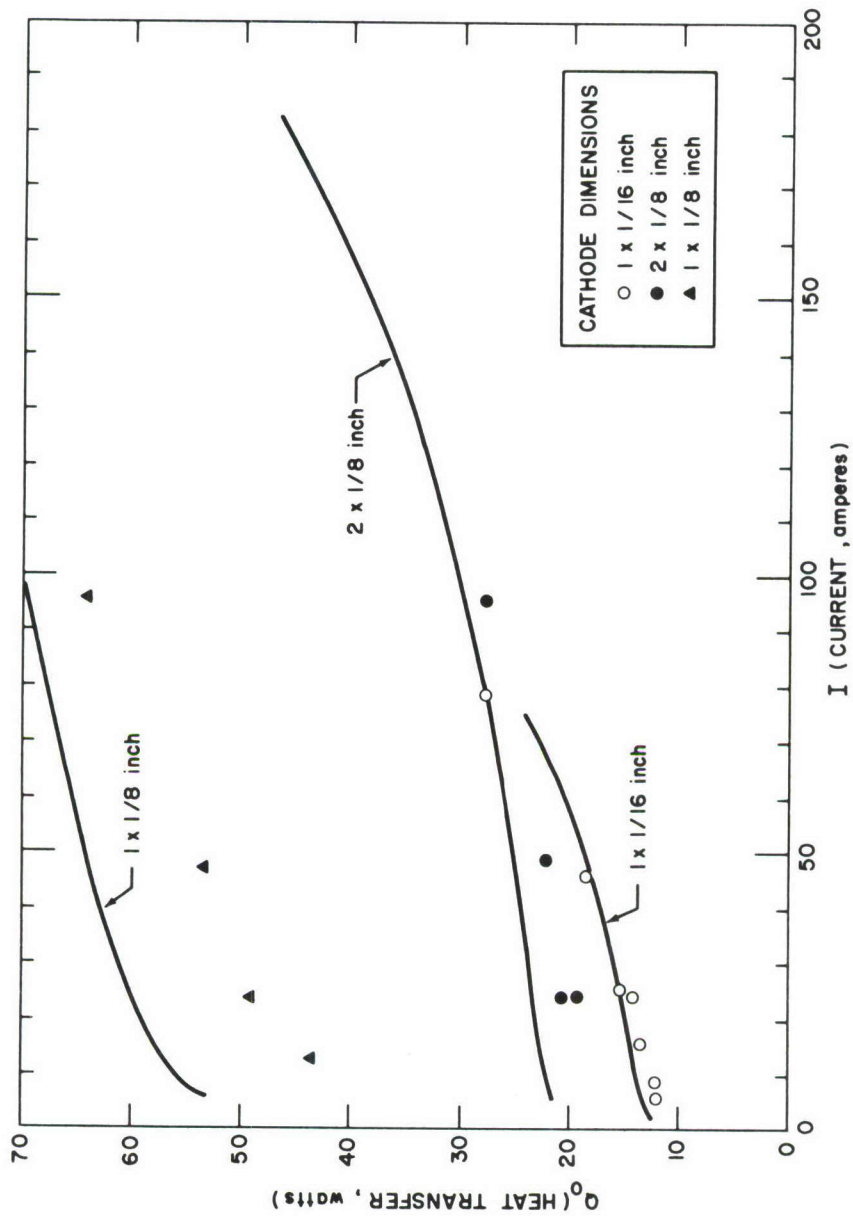


Figure 56 HEAT TRANSFER TO CATHODE COOLING SYSTEM VERSUS CURRENT (ARGON)

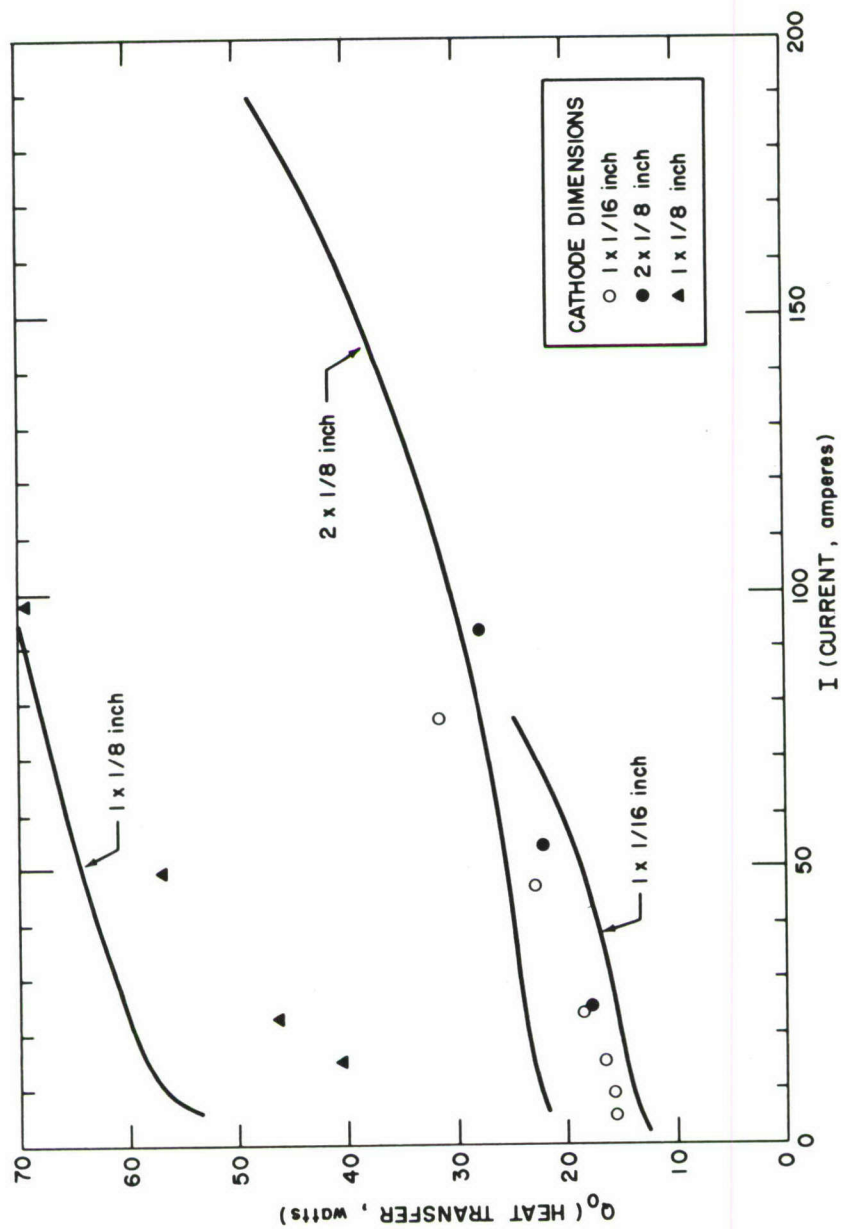


Figure 57 HEAT TRANSFER TO CATHODE COOLING SYSTEM VERSUS  
CURRENT (NITROGEN)

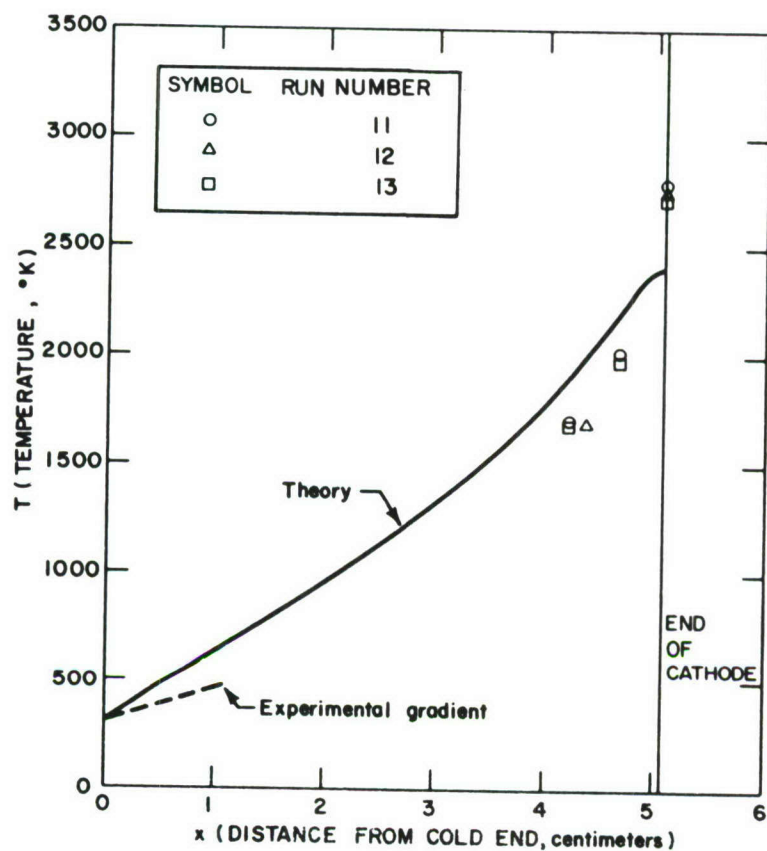


Figure 58 CATHODE TEMPERATURE DISTRIBUTION (HELIUM, TWO INCH BY ONE EIGHTH INCH CATHODE, TWENTY FIVE AMPERES)



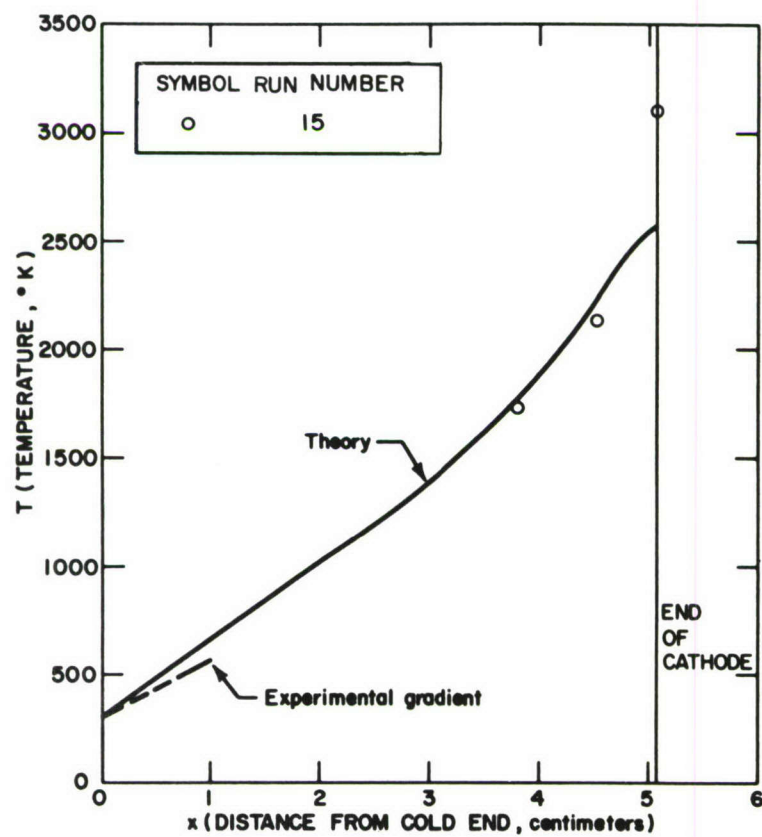


Figure 59 CATHODE TEMPERATURE DISTRIBUTION (HELIUM, TWO INCH BY ONE EIGHTH INCH CATHODE, FIFTY THREE AMPERES)

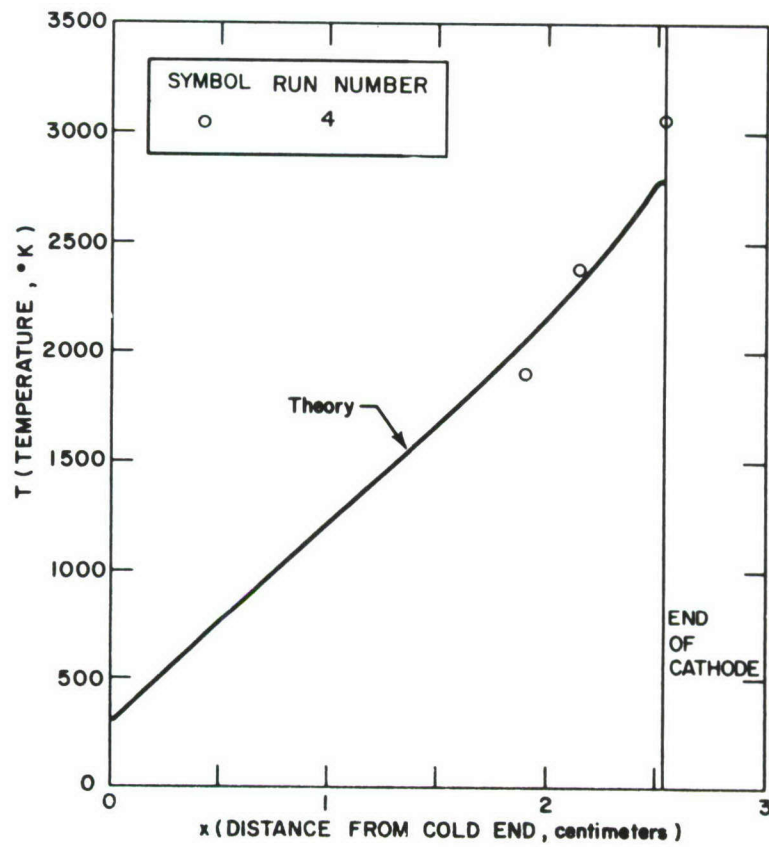


Figure 60 CATHODE TEMPERATURE DISTRIBUTION (HELIUM, ONE INCH BY ONE SIXTEENTH INCH CATHODE, FORTY ONE AMPERES)

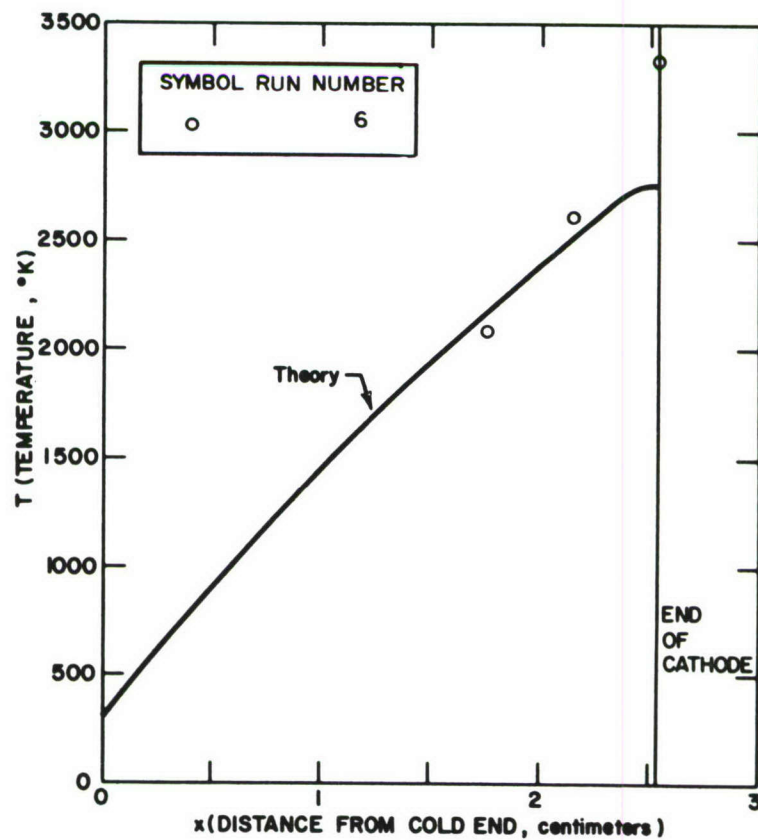


Figure 61 CATHODE TEMPERATURE DISTRIBUTION (HELIUM, ONE INCH BY ONE SIXTEENTH INCH CATHODE, SEVENTY FOUR AMPERES)



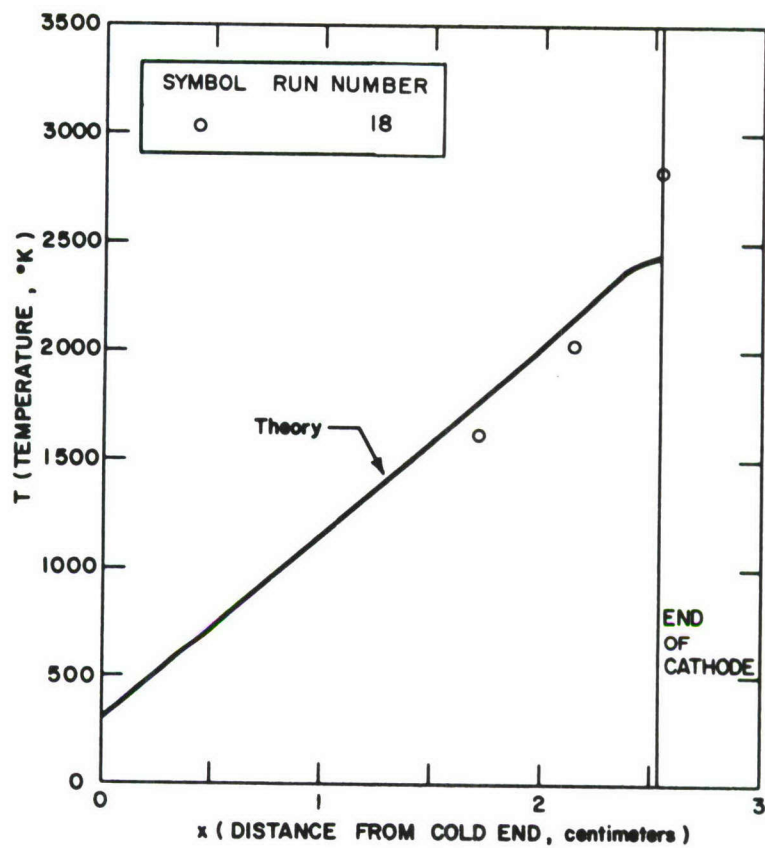


Figure 62 CATHODE TEMPERATURE DISTRIBUTION (HELIUM, ONE INCH BY ONE EIGHTH INCH CATHODE, TWENTY SIX AMPERES)

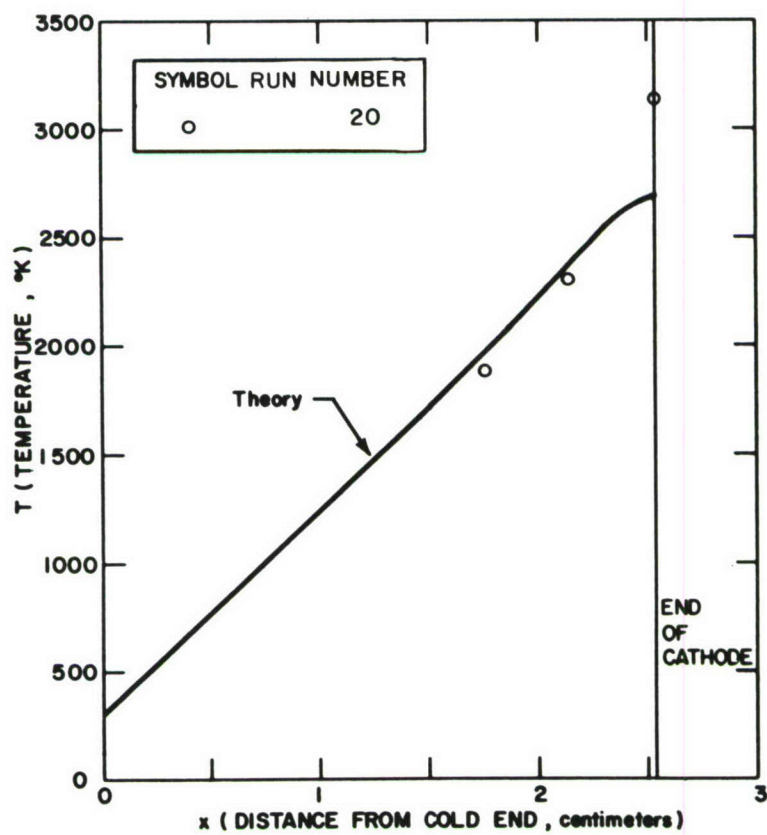


Figure 63 CATHODE TEMPERATURE DISTRIBUTION (HELIUM, ONE INCH BY ONE EIGHTH INCH CATHODE, NINETY SIX AMPERES)

theoretical model, while the points represent pyrometric measurements of temperature at various positions along the side of the cathode. The short broken line beginning at  $x = 0$  in figures 58 and 59 indicates the actual temperature gradient at the cold end, calculated from the experimental heat flux measurement assuming  $K = 0.94 \text{ w/cm}^2\text{K}$ . This broken line and the experimental points near the hot end, taken together, sketch out an approximation to the actual temperature distribution in the cathode. (Cold end temperature gradients are not indicated in figures 60 to 63, because the heat transfer data for the 1 inch cathodes are believed to be affected significantly by convective heating of the cathode base and by an unknown increase in the cold end temperature in the case of the 1 inch  $\times$  1/8 inch cathode.)

It is apparent from the figures that the actual temperature distribution is, in all cases, more concave upward than the theoretical distribution. In addition, the experimental tip temperatures are generally higher than the values predicted by theory. These differences can be accounted for, at least qualitatively, in terms of the hypothesis that substantial convective heat losses occur from the side of the cathode in helium. Such heat losses reduce the temperature in the midsection of the cathode, but cannot lower the tip temperature because the total current is "given." Thus, such losses tend to reduce the temperature gradient at the cold end of the cathode and to increase the gradient at the hot end, as shown in figures 58 to 63. Moreover, the substantial increase of the temperature gradient in the tip region drastically reduces the amount of arc overflow, and, thus (since the total current is given), increases the current density through the end of the cathode. The rise in current density entails an increase in tip temperature, in agreement with the data shown in the figures. This phenomenon is an instance of the general rule, pointed out in section IV E, that stronger cooling of the cathode tip region tends to raise the tip operating temperature.

In summary, the quasi-one-dimensional theory for spotless mode operation of rod shaped cathodes correctly predicts general trends in the variation of cathode temperature and heat transfer with cathode geometry and current, but a number of quantitative discrepancies occur. Some of these discrepancies, such as the dependence of calculated thermal conductivity upon cathode geometry in helium, are unrelated to the operation of the rod as a cathode, and simply betray the occurrence of heat transfer processes not included in the theory. Others, particularly those in the tip temperature and temperature gradient, can be accounted for at least partially by the effects of convective losses, but may also reflect errors in assumed material property values, in the approximations of the quasi-one-dimensional theory, or in the relations upon which the basic cathode model is based.



## VII. DISCUSSION

The operation of a thermionic cathode is a complex system of coupled physical processes occurring in the plasma of the cathode fall zone, at the plasma cathode interface, and in the cathode interior. The present report has set forth a theoretical model for this system. Although many of the important processes are represented by crude approximations, this model is physically complete in that it permits ab initio calculation of cathode performance solely from geometrical considerations and the physical properties of the cathode and the gas.

The essential physics of thermionic cathode operation, as viewed from the present perspective, may be summarized briefly as follows. Flow of electric current between the cathode and the plasma occurs predominantly by thermionic emission of electrons from the surface. Since each electron emerging from the surface carries away an energy equal to the thermionic work function, such a steady flow of emission current is possible only if energy is simultaneously supplied to the surface in sufficient quantity to balance this and other losses. In most cases, the bulk of this energy is provided by ion bombardment. Thus, although electron emission is the main charge transfer process, it can only occur if a substantial fraction (about 10 percent or more) of the current is carried by positive ions drawn from the plasma. Because of their greater mass, the ions move much more slowly than do the electrons in the electric field adjacent to the surface, and this region, therefore, contains a net positive space charge. This space charge layer is directly responsible for the cathode fall of potential and for the very high electric field intensity at the cathode surface. The thermionically emitted electrons are accelerated by this field to an energy equal to the cathode fall, and deposit most of this energy in the plasma near the cathode. The plasma absorbs this energy, in the steady state, by production of ion electron pairs. Thus, at least up to a point, an increase in electron emission current density leads to an increase in electron "beam" energy deposited in the gas, an increase in ion production, an increase in ion current to the surface, and an increase in surface heating due to ion bombardment. However, there is an upper limit to the ion current density which can be drawn from the plasma at a given pressure; it is given by the flux of ions across an arbitrary plane surface in a fully ionized gas. Once this limit for the ion current density has been reached, further increases of electron emission current density withdraw additional work function energy from the surface without leading to a compensatory increase in ion bombardment heating.

The net heat entering the cathode surface, after allowance for work function and radiative losses, flows by conduction into the cathode interior. The temperature and heat flow distributions inside the cathode are governed by the steady state heat conduction equation. A given distribution of heat flux over



the surface defines a solution of the cathode heat conduction problem which, in turn, gives a temperature distribution over the surface. This temperature distribution determines a distribution of electron emission current which, by the ion production and bombardment mechanisms discussed in the preceding paragraph, leads to a certain distribution of net heat flux into the surface. This heat flux distribution determined by the temperature field inside the cathode must be identical with the original distribution determining the temperature field as a solution of the heat conduction problem for the cathode interior.

No general methods are available at present for obtaining accurate analytical or numerical solutions of this rather intricate problem, but the main features of the system have been studied using approximate means. For a strongly cooled cathode, it turns out that the problem has no solution unless the ion current density is equal to its kinetic theory limiting value over a major part of the emitting region. Thus, the operating region of a strongly cooled cathode contracts to form a spot in which the current density is limited essentially by the density of particles in the plasma of the cathode fall zone. An increase of pressure raises this particle density, and hence increases the current density and the temperature of the surface in the spot region.

In a cathode which is sufficiently poorly cooled, the heat conduction equation requires a relatively large region of the cathode to be hot. Electron emission from the surface, then, leads to a relatively low current density spread over a large area. The resulting widely distributed moderate heat flux matches the requirements of the heat conduction problem for this case. Normally, the ion current density is below its limiting value over the entire surface. This type of cathode operation, in which the current density is limited only by the requirements of the cathode heat conduction problem, is tentatively identified with the spotless mode. The theory, in its present somewhat schematic form, predicts that the current density distribution over a cathode operating in the spotless mode should be pressure independent.

It is not yet altogether clear how the arc "chooses" between these two modes and, generally, between different possible solutions of either type. It is likely that, for some geometries and situations, the problem admits only a single nontrivial solution. However, circumstances clearly exist in which two or more solutions are possible mathematically. One instance is the case of a well cooled cylindrical cathode. It appears that this problem should admit an axisymmetric solution with the spot at the center of the end surface of the cathode. Experimentally, however, another solution is "chosen" with the spot on the rim of the end surface. Perhaps, problems such as this can be resolved by performing a stability analysis based upon the transient version of the problem.

## VIII. RECOMMENDATIONS FOR FURTHER WORK

The theory provides, in its present form, a conceptual framework for discussing and analyzing thermionic arc cathode behavior. Qualitative comparison with experimental data indicates that this framework is approximately correct. However, a considerable amount of additional work is needed to develop this model into a quantitative theory which can be used confidently in the design of cathodes for high pressure, high enthalpy plasma generators. The lines of effort which appear most likely to be fruitful are listed below.

### 1. Numerical Procedures for Solving Cathode Model

A method for computing accurate solutions of the model for particular cathode geometries is needed both for testing the model's validity and for engineering applications. Possible approaches to the development of such a numerical procedure have been discussed in paragraph 1 of section IV D.

### 2. Processes in Cathode Fall Zone and at Surface

The relations presented in section III for describing processes in the plasma and at the surface are all rather crude approximations. A number of these relations can clearly be improved. For example, the Mackeown formula (6) for the electric field at the surface should be modified, as shown by Ecker,<sup>12</sup> to take account of back diffusion of electrons from the plasma and thermal velocities of the ions. A somewhat detailed theory of charge and energy transport in the ion production zone should be developed, including some of the effects neglected in section III, such as Joule heating of the gas, heat conduction from the gas to the surface, radiative losses, and energy deposition in the gas by Auger ejected electrons from the surface and rebounding neutralized ions. Similarly, the cathode surface energy balance should be refined to include heat conduction from the gas and accommodation coefficient effects. Once these effects have been properly formulated, they should be incorporated into the cathode model.

### 3. Quasi-one-dimensional Cathode in Spot Mode Operation

It should be possible to obtain, from the theory, a criterion for spot mode operation on a rod shaped cathode. In addition, an approximate theory for a rod shaped cathode operating in the spot mode can probably be assembled by combining the existing quasi-one-dimensional theory (without overflow) with the approximate spot theory of paragraph 3 of section IV D. Such an approximate theoretical model would be useful for analysis of experimental data for rod shaped cathodes running in nitrogen and argon.



#### 4. Experiments

A further attempt should be made to obtain experimental data for quantitative comparison with the theory. It appears that this should be possible with some modifications of the apparatus described in section VI. A thermocouple or other sensor should be added to permit direct measurement of the temperature at the cold end of the cathode. An attempt should also be made to obtain interpretable data from operation in helium by reducing the convective heat transfer effects with the aid of a shield surrounding the cathode or a suitable change in the geometry of the arc chamber. Further experiments with other cathode geometries should also be valuable.

#### 5. Theory for Cold Cathodes

There is considerable interest, for plasma generator applications, in cold cathodes such as water cooled copper with a magnetic field applied to move the spot over the surface. Several experimental investigations have shown that the current enters a cold cathode through a number of "microspots," each of which carries a current density of  $10^7$  or  $10^8$  amp/cm<sup>2</sup>. The problem of explaining the mechanism of charge transport in these microspots has received much attention.<sup>6-9, 16-17, 37</sup> Various authors have invoked field emission, T-F emission, electron ejection by impact of excited atoms, and other processes. The most plausible assumption appears to be that the current is transported predominantly by the general mechanisms of ion neutralization and thermal field emission of electrons rather than by "special" mechanisms involving excited atoms. It would be a valuable exercise to attempt construction of a "complete" model for cold cathodes on the basis of this assumption. Other phenomena whose effects should be included in the model are Joule heating and heat conduction in the cathode, ion bombardment heating, space charge, kinetic theory limitations on ion current density, ion production in the gas, magnetic pinch pressure, electric pressure on the surface, and vaporization of cathode material.

## IX. REFERENCES

1. John, R.R. and W.L. Bade, Recent advances in electric arc plasma generation technology, ARS J. 31, 4-17 (1961).
2. Somerville, J.M., The Electric Arc, Methuen, London (1959), p. 58-78.
3. Weinstein, R.H. and R.V. Hess, New Experiments with Hollow Cathode Discharges (for Application to Plasma Accelerators), Third Symposium on Engineering Aspects of Magnetohydrodynamics, Rochester, N.Y. (March 1962).
4. Somerville, J. M., Ref.2, p. 64-65.
5. Ecker, G., Die Erscheinung des Beweglichen Einfach und Mehrfach-brennflecks an der Kathode des Elektrischen Lichtbogens, Z. Physik 136, 556-572 (1954).
6. Bauer, A., Untersuchungen über den Kathodenfall in den Übergangsbereichen vom Thermobogen zum Feldbogen und vom Bogen zur Glimmentladung, Ann. Physik 18, 387-400 (1956).
7. Lee, T.H., T-F theory of electron emission in high current arcs, J. Appl. Phys. 30, 166-171 (1959).
8. Lee, T.H., Energy distribution and cooling effect of electrons emitted from an arc cathode, J. Appl. Phys. 31, 924-927 (1960).
9. Lee, T.H. and A. Greenwood, Theory for the cathode mechanism in metal vapor arcs, J. Appl. Phys. 32, 916-923 (1961).
10. Weizel, W. and W. Thouret, Lichtbögen mit und ohne Brennfleck, Z. Physik 131, 170-184 (1952).
11. Ecker, G., Electrode components of the arc discharge, Ergeb. exakt. Naturwiss. 33, 1-104 (1961).
12. Ibid., p. 32-35.
13. Mackeown, S.S., [The] Cathode drop in an electric arc, Phys. Rev. 34, 611-614 (1929).
14. Somerville, J.M., Ref. 2, p. 67-68.
15. Moelwyn-Hughes, E.A., Physical Chemistry, Cambridge Univ. Press (1951), p. 63-64.

16. von Engel, A. and A. E. Robson, [The] Excitation theory of arcs with evaporating cathodes, Proc. Roy. Soc. (London) A242, 217-236 (1957).
17. Hernqvist, K. G., Emission mechanism of cold cathode arcs, Phys. Rev. 109, 636-646 (1958).
18. Dolan, W. W. and W. P. Dyke, Temperature and field emission of electrons from metals, Phys. Rev. 95, 327-332 (1954).
19. Murphy, E. L. and R. H. Good, Jr., Thermionic emission, field emission, and the transition region, Phys. Rev. 102, 1464-1473 (1956).
20. Nottingham, W. B., Thermionic Emission, In: Handbuch der Physik, vol. 21, Springer - Verlag, Berlin (1956), p. 6-7, 32.
21. Ecker, G., Ref. 11, p. 36-40.
22. Hagstrum, H. D., Auger ejection of electrons from tungsten by noble gas ions, Phys. Rev. 104, 317-318 (1956).
23. Somerville, J. M., Ref. 2, p. 66.
24. Carslaw, H. S. and J. C. Jaeger, Conduction of Heat in Solids, 2nd. ed. Clarendon Press, Oxford (1959), p. 10.
25. Rich, J. A., Resistance heating in the arc cathode spot zone, J. Appl. Phys. 32, 1023-1031 (1961).
26. Holm, R., [The] Vaporization of the cathode in the electric arc, J. Appl. Phys. 20, 715-716 (1949).
27. Carslaw, H. S. and J. C. Jaeger, Ref. 24, p. 215-216.
28. Müller, G. and W. Finkelburg, Über den Kathoden-und Anodenfall eines Kohlelichtbogens hoher Stromstärke, Naturwissenschaften 42, 294 (1955).
29. Neurath, P. W. and T. W. Gibbs, J. Appl. Phys. (to be published). (See also Part II, Vol. II of this report.)
30. Osburn, R. H., Thermal conductivities of tungsten and molybdenum at incandescent temperatures, J. Opt. Soc. Am. 31, 428-432 (1941).



31. AIP Handbook, McGraw-Hill, New York (1957), p. 4-67.
32. Handbook of Chemistry and Physics, 38th ed., Chemical Rubber Publ., Cleveland (1956), p. 2366.
33. Ref. 31, p. 6-79.
34. Nottingham, W.B., Ref. 20, p. 175.
35. Ref. 31, p. 6-7, 6-31.
36. Peterson, W., Avco RAD, Personal Communication.
37. Somerville, J.M., Ref. 2, p. 73-78.

## X. APPENDIXES

- A. NUMERICAL PROCEDURE FOR COMPUTATION  
OF SURFACE HEAT FLUX AS A FUNCTION OF  
SURFACE TEMPERATURE
- B. PROGRAM FOR SOLUTION OF QUASI-ONE-  
DIMENSIONAL CATHODE MODEL

## APPENDIX A

### NUMERICAL PROCEDURE FOR COMPUTATION OF SURFACE HEAT FLUX AS A FUNCTION OF SURFACE TEMPERATURE

The net heat flux into the surface,  $q_s$ , is determined as a function of surface temperature  $T_s$  for a given cathode fall voltage  $V_c$  by the relations (54) through (59),

$$q_s = j_i (V_c + V_I - \phi) - j_e \phi - \sigma \epsilon T_s^4 \quad (54)$$

$$j_e = A T_s^2 e^{-\theta/T_s} \quad (55a)$$

$$\theta = 11609 \phi - 4.40 \sqrt{E_c} \quad (55b)$$

$$E_c = 873 V_c^{1/4} [(1823W)^{1/2} j_i - j_e]^{1/2} \quad (56)$$

$$j_i = \min [a j_e / (1-a), (j_i)_{\max}] \quad (57)$$

$$\alpha = V_c / (V_c + V_I) \quad (58)$$

$$(j_i)_{\max} = \frac{P \epsilon_e}{\sqrt{8\pi M k T_g}} \quad (59)$$

Among the quantities appearing in these equations,  $M$ ,  $V_I$ , and  $W$  are gas properties, and  $\phi$ ,  $A$ , and  $\epsilon$  material properties of the cathode. The gas temperature  $T_g$  in the ion production zone under conditions of full ionization is about  $0.15 V_I/k$ . The cathode fall is taken as an input parameter (in place of the total current). Thus,  $\alpha$  is known from (58). The problem is to calculate values of  $q_s$  corresponding to known values of  $T_s$ . This can be accomplished most readily by introducing the nondimensional temperature,

$$\tau = T_s / \theta \quad , \quad (167)$$

in place of  $T_s$  as the independent variable of the computation. Then, (55a) becomes



$$j_e = A (\theta \tau)^2 e^{-1/\tau} \quad (168)$$

With given  $\tau$ , (168) is rather insensitive to uncertainty in  $\theta$ . Hence, one can proceed as follows:

1. Assume the initial approximation  $\theta \simeq 11609 \phi$ .
2. Calculate  $j_e$  from (168)
3. Calculate  $j_i$  from (57)
4. Calculate  $E_c$  from (56)
5. Calculate an improved value of  $\theta$  from (55b)
6. Repeat calculation of  $j_e, j_i$  with new  $\theta$ . Also calculate  $T_s$  from (167)
7. Calculate  $q_s$  from (54) using  $j_e, j_i, T_s$  values from step (5).

The procedure converges so rapidly that no further iterations are usually required.

## APPENDIX B

### PROGRAM FOR SOLUTION OF QUASI-ONE-DIMENSIONAL CATHODE MODEL

Figures 64 to 69 present a FORTRAN listing of the program for solving the quasi-one-dimensional cathode model (139). The correspondence between FORTRAN symbols used in this program and the mathematical notation employed in this report is as follows:

<u>FORTRAN Symbol</u>	<u>Mathematical Symbol</u>	<u>FORTRAN Symbol</u>	<u>Mathematical Symbol</u>
D	D	VØ	v
XL	L	VC	$V_c$
T0	$T_0$	XJ0	$j_0$
TAU	$\tau$	C	C
W	w	PSIS	$\psi_s$
VI	$V_I$	PSI0	$\psi_0$
A	A	Z	z
PHI	$\phi$	ETAS	$\eta_s$
XK	K	DELTA	$\Delta$
B	B	F	F
S	s	EC	$E_c$
EPS	$\epsilon$	XI	I
ZC	$z_c$	VR	$\Delta V$
THE TAO	$\theta_0$	Q0	$q_0 \pi D^2 / 4$
THETA	$\theta$	ALPHA	$\alpha$
TNP	$T_{ns}$	TS	$T_s$
TN	$T_{ns}$	QE	$q_E \cdot \pi D^2 / 4$
XLAMBD	$\lambda$		

```

C      QUASI ONE DIMENSIONAL CATHODE MODEL WITH OVERFLOW
      ARGF(X,Z)=1.0+X**5-Z*X**(S+1.)
      COMMON S,CG,CV,EPS,XK,B,A,PHI,DTNP,FF
      DIMENSION D(10),XL(10),TO(5),TAU(25),W(5),VI(5),PSI(20),ETA(20)
      DO 600 I=1,NG
      DO 500 J=1,ND
      DO 400 K=1,NL
      DO 300 L=1,NT0
      DO 200 M=1,NTAU
      WRITE OUTPUT TAPE 5,5,W(I),VI(I),D(J),XL(K),TO(L)
5      FORMAT(5H1 W=F7.3,5H VI=F6.3,4H D=F5.3,4H L=F5.2,5H TO=F5.0)
      MM=1
      NTH=1
      NDEL=1
      NTRY=0
      THETA0=11609.*PHI
      THETA=THETA0
      RADC=9.07E-12*EPS/XK/D(J)
      THMC=2.*B/XK/(S+1.)
      CALL START (TAU(M),D(J),VI(I),TNP,DTNP)
      GO TO 11
10     TNP=TNP+DTNP
11     MBS=0
      INTP=1
      TN=THETA*TAU(M)
      RF=A*TN**2*EXP(-1.0/TAU(M))
12     RADP=5.67E-12*EPS*TN**4
      CNP=XK*TNP
      TKD=THETA*XK*D(J)*TNP**2*0.5/TN**2
      XLAMD=(2.*RADP-TKD+SQRTF((TKD-2.*RADP)**2+4.*(CNP**2-RADP**2)))
X      *0.5/(CNP-RADP)
      V0=XLAMD*TKD/RF
      VC=-0.5*(VI(I)-PHI)+0.5*SQRTF((VI(I)+PHI)**2+4.*VI(I)*V0)
      XJO=RF*(1.+VC/VI(I))/(1.+XLAMD)**2*(1.+(1.+XLAMD)*4.*TN**2
X      /D(J)/THETA/TNP)
      C=TNP**2-RADC*TN**5+THMC*XJO**2*TN**(S+1.)
      NTRY=NTRY+1
      IF(NTRY-NMAX)66,66,67
67     WRITE OUTPUT TAPE 5,68,TAU(M),VC,TNP,C,DELTA,Z,THETA
68     FORMAT(21H ITERATION STOP TAU=F6.3,5H VC=F8.3,6H TNP=1PE10.3,
X      4H C=E10.3,8H DELTA=E10.3,4H Z=0PF8.4,8H THETA=1PE10.3)
      GO TO 200
66     IF(C)18,18,14
14     PSIS=(RADC/C)**0.2*TN
      PSIO=(RADC/C)**0.2*TO(L)
      Z=THMC*XJO**2*(RADC/C)**(-0.2*(S+1.))/C
      ETAS=SQRTF(C)*(RADC/C)**0.2*XL(K)
      GO TO (19,90),MM

```

Figure 64a FORTRAN LISTING OF MAIN PROGRAM FOR SOLUTION OF QUASI-ONE-DIMENSIONAL CATHODE MODEL



```

19 IF(Z-ZC)16,15,15
15 QARG=ARGF(PSIS,Z)
   IF(QARG-CARG)18,18,17
17 DARG=5.*PSIS**4-(S+1.0)*PSIS**S*Z
   IF(DARG)16,18,18
18 NTH=1
   GO TO 10
16 DELTA=ETAS-G(PSIO,PSIS,Z)
   IF(DELTA)20,21,21
20 DELTAN=DELTA
   TNP=TNP
   GO TO (22,25),INTP
22 NDEL=2
   NTH=1
   GO TO 10
21 GO TO (23,26),NTH
23 GO TO (27,24),NDEL
27 MBS=MBS+1
   IF(MBS-MBSTOP)28,28,29
28 TNP=TNP-0.5**MBS*DTNP
   GO TO 12
29 WRITE OUTPUT TAPE 5,30,TAU(M),VC,DELTA,Z,PSIS,TNP
30 FORMAT(22H BACKSPACE STOP TAU=F6.3,5H VC=F8.3,8H DELTA=
X      1PE10.3,4H Z=0PF8.4,7H PSIS=F8.4,6H TNP=1PE10.3)
   GO TO 200
26 TNP=TNP-DTNP
   GO TO 12
24 TNPP=TNP
   DELTAP=DELTA
25 ATNP=DELTAP*(TNPP-TNP)/(DELTAP-DELTAN)
   TNP1=TNPP-ATNP
   IF(ABSF(TNP1-TNP)-CTNP*TNP)40,40,35
35 TNP=TNP1
   INTP=2
   GO TO 12
40 TNP=TNP1
   F=16900.*SQRTF(A)*VC**0.25*SQRTF(VC/VI(1)*SQRTF(1823.*W(1))-1.)
X      *TAU(M)*EXPF(-0.5/TAU(M))/(1.+XLAMBD)
   THETA1=0.5*(2.*THETA0+F)-0.5*SQRTF(F**2+4.*F*THETA0)
   IF(ABSF(THETA-THETA1)-CTHETA)41,41,42
41 MM=2
42 THETA=THETA1
   NTH=2
   NDEL=1
   GO TO 11
90 CALL OUTPUT (THETA,XJO,C,TO(L),D(J),VC,PSIS,PSIO,Z,XLAMBD,TN,
X      TNP,ETAS,VI(1),TAU(M),XL(K),RADC,OHMC,RF)
200 CONTINUE
300 CONTINUE
400 CONTINUE
500 CONTINUE
600 CONTINUE

```

Figure 64b Concluded

```

SUBROUTINE START (TAUM,DJ,VII,TNP,DTNP)
COMMON S,CG,CV,EPS,XK,B,A,PHI,DTNP0,FF
RADC=9.07E-12*EPS/XK/DJ
ØHMC=2.*B/XK/(S+1.)
THETA=11609.*PHI
TN=THETA*TAUM
RF=A*TN**2*EXP(-1.0/TAUM)
RND=1.-0.3885E+24*XK*B*A*TN**(S-1.)*EXP(-2./TAUM)/EPS**2
X      /(S+1.)/THETA**2
IF(RND)701,701,702
702 TNPI=SQRTF((4.538E-12*EPS*TN**5/XK/DJ)*(1.+SQRTF(RND)))
RADP=5.67E-12*EPS*TN**4
CØNP=XK*TNPI
TKD=THETA*XK*DJ*TNPI**2*0.5/TN**2
XLAMBD=(2.*RADP-TKD+SQRTF((TKD-2.*RADP)**2+4.*(CØNP**2-RADP**2)))
X      *0.5/(CØNP-RADP)
VØ=XLAMBD*TKD/RF
VC=-0.5*(VII-PHI)+0.5*SQRTF((VII+PHI)**2+4.*VII*VØ)
XJØ=RF*(1.+VC/VII)/(1.+XLAMBD)**2*(1.+(1.+XLAMBD)**4.*TN**2
X      /DJ/THETA/TNPI)
RND2=RADC*TN**5-ØHMC*XJØ**2*TN**(S+1.)
IF(RND2)701,701,703
703 TNP=SQRTF(RND2)
IF(TNP-DTNP0/FF)701,711,711
701 TNP=DTNP0
DTNP=DTNP0
GØ TØ 750
711 DTNP=FF*TNP
TNP=TNP-DTNP
750 RETURN

```

Figure 65 FORTRAN LISTING OF SUBROUTINE START

```

FUNCTION G(X0,X1,Z)
  ARGF(X,Y)=1.0+X**5-Y*X**(S+1.0)
  INDF(X,Y)=1.0/SQRTF(ARGF(X,Y))
  COMMON S,CG,CV,EPS,XK,B,A,PHI,DTNPO,FF
  Q=0.0
  DX=0.1*(X1-X0)
301  G=0.0
     X=X0
302  DG=DX*(INDF(X,Z)+4.*INDF(X+DX,Z)+INDF(X+2.*DX,Z))/3.0
     X=X+2.*DX
     G=G+DG
     IF(X-X1+1.0E-6)302,303,303
303  IF(ABSF(G-Q)-CG)305,305,304
304  DX=0.5*DX
     Q=G
     GO TO 301
305  RETURN

```

Figure 66 FORTRAN LISTING OF FUNCTION G



```

FUNCTION V(X0,X1,Z)
  ARGF(X,Y)=1.0+X**5-Y*X*(S+1.0)
  VINP(X,Y)=X**S/SQRTF(ARGF(X,Y))
  COMMON S,CG,CV,EPS,XK,B,A,PHI,DTNPO,FF
  QV=0.0
  DX=0.1*(X1-X0)
201  V=0.0
     X=X0
202  DV=DX*(VINP(X,Z)+4.*VINP(X+DX,Z)+VINP(X+2.*DX,Z))/3.0
     X=X+2.*DX
     V=V+DV
     IF(X-X1+1.0E-6)202,203,203
203  IF(ABSF(V-QV)-CV)205,205,204
204  DX=0.5*DX
     QV=V
     GO TO 201
205  RETURN

```

Figure 67 FORTRAN LISTING OF FUNCTION V

```

SUBROUTINE DISTAN (X0,X1,Z,PSI,ETA)
  ARGF(X,Y)=1.0+X**5-Y*X**(S+1.0)
  INDF(X,Y)=1.0/SQRTF(ARGF(X,Y))
  COMMON S,CG,CV,EPS,XK,B,A,PHI,DTNPO,FF
  DIMENSION PSI(20),ETA(20)
  Q=0.0
  DX=0.05*(X1-X0)
  DXPRNT=DX
801  G=0.0
     X=X0
     XPRNT=X0+DXPRNT
     IP=1
802  DG=DX*(INDF(X,Z)+4.*INDF(X+DX,Z)+INDF(X+2.*DX,Z))/3.0
     X=X+2.*DX
     G=G+DG
     IF(X-XPRNT+1.0E-6)810,810,811
811  PSI(IP)=X
     ETA(IP)=G
     IP=IP+1
     XPRNT=XPRNT+DXPRNT
810  IF(X-X1+1.0E-6)802,803,803
803  IF(ABSF(G-Q)-CG)805,805,804
804  DX=0.5*DX
     Q=G
     GO TO 801
805  RETURN

```

Figure 68 FORTRAN LISTING OF SUBROUTINE DISTAN

```

SUBROUTINE OUTPUT (THETA,XJO,C,TOL,DJ,VC,PSIS,PSIO,Z,XLAMBD,TN,
X   TNP,ETAS,VII,TAUM,XLK,RADC,ØHMC,RF)
  ARGF(X1,X2)=1.0+X1**5-X2*X1**(S+1.0)
  SECHF(X)=2.0/(EXP(X)+EXP(-X))
  COMMON S,CG,CV,EPS,XK,B,A,PHI,DTNPO,FF
  DIMENSION PSI(20),ETA(20)
  THETA0=11609.*PHI
  EC=((THETA0-THETA)/4.4)**2
  XI=0.7854*DJ**2*XJO
  VR=XJO*B*(C/RADC)**(0.2*(S+1.0))/SQRTF(C)*V(PSIO,PSIS,Z)
  Q0=XK*SQRTF(RADC*TOL**5-ØHMC*TOL**(S+1.0)*XJO**2+C)*0.7854*DJ**2
  ALPHA=VC/(VC+VII)
  VEFF=Q0/XI
  TS=TN*(1.-2.*TN*LØGF(1.+XLAMBD))/THETA)
  XJE=RF*(1.+VC/VII)/(1.+XLAMBD)**2
  QE=((VC-PHI)*XJE-5.67E-12*EPS*TS**4)*0.7854*DJ**2
  DGRAD=SQRTF(ARGF(PSIS,Z))-SQRTF(ARGF(PSIO,Z))
  PRAD=0.3927*DJ**2*XK*SQRTF(C)*(2.*DGRAD+Z*(S+1.0)*V(PSIO,PSIS,Z))
  PJ=XI*VR
  ØVERF=TN**2*LØGF(2.+XLAMBD))/THETA/TNP
  VLØSS=(PRAD+Q0+5.67E-12*EPS*TS**4)*0.7854*DJ**2)/XI
  WRITE ØUTPUT TAPE 5,91,XI,TS,XJO,Q0,Z
  WRITE ØUTPUT TAPE 5,92,VC,TN,XJE,QE,PSIS
  WRITE ØUTPUT TAPE 5,93,VR,ALPHA,EC,PJ,PSIO
  WRITE ØUTPUT TAPE 5,94,VEFF,XLAMBD,TNP,PRAD,ETAS
  WRITE ØUTPUT TAPE 5,95,VLØSS,TAUM,ØVERF,THETA,C
91  FØRMAT(9HØCURRENT=F9.2,16H
X    1PE10.3,19H
92  FØRMAT(9H    VC=F9.2,16H
X    1PE10.3,19H
93  FØRMAT(9H    VR=F9.2,16H
X    1PE10.3,19H
94  FØRMAT(9H    VEFF=F9.2,16H
X    1PE10.3,19H
95  FØRMAT(9H    VLØSS=F9.2,16H
X    1PE10.3,19H
    WRITE ØUTPUT TAPE 5,96
    TNP=
    Z=E10.3)
    JE=
    PSIS=E10.3)
    EC=
    PSIO=E10.3)
    TNP=
    ETAS=E10.3)
    ØVERF=
    C=E10.3)

```

Figure 69a FORTRAN LISTING OF SUBROUTINE OUTPUT



```

96 FORMAT(110HTEMPERATURE    DISTANCE    CURR DENSITY    SIDE HEAT
X    RAD POWER    JOULE HEAT    PSI    ETA)
T=TOL
DIS=0.
ETA00=0.0
XJ=XJO
SHPUL=0.
RHPUL=1.782E-11*DJ*T**4*EPS
ØHPUL=0.7854*DJ**2*B*T**S*XJ**2
WRITE ØOUTPUT TAPE 5,97,T,DIS,XJ,SHPUL,RHPUL,ØHPUL,PSIO,ETA00
97 FØRMAT(1HØF7.0,F15.3,1P6E15.3)
CALL DISTAN (PSIO,PSIS,Z,PSI,ETA)
DØ 100 IP=1,20
DIS=(C/RADC)*Ø.2*ETA(IP)/SQRTF(C)
Y=XLK-DIS
PERTAG=0.5*THETA*TNP*Y/TN**2-0.5*LØGF(XLAMBD)
TPERT=TNP*Y+(TN**2/THETA)*LØGF(0.25/XLAMBD*(SECHF(PERTAG))**2)
T=(C/RADC)**0.2*PSI(IP)+TPERT
XJPERT=TNP*XK/(VC-PHI)*(TANH(PERTAG)-(1.-XLAMBD)/(1.+XLAMBD))
XJ=XJE+XJPERT
SHPUL=3.1416*DJ*(VC-PHI)*A*T**2*EXP(-THETA/T)
RHPUL=1.782E-11*DJ*T**4*EPS
ØHPUL=0.7854*DJ**2*B*T**S*XJ**2
WRITE ØOUTPUT TAPE 5,98,T,DIS,XJ,SHPUL,RHPUL,ØHPUL,PSI(IP),ETA(IP)
98 FØRMAT(F8.0,F15.3,1P6E15.3)
100 CONTINUE
RETURN

```

Figure 69b Concluded

As originally written, the program employs a special input routine (ENTERVAL) which is used on the Philco 2000 computer at Avco RAD. Since this routine is not generally available at other computing centers, the input statements have been omitted from the FORTRAN listing shown in figure 64. To prepare the program for operation on any machine with a FORTRAN compiler, it is necessary to add suitable input statements compatible with the particular machine. There are 27 input variables:

<u>Variable</u>	<u>Suggested Value</u>	<u>Significance</u>
D		cathode diameter (centimeters)
XL		cathode length (centimeters)
T0		temperature of cold end ( $^{\circ}\text{K}$ )
TAU		$T_{ns}/\theta$
W		molecular weight of ions (gm/mole)
VI		ionization potential (volts)
ND		number of D values
NL		number of XL values
NT0		number of T0 values
NTAU		number of TAU values
NG		number of gases
A		Richardson constant ( $\text{amp}/\text{cm}^2\text{ }^{\circ}\text{K}^2$ )
PHI		work function (volts)
XK		thermal conductivity ( $\text{w}/\text{cm }^{\circ}\text{K}$ )
B		resistivity constant in (87) ( $\text{ohm-cm}/^{\circ}\text{K}^8$ )
S		temperature exponent in (87)
EPS		total emissivity
DTNP0		input value of DTNP ( $^{\circ}\text{K}/\text{cm}$ )
ZC		$z_c$ (95)
MBSTØP	10	number of permissible iterations through statement 28
CTHETA	1.	convergence criterion for THETA ( $^{\circ}\text{K}$ )
CG	0.001	convergence criterion for numerical integration to obtain $G(X0, X1, Z)$
CARG	0.01	criterion for minimum value of ARGF (X, Z)
CTNP	0.0001	convergence criterion for TNP
CV	0.001	convergence criterion for numerical integration to obtain $V(X0, X1, Z)$
FF	0.2	factor for calculating DTNP (statement 711)
NMAX	50	number of permissible iterations through statement 12

The variables which are dimensionalized are indicated in the DIMENSION statement of the main program. D, XL, TO, and TAU are all indexed independently, but W and VI have the same index I. The suggested values for the control variables are intended as rough guides for getting the program into operation, and can be modified on the basis of experience to give better accuracy or shorter running time.

The flow chart for the main program between statements 5 and 200 is shown in figure 70. This is the section of the program which solves equations (139) for the principal unknowns. The following remarks are intended to aid in a study of the program.

1. Subroutine START selects initial values for TNP and DTNP which will enable the main program to find the correct TNP without an excessive number of passages through the incrementing statement, 10. The idea underlying this calculation is that the correct value of TNP is of the same order of magnitude as the larger of the two values which make C (139f) equal to zero,

$$0 = T_{ns}^{'2} - \frac{8\sigma\epsilon}{5KD} T_{ns}^{'5} + \frac{2B T_{ns}^{'s+1}}{(s+1)K} j_0^2. \quad (169)$$

Now,  $j_0$  is given by (139i and j). This variable is important in (169) only if it is large, and then it can be approximated roughly by

$$j_0 \sim \frac{2A T_{ns}^{'4} e^{-1/\tau}}{D \theta T_{ns}^{'}}. \quad (170)$$

Substitution of (170) converts (169) into a quadratic equation for  $T_{ns}^{'2}$ . The desired solution for  $T_{ns}'$  is

$$T_{ns}' = \sqrt{\frac{4\sigma\epsilon T_{ns}^{'5}}{5KD}} \left[ 1 + \sqrt{1 - \frac{25 KAB T_{ns}^{'s-1} e^{-2/\tau}}{2\sigma^2 \epsilon^2 (s+1) \theta^2}} \right]^{1/2}. \quad (171)$$

To improve on this rather crude value, START performs one loop of an iteration using equations (144), (145), (146), (147), and (169) and thus arrives at an improved estimate of the upper value of TNP for which  $C = 0$ . If  $FF * TNP$  is greater than or equal to  $DTNP0$ ,  $DTNP$  is taken equal to  $FF$  times the calculated TNP, and these values are returned to the main program. If  $FF * TNP$  is less than  $DTNP0$ , TNP and  $DTNP$  are both taken equal to  $DTNP0$ .





2. The loop (10, 66, 18) increases TNP until C becomes positive.
3. The loop (10, 19, 15 or 17) increases TNP until the values of Z, QARG, and DARG indicate that the function G (PSIS, PSI0, Z) can be evaluated. If  $Z < Z_C$ , the integration to obtain G can always be performed. If  $Z \geq Z_C$ , the integration encounters the square root of a negative number unless ARGF (PSIS, Z) is positive and to the left of its minimum (refer to discussion surrounding (95)) in which case the derivative DARG of ARGF is negative. In all other cases, the integration to obtain G is impossible.
4. The loop (10, 16, 22) increases TNP until DELTA, initially negative, becomes positive. Then, the interpolation routine beginning with statement 25 takes control until the change in TNP becomes less than  $CTNP * TNP$ . Once this criterion has been satisfied, the routine beginning at statement 40 calculates a new approximation to  $\theta$  and the program returns to statement 11 to begin calculating the corresponding new value of TNP. However, if the criterion on  $\theta$  (preceding statement 41) has been satisfied, MM is equal to 2, and the computed  $G\theta$   $T\theta$  preceding 19 transfers control to the subroutine  $\theta$ OUTPUT, which computes additional quantities and writes the results onto the output tape.
5. The loop (12, 28) deals with cases in which the first value of DELTA computed is already positive. It decreases TNP by successively smaller increments until DELTA becomes negative, control returns to statement 10 via 18, or the number of successive passages through 27 becomes equal to the input value MBSTOP. In this last case, the program prints a line of output and goes on to the next case according to the  $D\theta$  loop sequencing.
6. The loop (12, 21, 26) deals with cases in which control has reached statement 11 via 42 (i.e., cases in which an improved approximation to THETA has already been computed), and DELTA comes out positive on the first new passage through 16. In such cases, the new TNP might be less than the current value by more than the amount DTNP, and would thus escape the search carried out by the loop (12, 28). Statement 26 decreases TNP by DTNP until negative DELTA is obtained or one of the statements 66, 19 returns control to 10. Statement 18 or 22 then resets NTH to 1.
7. FUNCTION G (X0, X1, Z) is equal to the quantity  $G(X1, Z)$  minus  $G(X0, Z)$  as defined by (IV-10). Similarly,  $V(X0, X1, Z)$  is  $V(X1, Z) - V(X0, Z)$  as defined by (IV-13b). These functions are evaluated simply by Simpson-rule integration, with accuracy criteria CG and CV, respectively.
8. Subroutine  $\theta$ OUTPUT writes the output tape with instructions to print values of 25 quantities, plus a table giving the distribution of temperature and certain other quantities along the cathode. The 25 individual quantities are as follows:

<u>Symbol</u>	<u>Quantity</u>
XI	total current (amperes)
TS	tip temperature ( $^{\circ}\text{K}$ )
XJ0	current density at cold end ( $\text{amp}/\text{cm}^2$ )
Q0	heat flow at cold end (watts)
Z	(91c)
VC	cathode fall (volts)
TN	"unperturbed" tip temperature ( $^{\circ}\text{K}$ )
XJE	current density at hot end ( $\text{amp}/\text{cm}^2$ )
QE	heat flow into hot end (watts)
PSIS	(139c)
VR	resistive voltage drop along cathode (volts)
ALPHA	(58)
EC	field at surface ( $\text{v}/\text{cm}$ )
PJ	Joule dissipation (watts)
PSIO	(139d)
VEFF	$Q0/XI$
XLAMBD	$\lambda$
TNP	"unperturbed" temperature gradient at surface ( $^{\circ}\text{K}/\text{cm}$ )
PRAD	power radiated from cathode (watts)
ETAS	(139b)
VLØSS	total power loss from cathode by conduction and radiation, divided by I (volts)
TAU	$r$
ØVERF	$y0.5$ (135)
THETA	$\theta$ ( $^{\circ}\text{K}$ )
C	(139f)

9. Subroutine DISTAN calculates the values of  $\eta$  at  $\psi_s$  and at 19 equally spaced values of  $\psi$  between  $\psi_0$  and  $\psi_s$ . ØUTPUT then calculates the distance from the cold end in centimeters; the temperature (allowing for overflow effects) in  $^{\circ}\text{K}$ ; and the overflow side heating per unit length (SHPUL), the radiated heat per unit length (RHPUL), and the Joule heating per unit length (ØHPUL), all in  $\text{w}/\text{cm}$ . These quantities are printed out as a table.